

The nuclear Cooper pair

Structure and Reactions

G. Potel and R. A. Broglia

September 17, 2019

Preface

The elementary modes of nuclear excitation are vibrations and rotations, single-particle motion, and pairing vibrations and rotations. The specific reactions probing these modes are inelastic and Coulomb excitation, single- and two- particle transfer processes respectively.

The interweaving of the elementary modes of excitation lead to renormalization of the energy, wavefunction and particle content of the single-particles, as well as of the energy, width and collectivity of vibrations. This implies renormalization of the formfactors and transition densities, Q -value and effective deformation parameters both in 3D- and in gauge-space, and state and mass number dependence of the optical potential. As a consequence, the emergence of long range correlations. Also of resonance phenomena as a function of the bombarding energy of the projectile inducing the anelastic and/or transfer processes, implying also the need to go beyond lowest order distorted wave Born approximation (DWBA).

Within this context one can posit that nuclear structure (bound) and reactions (continuum) are but two aspects of the same physics. This is even more so concerning the study of light exotic halo nuclei, in which case the distinction between bound and continuum states is almost completely blurred. This is the reason why these two aspects are treated in the present monograph on equal footing within the framework of the unified nuclear field theory of structure and reactions (NFT)_(r+s).

This theory provides the (graphical) rules to diagonalize in a compact and economic way the nuclear Hamiltonian for both bound and continuum states. It does so in terms of Feynman diagrams which describe the coupling of elementary modes of excitation, correcting for the overcompleteness of the basis (structure) and for the non-orthogonality of the scattering states (reaction), as well as for Pauli principle violation. The outcome connects directly with observables: absolute reaction cross sections and decay probabilities.

In other words (NFT)_(r+s) focuses on the scattering amplitudes which determine the absolute cross sections for the variety of physical processes, involving also those in which bosons and fermions are created or annihilated, connecting such processes to formfactors and transition densities. Processes where one set of particles with given energies, momenta angular momenta, etc. go in and another group (or the same), comes out. That is, as it happens in the laboratory, let alone in nature.

Pairing vibrations and rotations, closely connected with nuclear superfluidity

are paradigms of quantal nuclear phenomena. They thus play an important role within the field of nuclear structure. It is only natural that two-nucleon transfer plays a similar role concerning the probing of the nucleus.

At the basis of fermionic pairing phenomena one finds Cooper pairs, weakly bound, extended, strongly overlapping (quasi-) bosonic entities, made out of pairs of nucleons dressed by collective vibrations and interacting through the exchange of these vibrations as well as through the bare NN -interaction, eventually corrected by $3N$ contributions. Cooper pairs not only change the statistics of the nuclear stuff around the Fermi surface and, condensing, the properties of nuclei close to their ground state. They also display a rather remarkable mechanism of tunnelling between target and projectile in direct two-nucleon transfer reaction.

Cooper pair partners being weakly bound ($\ll \epsilon_F$, Fermi energy), are correlated over distances (correlation length) much larger than nuclear dimensions ($\gg R$, nuclear radius). On the other hand, Cooper pairs are forced to be confined within regions in which normal density is present and thus, within nuclear dimensions. Within this context the mean field acts as a strong external field, strongly distorting the spatial structure of a Cooper pair in (infinite) nuclear matter.

Nonetheless, the correlation length paradigm comes into evidence, for example, when two nuclei are set into weak contact in a direct reaction. In this case, the partner nucleons of a Cooper pair have a finite probability to be confined within the mean field of a different nucleus. It is then natural that a Cooper pair can tunnel between target and projectile, equally well correlated, through simultaneous than through successive transfer processes.

Although one does not expects supercurrents in nuclei, one can study long-range pairing correlations in terms of individual quantal states and of the tunneling of single Cooper pairs. Such weak coupling Cooper pair transfer reminds the tunneling mechanism of electronic Cooper pairs across a barrier (e.g. a dioxide layer of dimensions much smaller than the correlation length) separating two superconductors, known as a Josephson junction. The main difference is that, as a rule, in the nuclear time dependent junction efigerely established in direct two-nucleon transfer process, only one or even none of the two weakly interacting nuclei are superfluid. On the other hand in nuclei, paradigmatic example of fermionic quantum finite many-body system, zero point fluctuations (ZPF) in general, and those associated with pair addition and pair subtraction modes known as pairing vibrations in particular, are much stronger than in condensed matter. Thus, pairing correlations based on even a single Cooper pair can lead to distinct pairing correlation effects in two-nucleon transfer processes.

Nucleonic Cooper pair tunneling has played and is playing a central role in the probing of these subtle quantal phenomena, both in the case of light exotic nuclei as well as of medium and heavy nuclei lying along the stability valley. They have been instrumental in shedding light on the subject of pairing in nuclei at large, and on nuclear superfluidity in particular. Consequently, and as said before, the subject of two-nucleon transfer occupies a central place in the present monograph. Both concerning the conceptual and the computational aspects of the description

of nuclear pairing, as well as regarding the quantitative confrontation of the results with the experimental findings in terms of absolute differential cross sections.

Concerning exotic nuclei, recent experiments carried out at TRIUMF (Canada) have provided, through the magnifying glass of $(NFT)_{(r+s)}$, a microscopic view of what can be considered a unique embodiment of Cooper's pair model¹: a pair of fermions (neutrons) moving in time reversal states on top of a quiescent Fermi surface and interacting through the exchange of a long wavelength vibration (phonon)², leading to a barely bound system. The two neutrons give rise to an isotropic halo. Because the vibration (phonon) results from the sloshing back and forth of the neutron halo against the core nucleons, one is in presence of a realization of Nambu's tumbling³ or, more precisely, symbiotic mechanism of spontaneously broken symmetry in gauge space.

Regarding the case of medium heavy nuclei lying along the stability valley, recent studies of heavy ion reactions between superfluid nuclei carried out at energies below the Coulomb barrier at the National Laboratory of Legnaro (Italy) have provided a measure of the neutron Cooper pair correlation length. Within this context, in the present monograph interdisciplinarity is used as a tool to attack concrete nuclear problems. But also, making use of the unique laboratory provided by the finite quantum many-body system of which the atomic nucleus is a paradigmatic example⁴, to shed light on condensed matter results, in terms of analogies involving individual, quantal single-particle states, let alone tunneling of single Cooper pairs.

Because of the central role the interweaving of the variety of elementary modes of nuclear excitation, namely single-particle motion and collective vibrations play in nuclear superfluidity, the study of Cooper pair tunneling in nuclei requires a consistent description of nuclear structure in terms of dressed quasiparticles and, making use of the resulting renormalized wavefunctions (formfactors), of one-nucleon transfer processes⁵. This is similar to the situation encountered in superconductors, in connection with strongly coupled systems, and experimentally studied through one- and two-electron tunneling experiments⁶

Thus, in the present monograph the general physical arguments and technical computational details concerning the calculation of absolute one-and two nucleon transfer differential cross sections, making use of state of the art NFT structure input, are discussed in detail.

As a result of this approach, theoretical and experimental nuclear practitioners, as well as fourth year and PhD students can use the present monograph at profit.

¹Cooper (1956).

²Fröhlich, H. (1952); Bardeen and Pines (1955); Bardeen et al. (1957a,b).

³Nambu (1991).

⁴Bohr (2019).

⁵Within this context one recognizes the difficulties of extracting spectroscopic factors from experiment, in terms of single-particle transfer cross sections calculated making use of mean field wavefunctions.

⁶Giaver (1973).

To help this use, the basic nuclear structure formalism, in particular that associated with pairing and with collective modes in nuclei, is economically introduced through general physical arguments. This is also in keeping with the availability in the current literature, of detailed discussions of the corresponding material. Within this context, the monographs *Nuclear Superfluidity* by Brink and Broglia and *Oscillations in Finite Quantum Systems* by Bertsch and Broglia, published also by Cambridge University Press can be considered companion volumes to the present one. Volume which shares with those a similar aim: to provide a broad physical view of central issues in the study of finite quantal many-body nuclear systems accessible to motivated students and practitioners. However, neither the present one, nor the other two are introductory texts. In particular the present one in which an attempt at unifying structure and reactions as it happens in nature is made. On the other hand, unifying discrete (mainly structure) and continuum (reactions), implies that we will be dealing with those structure results which can be tested by means of experiment. A fact which makes the subject of the present monograph a chapter of quantum mechanics, and thus close to what fourth year students have been learning.

Concerning the notation, we have divided each chapter into sections. Each section may, in turn, be broken down into subsections. Equations and Figures are identified by the number of the chapter and that of the section. Thus (5.1.33) labels the thirtythird equation of section 1 of chapter 5. Similarly, Fig. 5.1.2 labels the second figure of section 1 of chapter 5. Concerning the Appendices, they are labelled by the chapter number and by a Latin letter in alphabetical order, e.g. App. 2.A, App. 2.B, etc. Concerning equations and Figures, a sequential number is added. Thus (2.B.2) labels the second equation of Appendix B of chapter 2, while Fig. 2.B.1 labels the first figure of Appendix B of Chapter 2. References are called in terms of the author's surname and publication year and are found in alphabetic order in the bibliography at the end of each Chapter, as well as in the complete bibliography at the end of the monograph.

A methodological approach used in the present monograph concerns a certain degree of repetition. Similar, but not the same issues are dealt with more than once using different but equatable terminologies. This approach reflects the fact that useful concepts like reaction channels, or correlation length, let alone elementary modes of excitation, are easy to understand but difficult to define. This is because their validity is not exhausted in a single perspective. But even more important, because their power in helping at connecting⁷ seemingly unrelated results and phenomena is difficult to be fully appreciated the first time around, spontaneous symmetry breaking and associated emergent properties providing an example of this

⁷"The concepts and propositions get "meaning" viz. "content", only through their connection with sense-experience... The degree of certainty with which this connection, viz., intuitive combination, can be undertaken, and nothing else, differentiates empty fantasy from scientific "truth"... A correct proposition borrows its "truth" from the truth-content of the system to which it belongs" (A. Einstein, Autobiographical notes, in Albert Einstein, Ed. P. A. Schilpp, Harper, New York (1951)) p.1, Vol I.

fact.

Throughout, a number of footnotes are found. This is in keeping with the fact that footnotes can play a special role within the framework of an elaborated presentation. In particular, they are useful to emphasize relevant issues in an economic way. Being outside the main text, they give the possibility of stating eventual important results, without the need of elaborating on the proof, but referring to the corresponding sources. Within this context, and keeping the natural distances, one can mention that in the paper in which Born⁸ introduces the probabilistic interpretation of Schrödinger's wavefunction, the fact that this probability is connected with its modulus squared and not with the wavefunction itself, is only referred to in a footnote.

Most of the material contained in this monograph have been the subject of lectures of the four year course "Nuclear Structure Theory" which RAB delivered throughout the years at the Department of Physics of the University of Milan, as well as at the Niels Bohr Institute and at Stony Brook (State University of New York). It was also presented by the authors in the course Nuclear Reactions held at the PhD School of Physics of the University of Milan.

GP wants to thank the tutoring of Ben Bayman concerning specific aspects of two-particle transfer reactions. Discussions with Ian Thompson and Filomena Nunes on a variety of reaction subjects are gratefully acknowledged. RAB acknowledges the essential role the collaboration with Francisco Barranco and Enrico Vigezzi has played concerning nuclear structure aspects of the present monograph. Its debt with the late Aage Winther regarding the reaction aspects of it is difficult to express in words. The overall contributions of Daniel Bès, Ben Bayman and Pier Francesco Bortignon⁹ are only too explicitly evident throughout the text and constitute a daily source of inspiration. G. P. and R. A. B. have received important suggestions and comments regarding concrete points and the overall presentation of the material discussed below from Ben Bayman, Pier Francesco Bortignon, David Brink, Willem Dickhoff and Vladimir Zelevinsky and are here gratefully acknowledged.

Gregory Potel Aguilar
East Lansing

Ricardo A. Broglia
Copenhagen

Bibliography

- J. Bardeen and D. Pines. Electron-phonon interaction in metals. *Phys. Rev.*, 99: 1140, 1955.
- J. Bardeen, L. N. Cooper, and J. R. Schrieffer. Microscopic theory of superconductivity. *Physical Review*, 106:162, 1957a.

⁸Born (1926). Within this context, it is of notice that the extension of Born probabilistic interpretation to the case of many-particle systems is also found in a footnote (Pauli (1927), footnote on p. 83 of the paper).

⁹Deceased August 27, 2018.

- J. Bardeen, L. N. Cooper, and J. R. Schrieffer. Theory of superconductivity. *Physical Review*, 108:1175, 1957b.
- A. Bohr. Selected papers. In R. A. Broglia, editor, *The Finite Quantum Many-Body Problem*. World Scientific, Singapore, 2019.
- M. Born. Zur Quantenmechanik der Stoßvorgänge. *Zeitschr.f. Phys.*, 37:863, 1926.
- L. N. Cooper. Bound Electron Pairs in a Degenerate Fermi Gas. *Phys. Rev.*, 104: 1189, 1956.
- Fröhlich, H. Interaction of electrons with lattice vibrations. *Procs. Royal Soc.*, 215:291, 1952.
- I. Giaver. Electron tunneling and superconductivity. In P. Norstedt and Söner, editors, *Le Prix Nobel en 1973*, page 84. 1973.
- Y. Nambu. Dynamical symmetry breaking. In T. Eguchi and K. Nishigama, editors, *Broken Symmetry, Selected papers of Y. Nambu (1995)*, page 436. World Scientific, Singapore, 1991.
- W. Pauli. Über gasentartung und paramagnetismus. *Zeitschrift für Physik*, 41(2): 81, Jun 1927.

Contents

1	Introduction	15
1.1	Views of the nucleus	15
1.1.1	The liquid drop and the shell model	15
1.2	The particle-vibration coupling	23
1.3	Pairing vibrations	29
1.4	Spontaneous broken symmetry	32
1.4.1	Quadrupole deformations in 3D-space	32
1.4.2	Deformation in gauge space	39
1.5	Giant dipole resonance	47
1.6	Giant pairing vibrations	48
1.7	Sum rules	49
1.8	Ground state correlations	50
2	Structure and reactions	61
2.1	Elementary modes of excitation and specific probes	61
2.2	Sum rules	70
2.3	Particle–vibration coupling	77
2.3.1	Fluctuation and damping	79
2.3.2	Induced interaction	85
2.4	Well funneled nuclear structure landscape	88
2.5	Non–orthogonality	92
2.6	Coupling between intrinsic and relative motion	97
2.7	Nuclear Field Theory for pedestrians	99
2.7.1	The concept of elementary modes of excitation	104
2.7.2	NFT rules and applications	107
2.7.3	Spurious states	115
2.7.4	Applications	123
2.8	Competition between ZPF	129
2.9	Optical potential and transfer	133
2.9.1	Bare particles and Hartree–Fock field	133
2.9.2	Physical particles and optical potential	134
2.9.3	$^3_3\text{Li}_8$ structure in a nutshell	135
2.9.4	$^{11}\text{Li}(p, p)^{11}\text{Li}$ optical potential and transfer reaction channels	139

2.10 Characterization of an open–shell nucleus: ^{120}Sn	146
2.11 Summary	149
2.A Inelastic Scattering	149
2.A.1 (α,α') –scattering	150
2.B Technical details NFT	154
2.B.1 Graphical solution	154
2.B.2 Overlap	156
2.B.3 NFT($r+s$): linear theory	156
2.C NFT and reactions	158
2.C.1 Potential scattering	160
2.C.2 Transfer	161
2.D NFT vacuum polarization	167
3 Pairing with transfer	179
3.1 Nuclear Structure in a nutshell	179
3.2 Renormalization and spectroscopic amplitudes	191
3.3 Quantality Parameter	194
3.4 Cooper pairs	196
3.4.1 independent–particle motion	197
3.4.2 independent–pair motion	202
3.5 Pair vibration spectroscopic amplitudes	204
3.5.1 Pair removal mode	210
3.5.2 Pair addition mode	214
3.6 Halo pair addition mode and pygmy	217
3.6.1 Cooper pair binding: a novel embodiment of the Axel–Brink hypothesis.	220
3.7 Nuclear van der Waals Cooper pair	228
3.8 Renormalized coupling constants ^{11}Li : resumé	230
3.9 Phase transition and fluctuations	231
3.9.1 Pairing phase transition in small particles	232
3.9.2 Fine Sn particles	234
3.9.3 Time–reversal response function	234
3.A Lindemann criterion and quantality parameter	235
3.A.1 Lindemann (“disorder”) parameter for a nucleus	238
3.B The van der Waals interaction	239
3.B.1 van der Waals interaction between two hydrogen atoms . .	240
3.B.2 Critical dimension for van der Waals H–H interaction (protein folding domain)	243
3.B.3 van der Waals between two amino acids	244
3.B.4 Average interaction between two side chains	245

4 Simultaneous versus successive transfer	261
4.1 Simultaneous versus successive Cooper pair transfer in nuclei	261
4.2 Transfer probabilities, enhancement factor	262
4.2.1 Interplay between mean field and correlation length	275
4.3 Correlations in Cooper pair tunneling	278
4.4 Pair transfer	281
4.4.1 Cooper pair dimensions	281
4.5 Comments on the optical potential	287
4.6 Weak link between superconductors	291
4.7 Rotation in gauge space	296
4.7.1 Phase coherence	297
4.8 Hindsight	301
4.9 Medium polarization effects and pairing	304
4.9.1 Nuclei	306
4.9.2 Metals	315
4.9.3 Elementary theory of phonon dispersion relation	316
4.9.4 Pairing condensation (correlation) energy beyond level density	321
4.9.5 Hindsight	322
4.10 Cooper pair: radial dependence	324
4.10.1 Number of overlapping pairs	329
4.10.2 Coherence length and quantality parameter for (<i>ph</i>) vibrations	331
4.10.3 tunneling probabilities	335
4.10.4 Nuclear correlation (condensation) energy	336
4.10.5 Summary	337
4.11 Absolute Cooper pair tunneling cross section	339
4.11.1 Saturation density, spill out and halo	340
4.A pairing spatial correlation: simple estimate	346
4.B Coherent state	348
5 One-particle transfer	361
5.1 General derivation	362
5.1.1 Coordinates	369
5.1.2 Zero-range approximation	369
5.2 Examples and Applications	370
5.2.1 $^{120}\text{Sn}(p, d)^{119}\text{Sn}$ and $^{120}\text{Sn}(d, p)^{121}\text{Sn}$ reactions	370
5.2.2 Dressing of single-particle states: parity inversion in ^{11}Li	375
5.3 Minimal mean field theory	381
5.3.1 Density of levels	383
5.4 Single-particle strength function	385
5.5 Vacuum and medium polarization	388
5.6 The Lamb Shift	390
5.7 Self-energy and vertex corrections	391

5.8	Single-nucleon transfer for pedestrians	392
5.8.1	Plane-wave limit	396
5.9	One-particle knockout within DWBA	398
5.9.1	Spinless particles	398
5.9.2	Particles with spin	405
5.9.3	One-particle transfer	411
5.10	Dynamical shell model in a nutshell	414
6	Two-particle transfer	425
6.1	Summary of second order DWBA	426
6.2	Detailed derivation of second order DWBA	430
6.2.1	Simultaneous transfer: distorted waves	430
6.2.2	matrix element for the transition amplitude	431
6.2.3	Coordinates for the calculation of simultaneous transfer .	439
6.2.4	Matrix element for the transition amplitude (alternative derivation)	442
6.2.5	Coordinates used to derive Eq. (6.2.89)	445
6.2.6	Successive transfer	447
6.2.7	Coordinates for the successive transfer	452
6.2.8	Simplifying the vector coupling	453
6.2.9	non-orthogonality term	454
6.2.10	Arbitrary orbital momentum transfer	455
6.2.11	Successive transfer contribution	457
6.3	ZPF and Pauli principle	461
6.4	Coherence and effective formfactors	464
6.5	Succesive, simultaneous, non-orthogonality	469
6.5.1	Independent particle limit	476
6.5.2	Strong correlation (cluster) limit	477
6.A	Spherical harmonics and angular momenta	478
6.A.1	addition theorem	479
6.A.2	expansion of the delta function	479
6.A.3	coupling and complex conjugation	479
6.A.4	angular momenta coupling	480
6.A.5	integrals	480
6.A.6	symmetry properties	481
6.B	distorted waves	482
6.C	hole states and time reversal	483
6.D	Spectroscopic amplitudes in the BCS approximation	485
6.E	Bayman's two-nucleon transfer amplitudes	487
7	Structure with transfer	491
7.1	Evidence for phonon mediated pairing	491
7.1.1	Structure	495
7.1.2	Reaction	496

7.2	NFT of ^{11}Be : one-particle transfer in halo nuclei	498
7.2.1	Outlook	498
7.2.2	Calculations	500
7.3	Summary	505
7.4	Pairing rotational bands	505
7.4.1	Structure-reaction: stability of the order parameter α_0 . .	505
7.4.2	A two-nucleon transfer physical sum rule	509
7.5	Virtual states forced to become real	510
7.5.1	Empirical renormalization: $(\text{NFT})_{\text{ren}}(\mathbf{r}+\mathbf{s})$ (Feynman + S -matrix)	512
7.5.2	On-shell energy	513
7.6	Perturbation and beyond	514
7.6.1	One-particle transfer and optical potential	515
7.6.2	$(\text{NFT})_{\text{ren}}(\mathbf{r}+\mathbf{s})$ diagrams, S -matrix	515
7.6.3	The structure of “observable” Cooper pairs	515
7.6.4	Closing the circle	520
7.7	Bootstrap mechanism to break gauge invariance	521
7.7.1	Gedanken eksperiment	521
7.8	Alternative processes to populate $ ^9\text{Li}(1/2^-)\rangle$	522
7.9	Software	526
7.10	Statistics.	530
7.11	Correlation length and quantality parameter.	531
7.12	Multipole pairing vibrations.	533
7.A	Vacuum fluctuations: the Casimir effect	538
7.A.1	Measuring QED quantum fluctuations	539
7.A.2	The hydrophobic force	542

Chapter 1

Introduction

1.1 Views of the nucleus

In the atom, the nucleus provides the Coulomb field in which negatively charged electrons ($-e$) move independently of each other in single-particle orbitals. The filling of these orbitals explains Mendeleev's periodic table. Thus the valence of the chemical elements as well as the particular stability of the noble gases (He, N, Ar, Kr, Xe and Ra) associated with the closing of shells (Fig. 1.1.1). The dimension of the atom is measured in angstroms ($\text{\AA}=10^{-8}\text{cm}$), and typical energies in eV, the electron mass being $m_e \approx 0.5 \text{ MeV}$ ($\text{MeV}=10^6\text{eV}$).

The atomic nucleus is made out of positively charged protons ($+e$) and of (uncharged) neutrons, nucleons, of mass $\approx 10^3 \text{ MeV}$ ($m_p = 938.3 \text{ MeV}$, $m_n = 939.6 \text{ MeV}$). Nuclear dimensions are of the order of few fermis ($\text{fm}=10^{-13} \text{ cm}$). While the stability of the atom is provided by a source external to the electrons, namely the atomic nucleus, this system is self-bound as a result of the strong interaction of range $a_0 \approx 0.9 \text{ fm}$ and strength $v_0 \approx -100 \text{ MeV}$ acting among nucleons.

1.1.1 The liquid drop and the shell model

While most of the atom is empty space, the density of the atomic nucleus is conspicuous ($\rho = 0.17 \text{ nucleon/fm}^3$). The “closed packed” nature of this system implies a short mean free path as compared to nuclear dimensions. This can be estimated from classical kinetic theory $\lambda \approx (\rho\sigma)^{-1} \approx 1 \text{ fm}$, where $\sigma \approx 2\pi a_0^2$ is the nucleon-nucleon cross section. It seems then natural to liken the atomic nucleus to a liquid drop (Bohr and Kalckar). This picture of the nucleus provided the framework to describe the basic features of the fission process (Meitner and Frisch (1939); Bohr and Wheeler (1939)).

The leptodermic properties of the atomic nucleus are closely connected with the semi-empirical mass formula (Weizsäcker (1935))

$$m(N, Z) = (Nm_n + Zm_p) - \frac{1}{c^2}B(N, Z), \quad (1.1.1)$$

the binding energy being

$$B(N, Z) = \left(b_{vol}A - b_{surf}A^{2/3} - \frac{1}{2}b_{sym}\frac{(N-Z)^2}{A} - \frac{3}{5}\frac{Z^2e^2}{R_c} \right). \quad (1.1.2)$$

The first term is the volume energy representing the binding energy in the limit of large A , $N = Z$ and in the absence of the Coulomb interaction ($b_{vol} \approx 15.6$ MeV). The second term represents the surface energy, where

$$b_{surf} = 4\pi r_0^2 \gamma. \quad (1.1.3)$$

The nuclear radius is written as $R = r_0 A^{1/3}$, with $r_0 = 1.2$ fm, the surface tension energy being $\gamma \approx 0.95$ MeV/fm². The third term in (1.1.2) is the symmetry term which reflects the tendency towards stability for $N = Z$, with $b_{sym} = 50$ MeV. The symmetry energy can be divided into a kinetic and a potential energy part. A simple estimate of the kinetic energy part can be obtained by making use of the Fermi gas model which gives $(b_{sym})_{kin} \approx (2/3)\epsilon_F \approx 25$ MeV ($\epsilon_F \approx 36$ MeV). Consequently,

$$V_1 = (b_{sym})_{pot} = b_{sym} - (b_{sym})_{kin} \approx 25 \text{ MeV}. \quad (1.1.4)$$

The last term of (1.1.2) is the Coulomb energy corresponding to a uniformly charged sphere of radius $R_c = 1.24A^{1/3}$ fm.

When, in a heavy-ion reaction, two nuclei come within the range of the nuclear forces, the trajectory of relative motion will be changed by the attraction which will act between the nuclear surfaces. This surface interaction is a fundamental quantity in all heavy ion reactions. Assuming two spherical nuclei at a relative distance $r_{AA} = R_a + R_A$, where R_a and R_A are the corresponding half-density radii, the force acting between the two surfaces is

$$\left(\frac{\partial U_{AA}^N}{\partial r} \right)_{r_{AA}} = 4\pi\gamma \frac{R_a R_A}{R_a + R_A} \quad (1.1.5)$$

This result allows for the calculation of the ion-ion (proximity) potential which, supplemented with a position dependent absorption, can be used to accurately describe heavy ion reactions¹.

In such reactions, not only elastic processes are observed, but also anelastic processes in which one, or both surfaces of the interacting nuclei are set into vibration (Fig. 1.1.2). The restoring force parameter associated with oscillations of multipolarity λ is

$$C_\lambda = (\lambda - 1)(\lambda + 2)R_0^2\gamma - \frac{3}{2\pi} \frac{\lambda - 1}{2\lambda + 1} \frac{Z^2e^2}{R_c}, \quad (1.1.6)$$

where the second term corresponds to the contribution of the Coulomb energy to C_λ . Assuming the flow associated with surface vibration to be irrotational, the

¹Broglia and Winther (2004) and refs. therein.

associated inertia for small amplitude oscillations is,

$$D_\lambda = \frac{3}{4\pi} \frac{1}{\lambda} AMR^2, \quad (1.1.7)$$

the energy of the corresponding mode being

$$\hbar\omega_\lambda = \hbar \sqrt{\frac{C_\lambda}{D_\lambda}}. \quad (1.1.8)$$

The label λ stands for the angular momentum of the vibrational mode, μ being its third component (see Eq. (1.2.1)). Aside from λ, μ , surface vibrations can also be characterized by an integer $n (= 1, 2, \dots)$, an ordering number indicating increasing energy. For simplicity, a single common label α will also be used.

Experimental information associated with low-energy quadrupole vibrations, namely $\hbar\omega_2$ and the electromagnetic transition probabilities $B(E2)$, allow to determine C_2 and D_2 . The resulting C_2 values exhibit variations by more than a factor of 10 both above and below the liquid-drop estimate. The observed values of D_2 are large as compared with the mass parameter for irrotational flow.

A picture apparently antithetic to that of the liquid drop, the shell model, emerged from the study of experimental data, plotting them against either the number of protons (atomic number), or the number of neutrons in the nuclei, rather than against the mass number. One of the main nuclear features which led to the development of the shell model was the study of the stability and abundance of nuclear species and the discovery of what are usually called magic numbers (Elsasser (1933); Mayer (1948); Haxel et al. (1949)). What makes a number magic is that a configuration of a magic number of neutrons, or of protons, is unusually stable whatever the associated number of other nucleons is (Mayer (1949); Mayer and Teller (1949)).

The strong binding of a magic number of nucleons and weak binding for one more reminds, only relatively weaker, the results displayed in Fig. 1.1.1 concerning the atomic stability of rare gases. In the nuclear case, at variance with the atomic case, the spin-orbit coupling play an important role, as can be seen from the level scheme shown in Fig. 1.1.3, obtained by assuming that nucleons move independently of each other in an average potential of spherical symmetry.

A closed shell, or a filled level, has angular momentum zero. Thus, nuclei with one nucleon outside (missing from) closed shell, should have the spin and parity of the orbital associated with the odd nucleon (-hole), a prediction confirmed by the data (available at that time) throughout the mass table. Such a picture implies that the nucleon mean free path is large compared to nuclear dimensions.

The systematic studies of the binding energies leading to the shell model found also that the relation (1.1.2), has to be supplemented to take into account the fact that nuclei with both odd number of protons and of neutrons are energetically unfavored compared with even-even ones (inset Fig. 1.1.1) by a quantity of the order of $\delta \approx 33 MeV/A^{3/4}$ called the pairing energy².

²Connecting with further developments associated with the BCS theory of superconductivity

The low-lying excited state of closed shell nuclei can be interpreted as a rule, as harmonic quadrupole or octupole collective vibrations (Fig. 1.1.4) described by the Hamiltonian³

$$H_{coll} = \sum_{\lambda\mu} \left(\frac{1}{2D_\lambda} |\Pi_{\lambda\mu}|^2 + \frac{C_\lambda}{2} |\alpha_{\lambda\mu}|^2 \right) \quad (1.1.9)$$

Following Dirac (1930) one can describe the oscillatory motion introducing boson creation (annihilation) operator $\Gamma_{\lambda\mu}^\dagger$ ($\Gamma_{\lambda\mu}$) obeying

$$[\Gamma_\alpha, \Gamma_{\alpha'}^\dagger] = \delta(\alpha, \alpha'), \quad (1.1.10)$$

leading to

$$\hat{\alpha}_{\lambda\mu} = \sqrt{\frac{\hbar\omega_\lambda}{2C_\lambda}} (\Gamma_{\lambda\mu}^\dagger + (-1)^\mu \Gamma_{\lambda-\mu}), \quad (1.1.11)$$

and a similar expression for the conjugate momentum variable $\hat{\Pi}_{\lambda\mu}$, resulting in

$$\hat{H}_{coll} = \sum \hbar\omega_\lambda ((-1)^\mu \Gamma_{\lambda\mu}^\dagger \Gamma_{\lambda-\mu} + 1/2). \quad (1.1.12)$$

The frequency is $\omega_\lambda = (C_\lambda/D_\lambda)^{1/2}$, while $(\hbar\omega_\lambda/2C_\lambda)^{1/2}$ is the amplitude of the zero-point fluctuation of the vacuum state $|0\rangle_B, |n_{\lambda\mu} = 1\rangle = \Gamma_{\lambda\mu}^\dagger |0\rangle_B$ being the one-phonon state. To simplify the notation, in many cases one writes $|n_\alpha = 1\rangle$.

The ground and low-lying states of nuclei with one nucleon outside closed shell can be described by the Hamiltonian

$$H_{sp} = \sum_\nu \epsilon_\nu a_\nu^\dagger a_\nu, \quad (1.1.13)$$

where $a_\nu^\dagger (a_\nu)$ is the single-particle creation (annihilation) operator,

$$|\nu\rangle = a_\nu^\dagger |0\rangle_F, \quad (1.1.14)$$

being the single-particle state of quantum numbers $\nu (\equiv nljm)$ and energy ϵ_ν , while $|0\rangle_F$ is the Fermion vacuum. It is of notice that

$$[H_{coll}, \Gamma_{\lambda'\mu'}^\dagger] = \hbar\omega_{\lambda'} \Gamma_{\lambda'\mu'}^\dagger \quad (1.1.15)$$

and

$$[H_{sp}, a_{\nu'}^\dagger] = \epsilon_{\nu'} a_{\nu'}^\dagger. \quad (1.1.16)$$

(Bardeen et al. (1957a,b)) and its extension to the atomic nucleus (Bohr et al. (1958)), the quantity δ is identified with the pairing gap Δ parametrized according to $\Delta = 12 \text{MeV}/\sqrt{A}$ (Bohr and Mottelson (1969)). It is of notice that for typical superfluid nuclei like ^{120}Sn , the expression of δ leads to a numerical value which can be parametrized as $\delta \approx 10 \text{ MeV}/\sqrt{A}$.

³Classically $\Pi_{\lambda\mu} = D_\lambda \dot{\alpha}_{\lambda\mu}$.

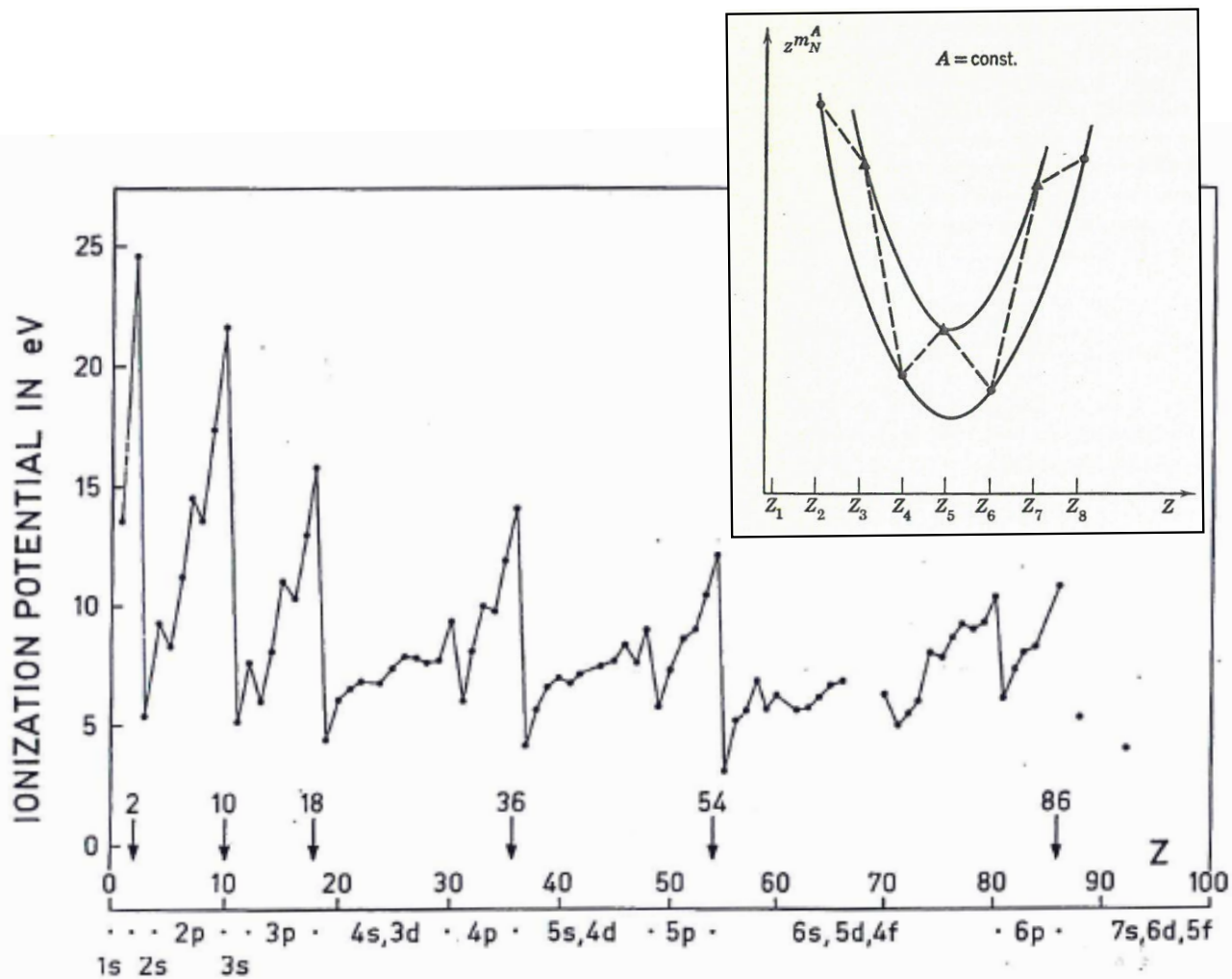


Figure 1.1.1: The values of the atomic ionization potentials. The closed shells, corresponding to electron number 2(He), 10(Ne), 18(Ar), 36(Kr), 54(Xe), and 86(Ra), are indicated. After Bohr and Mottelson (1969). In the inset, masses of nuclei with even A are shown (after Mayer and Jensen (1955)).

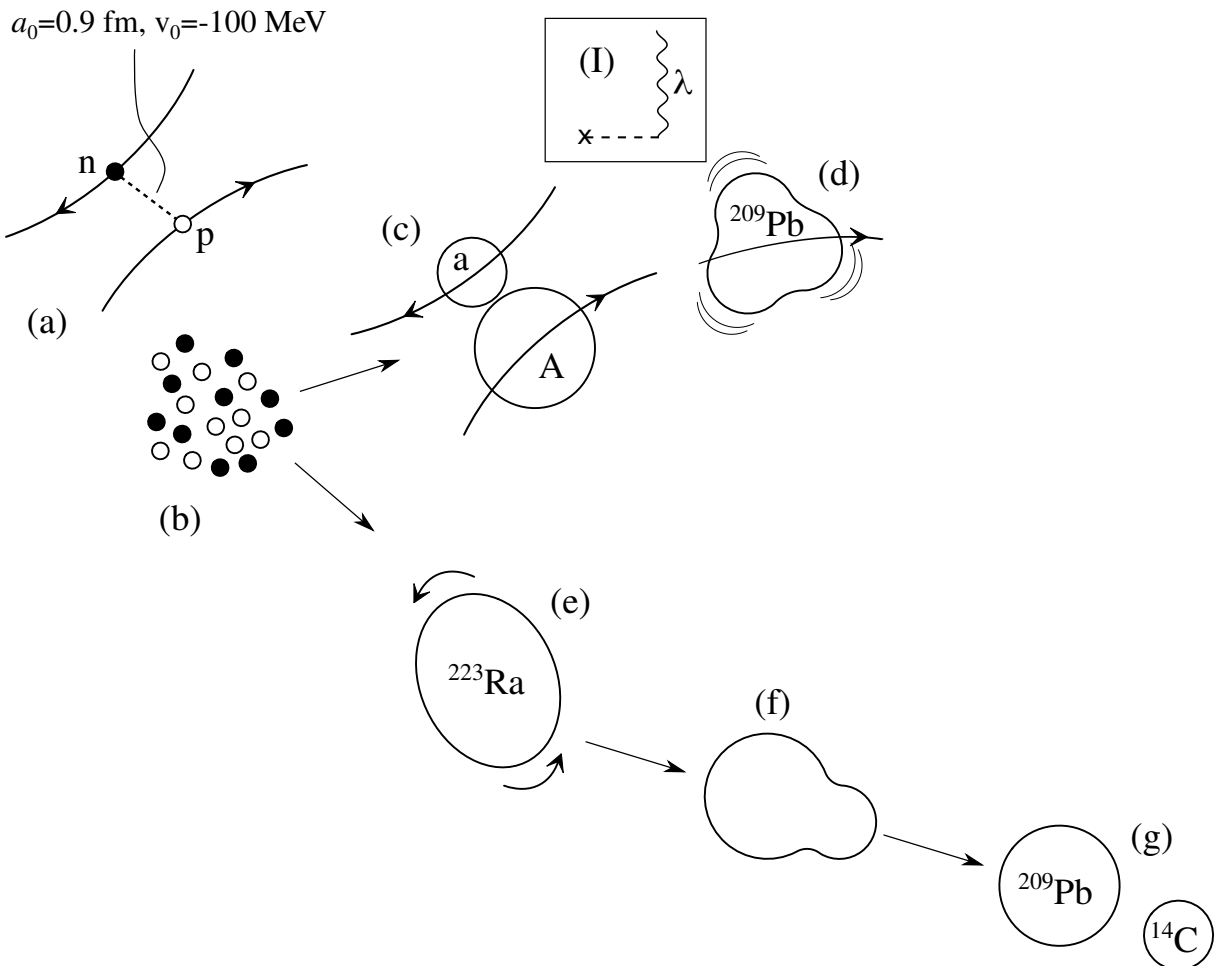


Figure 1.1.2: Emergent properties (collective nuclear models) (a) Nucleon-Nucleon (NN) interaction in a scattering experiment; (b) assembly of a swarm of nucleons condensing into drops of nuclear matter, examples shown in (c) and (e); (c) anelastic heavy ion reaction $a + A \rightarrow a + A^*$ setting the nucleus A into an octupole surface oscillations (d); in inset (I) the time-dependent nuclear plus Coulomb fields associated with the reaction (c) is represented by a cross followed by a dashed line, while the wavy line labeled λ describes the propagation of the surface vibration shown in (d), time running upwards; (e) another possible outcome of nucleon condensation: the (weakly) quadrupole deformed nucleus ^{223}Ra which can rotate as a whole with moment of inertia smaller than the rigid moment of inertia, but much larger than the irrotational one; (f) the zero point fluctuations (quadrupole ($\lambda = 2$), octupole ($\lambda = 3$), etc.) can get, with a small but finite probability ($P \approx 10^{-10}$), spontaneously in phase and produce a neck-in (saddle conformation) leading eventually to the (exotic) decay mode $^{223}\text{Ra} \rightarrow ^{209}\text{Pb} + ^{14}\text{C}$, as experimentally observed (g) (see Brink, D. and Broglia (2005), Ch. 7).

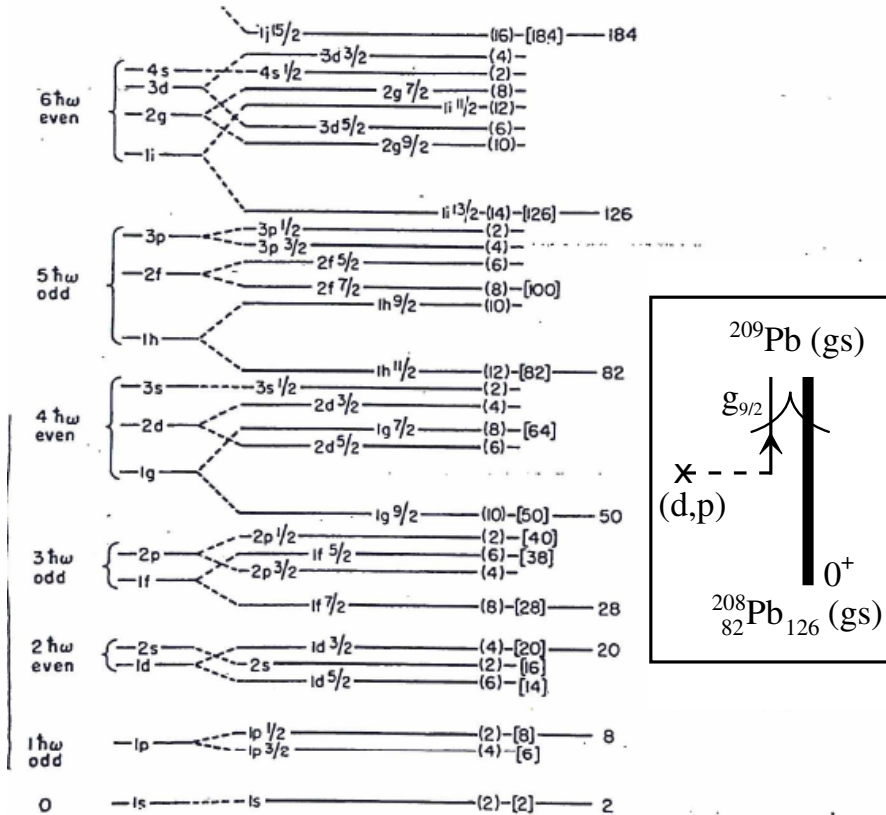


Figure 1.1.3: To the left (first column), the sequence of levels of the harmonic oscillator potential labeled with the total oscillator quantum number and parity $\pi = (-1)^N$. The next column shows the splitting of major shell degeneracies obtained using a more realistic potential (Woods-Saxon), the quantum number being the number of radial nodes of the associated single-particle s, p, d , etc., states. The levels shown at the center result when a spin-orbit term is also considered, the quantum numbers nlj characterizing the states of degeneracy $(2j + 1)$ ($j = l \pm 1/2$) (After Mayer (1963)). In the inset, a schematic graphical representation of the reaction $^{208}_{82}\text{Pb}_{126}(d, p)^{209}\text{Pb}(\text{gs})$ is shown. A cross followed by a horizontal dashed line represents the (d, p) field, while a single arrowed line describes the odd nucleon moving in the $g_{9/2}$ orbital above the $N = 126$ shell closure (and belonging to the $N = 6$ major shell) drawn as a bold line labeled 0^+ (after Bohr and Mottelson (1969)).

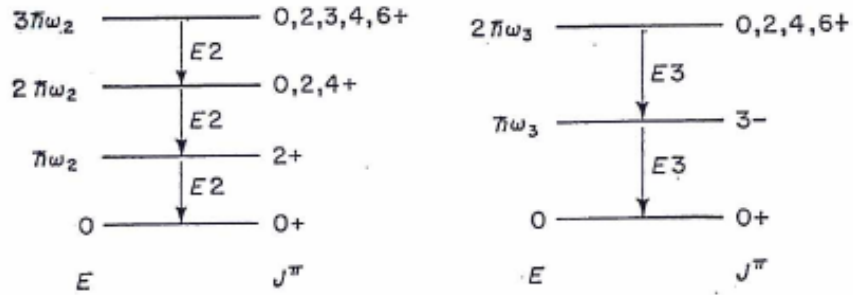


Figure 1.1.4: Schematic representation of harmonic quadrupole and octupole liquid drop collective surface vibrational modes (after Rowe (1970)).

This is an obvious outcome resulting from the bosonic

$$[\Gamma_\alpha, \Gamma_{\alpha'}^\dagger] = \delta(\alpha, \alpha') \quad (1.1.17)$$

and fermionic

$$\{a_\nu, a_{\nu'}^\dagger\} = \delta(\nu, \nu') \quad (1.1.18)$$

commutation (anti-commutation) relations.

Both the existence of drops of nuclear matter displaying collective surface vibrations, and of independent-particle motion in a self-confining mean field are emergent properties not contained in the particles forming the system, neither in the NN -force, but on the fact that these particles behave according to the rules of quantum mechanics, move in a confined volume and that there are many of them.

Generalized rigidity as measured by the inertia parameter D_λ , as well as surface tension closely connected to the restoring force C_λ , implies that acting on the system with an external time-dependent (nuclear and/or Coulomb) field, the system reacts as a whole. This behavior is to be found nowhere in the properties of the nucleons, nor in the nucleon-nucleon scattering phase shifts consistent with Yukawa's predictions of the existence of a π -meson as the carrier of the strong force acting among nucleons.

Similarly, the fact that nuclei probed through fields which change in one unit particle number (e.g. (d, p) and (p, d) reactions) react in term of independent particle motion, feeling the pushings and pullings of the other nucleons only when trying to leave the nucleus, is not apparent in the detailed properties of the NN -forces, not even in those carrying the quark-gluon input. Within this context, independent particle motion can be considered a *bona fide* emergent property.

Collective surface vibrations and independent particle motion are examples of what are called elementary modes of excitation in many-body physics, and collective variables in soft-matter physics.

1.2 The particle-vibration coupling

The oscillation of the nucleus under the influence of surface tension implies that the potential $U(R, r)$ in which nucleons move independently of each other change with time. For low-energy collective vibrations this change is slow as compared with single-particle motion. Within this scenario the nuclear radius can be written as

$$R = R_0 \left(1 + \sum_{LM} \alpha_{LM} Y_{LM}^*(\hat{r}) \right) \quad (1.2.1)$$

Assuming small amplitude motion,

$$U(r, R) = U(r, R_0) + \delta U(r), \quad (1.2.2)$$

where

$$\delta U = -\kappa \hat{a} \hat{F}, \quad (1.2.3)$$

and

$$\hat{F} = \sum_{\nu_1 \nu_2} \langle \nu_1 | F | \nu_2 \rangle a_{\nu_1}^\dagger a_{\nu_2}, \quad (1.2.4)$$

while

$$F = \frac{R_0}{\kappa} \frac{\partial U}{\partial r} Y_{LM}^*(\hat{r}). \quad (1.2.5)$$

The coupling between surface oscillation and single-particle motion, namely the particle vibration coupling (PVC) Hamiltonian δU (Fig. 1.2.1) is a consequence of the overcompleteness of the basis. Diagonalizing δU making use of the graphical (Feynman) rules of nuclear field theory (NFT) to be discussed in following Chapter, one obtains structure results which can be used in the calculation of transition probabilities and reaction cross sections, quantities which can be compared with experimental findings.

In fact, within the framework of NFT, single-particles are to be calculated as the Hartree–Fock solution of the NN -interaction $v(|\mathbf{r} - \mathbf{r}'|)$ (Fig. 1.2.2), in particular

$$U(r) = \int d\mathbf{r}' \rho(r') v(|\mathbf{r} - \mathbf{r}'|) \quad (1.2.6)$$

being the Hartree field⁴ expressing the selfconsistency between density ρ and potential U (Fig. 1.2.2 (b) (1) and (3)), while vibrations are to be calculated in the

⁴To this potential one has to add the Fock potential resulting from the fact that nucleons are fermions. This exchange potential (Fig. 1.2.2 (b) (2 and 4)) is essential in the determination of single-particle energies and wavefunctions. Among other things, it takes care of eliminating the nucleon self interaction from the Hartree field.

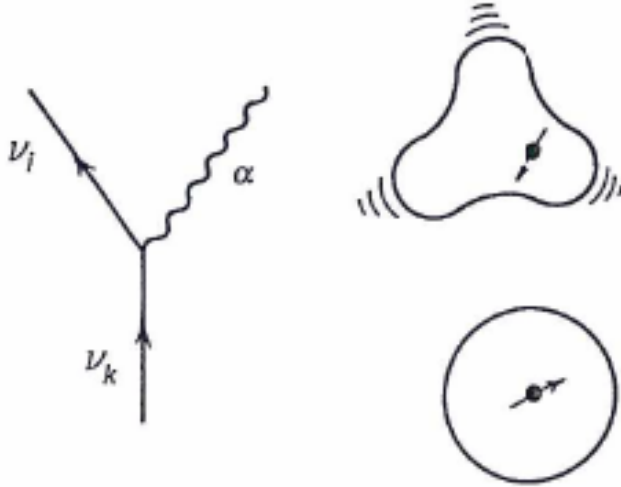


Figure 1.2.1: Graphical representation of process by which a fermion, bouncing inelastically off the surface, sets it into vibration. Particles are represented by an arrowed line pointing upwards which is also the direction of time, while the vibration is represented by a wavy line. In the cartoon to the right, the black dot represents a nucleon moving in a spherical mean field of which it excites an octupole vibration after bouncing inelastically off the surface.

Random Phase Approximation (RPA) making use of the same interaction⁵ (Fig. 1.2.3), extending the selfconsistency to fluctuations $\delta\rho$ of the density and δU of the mean field, that is,

$$\delta U(r) = \int d\mathbf{r}' \delta\rho(\mathbf{r}') v(|\mathbf{r} - \mathbf{r}'|). \quad (1.2.7)$$

Making use of the solution to this relation one obtains the transition density $\delta\rho$. The matrix elements $\langle n_\lambda = 1, \nu_i | \delta\rho | \nu_k \rangle$ provide the particle-vibration coupling strength to work out the variety of coupling processes between single-particle and collective motion (Fig. 1.2.1). That is, the matrix element of the PVC Hamiltonian H_c . Diagonalizing

$$H = H_{HF} + H_{RPA} + H_c + v, \quad (1.2.8)$$

applying in the basis of single-particle and collective modes, that is solutions of H_{HF} and of H_{RPA} respectively, the NFT rules (see next chapter) one obtains a solution of the total Hamiltonian. Concerning the rules of NFT (Sect. 2.7), they codify the way in which H_c (three-point vertices) and v (four-point vertices) are to

⁵The sum of the so called ladder diagrams (see Fig. 1.2.3) are taken into account to infinite order in RPA. This is the reason why bubble contributions in the diagonalization of Eq. (1.2.8) are not allowed in NFT, being already contained in the basis states (see next chapter, Sect. 2.7).

be treated to all orders of perturbation theory. Also which processes (diagrams) are not allowed because they will imply overcounting of correlations already included in the basis states⁶.

Because of quantal zero point fluctuations, a nucleon propagating in the nuclear medium moves through a cloud of bosonic virtual excitations to which it couples becoming dressed and acquiring effective mass, charge, etc. (Fig. 1.2.4; see also App. 5.3 and 5.10). Vice versa, vibrational modes can become renormalized through the coupling to dressed nucleons which, in intermediate virtual states, can exchange the vibrations which produce their clothing, with the second fermion (hole state). Such a process leads to a renormalization of the PVC vertex⁷ (Fig. 1.2.5), as well as of the bare NN -interaction, in particular 1S_0 component (bare pairing interaction)⁸.

The analytic procedures equivalent to the diagrammatic ones to obtain the HF (Fig. 1.2.2) and RPA (Fig. 1.2.3) solutions associated with the bare NN -interaction v is provided by the relations (1.1.16) and (1.1.15) respectively, replacing the corresponding Hamiltonians by $(T + v)$, where T is the kinetic energy operator. The phonon operator associated with surface vibrations is defined as,

$$\Gamma_\alpha^\dagger = \sum_{ki} X_{ki}^\alpha \Gamma_{ki}^\dagger + Y_{ki}^\alpha \Gamma_{ki}, \quad (1.2.9)$$

the normalization condition being,

$$[\Gamma_\alpha, \Gamma_\alpha^\dagger] = \sum_{ki} (X_{ki}^{\alpha 2} - Y_{ki}^{\alpha 2}) = 1. \quad (1.2.10)$$

The operator $\Gamma_{ki}^\dagger = a_k^\dagger a_i (\epsilon_k > \epsilon_F, \epsilon_i \leq \epsilon_F)$ creates a particle-hole excitation acting on the HF vacuum state $|0\rangle_F$. It is assumed that

$$[\Gamma_{ki}, \Gamma_{k'i'}^\dagger] = \delta(k, k')\delta(i, i'). \quad (1.2.11)$$

Within this context, RPA is a harmonic, quasi-boson approximation.

From being antithetic views of the nuclear structure, a proper analysis of the experimental data testifies to the fact that the collective and the independent particle pictures of the nuclear structure require and support each other (Bohr, A. and Mottelson (1975)). To obtain a quantitative description of nucleon motion and nuclear phonons (vibrations), one needs a proper description of the k - and ω -dependent “dielectric” function of the nuclear medium, in a similar way in which a proper

⁶A simple, although not directly related but only in a general way, example is provided by Eq. (2A-31) of Bohr and Mottelson (1969) i.e. $G = \frac{1}{4} \sum_{\nu_1 \nu_2 \nu_3 \nu_4} \langle \nu_3 \nu_4 | G | \nu_1 \nu_2 \rangle_a a^\dagger(\nu_4) a^\dagger(\nu_3) a(\nu_1) a(\nu_2) = \frac{1}{2} \sum_{\nu_1 \nu_2 \nu_3 \nu_4} \langle \nu_3 \nu_4 | G | \nu_1 \nu_2 \rangle_a a^\dagger(\nu_4) a^\dagger(\nu_3) a(\nu_1) a(\nu_2)$ where $\langle \cdot \rangle_a$ is the antisymmetric matrix element.

⁷Bertsch et al. (1983); Barranco et al. (2004) and refs. therein. It is to be noted that in the case in which the renormalized vibrational modes, i.e. the initial and final wavy lines in Fig. 1.2.5 have angular momentum and parity $\lambda^\pi = 0^+$, and one uses a model in which there is symmetry between the particle and the hole subspaces, the four diagrams sum to zero, because of particle (gauge) conservation.

⁸See e.g. Brink, D. and Broglia (2005) Ch. 10 and references therein.

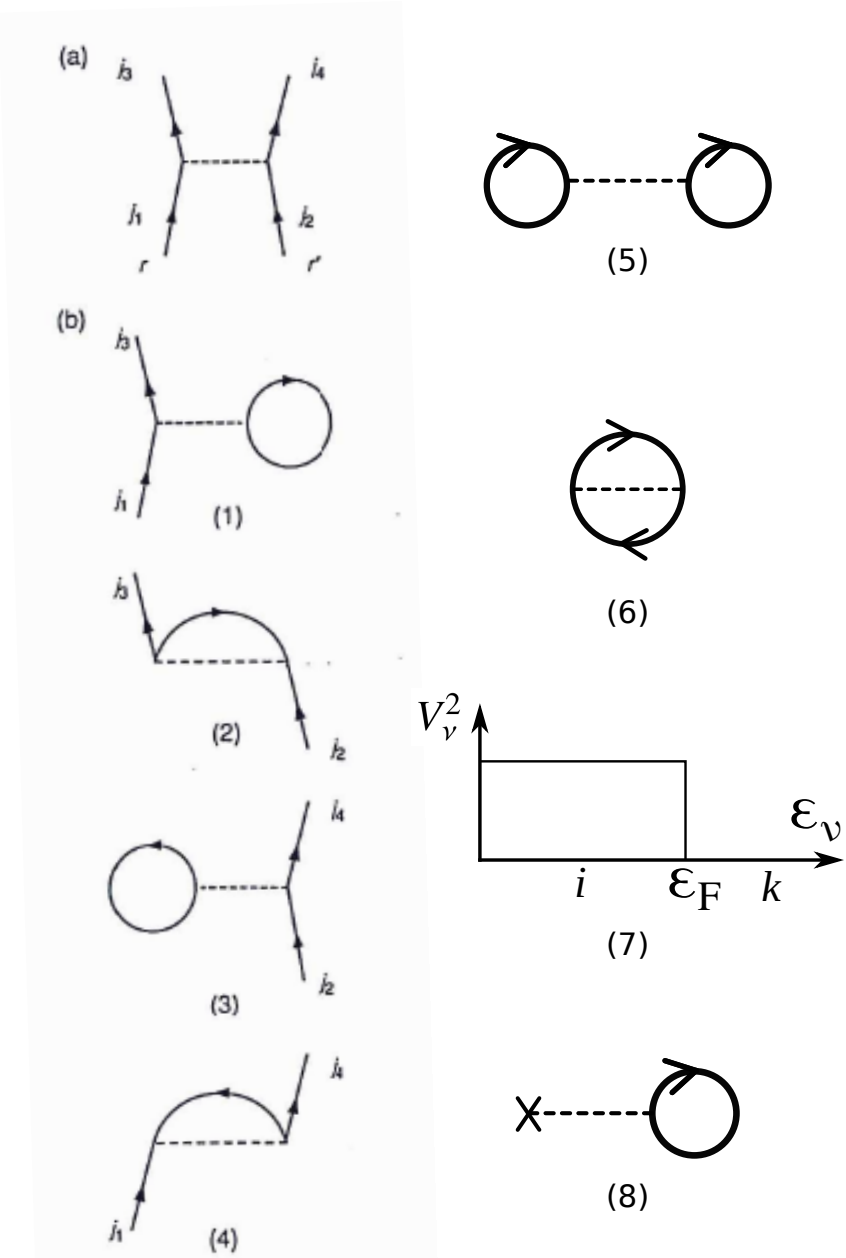


Figure 1.2.2: (a) Scattering of two nucleons through the bare NN -interaction; (b) (1) and (3): Contributions to the (direct) Hartree potential; (2) and (4): contributions to the (exchange) Fock potential. In (5) and (6) the ground state correlations associated with the Hartree- and the Fock-terms are displayed. (7) States $|i\rangle$ ($\epsilon_i \leq \epsilon_F$) are occupied with probability $V_i^2 = 1$. States $|k\rangle$ ($\epsilon_k > \epsilon_F$) are empty $V_k^2 = 1 - U_k^2$. (8) Nuclear density, the density operator being represented by a cross followed by a dashed horizontal line. (After Brink, D. and Broglia (2005)).

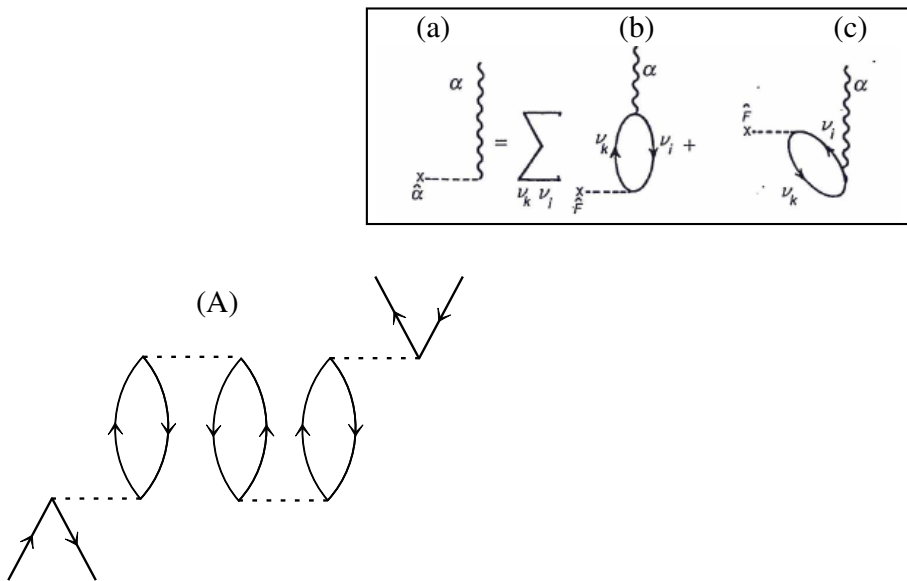


Figure 1.2.3: (A) typical Feynman diagram diagonalizing the NN -interaction $v(|\mathbf{r} - \mathbf{r}'|)$ (horizontal dashed line) in a particle-hole basis provided by the Hartree-Fock solution of v , in the harmonic approximation (RPA). Bubbles going forward in time (inset (b); leading to the amplitudes $X_{ki}^\alpha = \frac{\Lambda_\alpha(\tilde{i}|F|k)}{(\epsilon_k - \epsilon_i) - \hbar\omega_\alpha}$) are associated with configuration mixing of particle-hole states. Bubbles going backwards in time (inset (c); leading to the amplitudes $Y_{ki}^\alpha = -\frac{\Lambda_\alpha(\tilde{i}|F|k)}{(\epsilon_k - \epsilon_i) + \hbar\omega_\alpha}$) are associated with zero point motion (fluctuations ZPF) of the ground state (term $(1/2)\hbar\omega$ for each degree of freedom in Eq. 1.1.12). The self consistent solutions of A , eigenstates of the dispersion relation $\sum_{ki} \frac{2(\epsilon_k - \epsilon_i)(\tilde{i}|F|k)|^2}{(\epsilon_k - \epsilon_i)^2 - (\hbar\omega_\alpha)^2} = 1/\kappa$ are represented by a wavy line (inset (a)), that is a collective mode which can be viewed as a correlated particle (arrowed line going upward)- hole (arrowed line going downward) excitation.

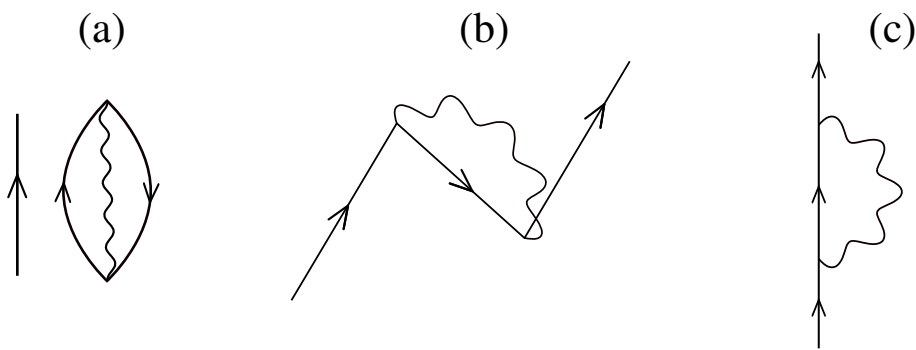


Figure 1.2.4: **(a)** a nucleon (single arrowed line pointing upward) moving in presence of the zero point fluctuation of the nuclear ground state associated with a collective surface vibration; **(b)** Pauli principle leads to a dressing process of the nucleon; **(c)** time ordering gives rise to the second possible lowest order clothing process (time assumed to run upwards).

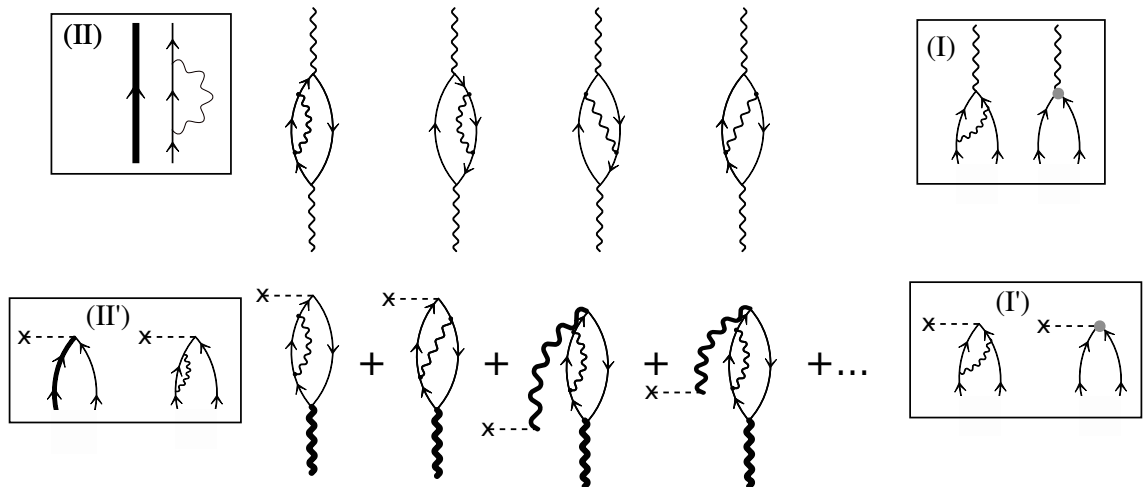


Figure 1.2.5: (Upper part) Examples of renormalization processes dressing a surface collective vibrational state. (Lower part) Intervening with an external electromagnetic field ($E\lambda$: cross followed by dashed horizontal line; bold wavy lines, renormalized vibration of multipolarity λ) the $B(E\lambda)$ transition strength can be measured. In insets (I) and (I'), the hatched circle in the diagram to the right stands for the renormalized PVC strength resulting from the processes described by the corresponding diagrams to the left (vertex corrections). In (II') the bold face arrowed curve represent (left diagram) the motion of a nucleon of effective mass m^* in a potential $(m/m^*)U(r)$, generated by the self-energy process shown to the right (see also (II) right diagram), $U(r)$ being the potential describing the motion of nucleons (drawn as a thin arrowed line) of bare mass m (inset (II), left diagram; Brink, D. and Broglia (2005) App. B).

description of the reaction processes used as probes of the nuclear structure requires the use of the optical potential (continuum “dielectric” function). The NFT solution of (1.2.8) provides all the elements to calculate the structure properties of nuclei, and also the optical potential needed to describe nucleon-nucleus as well as the nucleus-nucleus scattering and reaction processes. It furthermore shows that both single-particle and vibrational elementary modes of excitation emerge from the same properties of the NN -interaction, the main task being that of relating these modes with the observables. Namely with the absolute differential cross sections, in keeping with the central role played by the quantal many-body renormalization processes and associated emergent properties. Renormalization which acts on par on the radial dependence of the wavefunctions (formfactors) and on the single-particle content of the orbitals involved in the reaction process under discussion (see e.g. Sect. 7.2). In other words, structure ad reactions are to be treated on equal footing⁹.

The development of experimental techniques and associated hardware has allowed for the identification of a rich variety of elementary modes of excitation aside from collective surface vibrations and of independent particle motion: quadrupole and octupole rotational bands, giant resonance of varied multipolarity and isospin, as well as pairing vibrations and rotation, together with giant pairing vibrations of transfer quantum number $\beta \pm 2$. Modes which can be specifically excited in inelastic and Coulomb excitation processes (see App. 2.A), and one- and two-particle transfer reactions (Ch. 6).

1.3 Pairing vibrations

Let us introduce this new type of elementary mode of excitation by making a parallel with quadrupole surface vibrations within the framework of RPA, namely

$$[(H_{sp} + H_i), \Gamma_{k'i'}^\dagger] = \hbar\omega_\alpha \Gamma_{k'i'}^\dagger, \quad (1.3.1)$$

where for simplicity we use, instead of v , a quadrupole-quadrupole separable interaction ($i = QQ$) defined as

$$H_{QQ} = -\kappa Q^\dagger Q \quad (1.3.2)$$

with

$$Q^\dagger = \sum_{ki} \langle k | r^2 Y_{2\mu} | i \rangle a_k^\dagger a_i, \quad (1.3.3)$$

while H_{sp} and Γ_α^\dagger are defined in (1.1.13) and (1.2.9) supplemented by (1.2.10).

⁹Within this context, and referring to one-particle transfer reactions for concreteness, the prescription of using the ratio of the absolute experimental cross section and the theoretical one – calculated in the Distorted Wave Born Approximation (DWBA) making use of Saxon-Woods single-particle wavefunctions as formfactors – to extract the single-particle content of the orbital under study (see e.g. Schiffer, J. P. et al. (2012)), may not be appropriate.

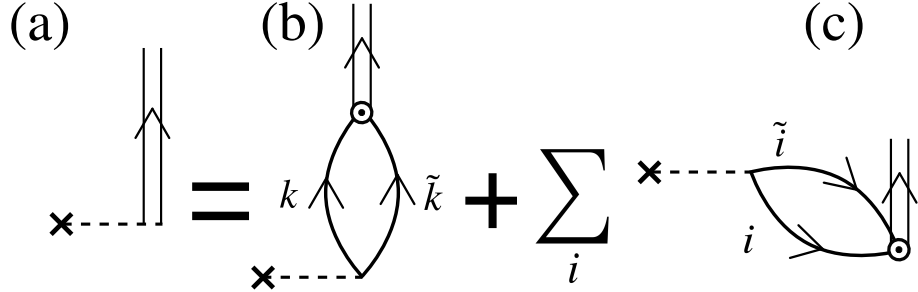


Figure 1.3.1: Graphical representation of the RPA dispersion relation describing the pair addition pairing vibrational mode, represented by a double arrowed line. Making use of the unitary transformation (1.3.6), a cross followed by a dashed horizontal line stands for: (a) the collective operator Γ_α^\dagger , (b) the operator Γ_k^\dagger creating a pair of nucleons moving in time reversal states associated with ground state correlations (k, \tilde{k}) above the Fermi energy ($\epsilon_k > \epsilon_F$); (c) The operator Γ_i^\dagger filling a pair of time reversal holes associated with ground state correlations ($\epsilon_i \leq \epsilon_F$).

In connection with the pairing energy mentioned in relation with the inset to Fig. 1.1.1, it is a consequence of correlation of pairs of like nucleons moving in time reversal states. A similar phenomenon to that found in metals at low temperatures and giving rise to superconductivity. The pairing interaction ($i = p$) can be written, within the approximation (1.3.2) used in the case of the quadrupole-quadrupole force, as

$$H_P = -P^\dagger P, \quad (1.3.4)$$

where

$$P^\dagger = \sum_{\nu>0} a_\nu^\dagger a_\nu^\dagger. \quad (1.3.5)$$

Consequently, in this case the concept of independent particle field \hat{Q} (see also (1.2.4)) associated with particle-hole (ph) excitations and carrying transfer quantum number $\beta = 0$ has to be generalized to include fields describing independent pair motion, in which case $\alpha \equiv (\beta = +2, J^\pi = 0^+)$

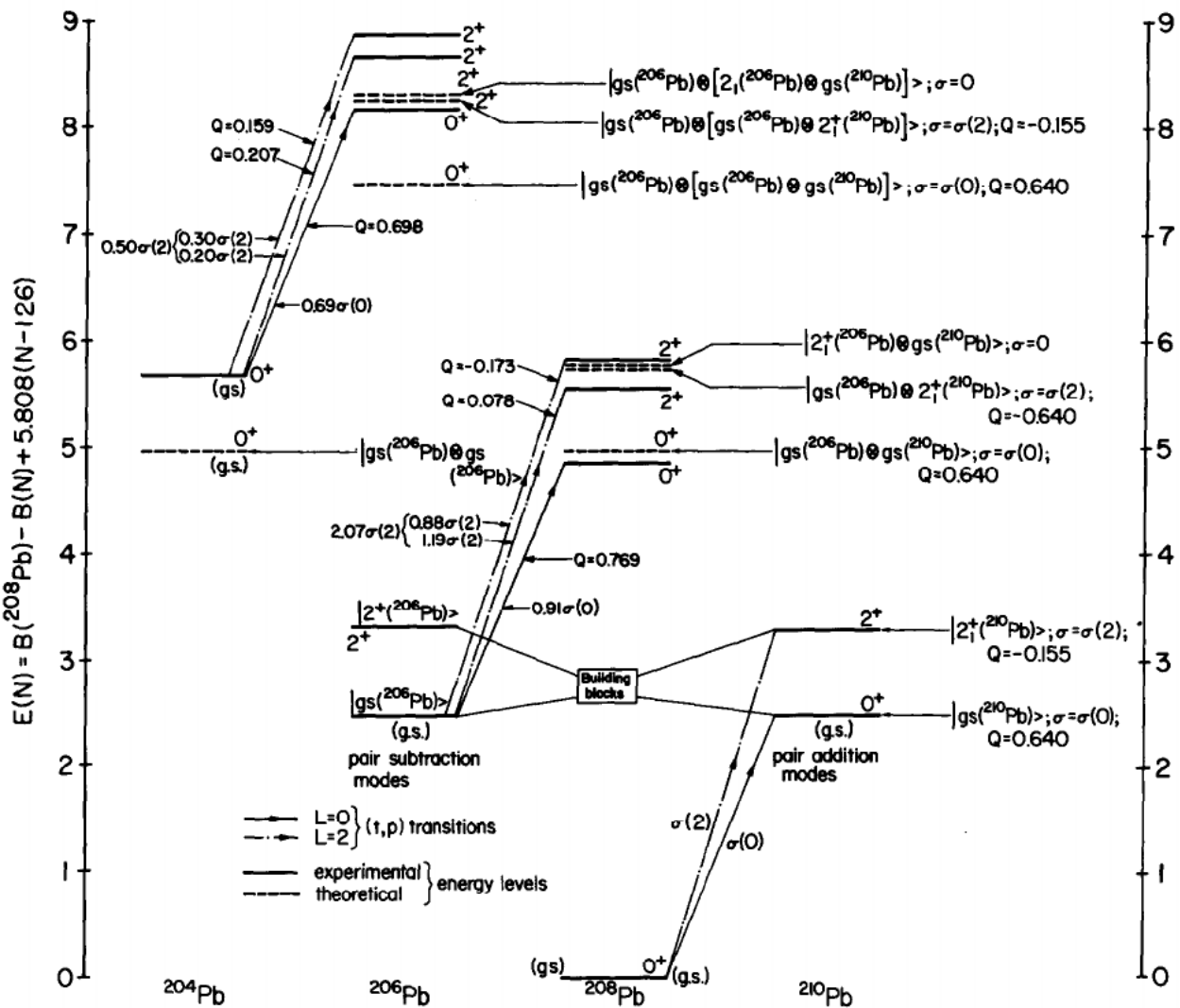
$$\Gamma_\alpha^\dagger = \sum_k X_{kk}^\alpha \Gamma_k^\dagger + \sum_i Y_{ii}^\alpha \Gamma_i^\dagger \quad (1.3.6)$$

with

$$\Gamma_k^\dagger = a_k^\dagger a_{\tilde{k}}^\dagger \quad (\epsilon_k > \epsilon_F), \quad \Gamma_i^\dagger = a_i^\dagger a_{\tilde{i}}^\dagger \quad (\epsilon_i \leq \epsilon_F), \quad (1.3.7)$$

and

$$\sum_k X_{kk}^{\alpha 2} - \sum_i Y_{ii}^{\alpha 2} = 1, \quad (1.3.8)$$



Theoretical predictions of the pairing vibrational model for the $J\pi = 0^+$ and 2^+ excited states of ^{208}Pb and ^{206}Pb expected to display the same Q -value, angular distribution and intensities in the $^{206}, ^{204}\text{Pb} (t, p)$ reactions as the ground state and first excited 2^+ state of ^{210}Pb in the $^{208}\text{Pb} (t, p)$ ^{210}Pb reaction.

These levels are depicted as dotted lines and their structure in terms of the pair addition and pair subtraction phonons (building blocks) are explicitly given.

The corresponding cross section and Q -values expected for each transition are also quoted for each state. The experimental energies (solid lines) and (t, p) cross sections are also given. In this case, the levels are joined by a continuous line ($L = 0$ transitions) or by a dotted line ($L = 2$ transitions) and the corresponding intensities in terms of the cross sections $\sigma(0) = \sigma(^{208}\text{Pb}(t, p)^{210}\text{Pb}(\text{gs}))$ and $\sigma(2) = \sigma(^{208}\text{Pb}(t, p)^{210}\text{Pb}(2^+))$ are given. Also quoted are the observed Q -values.

The experimental energy of the different ground states is given relative to the ^{208}Pb ground state and corrected by a linear function of the number of neutrons outside (or missing from) the $N = 126$ closed shell such that $E(^{206}\text{Pb}(\text{gs})) = E(^{210}\text{Pb}(\text{gs}))$. The corresponding expression [6] is $E_{\text{exp}}(N, Z = 82) = B(^{208}\text{Pb}) - B(N, Z = 82) + 5.808(N - 126)$, where $B(N, Z)$ is the binding energy of the nucleus $A = N + Z$. Note that $\hbar\omega(0) = E_{\text{theor}}(^{206}\text{Pb}(\text{gs})) = E_{\text{theor}}(^{210}\text{Pb}(\text{gs})) = E_{\text{exp}}(^{206}\text{Pb}(\text{gs})) = E_{\text{exp}}(^{210}\text{Pb}(\text{gs})) = 2.493$ MeV, that $E_{\text{theor}}(^{206}\text{Pb}(2^+)) = E_{\text{exp}}(^{206}\text{Pb}(2^+)) = 3.294$ MeV and $E_{\text{theor}}(^{210}\text{Pb}(2^+)) = E_{\text{exp}}(^{210}\text{Pb}(2^+)) = 3.288$ MeV. The theoretical energy of any other state, for example of the 2^+ state $|gs(^{206}\text{Pb}) \otimes 2(^{210}\text{Pb}); 2^+\rangle$ of ^{206}Pb is equal to $2.493 + 3.294 + 2.493 = 8.280$ MeV (as measured from $^{208}\text{Pb}(\text{gs})$).

Figure 1.3.2: (After Flynn, E. R. et al. (1972)).

for the pair addition ($(pp), \beta = +2$) mode, and a similar expression for the pair removal ($(hh), \beta = -2$) mode. In Fig. 1.3.1 the NFT graphical representation of the RPA equations for the pair addition mode is given. The state $\Gamma_\alpha^\dagger(\beta = +2)|\tilde{0}\rangle$, where $|\tilde{0}\rangle$ is the correlated ground state of a closed shell nucleus, can be viewed as the nuclear embodiment of a Cooper pair found at the basis of the microscopic theory of superconductivity.

While surface vibrations are associated with the normal ($\beta = 0$) nuclear density, pairing vibrations are connected with the so called abnormal ($\beta = \pm 2$) nuclear density (density of Cooper pairs), both static and dynamic.

Similar to the quadrupole and octupole vibrational bands built out of n_α phonons of quantum numbers $\alpha \equiv (\beta = 0, \lambda^\pi = 2^+, 3^-)$ schematically shown in Fig. 1.1.4 and experimentally observed in inelastic and Coulomb excitation and associated γ -decay processes, pairing vibrational bands build of n_α phonons of quantum numbers $\alpha \equiv (\beta = \pm 2, \lambda^\pi = 0^+, 2^+)$ have been identified around closed shells in terms of two-nucleon transfer reactions throughout the mass table (see e.g. Fig. 1.3.2).

1.4 Spontaneous broken symmetry

Because empty space is homogeneous and isotropic, the nuclear Hamiltonian is translational and rotational invariant. It also conserves particle number and is thus gauge invariant. According to quantum mechanics, the corresponding wavefunctions transform in an irreducible way under the corresponding groups of transformation. When the solution of the Hamiltonian does not have some of these symmetries, for example defines a privileged direction in space violating rotational invariance, one is confronted with the phenomenon of spontaneous broken symmetry. Strictly speaking, this can take place only for idealized systems that are infinitely large. But when one sees similar phenomena in atomic nuclei, although not so clear or regular, one recognizes that this system is after all a finite quantum many-body system (FQMBS).

1.4.1 Quadrupole deformations in 3D-space

A nuclear embodiment of the spontaneous symmetry breaking phenomenon is provided by a quadrupole deformed mean field. A situation one is confronted with, when the value of the lowest quadrupole frequency ω_2 of the RPA solution (1.1.15) tends to zero ($C_2 \rightarrow 0, D_2$ finite). A phenomenon resulting from the interplay of the interaction v (H_{QQ} in (1.3.2)), and of the nucleons outside closed shell, leading to tidal-like polarization of the spherical core.

Coordinate and linear momentum ((x, p_x) single-particle motion) as well as Euler angles and angular momentum ((φ, I_z) rotational in two-dimensional (2D)-space) are conjugate variables. Similarly, the gauge angle and the number of particles ((ϕ, N) rotation in gauge space), fulfill $[\phi, N] = i$. The operators $e^{-ip_x x}, e^{-i\varphi I_z}$ and $e^{-iN\phi}$ induce Galilean transformation and rotations in 2D- and in gauge space

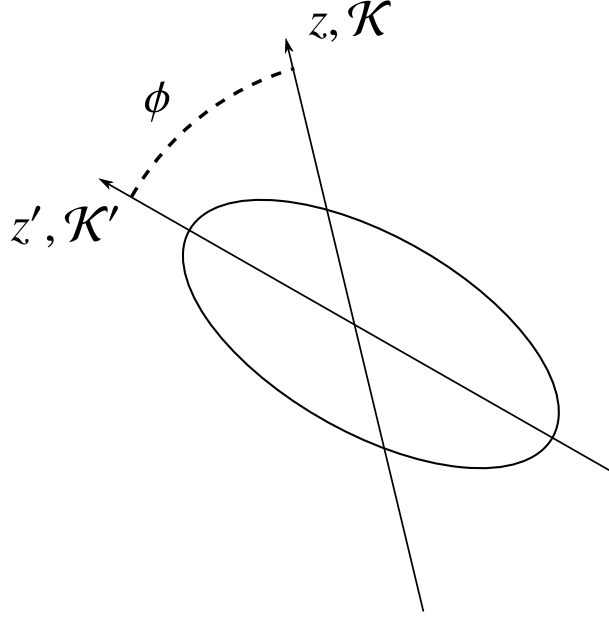


Figure 1.4.1: Schematic representation of deformation in gauge space, where the laboratory (\mathcal{K}) and the intrinsic (\mathcal{K}' , body fixed) frames of reference are also indicated.

respectively.

Making again use, for didactical purposes, of H_{QQ} instead of v , and calling $|N\rangle$ the eventual mean field solution of the Hamiltonian $T + H_{QQ}$, one expects

$$\langle N | \hat{Q} | N \rangle = Q_0, \quad (1.4.1)$$

where, for simplicity, we assumed axial symmetry ($\lambda = 2, \mu = 0$). That is, the emergence of a static quadrupole deformation. Rewriting H_{QQ} in terms of $(\hat{Q}^\dagger - Q_0 + Q_0)$ and its Hermitian conjugate, one obtains

$$H = H_{sp} + H_{QQ} = H_{MF} + H_{fluct}, \quad (1.4.2)$$

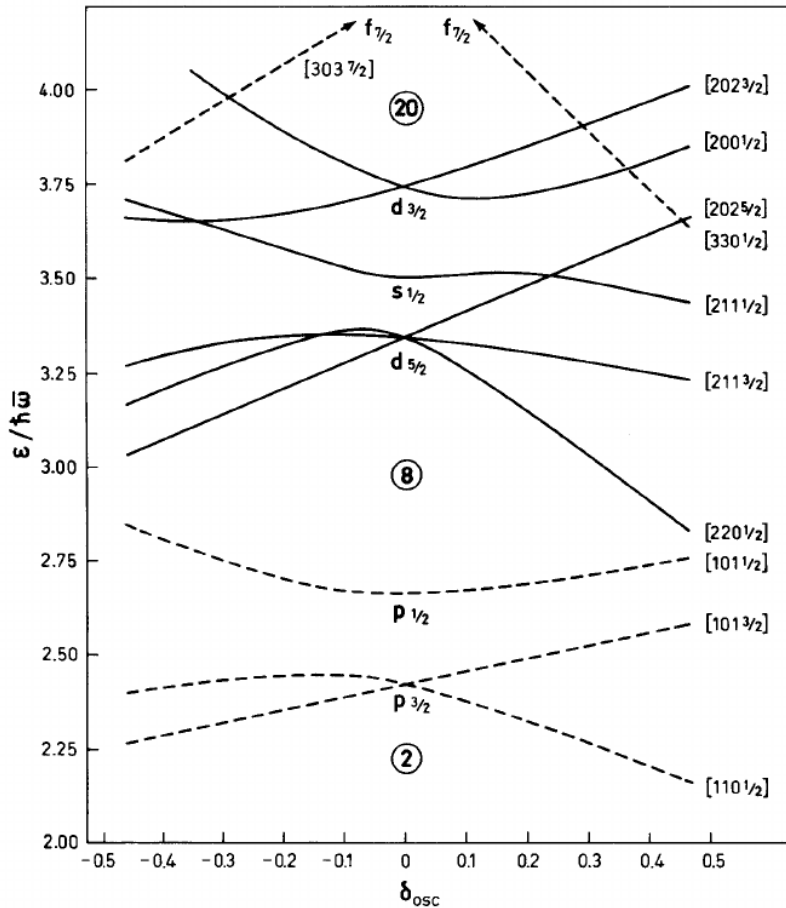
where

$$H_{MF} = H_{sp} - \kappa(\hat{Q}^\dagger + \hat{Q}), \quad (1.4.3)$$

is the mean field, and

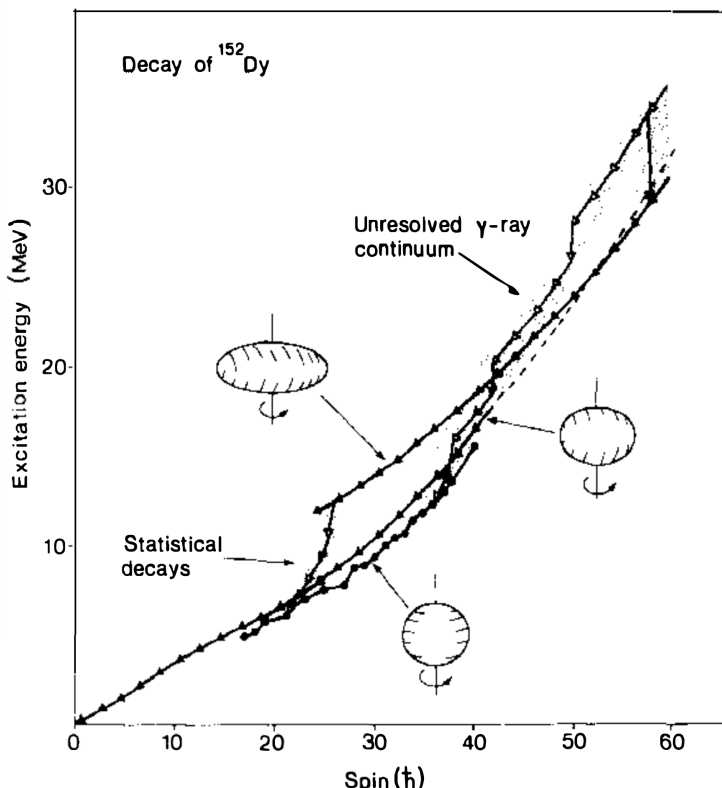
$$H_{fluct} = -\kappa(\hat{Q}^\dagger - Q_0)(\hat{Q} - Q_0) \quad (1.4.4)$$

the residual interaction inducing fluctuations around Q_0 . Assuming $Q_0 \gg (\hat{Q}^\dagger - Q_0)(\hat{Q} - Q_0)$, we concentrate on H_{MF} . The original realization of it is known as the Nilsson Hamiltonian (Nilsson (1955)). It describes the motion of nucleons in



Spectrum of single-particle orbits in spheroidal potential (N and $Z < 20$). The spectrum is taken from B. R. Mottelson and S. G. Nilsson, *Mat. Fys. Skr. Dan. Vid. Selsk.* **1**, no. 8 (1959). The orbits are labeled by the asymptotic quantum numbers $[Nn_l\Lambda\Omega]$ referring to large prolate deformations. Levels with even and odd parity are drawn with solid and dashed lines, respectively.

Figure 1.4.2: (After Bohr, A. and Mottelson (1975)).



A schematic of the proposed γ -ray decay paths from a high-spin entry point in ^{152}Dy . The major initial decay flow occurs mainly via E2 transitions in the unresolved γ -ray continuum and reaches the oblate yrast structures between $30\hbar$ and $40\hbar$. A small 1% branch feeds the superdeformed band, which is assumed to become yrast at a spin of $50\hbar$ – $55\hbar$. The deexcitation of the superdeformed band around $26\hbar$ occurs when the band is 3–5 MeV above yrast, and a statistical type of decay flow takes it into the oblate states between $19\hbar$ and $25\hbar$.

Figure 1.4.3: (After Nolan and Twin (1988)).

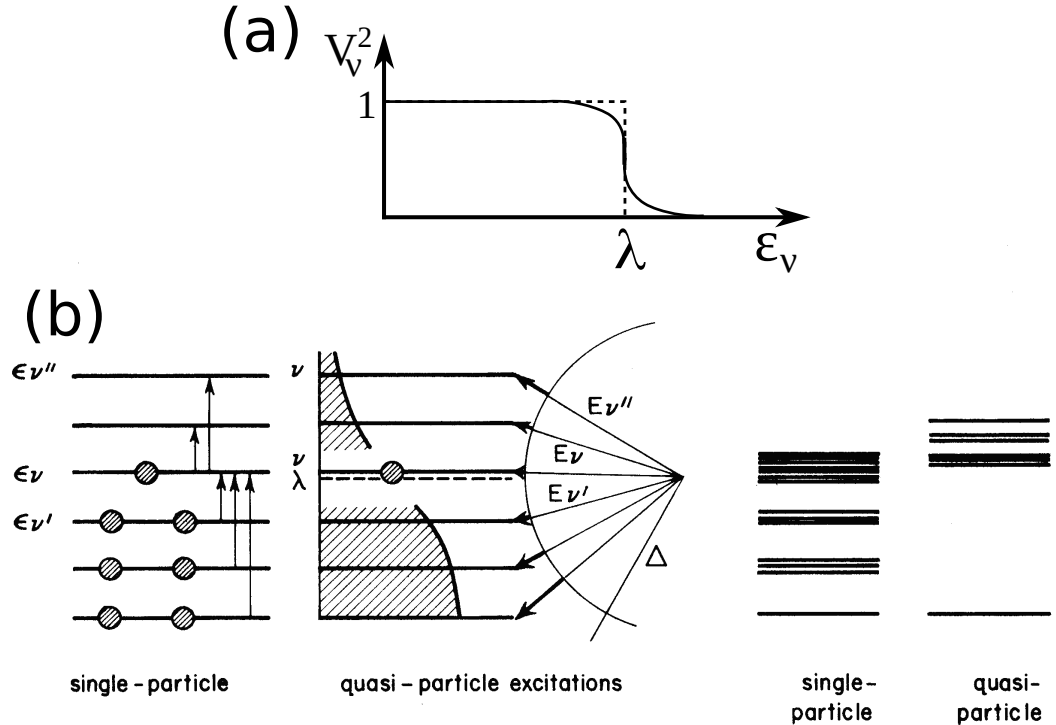


Figure 1.4.4: (a) Independent (dashed line) and BCS occupation numbers; (b) ground state and excited states in the extreme single-particle model and in the pairing-correlated, superfluid model in the case of a system with an odd number of particles. In the first case, the energy of the ground state of the odd system differs from that of the even with one particle fewer by the energy difference $\epsilon_v - \epsilon_{v'}$, while in the second case by the energy $E_v = \sqrt{(\epsilon_v - \lambda)^2 + \Delta^2} \approx \Delta$, associated with the fact the odd particle has no partner. Excited states can be obtained in the independent particle case, where it is assumed that levels are two-fold degenerate (Kramers degeneracy) by promoting the odd particle to states above the level ϵ_v , or one particle to states above ν' (arrows). To the left only a selected number of these excitations are shown. In the superfluid case excited states can be obtained by breaking of pairs in any orbit. The associated quasiparticle energy is drawn also here by an arrow of which the thin part indicates the contribution of the pairing gap and the thick part indicates the kinetic energy contribution, i.e. the contribution arising from the single-particle motion. Note the very different density of levels emerging from these two pictures, which are shown at the far right of the figure (after Nathan and Nilsson (1965)).

a single-particle potential of radius $R_0(1 + \beta_2 Y_{20}(\hat{r}))$, with β_2 proportional to the intrinsic quadrupole moment Q_0 ($\beta_2 \approx Q_0/(ZR_0^2)$). The reflection invariance and axial symmetry of the Nilsson Hamiltonian implies that parity π and projection Ω of the total angular momentum along the symmetry axis are constants of motion for the one-particle Nilsson states. These states, are two-fold degenerate, since two orbits that differ only in the sign of Ω represent the same motion, apart from the clockwise and anticlockwise sense of revolution around the symmetry axis. One can thus write the Nilsson creation operators in terms of a linear combination of creation operators carrying good total angular momentum j ,

$$\gamma_{a\Omega}^\dagger = \sum_j A_j^a a_{aj\Omega}^\dagger, \quad (1.4.5)$$

where the label a stands for all the quantum numbers aside from Ω , which specify the orbital.

Expressed in the intrinsic, body-fixed, system of coordinates \mathcal{K}' (Fig. 1.4.1) where the 3 (z') axis lies along the symmetry axis and the 1 and 2 (x', y') axis lie in a plane perpendicular to it, namely

$$\gamma'_{a\Omega}^\dagger = \sum_j A_j^a \sum_{\Omega'} \mathcal{D}_{\Omega\Omega'}^2(\omega) a_{aj\Omega'}^\dagger, \quad (1.4.6)$$

one can write the Nilsson state as

$$|N(\omega)\rangle_{\mathcal{K}'} = \prod_{a\Omega>0} \gamma_{a\Omega}^{\dagger} \gamma'_{a\Omega}^{\dagger} |0\rangle_F, \quad (1.4.7)$$

where ω represent the Euler angles, $|0\rangle_F$ is the particle vacuum, and $|a\tilde{\Omega}\rangle = \gamma_{a\Omega}^{\dagger} |0\rangle_F$ is the state time-reversed to $|a\Omega\rangle$. For well deformed nuclei, a conventional description of the one-particle motion is based on the similarity of the nuclear potential to that of an anisotropic nuclear potential,

$$V = \frac{1}{2} M \left(\omega_3^2 x_3^2 + \omega_\perp^2 (x_1^2 + x_x^2) \right) = \frac{1}{2} M \omega_0 r^2 \left(1 - \frac{4}{3} \delta P_2(\cos \theta) \right), \quad (1.4.8)$$

with $\omega_3 \omega_\perp^2 = \omega_0^3$. That is a volume which is independent of the deformation $\delta \approx 0.95\beta_2$. The corresponding single-particle states have energy

$$\epsilon(n_3 n_\perp) = (n_3 + \frac{1}{2})\hbar\omega_3 + (n_\perp + \frac{1}{2})\hbar\omega_\perp, \quad (1.4.9)$$

where n_3 and $n_\perp = n_1 + n_2$ are the number of quanta along and perpendicular to the symmetry axis. The degenerate states with the same value of n_\perp can be specified by the component Λ of the orbital angular momentum along the symmetry axis,

$$\Lambda = \pm n_\perp, \pm(n_\perp - 2), \dots, \pm 1 \text{ or } 0. \quad (1.4.10)$$

One can then label the Nilsson levels in terms of the asymptotic quantum numbers $[N n_3 \Lambda \Omega]$, where $N = n_3 + n_\perp$, is the total oscillator quantum number. The complete

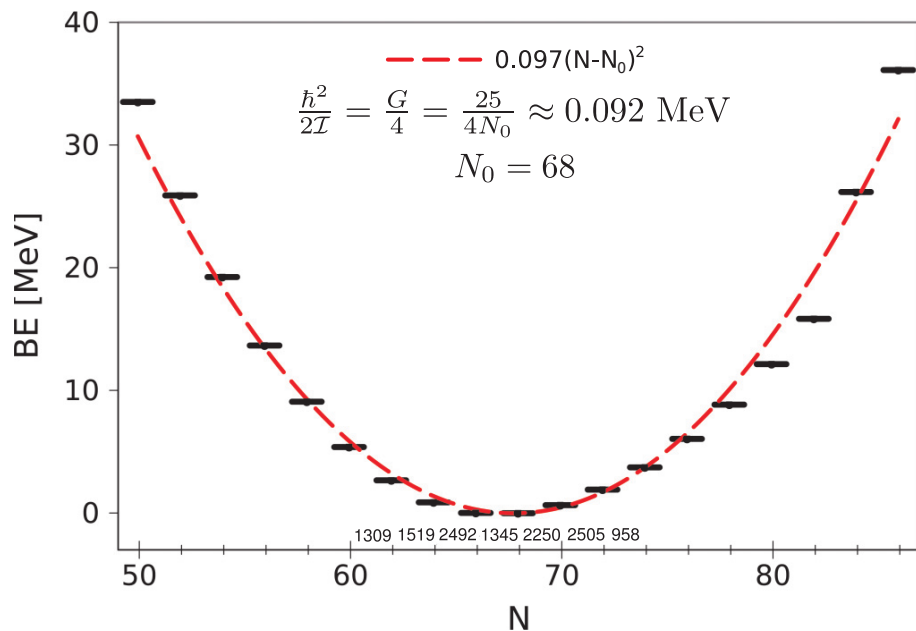


Figure 1.4.5: Pairing rotational band associated with the ground states of the Sn-isotopes. The lines represent the energies calculated according to the expression $BE = B(^{50+N}\text{Sn}_N) - 8.124N + 46.33$ (Brink, D. and Broglia (2005)), subtracting the contribution of the single nucleon addition to the nuclear binding energy obtained by a linear fitting of the binding energies of the whole Sn chain. The estimate of $\hbar^2/2I$ was obtained using the single j -shell model (see, e.g., Brink, D. and Broglia (2005), Appendix H). The numbers given on the abscissa are the absolute value of the experimental $gs \rightarrow gs$ cross section (in units of μb). (After Potel, G. et al. (2013)).

expression of the Nilsson potential includes, aside from the central term discussed above, a spin-orbit and a term proportional to the orbital angular momentum quantity squared, so as to make the shape of the oscillator to resemble more that of a Saxon-Woods potential. The resulting levels provide an overall account of the experimental findings, providing detailed evidence in terms of individual states of the interplay between the single-particle and the collective aspects of nuclear structure. An example of relevance for light nuclei (N and $Z < 20$) is given in Fig. 1.4.2.

The Nilsson intrinsic state (1.4.7) does not have a definite angular momentum but is rather a superposition of such states,

$$|N(\omega)\rangle_{\mathcal{K}'} = \sum C_I |I\rangle. \quad (1.4.11)$$

Because there is no restoring force associated with different orientations of $|N(\omega)\rangle_{\mathcal{K}'}$, fluctuations in the Euler angle diverge in the right way to restore rotational invariance, leading to a rotational band whose members are

$$|IKM\rangle \sim \int d\omega \mathcal{D}_{MK}^I(\omega) |N(\omega)\rangle_{\mathcal{K}'}, \quad (1.4.12)$$

with energy

$$E_I = \frac{\hbar^2}{2I} I(I+1). \quad (1.4.13)$$

The quantum numbers I, M, K are the total angular momentum I , and its third component M and K along the laboratory (z) and intrinsic (z') frame references respectively. Rotational bands have been observed up to rather high angular momenta in terms of individual transitions. An example extending up to $I = 60\hbar$ is given in Fig. 1.4.3.

1.4.2 Deformation in gauge space

Let us now turn to the pairing Hamiltonian. In the case in which $\hbar\omega_{\beta=-2} = \hbar\omega_{\beta=2} = 0$, the system deforms, this time in gauge space. Calling $|BCS\rangle$ the mean field solution of the pairing Hamiltonian, leads to the finite expectation value

$$\alpha_0 = \langle BCS | P^\dagger | BCS \rangle, \quad (1.4.14)$$

of the pair creation operator P^\dagger , quantity which can be viewed as the order parameter of the new deformed phase of the system in gauge space. The total Hamiltonian can be written as

$$H = H_{MF} + H_{fluct}, \quad (1.4.15)$$

where

$$H_{MF} = H_{sp} - \Delta(P^\dagger + P) + \frac{\Delta^2}{G} \quad (1.4.16)$$

and

$$H_{fluct} = -G(P^\dagger - \alpha_0)(P - \alpha_0). \quad (1.4.17)$$

The quantity

$$\Delta = G\alpha_0, \quad (1.4.18)$$

is the so called pairing gap (Fig. 1.4.4), which measures the binding energy of Cooper pairs, the quantity α_0 being the number of Cooper pairs.

The mean field pairing Hamiltonian

$$H_{MF} = \sum_{\nu>0} (\epsilon_\nu - \lambda) (a_\nu^\dagger a_\nu + a_{\tilde{\nu}}^\dagger a_{\tilde{\nu}}) - \Delta \sum_{\nu>0} (\epsilon_\nu - \lambda) (a_\nu^\dagger a_{\tilde{\nu}}^\dagger + a_{\tilde{\nu}} a_\nu) + \frac{\Delta^2}{G} \quad (1.4.19)$$

is a bilinear expression in the creation and annihilation operator, ν labeling the quantum numbers of the single-particle orbitals where nucleons are allowed to correlate e.g. $(nljm)$ while $\tilde{\nu}$ denotes the time reversal state which in this case is degenerate with ν and has quantum numbers $(nlj - m)$, $\nu > 0$ implying that one sums over $m > 0$. It is of notice that

$$\hat{N} = \sum_{\nu>0} (a_\nu^\dagger a_\nu + a_{\tilde{\nu}}^\dagger a_{\tilde{\nu}}), \quad (1.4.20)$$

is the number operator, and $\lambda \hat{N}$ in Eq. (1.4.19) acts as the Coriolis force in the body-fixed frame of reference in gauge space.

One can diagonalize H_{MF} by a rotation in the (a^\dagger, a) -space. This can be accomplished through the Bogoliubov-Valatin transformation

$$\alpha_\nu^\dagger = U_\nu a_\nu^\dagger - V_\nu a_{\tilde{\nu}}, \quad (1.4.21)$$

The BCS solution does not change the energies ϵ_ν (measured in (1.4.19) from the Fermi energy λ) of the single-particle levels or associated wavefunctions $\varphi_\nu(\mathbf{r})$, but the occupation probabilities for levels around the Fermi energy within an energy range 2Δ ($2\Delta/\lambda \approx 2 \text{ MeV}/36 \text{ MeV} \approx 0.06$). The quasiparticle operator α_ν^\dagger creates a particle in the single-particle state ν with probability U_ν^2 , while it creates a hole (annihilates a particle) with probability V_ν^2 . To be able to create a particle, the state ν should be empty, while to annihilate a particle it has to be filled, so U_ν^2 and V_ν^2 are the probabilities that the state ν is empty and is occupied respectively. Within this context, the one quasiparticle states

$$|\nu\rangle = \alpha_\nu^\dagger |BCS\rangle \quad (1.4.22)$$

are orthonormal. In particular

$$\langle \nu | \nu \rangle = 1 = \langle BCS | \alpha_\nu \alpha_\nu^\dagger | BCS \rangle = \langle BCS | \{\alpha_\nu, \alpha_\nu^\dagger\} | BCS \rangle = U_\nu^2 + V_\nu^2, \quad (1.4.23)$$

where the relations

$$\{a_\nu, a_{\nu'}^\dagger\} = \delta(\nu, \nu') \quad (1.4.24)$$

and

$$\{a_\nu, a_{\nu'}\} = \{a_\nu^\dagger, a_{\nu'}^\dagger\} = 0 \quad (1.4.25)$$

have been used. Note that the $|BCS\rangle$ state is the quasiparticle vacuum

$$\alpha_\nu |BCS\rangle = 0, \quad (1.4.26)$$

in a similar way in which $|0\rangle_F$ is the particle vacuum. Inverting the quasiparticle transformation (1.4.21) and its complex conjugate, i.e. expressing a_ν^\dagger and a_ν (and time reversals (tr)) in terms of α_ν^\dagger and α_ν (and tr) one can rewrite (1.4.19) in terms of quasiparticles.

Minimizing the energy $E_0 = \langle BCS|H|BCS\rangle$ in terms of V_ν

$$\frac{\partial E_0}{\partial V_\nu} = 0 \quad (1.4.27)$$

and making use of the expression for the average of particles

$$N_0 = \langle BCS|\hat{N}|BCS\rangle = 2 \sum_{\nu>0} V_\nu^2, \quad (1.4.28)$$

and of the number of Cooper pairs

$$\alpha_0 = \langle BCS|P^\dagger|BCS\rangle = \sum_{\nu>0} U_\nu V_\nu \quad (1.4.29)$$

and of the pairing gap

$$\Delta = G \sum_{\nu>0} U_\nu V_\nu, \quad (1.4.30)$$

one obtains,

$$H_{MF} = H_{11} + U \quad (1.4.31)$$

where

$$H_{11} = \sum_\nu E_\nu \alpha_\nu^\dagger \alpha_\nu \quad (1.4.32)$$

and

$$U = 2 \sum_{\nu>0} (\epsilon_\nu - \lambda) V_\nu^2 - \frac{\Delta^2}{G}. \quad (1.4.33)$$

The quantity

$$E_\nu = \sqrt{(\epsilon_\nu - \lambda)^2 + \Delta^2} \quad (1.4.34)$$

is the quasiparticle energy, while the probability amplitudes are

$$V_\nu = \frac{1}{\sqrt{2}} \left(1 - \frac{\epsilon_\nu - \lambda}{E_\nu} \right)^{1/2} \quad (1.4.35)$$

$$U_\nu = \frac{1}{\sqrt{2}} \left(1 + \frac{\epsilon_\nu - \lambda}{E_\nu} \right)^{1/2} \quad (1.4.36)$$

From the relations (1.4.28) and (1.4.30) one obtains

$$N_0 = 2 \sum_{\nu>0} V_\nu^2 \quad (1.4.37)$$

and

$$\frac{1}{G} = \sum_{\nu>0} \frac{1}{2E_\nu}. \quad (1.4.38)$$

These equations allow one to calculate the parameters λ and Δ from the knowledge of G and ϵ_ν , parameters which completely determine E_ν , V_ν and U_ν and thus the BCS mean field solution (Fig. 1.4.4). The validity of the BCS description of superfluid open shell nuclei have been confirmed throughout the mass table. We provide below recent examples.

The relation (1.4.26) implies that

$$\begin{aligned} |BCS\rangle &= \frac{1}{\text{Norm}} \prod_{\nu>0} \alpha_\nu \alpha_{\tilde{\nu}} |0\rangle_F = \prod_{\nu>0} (U_\nu + V_\nu P_\nu^\dagger) |0\rangle_F \\ &= \left(\prod_{\nu>0} U_\nu \right) \sum_{N \text{ even}} \frac{(c_\nu P_\nu^\dagger)^{N/2}}{(N/2)!} |0\rangle_F, \end{aligned} \quad (1.4.39)$$

where

$$P_\nu^\dagger = a_\nu^\dagger a_{\tilde{\nu}}^\dagger \quad \left(P^\dagger = \sum_{\nu>0} P_\nu^\dagger \right), \quad c_\nu = V_\nu / U_\nu. \quad (1.4.40)$$

In the above discussion of BCS we have treated in a rather cavalier fashion the fact that the amplitudes U_ν and V_ν are in fact complex quantities. A possible choice of phasing is¹⁰

$$U_\nu = U'_\nu; \quad V_\nu = V'_\nu e^{-2i\phi}, \quad (1.4.41)$$

¹⁰The same results as those which will be derived are obtained with the alternative choice $U_\nu = U'_\nu e^{i\phi}$, $V_\nu = V'_\nu e^{-i\phi}$.

U'_ν and V'_ν being real quantities, while ϕ is the gauge angle, conjugate variable to the number of particles operator (1.4.20). Then¹¹

$$\hat{\phi} = i\partial/\partial\mathcal{N}, \quad \mathcal{N} \quad (1.4.42)$$

and

$$[\hat{\phi}, \mathcal{N}] = i \quad (1.4.43)$$

where $\mathcal{N} \equiv \hat{N}$ (Eq. (1.4.20)), gauge transformations being induced by the operator

$$\mathcal{G}(\phi) = e^{-i\mathcal{N}\phi}. \quad (1.4.44)$$

Let us introduce the amplitudes (1.4.41) in (1.4.23)

$$|BCS\rangle = \left(\prod_{\nu>0} U'_\nu \right) \sum_{N \text{ even}} e^{-iN\phi} |\Phi_N\rangle = \left(\prod_{\nu>0} U'_\nu \right) \sum_{N \text{ even}} e^{-iN\phi} |\Phi_N\rangle \quad (1.4.45)$$

where

$$|\Phi_N\rangle = \frac{\left(\sum_{\nu>0} c'_\nu P_\nu^\dagger \right)^{N/2}}{(N/2)!} |0\rangle_F, \quad (1.4.46)$$

with $c'_\nu = V'_\nu/U'_\nu$. It is of notice that

$$\sum_{\nu>0} c'_\nu P_\nu^\dagger |0\rangle_F \quad (1.4.47)$$

is the single Cooper pair state. The $|BCS\rangle$ state does not have a definite number of particles, but only in average being a wavepacket in N .

In fact, (1.4.44) defines a privileged direction in gauge space, being an eigenstate of $\hat{\phi}$

$$\hat{\phi}|BCS\rangle = i \frac{\partial}{\partial\mathcal{N}} \left(\prod_{\nu>0} U'_\nu \right) \sum_{N \text{ even}} e^{-iN\phi} |\Phi_N\rangle = \phi |BCS\rangle. \quad (1.4.48)$$

Expressing it differently (1.4.44) can be viewed as an axially symmetric deformed system in gauge space, whose symmetry axis coincides with the z' component of the body-fixed frame of reference \mathcal{K}' , which makes an angle ϕ with the laboratory z -axis (Fig. 1.4.1).

With the help of Eq. (1.4.39) (first line) one can write

$$|BCS(\phi=0)\rangle_{\mathcal{K}'} = \prod_{\nu>0} (U'_\nu + V'_\nu P_\nu^\dagger) |0\rangle_F, \quad (1.4.49)$$

¹¹See e.g. Brink, D. and Broglia (2005) App. H and refs. therein.

where use was made of the relations

$$\mathcal{G}(\phi) a_\nu^\dagger \mathcal{G}^{-1}(\phi) = e^{-i\phi} a_\nu^\dagger = a_\nu'^\dagger, \quad (1.4.50)$$

and

$$\mathcal{G}(\phi) P_\nu^\dagger \mathcal{G}^{-1}(\phi) = e^{-2i\phi} P_\nu^\dagger = P_\nu'^\dagger. \quad (1.4.51)$$

It is to be noted that \mathcal{G} induces a counter clockwise rotation,

$$\mathcal{G}(\chi) \hat{\phi} \mathcal{G}^{-1}(\chi) = \hat{\phi} - \chi. \quad (1.4.52)$$

As a consequence, to rotate $|BCS(\phi = 0)\rangle_{\mathcal{K}'}$ back into the laboratory system, use has to be made of the clockwise rotation of angle ϕ induced by $\mathcal{G}^{-1}(\phi)$,

$$\begin{aligned} \mathcal{G}^{-1}(\phi) |BCS(\phi = 0)\rangle_{\mathcal{K}'} &= \prod_{\nu>0} (U'_\nu + V'_\nu \mathcal{G}^{-1}(\phi) P_\nu'^\dagger) |0\rangle_F \\ &= \prod_{\nu>0} (U'_\nu + e^{2i\phi} V_\nu P_\nu^\dagger) |0\rangle_F = |BCS(\phi)\rangle_{\mathcal{K}} \end{aligned} \quad (1.4.53)$$

where use was made of (1.4.49)

$$\mathcal{G}^{-1}(\phi) (\mathcal{G}(\phi) P_\nu^\dagger \mathcal{G}^{-1}(\phi)) \mathcal{G}(\phi) = \mathcal{G}^{-1}(\phi) P_\nu'^\dagger \mathcal{G}(\phi). \quad (1.4.54)$$

We note furthermore

$$|BCS(\phi = 0)\rangle_{\mathcal{K}'} = \prod_{\nu>0} (U'_\nu + V'_\nu P_\nu'^\dagger) |0\rangle_F = \prod_{\nu>0} (U_\nu + V_\nu P_\nu^\dagger) |0\rangle_F. \quad (1.4.55)$$

Spontaneous broken symmetry in nuclei is, as a rule associated with the presence of rotational bands, as already found in the case of quadrupole deformed nuclei. Consequently, one expects in nuclei with $\Delta \neq 0$ rotational bands in which particle number plays the role of angular momentum. That is pairing rotational bands.

In what follows we will discuss the structure of H_{fluct} and single out the term responsible for restoring gauge invariance to the BCS mean field solution giving thus, rise to pairing rotational bands. In terms of quasiparticles, H_{fluct} can be expressed as

$$H_{fluct} = H'_p + H''_p + C \quad (1.4.56)$$

where

$$H'_p = -\frac{G}{4} \left(\sum_{\nu>0} (U_\nu^2 - V_\nu^2) (\Gamma_\nu^\dagger + \Gamma_\nu) \right)^2 \quad (1.4.57)$$

and

$$H''_p = \frac{G}{4} \left(\sum_{\nu} (\Gamma_\nu^\dagger - \Gamma_\nu) \right)^2, \quad (1.4.58)$$

with

$$\Gamma_\nu^\dagger = \alpha_\nu^\dagger \alpha_{\bar{\nu}}^\dagger. \quad (1.4.59)$$

The term C stands for constant terms, as well as for terms proportional to the number of quasiparticles, which consequently vanish when acting on $|BCS\rangle$. The term H'_p gives rise to two-quasiparticle pairing vibrations with energies $\gtrsim 2\Delta$. It can be shown that it is the term H''_p which restores gauge invariance¹²,

$$[H_{MF} + H''_p, \hat{N}] = 0 \quad (1.4.60)$$

We now diagonalize $H_{MF} + H''_p$ in the quasiparticle RPA (QRPA),

$$[H_{MF} + H''_p, \Gamma_n^\dagger] = \hbar\omega_n \Gamma_n^\dagger, \quad [\Gamma_n, \Gamma_{n'}^\dagger] = \delta(n, n'), \quad (1.4.61)$$

where

$$\Gamma_n^\dagger = \sum_\nu (a_{n\nu} \Gamma_\nu^\dagger + b_{n\nu} \Gamma_\nu), \quad \Gamma_\nu^\dagger = \alpha_\nu^\dagger \alpha_{\bar{\nu}}^\dagger, \quad (1.4.62)$$

is the creation operator of the n th vibrational mode. In the case of the $n = 1$, lowest energy root, it can be written as

$$|1''\rangle = \Gamma_1^{\prime\dagger} |0''\rangle = \frac{\Lambda_1''}{2\Delta} (\hat{N} - N_0) |0''\rangle, \quad (1.4.63)$$

where \hat{N} is the particle number operator written in terms of Γ_ν^\dagger and Γ_ν , and Λ_1'' is the strength of the quasiparticle-mode coupling. The prefactor is the zero point fluctuation (ZPF) of the mode, that is (see Eq. (1.1.11) in the case of surface vibration),

$$\sqrt{\frac{\hbar\omega_1''}{2C_1'}} = \sqrt{\frac{\hbar^2}{2D_1''\hbar\omega_1''}}. \quad (1.4.64)$$

Because the lowest frequency is $\omega_1'' = 0$, the associated ZPF diverge ($\Lambda_1'' \sim (\hbar\omega_1'')^{-1/2}$). It can be seen that this is because $C_1'' \rightarrow 0$, while D_1'' remains finite. In fact,

$$\frac{D_1''}{\hbar^2} = \frac{2\Delta^2}{\Lambda_1''^2 \hbar\omega_1''} = 4 \sum_{\nu>0} \frac{U_\nu^2 V_\nu^2}{2E_\nu}. \quad (1.4.65)$$

A rigid rotation in gauge space can be generated by a series of infinitesimal operations of type $\mathcal{G}(\delta\phi) = e^{i(\hat{N}-N_0)\delta\phi}$, the one phonon state $|1''\rangle = \Gamma_1^{\prime\dagger} |0''\rangle$, is obtained from rotations in gauge space of divergent amplitude. That is, fluctuations of ϕ

¹²For details see Brink, D. and Broglia (2005).

over the whole $0 - 2\pi$ range. By proper inclusion of these fluctuations one can restore gauge invariance violated by $|BCS\rangle_{\mathcal{K}'}$. The resulting states

$$|N_0\rangle \sim \int_0^{2\pi} d\phi e^{-iN_0\phi} |BCS(\phi)\rangle_{\mathcal{K}'} \left(\sum_{\nu>0} c'_\nu P_\nu^\dagger \right)^{N/2} |0\rangle_F \quad (1.4.66)$$

have a definite number of particles and constitute the members of a pairing rotational band. Making use of a simplified model (single j -shell) it can be shown that the energies of those states can be written as,

$$E_N = \lambda(N - N_0) + \frac{G}{4} (N - N_0)^2, \quad (1.4.67)$$

where

$$\frac{G}{4} = \frac{\hbar^2}{2D'_1}. \quad (1.4.68)$$

An example of pairing rotational bands is provided by the ground state of the single open closed shell superfluid isotopes of the $^{50}_{50}\text{Sn}_N$ -isotopes (Fig. 1.4.5), $N_0 = 68$ having been used in the solution of the BCS number equation (1.4.37). Theory provides an overall account of the experimental findings. Making use of the BCS pair transfer amplitudes,

$$\langle BCS | P_\nu^\dagger | BCS \rangle = U_\nu V_\nu \quad (1.4.69)$$

in combination with a reaction software and of global optical parameters, one can account for the absolute value of the pair transfer differential cross section, within experimental errors (see Sect. 3.1 and Chapters 4 and 7). The fact that projecting out the different Sn-isotopes from the intrinsic BCS state describing ^{118}Sn one obtains a quantitative description of observations carried out with the help of the specific probe of pairing correlations (Cooper pair transfer), testifies to the fact that pairing rotational bands can be considered elementary modes of nuclear excitation, emergent properties of spontaneous symmetry braking of gauge invariance.

Furthermore, the fact that these results follow the use of QRPA¹³ in the calculation of the ZPF of the collective solutions of the pairing Hamiltonian indicates the importance of conserving approximations to describe quantum many-body problems in general, and the finite size quantum many-body problem (FSQMB), of which the nuclear case represents a paradigmatic example, in particular.

Aside from low-lying collective states, that is rotations and low-energy vibrations, nuclei also display high-lying collective modes known as giant resonances.

¹³Using the Tamm-Dancoff approximation, i.e. setting $Y \equiv 0$ (and thus $\sum X^2 = 1$) in the QRPA approximation does not lead to particle number conservation, in keeping with the fact that the amplitudes Y are closely connected with ZPF.

1.5 Giant dipole resonance

If one shines a beam of photons on a nucleus it is observed that the system absorbs energy resonantly essentially at a single frequency, of the order of¹⁴ $\nu = 5 \times 10^{21}$ Hz, corresponding to an energy of $h\nu \approx 20$ MeV.

It is not difficult to understand how γ -rays excite a nuclear dipole vibration. A photon carries with it an oscillating electric field. Although the wavelength of a 20 MeV γ -ray is smaller than that of other forms of electromagnetic radiation such as visible light, it is still large ($\lambda \approx 63$ fm) compared to the dimensions of e.g. ^{40}Ca ($R_0 \approx 4.1$ fm). As a result the photon electric field is nearly uniform across the nucleus at any time. The field exerts a force on the positively charged protons. Consequently, it can set the center of mass into an antenna like, dipole oscillation (Thompson scattering), in which case no photon is absorbed. Another possibility is that it leads to an internal excitation of the system. In this case because the center of mass of the system does not move, the neutrons have to oscillate against the protons, again in an antenna-like motion. The restoring force of the vibration, known as the giant dipole resonance (GDR), is provided by the attractive force between protons and neutrons.

The connotation of giant is in keeping with the fact that it essentially carries the full photo absorption cross section (energy weighted sum rule, see below), and resonance because it displays a Lorentzian-like shape with a full width at half maximum of few MeV ($\lesssim 5$ MeV), considerably smaller than the energy centroid¹⁵ $\hbar\omega_{GDR} \approx 80/A^{1/3}$ MeV. Microscopically, the GDR can be viewed as a correlated particle-hole excitation, that is a state made out of a linear contribution of proton and neutron particle-hole excitations with essentially $\Delta N = 1$, as well as small $\Delta N = 3, 5, \dots$ components (Fig. 1.1.3). Because the difference in energy between major shells is $\hbar\omega_0 \approx 41A^{1/3}$ MeV, one expects that about half of the contribution to the energy arises from the neutron-proton interaction. More precisely, from the so called (repulsive) symmetry potential V_1 (see Eq. (1.1.4)), which measures the energy price the system has to pay to separate protons from neutrons. Theoretical estimates lead to

$$(\hbar\omega_{GDR})^2 = (\hbar\omega_0)^2 + \frac{3\hbar^2 V_1}{m\langle r^2 \rangle} = \frac{1}{A^{2/3}} [(41)^2 + (60)^2] \text{ MeV}^2, \quad (1.5.1)$$

resulting in

¹⁴Making use of $h = 4.1357 \times 10^{-15}$ eVs one obtains for $h\nu = 1$ eV the frequency $\nu = 2.42 \times 10^{14}$ Hz and thus $\nu = 4.8 \times 10^{21}$ Hz for $h\nu = 20$ MeV. The wavelength of a photon of energy E is $\lambda = hc/E \approx 2\pi \times 200$ MeV fm/ E , which for $E = 20$ MeV leads to $\lambda \approx 63$ fm.

¹⁵Within this context we refer to the discussion concerning the renormalization of collective modes carried out in the text after equation (1.2.8), in particular regarding the cancellation between self-energy and vertex corrections (see Fig. 1.2.5 and footnote 7). This is a basic result of NFT –as discussed in later chapters– being connected with sum rule arguments in general, and particle conservation in particular. Argument which has been extended to the case of finite temperature as well as to include relativistic effects Ward (1950); Nambu (1960); Bortignon and Broglia (1981); Bertsch et al. (1983); Bortignon, P. F. et al. (1998); Litvinova and Wibowo (2018); Wibowo and Litvinova (2019).

$$\hbar\omega_{GDR} \approx \frac{73}{A^{1/3}} \approx \frac{87}{R} \text{ MeV}, \quad (1.5.2)$$

where $R = 1.2A^{1/3}$ is the numerical value of the nuclear radius measured in fm. The above quantity is to be compared with the empirical value $\hbar\omega_{GDR} \approx (80/A^{1/3})$ MeV $\approx (95/R)$ MeV. It is of notice that the elastic vibrational frequency of a spherical solid made out of particles of mass m can be written as $\omega_{el}^2 \sim \mu/(m\rho R^2) \sim v_t^2/R^2$, where R is the radius, ρ the density and v_t the transverse sound velocity proportional to the Lamé shear modulus of elasticity μ . In other words, giant resonance in general, and the GDR in particular, are embodiments of the elastic response of the nucleus to an impulsive external fields, like that provided by a photon. The nuclear rigidity to sudden solicitations is provided by the shell structure, quantitatively measured by the energy separation between major shells.

1.6 Giant pairing vibrations

Due to spatial quantization, in particular to the existence of major shells of pair degeneracy $\Omega (\equiv (2j+1)/2)$, and separated by an energy $\hbar\omega_0 \approx 41/a^{1/3}$ MeV, the Cooper pair model can be extended to encompass pair addition and pair subtraction modes across major shells¹⁶ Assuming both ϵ_k and ϵ_i appearing in Fig. 1.3.1 are both at an energy $\hbar\omega_0$ away from the Fermi energy, one obtains the dispersion relation

$$-\frac{1}{G} = \frac{\Omega}{W - 2\hbar\omega_0} - \frac{\Omega}{W + 2\hbar\omega_0}, \quad (1.6.1)$$

leading to

$$(2\hbar\omega_0)^2 - W^2 = 4\hbar\omega_0 G, \quad (1.6.2)$$

and implying a high lying pair addition mode of energy

$$W = 2\hbar\omega_0 \left(1 - \frac{G\Omega}{\hbar\omega_0}\right)^{1/2}. \quad (1.6.3)$$

The forwards (backwards) going RPA amplitudes are, in the present case

$$X = \frac{\Lambda_0^2 \Omega^{1/2}}{2\hbar\omega_0 - W} \quad \text{and} \quad Y = \frac{\Lambda_0^2 \Omega^{1/2}}{2\hbar\omega_0 + W} \quad (1.6.4)$$

normalized according to the relation

$$1 = X^2 - Y^2 = \Lambda_0^2 \Omega \frac{8\hbar\omega_0 W}{((2\hbar\omega_0)^2 - W^2)^2}, \quad (1.6.5)$$

¹⁶Broglia and Bes (1977).

where Λ_0 stands for the particle-pair vibration coupling vertex. Making use of (1.6.2) one obtains

$$\left(\frac{\Lambda_0}{G}\right)^2 = \Omega \left(1 - \frac{G\Omega}{\hbar\omega_0}\right)^{-1/2} \quad (1.6.6)$$

quantity corresponding, within the framework of the simplified model used, to the two-nucleon transfer cross section. Summing up, the monopole giant pairing vibration has an energy close to $2\hbar\omega_0$, and is expected to be populated in two-particle transfer processes with a cross section of the order of that associated with the low-lying pair addition mode, being this one of the order of Ω . Simple estimates of (1.6.3) and (1.6.6) can be obtained making use of $\Omega \approx \frac{2}{3}A^{2/3}$ and $G \approx 17/A$ MeV lead to

$$W = 0.85 \times 2\hbar\omega_0, \quad \left(\frac{\Lambda_0}{G}\right)^2 \approx 1.2\Omega. \quad (1.6.7)$$

Experimental evidence of GPV in light nuclei have been reported¹⁷

1.7 Sum rules

There are important operator identities which restrict the possible matrix elements in a physical system. Let us calculate the double commutator of the Hamiltonian describing the system and a single-particle operator F . That is

$$[\hat{F}, [H, \hat{F}]] = (2\hat{F}H\hat{F} - \hat{F}^2H - H\hat{F}^2) \quad (1.7.1)$$

Let us assume that $\hat{F} = \sum_k F(\mathbf{r}_k)$ and $H = T + v(\mathbf{r}, \mathbf{r}')$, where $v(\mathbf{r}, \mathbf{r}') = -\kappa_1 \hat{F}(\mathbf{r})\hat{F}(\mathbf{r}')$. Thus

$$[\hat{F}, [H, \hat{F}]] = \sum_k \frac{\hbar^2}{m} (\nabla_k F(\mathbf{r}_k))^2 \quad (1.7.2)$$

Let us take the average value on the correlated ground state

$$S(F) = \sum_{\alpha'} |\langle \alpha' | F | \tilde{0} \rangle|^2 (E_{\alpha'} - E_0) = \frac{\hbar^2}{2m} \int d\mathbf{r} |\nabla F|^2 \rho(\mathbf{r}), \quad (1.7.3)$$

where we have used $H|\alpha\rangle = E_\alpha$ and $H|\tilde{0}\rangle = E_0|\tilde{0}\rangle$, and the sum $\sum_{\alpha'}$ is over the complete set of eigenstates of the system. The above result describes the reaction of a system at equilibrium to which one applies an impulsive field, which gives the particles a momentum ∇F . On the average, the particles started at rest so their average energy after the sudden impulse is $\hbar^2|\nabla F|^2/2m$, a result which is model

¹⁷Cappuzzello et al. (2015), Bortignon and Broglia (2016). See also Laskin et al. (2016); Id Betan et al. (2002); Dussel et al. (2009); Mouginot et al. (2011); Khan et al. (2004).

independent not depending on the interaction among the nucleons, the energy being absorbed from the (instantaneous) external field before the system is disturbed from equilibrium. The result (1.7.3) is known as the energy weighted sum rule (EWSR).

An important application of (1.7.3) implies a situation where F has a constant gradient. Inserting $\mathbf{F} = z\mathbf{z}$ in (1.7.3), the integral simplifies because $\nabla F = 1$, and the integral leads just to the number of particles,

$$\sum_{\alpha} |\langle \alpha | F | \tilde{0} \rangle|^2 (E_{\alpha} - E_0) = \frac{\hbar^2 N}{2m} \quad (1.7.4)$$

The electric field of a photon is of this form in the dipole approximation, which is valid when the size of the system is small compared to the wavelength of the photon, the single-particle field being

$$F(\mathbf{r}_k) = e \left[\frac{N - Z}{A} - t_z(k) \right] r_k Y_{1\mu}(\hat{r}_k), \quad (1.7.5)$$

with $t_z = -1/2$ for protons and $+1/2$ for neutrons. For the dipole operator referred to the nuclear center of mass one obtains

$$\sum_{\alpha'} |\langle \alpha' | F | \tilde{0} \rangle|^2 (E_{\alpha'} - E_0) = \frac{9}{4\pi} \frac{\hbar^2 e^2}{2m} \frac{NZ}{A}. \quad (1.7.6)$$

The above relation is known as the Thomas-Reiche-Kuhn (TRK) sum rule, and is equal to the maximum energy a system can absorb from the dipole field. The RPA solution respect the EWSR, while the Tamm-Dancoff approximation (TDA), resulting by setting $Y_{ki}^{\alpha} = 0$ and normalizing the X-components ($\sum_{ki} X_{ki}^{\alpha 2} = 1$) fulfill the non-energy weighted sum rule. A fact which testifies to the important role ZPF play in nuclei.

1.8 Ground state correlations

The zero point fluctuations associated with collective vibrations of protons and of neutrons affect the nuclear mean field static properties. In particular concerning the nuclear density distribution¹⁸ ρ and radius R . According to the indeterminacy relations,

$$\Delta \alpha_{\lambda\mu}^{(n)} \Delta \pi_{\lambda\mu}^{(n)} \geq \frac{\hbar}{2}. \quad (1.8.1)$$

Making use of the virial theorem ($\Delta \pi_{\lambda\mu}^2 / D_{\lambda} = C_{\lambda} \alpha_{\lambda\mu}^2$) one can write

$$\Delta \alpha_{\lambda\mu}^{(n)} \geq \frac{\hbar \omega_{\lambda}}{2C_{\lambda}}. \quad (1.8.2)$$

¹⁸Gogny (1978); Esbensen and Bertsch (1983); Reinhard and Drechsel (1979); Khodel et al. (1982); Barranco and Broglia (1987) see also Brown and Jacob (1963); Anderson and Thouless (1962) (it is likely a coincidence in connection with this inaugural issue of Phys. Lett. that short of hundred pages after, one finds the paper of B. D. Josephson, Possible new effects in superconducting tunneling, Phys. Lett. **1**, 251 (1962)).

Let us compare this relation with the expectation value of $\Delta\alpha_{\lambda\mu}^2$ in the ground state of the collective Hamiltonian (1.1.9) described by the wavefunction $\Psi_0(\alpha_{\lambda\mu}^{(n)}) = \left(\frac{D_\lambda^{(n)}\omega_\lambda^{(n)}}{\hbar\pi}\right)^{1/4} \exp\left(-\frac{D_\lambda^{(n)}\omega_\lambda^{(n)}}{2\pi}\alpha_{\lambda\mu}^2\right)$. The result coincides with the lowest limit of (1.8.1) in keeping with the fact that $|\Psi_0|^2$ is mathematically a Poisson distribution¹⁹ The fact that $\Delta\alpha_{\lambda\mu}^2(n) = \hbar\omega_\lambda(n)/2C_\lambda(n)$ implies that the mean square radius will be modified from its mean field value R_0 (Eq. (1.8.1)) and thus also the nuclear density distribution. The value of $\hbar\omega_\lambda(n)/2C_\lambda(n)$ can be determined by calculating the collective mode $|n_\lambda(n)=1\rangle = \Gamma_{\lambda\mu}^\dagger(n)|\tilde{0}\rangle$ in RPA. As seen from the caption to Fig. 1.2.3 the zero point fluctuation of the mode enter the definition of the X, Y -amplitudes of the mode. Let us start by calculating the effect of the zero point fluctuations on the nuclear density distribution. The corresponding operator can be written as

$$\hat{\rho}(\mathbf{r}) = a^\dagger(\mathbf{r})a(\mathbf{r}), \quad (1.8.3)$$

where $a^\dagger(\mathbf{r})$ is the creation operator of a nucleon at point \mathbf{r} . It can be expressed in terms of the phase space creation operators $a_v^\dagger(v \equiv n, l, j, m)$ as

$$a^\dagger(\mathbf{r}) = \sum_v \varphi_v^*(\mathbf{r})a_v^\dagger, \quad (1.8.4)$$

where $\varphi_v(\mathbf{r})$ are the single-particle wavefunctions. Thus

$$\hat{\rho}(\mathbf{r}) = \sum_{vv'} \varphi_v^*(\mathbf{r})\varphi_{v'}(\mathbf{r})a_v^\dagger a_{v'}. \quad (1.8.5)$$

The matrix element in the HF ground state is (Fig. 1.2.2)

$$\rho_0(\mathbf{r}) =_F \langle 0|\hat{\rho}(\mathbf{r})|0\rangle_F = \sum_{i,(\epsilon_i \leq \epsilon_F)} |\varphi_i(\mathbf{r})|^2. \quad (1.8.6)$$

To lowest order of perturbation theory in the particle-vibration coupling vertex, the NFT diagrams associated with the change of ρ_0 due to ZPF are shown in Fig. 1.8.1.

¹⁹The same result is found for Ψ_n describing a state with n -quanta, and the basis that solutions with $n \gg 1$ behaves as “quasiclassical” or “coherent” states of the harmonic oscillator (Glauber (2007)) in keeping with the fact that the contribution of the zero point energy is negligible in such case ($(n + 1/2)\hbar\omega \approx n\hbar\omega$) and that the many quanta wavepacket always attain the lower limit of (1.8.1) (Basdevant and Dalibard (2005) pp. 153,465) (discussions with Pier Francesco Bortignon in March 2018 concerning coherent states are gratefully acknowledged). Schrödinger was the first to find this result which he used in a paper (Schrödinger, E. (1926)) to suggest that waves (material waves) described by his wave function are the only reality, particles being only derivative things. In support of his view he considered a superposition of linear harmonic oscillator wavefunctions and showed that the wave group holds permanently together in the course of time. And he adds that the same will be true for the electron as it moves in high orbits of the hydrogen atom, hoping that wave mechanics would turn out to be a branch of classical physics (Pais (1986)). It was Born who first provided the correct interpretation of Schrödinger’s wavefunction (modulus square) in his paper “Quantum mechanical collision phenomena” (Born (1926)). In it it is stated that the result of solving with wave mechanics the process of elastic scattering of a beam of particles by a static potential is not what the state after the collision is, but how probable is a given effect of the collision.

Graphs (a) and (b) and (c) and (d) describe the changes in the density operator and in the single-particle potential respectively. This can be seen from the insets (I) and (II). The dashed horizontal line starting with a cross and ending at a hatched circle represents the renormalized density operator. This phenomenon is similar to that encountered in connection with vertex renormalization in Fig. 1.2.5, that is the renormalization of the particle-vibration coupling (insets (I) and (I')). Concerning potential renormalization, the bold face arrowed line shown in inset (II) of Fig. 1.8.1 represents the motion of a renormalized nucleon due to the self-energy process induced by the coupling to vibrational modes. A phenomenon which can be described at profit through an effective mass, the so called ω -mass m_ω , in which case particle motion is described by the Hamiltonian²⁰ $(\hbar^2/2m_\omega)\nabla^2 + (\frac{m}{m_\omega})U(r)$. The ω -mass can be written as $m_\omega = (1 + \lambda)m$, where λ is the so called mass enhancement factor $\lambda = N(0)\Lambda$, where $N(0)$ is the density of levels at the Fermi energy, and Λ the PVC vertex strength, typical values being $\lambda = 0.4$.

The fact that in calculating $\delta\rho$, that is, the correction to the nuclear density distribution (renormalization of the density operator), one finds to the same order of perturbation a correction to the potential, is in keeping with the self consistency existing between the two quantities (Eq. (1.2.6)). Now, what changes is not only the single-particle energy, but also the single-particle content as well as the radial dependence of the wavefunctions of the states measured by $Z_\omega = m/m_\omega$. It is of notice that the effective mass approximation, although being quite useful, cannot take care of the energy dependence of the renormalization process which leads, in the case of single-particle motion to renormalized energies, spectroscopic amplitudes and wavefunctions. The analytic expressions associated with diagrams (a) and (c) of Fig. 1.8.1 are

$$\delta\rho(r)_{(a)} = \frac{(2\lambda + 1)}{4\pi} \sum_{\nu_1\nu_2n} [Y_n(\nu_1\nu_2; \lambda)]^2 R_{\nu_1}(r)R_{\nu_2}(r), \quad (1.8.7)$$

and

$$\begin{aligned} \delta\rho(r)_{(b)} &= (2\lambda + 1)\Lambda_n(\lambda) \sum_{\nu_1\nu_2\nu_3} \frac{M(\nu_1, \nu_3; \lambda)}{\epsilon_{\nu_1} - \epsilon_{\nu_2}} (2j_1 + 1)^{-1/2} \\ &\times Y_n(\nu_3\nu_2; \lambda) \times R_{\nu_1}(r)R_{\nu_2}(r), \end{aligned} \quad (1.8.8)$$

where M is the matrix element of $\frac{R_0}{\kappa} \frac{\partial U}{\partial r} Y_{\lambda\mu}(\hat{r})$ and $n = 1, 2 \dots$ the first, second, etc vibrational modes as a function of increasing energy, and Λ_n is the strength of the particle-vibration coupling associated with the n -mode of multipolarity λ . While $\delta\rho_{(a)}$ can be written in terms of the RPA Y -amplitudes which are directly associated with the zero point fluctuations of harmonic motion (Fig. 1.2.3 (c)), $\delta\rho_{(c)}$ contains a scattering vertex not found in RPA – that is going beyond the harmonic approximation – and essential to describe renormalization processes of the different degrees of freedom, namely single-particle (energy, single-particle

²⁰Brink, D. and Broglia (2005).

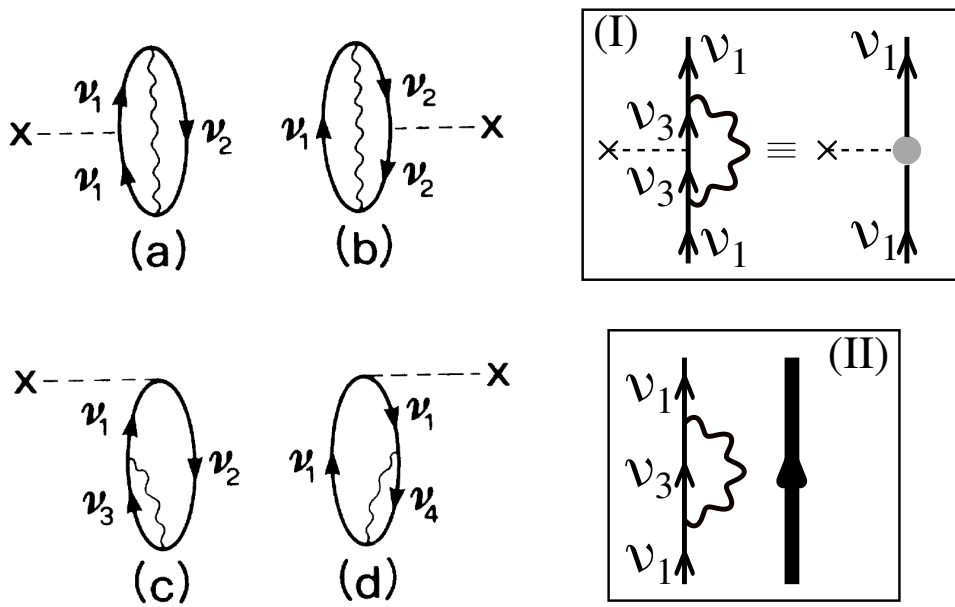


Figure 1.8.1: Lowest-order corrections in the particle-vibration coupling vertex of the nuclear density due to the presence of zero-point fluctuations associated with density vibrations. An arrowed line pointing upwards denotes a particle, while one pointing downward a hole. A wavy line represents a surface phonon. The density operator is described through a dotted horizontal line starting with a cross. Graphs (a) and (b) are typical examples of density contributions to $\delta\rho$ (see inset (I)); the dashed horizontal line starting with a cross and ending at a hatched circle in the diagram to the right, represents the renormalized density operator, resulting from the processes displayed to the left; (c) and (d) are of potential contributions (see inset (II)); the bold face arrowed line represents the renormalized single-particle state due to the coupling to the vibrations leading to the self energy process shown to the left. (After Barranco and Broglia (1987)).

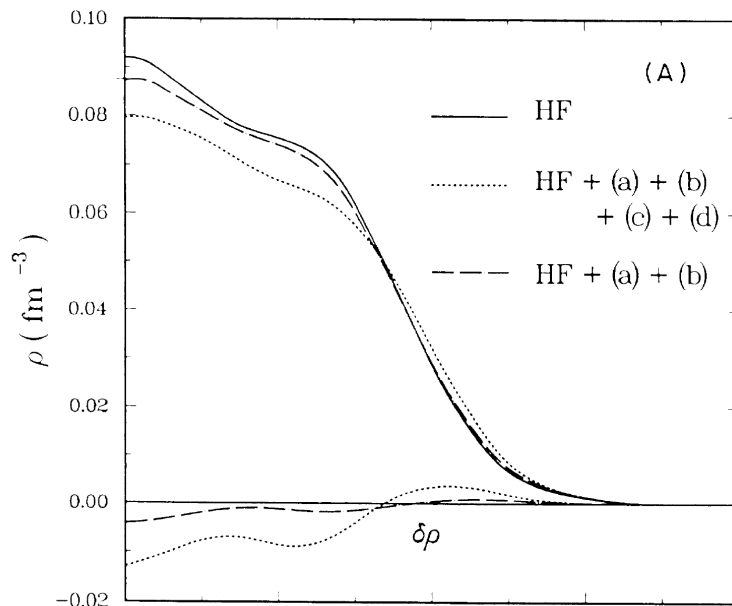


Figure 1.8.2: Modification in the charge density of ${}^{40}\text{Ca}$ induced by the zero-point fluctuations associated with vibrations of the surface modes. The results labeled HF, HF+(a)+(b), and HF+(a)+(b)+(c)+(d) are the Hartree-Fock density, and that resulting from adding to it the corrections $\delta\rho$ associated with the processes (a)+(b) and (a)+(b)+(c)+(d) displayed in Fig. 1.8.1, respectively. In the lower part of the figure the quantities $\delta\rho$ are displayed. (After Barranco and Broglia (1987)).

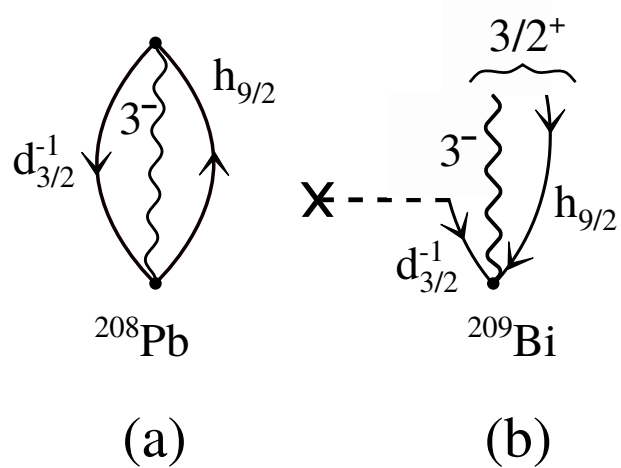


Figure 1.8.3: (a) Example of zero point fluctuation of the ground state of the double-magic nucleus $^{208}_{82}\text{Pb}_{126}$ associated with the low-lying octupole vibration of this system, observed at an energy of 2.615 MeV and displaying a collective electromagnetic decay to the ground state. The proton particle-hole component $(h_{9/2}, d_{3/2}^{-1})_{3^-}$ displayed carries a large amplitude in the octupole vibration wavefunction. (b) Diagram representing the transfer of one proton to ^{208}Pb , which fills the $d_{3/2}^{-1}$ hole state leading to a $3/2^+$ in $^{209}_{83}\text{Bi}_{126}$, member of the septuplet of states $|(3^- \otimes h_{9/2} J^\pi)\rangle$ with $J^\pi = 3/2^+, 5/2^+, \dots, 15/2^+$. The horizontal dashed line starting with a cross stands for the stripping process $(^3\text{He}, d)$.

content and radial dependence of the wavefunction) and collective motion, as well as interactions. In particular the pairing interaction.

In Fig. 1.8.2 we show the results of calculations of $\delta\rho$ carried out for the closed shell nucleus ^{40}Ca . The vibrations were calculated by diagonalizing separable interactions of multipolarity λ in the RPA. All the roots of multipolarity and parity $\lambda^\pi = 2^+, 3^-, 4^+$ and 5^- which exhaust the EWSR were included in the calculations. Both isoscalar and isovector degrees of freedom were included, and low-lying and giant resonances.

From the point of view of the single-particle motion the vibrations associated with low-lying modes display very low frequency ($\hbar\omega_\lambda/\epsilon_F \approx 0.1$) and lead to an ensemble of deformed shapes. Nucleons can thus reach to distances from the nuclear center which are considerably larger than the radius R of the static spherical potential. Because the frequency of the giant resonances are of similar magnitude to those corresponding to the single-particle motion, the associated surface deformations average out.

Said it differently, the low-lying vibrational modes account for most of the contributions to the changes in the density distribution²¹. Making use of the corresponding $(\delta\rho)_{low-lying}$, the mean square radius of ^{40}Ca was calculated²², leading to $\langle r^2 \rangle = (3/5)R_0^2 = 10.11 \text{ fm}^2$ ($R_0 = 1.2A^{1/3} \text{ fm} = 4.1 \text{ fm}$), in overall agreement with the experimental findings. Similar calculations to the ones discussed above, but in this case taking into account only the contributions of the low-lying octupole vibration²³ indicate that nucleons are to be found a reasonable part of the time in higher shells than those assigned to them by the shell model. The average number of “excited” particles being ≈ 2.4 . If these are present, pickup reactions such as (p, d) and (d, t) will show them. From the nature of the correlations, the pickup of such a particle will leave a hole and a vibration. That is, the final nucleus will be in one of the states which can be related by coupling the hole and the vibration. Conversely, because of the presence of hole states in the closed shell nucleus, one can transfer a nucleon to states below the Fermi energy in, for example, (d, p) or $(^3\text{He}, d)$ one-neutron or one-proton stripping reactions respectively, leaving the final nucleus with one-nucleon above closed shell coupled to the vibrations.

Systematic studies of such multiplets have been carried out throughout the mass table. In particular around the closed shell nucleus $^{208}_{82}\text{Pb}_{126}$ (Fig. 1.8.3). Within this context it is not only quite natural but also necessary, to deal with structure and reactions on equal footing. This is one of the main goals of the present monograph, as will become clear already from the next chapter.

²¹Another example of the recurrent central role played by low-frequency modes in determining the properties and behavior of systems at all levels of organization, from the atomic nucleus to the Casimir effect in QED, to phonons in superconductors as well as to the folding of proteins and brain activity ($\nu < 0.1 \text{ Hz}$) (Mitra et al. (2018)).

²²Barranco and Broglia (1987).

²³Brown and Jacob (1963).

Bibliography Ch 1

- P. Anderson and D. Thouless. Diffuseness of the nuclear surface. *Physics Letters*, 1(5):155 – 157, 1962.
- J. Bardeen, L. N. Cooper, and J. R. Schrieffer. Microscopic theory of superconductivity. *Physical Review*, 106:162, 1957a.
- J. Bardeen, L. N. Cooper, and J. R. Schrieffer. Theory of superconductivity. *Physical Review*, 108:1175, 1957b.
- F. Barranco and R. A. Broglia. Effect of surface fluctuations on the nuclear density. *Phys. Rev. Lett.*, 59:2724, 1987.
- F. Barranco, R. A. Broglia, G. Colò, G. Gori, E. Vigezzi, and P. F. Bortignon. Many-body effects in nuclear structure. *European Physical Journal A*, 21:57, 2004.
- J. L. Basdevant and J. Dalibard. *Quantum Mechanics*. Springer, Berlin, 2005.
- G. F. Bertsch, P. F. Bortignon, and R. A. Broglia. Damping of nuclear excitations. *Rev. Mod. Phys.*, 55:287, 1983.
- A. Bohr and B. R. Mottelson. *Nuclear Structure, Vol.I*. Benjamin, New York, 1969.
- A. Bohr, B. R. Mottelson, and D. Pines. Possible analogy between the excitation spectra of nuclei and those of the superconducting metallic state. *Physical Review*, 110:936, 1958.
- N. Bohr and J. A. Wheeler. The mechanism of nuclear fission. *Phys. Rev.*, 56:426, 1939.
- Bohr, A. and B. R. Mottelson. *Nuclear Structure, Vol.II*. Benjamin, New York, 1975.
- M. Born. Zur Quantenmechanik der Stoßvorgänge. *Zeitschr.f. Phys.*, 37:863, 1926.
- P. Bortignon and R. Broglia. Elastic response of the atomic nucleus in gauge space: Giant pairing vibrations. *The European Physical Journal A*, 52(9):280, 2016.
- P. F. Bortignon and R. A. Broglia. Role of the nuclear surface in an unified description of the damping of single-particle states and giant resonances. *Nucl. Phys. A*, 371:405, 1981.
- Bortignon, P. F., A. Bracco, and R. A. Broglia. *Giant Resonances*. Harwood Academic Publishers, Amsterdam, 1998.
- Brink, D. and R. A. Broglia. *Nuclear Superfluidity*. Cambridge University Press, Cambridge, 2005.

- R. A. Broglia and D. R. Bes. High-lying pairing resonances. *Physics Letters B*, 69:129, 1977.
- R. A. Broglia and A. Winther. *Heavy Ion Reactions*. Westview Press, Boulder, CO., 2004.
- G. Brown and G. Jacob. Zero-point vibrations and the nuclear surface. *Nuclear Physics*, 42:177 – 182, 1963.
- F. Cappuzzello, D. Carbone, M. Cavallaro, M. Bondí, C. Agodi, F. Azaiez, A. Bonaccorso, A. Cunsolo, L. Fortunato, A. Foti, S. Franchoo, E. Khan, R. Linares, J. Lubian, J. A. Scarpaci, and A. Vitturi. Signatures of the Giant Pairing Vibration in the ^{14}C and ^{15}C atomic nuclei. *Nature Communications*, 6:6743, 2015.
- P. A. M. Dirac. *The principles of quantum mechanics*. Oxford University Press, London, 1930.
- G. G. Dussel, R. I. Betan, R. J. Liotta, and T. Vertse. Collective excitations in the continuum. *Phys. Rev. C*, 80:064311, Dec 2009. doi: 10.1103/PhysRevC.80.064311. URL <https://link.aps.org/doi/10.1103/PhysRevC.80.064311>.
- W. Elsasser. Sur le principe de Pauli dans les noyaux. *J. Phys. Radium*, 4:549, 1933.
- H. Esbensen and G. F. Bertsch. Nuclear surface fluctuations: Charge density. *Phys. Rev. C*, 28:355, 1983.
- Flynn, E. R., G. J. Igo, and R. A. Broglia. Three-phonon monopole and quadrupole pairing vibrational states in ^{206}Pb . *Phys. Lett. B*, 41:397, 1972.
- R. J. Glauber. *Quantum theory of optical coherence*. Wiley, Weinheim, 2007.
- D. Gogny. Lecture notes in physics, vol. 108. In H. Arenhövd and D. Drechsel, editors, *Nuclear Physics with Electromagnetic Interactions*, p.88, page 55, Heidelberg, 1978. Springer Verlag.
- O. Haxel, J. H. D. Jensen, and H. E. Suess. On the “Magic Numbers” in nuclear structure. *Phys. Rev.*, 75:1766, 1949.
- R. Id Betan, R. J. Liotta, N. Sandulescu, and T. Vertse. Two-particle resonant states in a many-body mean field. *Phys. Rev. Lett.*, 89:042501, Jul 2002. doi: 10.1103/PhysRevLett.89.042501. URL <https://link.aps.org/doi/10.1103/PhysRevLett.89.042501>.
- E. Khan, N. Sandulescu, N. V. Giai, and M. Grasso. Two-neutron transfer in nuclei close to the drip line. *Physical Review C*, 69:014314, 2004.

- V. A. Khodel, A. P. Platonov, and E. E. Saperstein. On the 40ca-48ca isotope shift. *Journal of Physics G: Nuclear Physics*, 8(7):967–973, jul 1982.
- M. Laskin, R. F. Casten, A. O. Macchiavelli, R. M. Clark, and D. Bucurescu. Population of the giant pairing vibration. *Phys. Rev. C*, 93:034321, 2016.
- E. Litvinova and H. Wibowo. Finite-temperature relativistic nuclear field theory: An application to the dipole response. *Phys. Rev. Lett.*, 121: 082501, Aug 2018. doi: 10.1103/PhysRevLett.121.082501. URL <https://link.aps.org/doi/10.1103/PhysRevLett.121.082501>.
- M. Mayer and J. Jensen. *Elementary Theory of Nuclear Structure*. Wiley, New York, NY, 1955.
- M. G. Mayer. On closed shells in nuclei. *Phys. Rev.*, 74:235, 1948.
- M. G. Mayer. On closed shells in nuclei. ii. *Phys. Rev.*, 75:1969, 1949.
- M. G. Mayer. The shell model. *Nobel Lecture*, 1963.
- M. G. Mayer and E. Teller. On the origin of elements. *Phys. Rev.*, 76:1226, 1949.
- L. Meitner and O. R. Frisch. Products of the fission of the uranium nucleus. *Nature*, 143:239, 1939.
- A. Mitra, A. Kraft, P. Wright, B. Acland, A. Z. Snyder, Z. Rosenthal, L. Czerniewski, A. Bauer, L. Snyder, J. Culver, et al. Spontaneous infra-slow brain activity has unique spatiotemporal dynamics and laminar structure. *Neuron*, 98: 297, 2018.
- B. Mouginot, E. Khan, R. Neveling, F. Azaiez, E. Z. Buthelezi, S. V. Förtsch, S. Franschoo, H. Fujita, J. Mabiala, J. P. Mira, P. Papka, A. Ramus, J. A. Scarpaci, F. D. Smit, I. Stefan, J. A. Swartz, and I. Usman. Search for the giant pairing vibration through (p,t) reactions around 50 and 60 MeV. *Phys. Rev. C*, 83: 037302, 2011.
- Y. Nambu. Quasi-particles and gauge invariance in the theory of superconductivity. *Physical Review*, 117:648, 1960.
- O. Nathan and S. G. Nilsson. Collective nuclear motion and the unified model. In K. Siegbahn, editor, *Alpha- Beta- and Gamma-Ray Spectroscopy, Vol 1*, page 601, Amsterdam, 1965. North Holland Publishing Company.
- S. G. Nilsson. Binding states of individual nucleons in strongly deformed nuclei. *Mat. Fys. Medd. Dan. Vid. Selsk.*, 29, 1955.
- P. J. Nolan and P. J. Twin. Superdeformed shapes at high angular momentum. *Annual Review of Nuclear and Particle Science*, 38:533, 1988.

- A. Pais. *Inward bound*. Oxford University Press, Oxford, 1986.
- Potel, G., A. Idini, F. Barranco, E. Vigezzi, and R. A. Broglia. Quantitative study of coherent pairing modes with two-neutron transfer: Sn isotopes. *Phys. Rev. C*, 87:054321, 2013.
- P. G. Reinhard and D. Drechsel. Ground state correlations and the nuclear charge distribution. *Zeitschrift für Physik A Atoms and Nuclei*, 290(1):85–91, Mar 1979.
- D. J. Rowe. *Nuclear Collective Motion. Models and Theory*. Methuen & Co., London, 1970.
- Schiffer, J. P., C. R. Hoffman, B. P. Kay, J. A. Clark, C. M. Deibel, S. J. Freeman, A. M. Howard, A. J. Mitchell, P. D. Parker, D. K. Sharp, and J. S. Thomas. Test of sum rules in nucleon transfer reactions. *Phys. Rev. Lett.*, 108:022501, 2012.
- Schrödinger, E. *Naturw.*, 14:644, 1926.
- J. C. Ward. An identity in quantum electrodynamics. *Phys. Rev.*, 78:182–182, Apr 1950. doi: 10.1103/PhysRev.78.182. URL <https://link.aps.org/doi/10.1103/PhysRev.78.182>.
- C. F. Weizsäcker. Zur theorie der kernmassen. *Z. Phys.*, 96:431, 1935.
- H. Wibowo and E. Litvinova. Nuclear dipole response in the finite-temperature relativistic time-blocking approximation. *Phys. Rev. C*, 100:024307, Aug 2019. doi: 10.1103/PhysRevC.100.024307. URL <https://link.aps.org/doi/10.1103/PhysRevC.100.024307>.

Chapter 2

Structure and reactions

In what follows the connection between the concept of elementary modes of excitation and associated specific probes is discussed in terms of selected experiments. Connection which finds its ultimate test in terms of predicted and measured absolute transition probabilities and differential cross sections.

2.1 Elementary modes of excitation and specific probes

Subject to external probes which couple weakly to the nucleus, that is in such a way that the system can be expressed in terms of the properties of the excitation in the absence of probes¹, the nucleus reacts in terms of single-particle (-hole) motion (one-particle transfer), vibrations (surface, spin, etc.) and rotations (Coulomb excitation and inelastic scattering) and pairing vibrations and rotations (two-nucleon transfer reactions), that is, in terms of elementary modes of excitation.

Collective vibrations in nuclei can be characterized by a variety of quantum numbers. In particular angular momentum (J), parity (π) and transfer quantum number (β). Let us consider the doubly magic nucleus $^{208}_{82}\text{Pb}_{126}$ to illustrate some aspects of β . The ground state of this nucleus $|\text{gs}(^{208}\text{Pb})\rangle$ has angular momentum 0 and positive parity. It can be viewed as the vacuum state of the variety of elementary modes of excitation at the basis of the nuclear field theory (NFT) description of this system. The lowest lying collective vibration ($E_x \approx 2.6$ MeV) is an octupole surface vibration. Microscopically, it can be viewed as a correlated particle-hole (p, h) excitation. Consequently, this state is characterized by the quantum numbers $J^\pi = 3^-, \beta = 0$. A neutron moving around ^{208}Pb in levels above the Fermi energy can have quantum numbers $j^\pi = 9/2^+, 11/2^+, 5/2^+, \dots (2g_{9/2}, 1i_{11/2}, 3d_{5/2}, \dots)$, all of them having $\beta = 1$.

In the case of quantum electrodynamics (Feynman graphical formulation²),

¹See e.g. Pines, D. and Nozières (1966), Bohr, A. and Mottelson (1975) and refs. therein. Within the context of linear response see however Sect. 7.6.3.

²“The practical usefulness of the Feynman rules and diagrams made them one of the most essential elements of the scientific training of every theoretical physicist” J. Mehra.

theory after which NFT was worked out, these two modes (octupole and single-particle modes) parallel the photon and the electron. The nucleus, aside from having a rich variety of $\beta = 0$ collective (p, h) correlated modes (“photons”) like the $J^+ = 2^+$ (4.1 MeV) and 5^- (3.2 Mev) states, it displays collective $\beta = \pm 2$ modes. These pairing vibrations can be viewed as correlated two-particle ($\beta = +2$), two-hole ($\beta = -2$) vibrations. For example, pair addition modes with quantum numbers $J^\pi = 0^+, 2^+, 4^+, \dots, \beta = +2$ correspond to the ground state and to the lowest $2^+, 4^+, \dots$ states of ^{210}Pb . In particular, the $|J^\pi = 0_1^+, \beta = 2\rangle \equiv |\text{gs}({}^{210}\text{Pb})\rangle$ can be viewed as a nuclear embodiment of a Cooper pair: a weakly correlated pair of fermions moving in time reversal states lying close to the Fermi energy. Cooper pairs are the building blocks of the microscopic theory of superconductivity developed by Bardeen, Cooper, Schrieffer (BCS)³.

In Figs. 2.1.1–2.1.3, examples of specific reactions which have identified different elementary modes of excitation of ^{208}Pb mentioned above, are given.

In the figures, a cartoon representation (color online) of elastic, inelastic, one- and two-particle direct transfer reactions induced by alpha, deuteron and triton projectiles impinging on ^{208}Pb are shown. In all cases a standard setup is used, in which a light projectile is aimed at a fixed target (thin foil made out of ^{208}Pb). The outgoing particles carrying the corresponding physical information, i.e. momentum, angular momentum, energy, etc. transferred to or from the target, are deflected by the electromagnetic fields of a spectrometer and eventually recorded at a given angle by particle detectors (points a,b,... in magnet). Those events provide structural information as shown in the two dimensional strength function displayed below the cartoon laboratory setup.

These strength functions, recorded at a wide range of angles provide the absolute differential cross sections associated with each of the nuclear states populated in the process. They are typically measured in⁴ millibarns per steradian (mb/sr). To translate these quantities into nuclear structure information, a model of structure and of reactions is needed to calculate the absolute cross sections, to be compared with the data. The risks of using relative cross section is that of overlooking limitations in the description of the reaction mechanism or in that of the structure description of the states involved in the reaction under study. Or of both.

In this connection, it is of notice that either one sets equal weight in correctly calculating the static and dynamic properties of the single-particles and of the collective modes respectively, and on their interweaving leading to renormalized, physical modes, than in working out the reaction mechanism, or the confrontation between theoretical predictions and experimental observation may not be fruitful⁵.

³Bardeen et al. (1957a,b). See also Brink, D. and Broglia (2005) and references therein.

⁴A barn is defined as $1\text{b}=10^{-28}\text{m}^2 = 100\text{fm}^2$. In three dimensions, the solid angle Ω is related to the area of the spherical surface A it spans ($\Omega = A/R^2$ sr), in a similar way in which in two dimensions, an angle θ is related to the length L of the circular arc it spans. $\theta = L/R$ rad.

⁵*Structure and Reactions.* Within this context one can ask how one understands which the correct elements are to describe a reaction process, if one does not know in detail the structure of the initial and final states? In a nutshell: how can one understand reaction without knowing structure

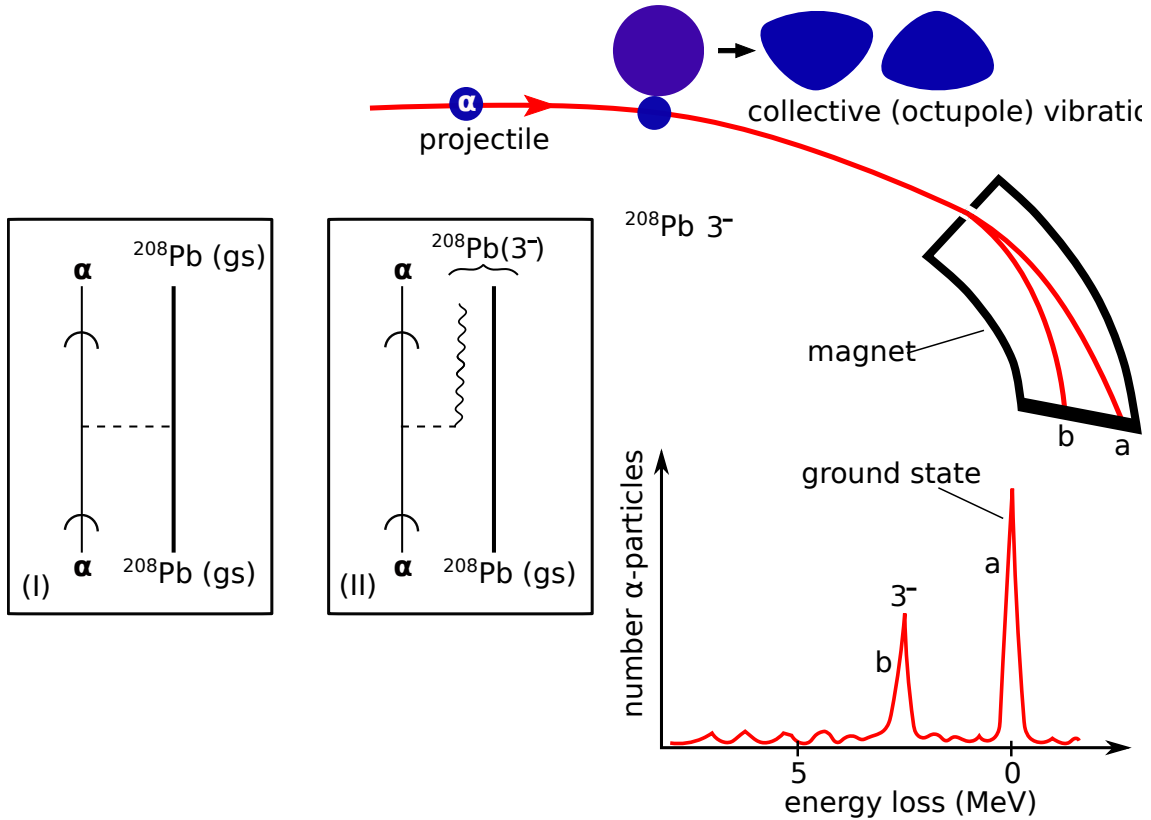


Figure 2.1.1: (color online) Schematic representation of: **elastic** a (population of the ground state), and **inelastic** b (population lowest octupole vibration at 2.62 MeV) processes associated with the reaction $^{208}\text{Pb}(\alpha, \alpha')^{208}\text{Pb}^*$ (for more details see Sect. 2.3 and App. 2.A). In the inset (I) a schematic Nuclear Field Theory (reaction plus structure) (NFT(r+s)) diagram describing the elastic process (potential scattering, dashed horizontal line) is displayed (see e.g. Broglia et al. (2016) and refs. therein). The α -projectile moving in the continuum is represented by an arrowed (curved) line. From the measurement of the elastic differential cross section one can deduce the partial wave phase shifts (Appendix 2.C). In the inset (II) a schematic NFT(r+s) diagram describing the inelastic excitation (see Fig. 2.C.1) of the low-lying octupole vibration (wavy line) of ^{208}Pb by the action of the transient field created by the α -particle on the target (horizontal dashed line) is given (see App. 2.A). Outgoing α particles are deflected in a spectograph and recorded in a detector. The corresponding excitation function is given in the lowest part of the figure (after Mottelson (1976b)).

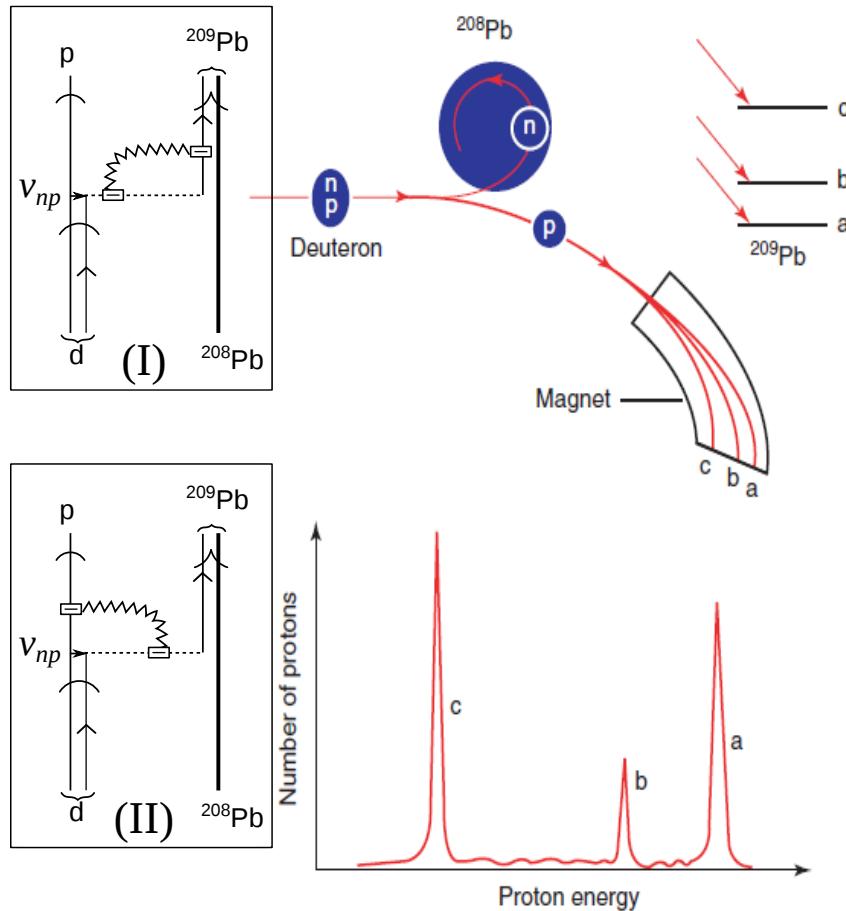


Figure 2.1.2: (Color online) Schematic representation of the one-nucleon transfer reaction $^{208}\text{Pb}(d, p)^{209}\text{Pb}$ populating valence single-particle states of ^{209}Pb . In the inset a schematic NFT($r+s$) diagram describing the process is shown. Curved arrowed lines describe the projectile d (deuteron) and outgoing particle p (proton) moving in the continuum. The short horizontal arrowed line labeled v_{np} represents the proton–neutron interaction inducing the transfer process (dashed horizontal line) while the open dashed rectangle indicates the Particle Recoil Coupling (PRC) vertex. That is, the coupling of the relative motion to the recoil process described in terms of a jagged line (App. 2.C). This information is carried out in the center of mass system by the outgoing particles in the final channel. Within this context the jagged line is involved in a virtual process (insets (I) and (II)). The energy and momentum of the outgoing proton reflects the recoil, the Q -value of the reaction and the excitation energy of the final state as analyzed in the magnet and recorded in the particle detector (a,b,c) (after Mottelson (1976b)).

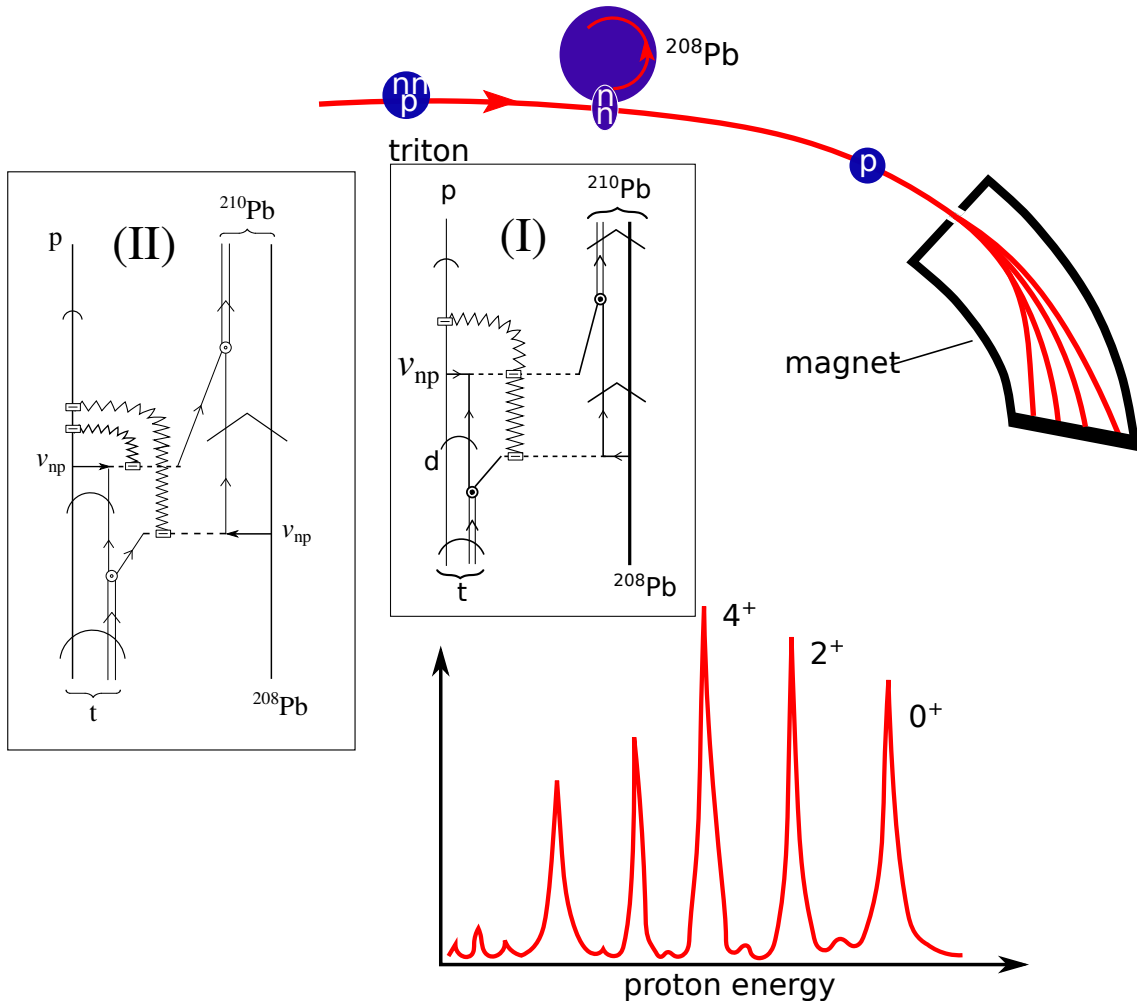


Figure 2.1.3: (Color online) Schematic representation of the two–nucleon transfer reaction $^{208}\text{Pb}(t, p)^{210}\text{Pb}$ process populating the ground state 0^+ , and two particle excited states 2^+ and 4^+ . That is, monopole, quadrupole and hexadecapole pair addition modes (multipole pairing vibrations) of ^{208}Pb (App. 7.12; see also Brink, D. and Broglia (2005) Sect. 5.3.1 p. 108). In the inset (I) a $\text{NFT}(r+s)$ diagram of the (successive) transfer process is displayed. The jagged line brings information to the outgoing nuclei in the exit channel (CM system), of the change in scaling in the asymptotic outgoing waves with respect to the incoming ones, concerning the different mass partitions (recoil) of summed value $2m$ (App. 2.C; concerning the apparent non–linearity that is the direct coupling of two recoil modes, this can be avoided drawing the process as shown in inset (II); see also Sect. 2.B.3; see also Fig. 2.7.10), this information is carried out to the detector by the outgoing proton (see App. 2.B, Sect. 2.B.3) (after Mottelson (1976b)).

Echoing Heisenberg's requirement⁶ that no concept enters the quantal description of a physical system which has no direct relation to experiments, and Landau's findings that a weakly excited state of a quantal many-body system may be regarded as a gas of weakly interacting elementary modes of excitation⁷, Bohr, Mottelson⁸ and coworkers developed a unified description of the nuclear structure. In particular, a Nuclear Field Theory (NFT)⁹ in terms of Feynman diagrams describing the behavior of quasiparticles, vibrations and rotations, and of their couplings both in 3D¹⁰ – as well as in gauge¹¹ – and other “abstract” spaces, which had close connections with direct nuclear reactions¹². Within this context one gives in Figs. 2.1.1–2.1.3 (insets) schematic representations of *unified NFT diagrams of structure and reactions (NFT(s+r))*¹³, which microscopically describe the variety of structure and reaction processes in terms of Feynman diagrams in a basis of elementary modes of excitation. That is, in the present case in which the target is a closed shell system, a particle-hole (inelastic scattering), one-particle (single-particle stripping) and two-particle (Cooper pair transfer) modes.

In inset (I) of Fig. 2.1.1 a diagram describing elastic scattering is shown, while in inset (II) a NFT(r+s) diagram describing the inelastic excitation of the low-lying octupole vibration of ^{208}Pb is displayed. A pointed (curved) arrow on a line indicates propagation of a nucleon inside the projectile or in the target nucleus (in the continuum with asymptotic waves). An up (down) pointing arrowed line indicates a nucleon (nucleon-hole) moving above (in) the Fermi sea. The horizontal dashed line represents the action of the mean field or of the bare interaction (see also Fig. 2.2.1), while the solid dot stands for the particle-vibration coupling vertex in the case of particle-hole collective modes.

In the insets of Fig. 2.1.2 a NFT(r+s) diagrams describing the process $^{208}\text{Pb}(d, p)^{209}\text{Pb}$ are schematically shown. A standard pointed arrowed line indicates the neutron moving with the proton in the deuteron (double, curve arrowed, line), or around the (assumed, for simplicity, inert) ^{208}Pb core (bold face line). The

(eyes without object)? Vice versa, how can one understand what the elements needed for a correct description of the structure of levels is, if one does not know how to observe them (specific probe), how to bring that information to the detector?. In other words, how can one understand structure without knowing reaction (object without eyes)? The answer to both questions is that one cannot.

⁶Heisenberg (1949).

⁷Landau (1941).

⁸Bohr (1964), Bohr and Mottelson (1969), Bohr (1976), Mottelson (1976a), Bohr, A. and Mottelson (1975), Bohr et al. (1958) and references therein.

⁹Bès et al. (1974); Bohr, A. and Mottelson (1975); Bès, D. R. and Kurchan (1990); Mottelson (1976a) and refs. therein.

¹⁰Nilsson (1955); Bohr, A. and Mottelson (1975) and refs. therein.

¹¹Bohr et al. (1958); Belyaev (1959); Högaasen-Feldman (1961); Bjerregaard, J. H. et al. (1966); Broglia and Riedel (1967); Bohr, A. and Mottelson (1975).

¹²Alder et al. (1956), Alder and Winther (1975), Broglia and Winther (2004); concerning the general development of direct nuclear reactions see Austern (1970), Jackson (1970), Satchler (1980), Satchler (1983), Brink, D. M. (1985), Glendenning, N. K. (2004); Thompson and Nunes (2009), and refs. therein.

¹³Broglia (1975); Broglia and Winther (2004); Potel, G. et al. (2013a); Broglia et al. (2016).

jagged curve represents the recoil mode coupling the intrinsic and the relative motion¹⁴, thus accounting for the mass partition and the change in scaling between entrance and exit channel distorted waves. The corresponding momentum mismatch being taken care of by a Galilean transformation (recoil effects)¹⁵. Because one is working in the center of mass (CM) system, the jagged curve can transfer the information of momentum mismatch to either the residual nucleus (inset (I)) or to the outgoing particle, i.e. the proton (inset (II)). Horizontal short arrowed lines stand for the proton–neutron (nucleon–nucleon) bare interaction inducing transfer¹⁶. It is of notice that choosing in an appropriate way the (post or prior) representation to describe the reaction process (energy conservation), one can evidence the single-particle mean field or the proton–neutron interaction as inducing the transfer process¹⁷.

In Fig. 2.1.3 a schematic representation of the $^{208}\text{Pb}(t, p)^{210}\text{Pb}$ process is given. In the insets a schematic NFT(r+s) diagram describing the $^{208}\text{Pb}(t, p)^{210}\text{Pb}$ process is shown. The dineutron moving in the triton and around the ^{208}Pb core, (pair addition mode) is represented by a double arrowed line. Each individual transferred neutron is indicated with a single arrowed line. The curved arrows on the triton and on the proton indicate motion in the continuum with outgoing and incoming asymptotic waves, respectively. The pointed arrow encompassing the pair addition mode and the core ^{208}Pb , indicate intrinsic (structure) motion. In selecting this NFT diagram the assumption was made, following the results of detailed calculations, that the main contribution to the process arises from the successive transfer of the nucleons. Two jagged curves are shown. One connecting the first and the second transfer process at the particle–recoil mode coupling vertex (PRCV, dashed open square), in keeping with the fact that the channel $^{209}\text{Pb}+d$ has no asymptotic waves. The second one emerges from the second PRCV and carries the mismatch information associated with a transfer of mass $2m$ to either the outgoing proton (not shown) or residual nucleus ^{210}Pb (CM description; see App. 2.C, in particular paragraph after Eq. (2.C.40))¹⁸. Within this context, see also inset (II).

It is of notice that the successive transfer of neutrons described in insets (I) and (II) can be related to the successive tunneling of pairs of electrons involved in the Josephson effect, in particular in connection with what is known as direct current effect (dc effect; see Sect. 4.6, in particular the discussion following Eq. (4.6.20)), as well as Josephson effect¹⁹.

As discussed in the following Chapters, Cooper pairs are extended objects, the fermionic partners being correlated over distances much larger than nuclear

¹⁴See App. 2.C.

¹⁵See App. 2.C; also Ch. 6, in particular Figs. 6.5.1 and 6.5.2.

¹⁶For more details see Figs. 2.9.2 and 2.9.3, see also Ch. 5 and Fig. 5.1.1 as well as App. 2.C and Sect. 6.5.

¹⁷See Sects. 4.1, 6.1, Fig. 5.1.1 and App. 6.5.

¹⁸Concerning the apparent non linearity of the recoil process (two jagged lines associated with a single PRCV, we refer to App. 2.B Sect. 2.B.3).

¹⁹Josephson (1962); Anderson (1964). See also Brink, D. and Broglia (2005) App. L and refs. therein.

dimensions (correlation length $\xi \approx 15$ fm $\gg R_0 \approx 6$ fm ($A = 120$)). Because the single particle potential acts on these pairs as a rather strong external field, this correlation length feature is not obvious in structure calculations, becoming apparent in reaction calculations.

Elementary modes of excitation, that is single-particle motion and collective motion, are the way nuclei react to external probes, and thus closely connected with the physical observables. Namely, absolute transition probabilities and absolute differential cross sections. Within this context, bare elementary modes of excitation already contain an important fraction of nuclear many-body correlations, thus making the diagonalization of the nuclear Hamiltonian leading to dressed elementary modes of excitation, a low-dimension problem. For example, in terms of matrices $10^2 \times 10^2$, each matrix element containing much physical insight into nuclear structure at large²⁰.

In keeping with the fact that all the nuclear degrees of freedom are exhausted by those of the nucleons, and that the different reactions, that is elastic, Coulomb and inelastic excitations, as well as one- and two-particle transfer reactions project particular, but somewhat overlapping components of the total wavefunction, the nuclear elementary modes of excitation give rise to an overcomplete, non orthogonal, Pauli principle violating basis, both concerning structure as well as reactions. The coupling between unperturbed fermionic and bosonic degrees of freedom is proportional to this overlap between single-particle and collective modes. Nuclear Field Theory²¹, provides the conserving sum rules protocol to diagonalize these couplings to any order of perturbation theory, also infinite if so required for specific processes (see Sect. 2.7). The dressed physical elementary modes resulting from the interweaving of the bare modes are orthogonal to each other and fulfill Pauli principle, providing a microscopic solution to the many-body nuclear problem. The NFT(s+r) diagrams²² (see e.g. Figs. 2.9.2 and 2.9.5) predictions are embodied in absolute cross sections and transition probabilities, which can be directly compared with the observables whose values are obtained by studying the nuclear system with the variety of ever more precise and varied arsenal of experimental probes (see e.g. Fig. 7.1.3).

At this point a proviso or two are in place. The original elementary modes of nuclear excitation melt together, due to their interweaving, into effective fields²³. Each of them display properties which reflect that of all the others, their individuality resulting from the actual relative importance of each one of them. What

²⁰Illuminating discussion with B. A. Brown during the 15th International Conference on Nuclear Reactions Mechanisms (Varenna, June 2018) regarding this, and related issues are gratefully acknowledged (RAB).

²¹Bès et al. (1974), Bès et al. (1976b), Bès et al. (1976c), Bès et al. (1976a), Bès and Broglia (1975), Broglia et al. (1976), Bès, D. R. and Broglia, R. A. and Dussel, G. G. and Liotta (1975), Mottelson (1976a), Bès and Broglia (1977), Bortignon, P. F. et al. (1977), Bortignon, P. F. et al. (1978), Broglia and Winther (2004), Reinhardt (1975), Reinhardt (1978a), Reinhardt (1978b), Reinhardt (1980).

²²Broglia (1975); Broglia and Winther (2004); Broglia et al. (2016).

²³Within this context see Dickhoff, W. and Van Neck (2005) and references therein.

one calls a physically (clothed) particle is only partially to be associated with that particle field alone. It is also partially to be associated with the vibrational fields (surface, density, spin²⁴, pairing²⁵, etc. vibrational modes), because they are in interaction through the particle–vibration coupling vertices²⁶. And conversely, what one calls a nuclear vibration can couple to particle–hole (in the case of a surface vibration), two–particle (in the case of a pair addition) or a two–hole (in the case of a pair removal) configurations.

Thus nucleons (fermions) couple to vibrational modes (bosons) and, eventually, can reabsorb them returning to the original state. The same is true concerning bosons degrees of freedom and their coupling to fermions. The outcome of such processes, namely the dressed physical elementary modes of excitation, is closely connected with the renormalization program of quantum electrodynamics (QED)²⁷ implemented in NFT in terms of Feynman diagrams. Renormalized NFT, i.e (NFT)_{ren} implies that the intermediate, virtual states clothing the elementary modes of excitation, are fully dressed²⁸.

The specific experimental probes of the bare elementary modes of nuclear excitation reveal only one aspect, in most cases likely the most important one of the physical (clothed) elementary modes. Renormalized NFT reflects the physical unity of low–energy nuclear research requiring the melting not only of elementary modes of excitation but also of structure and reaction theory, let alone of the different experimental techniques developed to study the atomic nucleus. In other words the need for a complete set of experimental probes to reveal the multi faceted properties of clothed elementary modes of excitation resulting from the implementation of a consistent program of structure and reactions (within this context see Fig. 2.10.1).

As seen from the contents of the present monograph, the accent is set at relating theoretical predictions with experimental findings, through the unification of structure and reactions. In particular the unification of pairing and two–nucleon transfer processes, where the two subjects are blended together, which is what happens in nature. Once the NFT rules to work out the variety of elements (spectroscopic and, with the help of them, reaction amplitudes) have been laid out and/or the pertinent literature refer to, concrete embodiments are provided and eventual absolute cross sections and transition probabilities calculated and confronted with the experimental data.

An essential test theory has to pass is particle-pair conservation. Test closely connected with some operator identities which go under the name of sum rules. An overcomplete basis of states will violate sum rules, resulting in couplings between the basis states. Couplings which are proportional to the overlap (non-orthogonality) between these states. This is so, not only for structure calculations,

²⁴Bertsch and Broglia (2005) Chs. 6,7,8.

²⁵Brink, D. and Broglia (2005) Ch. 5.

²⁶Bohr, A. and Mottelson (1975).

²⁷Feynman (1975); Schwinger (2001).

²⁸Barranco et al. (2017), see also Broglia et al. (2016).

in which e.g. hole and pair addition modes are non orthogonal to particle and surface (p, h) vibrational states. Also for reactions calculations, as the single-particle states in projectile and target are, as a rule, non orthogonal. Sum rules play a central role not only in the validation of a theory, but also in defining the variety of couplings which dress the bare basis states as well as to eliminate spurious components from reaction amplitudes.

2.2 Sum rules

A quantitative measure of the overcompleteness of the elementary modes of excitation basis is provided by the use of exact and of empirical sum rules that the observables (cross sections) associated with the variety of probes to which the nucleus is subject, have to fulfill. An example of the first type is given by the Thomas–Reiche–Kuhn (TRK) sum rule^{29,30}, while of the second type, by some of the two–nucleon transfer reaction (TNTR) sum rules³¹. Others, which relate one–with two–particle transfer processes³² being exact. In all cases they embody particle (pair) number conservation. Charged particles in the first case (electrons in atoms and molecules, effective charges of neutrons and protons in nuclei). Number of Cooper pairs in nuclei in the second³³. Physically, they provide information concerning: 1) the maximum amount of energy which the quantal system can absorb from a beam of photons (γ -rays) shined on it; 2) the total two–nucleon transfer cross section (ring area fraction of the geometrical reaction cross section) exhausted by the final ($A \pm 2$) states populated in the transfer process.

In other words, these sum rules provide a quantitative measure of the single–particle subspace the quantal system under study, in particular the nucleus, uses to correlate particle–hole excitations and thus induce the antenna–like motion of protons against neutrons or, to correlate pairs of nucleons moving in time reversal states around the Fermi energy, leading to a, static or dynamic, sigmoidal distribution of the associated pair ($\nu, \bar{\nu}$) level occupancy around the Fermi energy.

The TRK sum rule can, in the nuclear case, be written as³⁴

$$S(E1) = \sum_{\alpha} \left| \langle \alpha | F | \tilde{0} \rangle \right|^2 (E_{\alpha} - E_0) = \frac{9}{4\pi} \frac{\hbar^2 e^2}{2m} \frac{NZ}{A}, \quad (2.2.1)$$

²⁹Bohr, A. and Mottelson (1975), Sect. 6-4.

³⁰Bertsch and Broglia (2005), Chapter 3, in particular Sect. 3.3.

³¹Broglia, R. A. et al. (1972)

³²Bayman, B. F. and Clement (1972); Lanford (1977)

³³Within this context, the absolute two–nucleon transfer cross section populating the ground state of a superfluid nucleus is proportional to the number of Cooper pairs contributing to the nuclear condensate (modulus squared). This quantity is rather stable along a pairing rotational band, in keeping with the fact that the “intrinsic” $|BCS\rangle$ –state of the deformed system in gauge space, is essentially the same for all members of the band. This fact is at the basis of a newly found physical sum rule (Potel et al. (2017); see also Ch. 7 Sect. 7.4.1).

³⁴Bohr, A. and Mottelson (1975); Bertsch and Broglia (2005); Bortignon, P. F. et al. (1998)

where $|\alpha\rangle$ labels the complete set of excited dipole states which can be reached acting with the dipole operator F on the initial correlated vacuum state $|\tilde{0}\rangle$ (see Eq. (2.2.4)). Within this context, each bosonic elementary mode of excitation provides, within the harmonic approximation, a specific contribution to the total zero point fluctuations of the ground state (ZPF, see introduction to Sect. 2.7 and Sect. 2.8), that is,

$$\langle \tilde{0}|F^2|\tilde{0}\rangle = \frac{\hbar\omega}{2C_\alpha} = \frac{\hbar^2}{2D_\alpha} \frac{1}{\hbar\omega_\alpha}. \quad (2.2.2)$$

Where C_α and D_α are the restoring force and the inertia parameters of the collective mode of frequency ω_α ($= (C_\alpha/D_\alpha)^{1/2}$). The label α indicates the quantum numbers characterizing the vibrational mode. For example, in the case of surface multipole vibrations $\alpha \equiv (\beta = 0, \lambda\mu, \pi)$.

The ZPF perturb the static nucleon Fermi sea, that is the set of occupied levels of the mean field potential (Fig. 2.2.1)

$$U(r) = \int d\mathbf{r}' \rho(r') v(|\mathbf{r} - \mathbf{r}'|), \quad (2.2.3)$$

inducing virtual particle-hole excitations (k, i , i.e. $\epsilon_i \leq \epsilon_F$ and $\epsilon_k > \epsilon_F$, Eqs. (2.2.6) and (2.4.1); see Fig. 2.2.2). In the above equation, $\rho(r)$ is the nuclear density and v is the nuclear two-body interaction.

In Eq. (2.2.1), the quantity

$$F = e \sum_n \left(\left(\frac{N-Z}{2A} - t_z(n) \right) r_n Y_{1\mu}(\hat{r}_n) \right), \quad (2.2.4)$$

is the dipole operator referred to the nucleus center-of-mass acting both on the protons ($t_z = -1/2$) and on the neutrons ($t_z = 1/2$), t_z being the third component of the isospin operator.

Because $|\langle \alpha | F | \tilde{0} \rangle|^2$ measures the probability with which the state $|\alpha\rangle$ is populated, the α -sum in (2.2.1) gives a measure of the maximum energy that the nucleus can absorb from the γ -beam. It is customary to measure $|\langle \alpha | F | \tilde{0} \rangle|^2$ in single-particle (sp) units (Weisskopf (W) units)

$$\begin{aligned} B_{sp}(E1; j_1 \rightarrow j_2) &= \frac{3}{4\pi} e_{E1}^2 \langle j_1 \frac{1}{2} 1 0 | j_2 \frac{1}{2} \rangle^2 \times \langle j_2 | r | j_1 \rangle^2, \\ &\approx \frac{0.81}{4\pi} A^{2/3} e_{E1}^2 \text{ fm}^2 = B_W(E1), \end{aligned} \quad (2.2.5)$$

where $(e)_{E1} = (N/A)e$ for protons and $(e)_{E1} = -(Z/A)e$ for neutrons, in keeping with the fact that the motion of a nucleon is associated with a recoil of the rest of the nucleus. This is because the center of mass of the system remains, in an intrinsic excitation³⁵, at rest.

Within this context is that independent-particle motion in general and the existence of a mean field ((MF), Hartree–Fock (HF) solution) in particular can be viewed as the most collective of all nuclear phenomena³⁶, in keeping with the fact

³⁵See, e.g. Broglia et al. (2016) App. G and references therein.

³⁶Mottelson (1962).

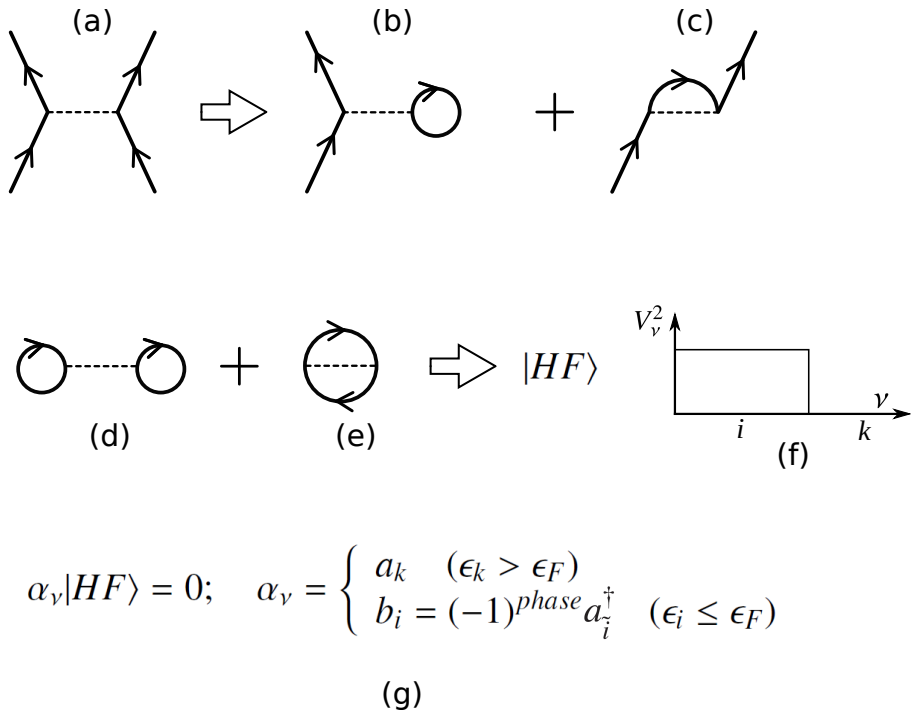


Figure 2.2.1: Schematic representation of the processes characterizing the Hartree–Fock ground state (single-particle vacuum), in terms of Feynman diagrams. **(a)** nucleon–nucleon interaction through the bare (instantaneous) NN –potential. **(b)** Hartree mean field contribution. **(c)** Fock mean field contribution. **(d,e)** ground state correlations (ZPF) associated with the Hartree and Fock processes. **(f)** There is, in HF (mean field) theory, a complete decoupling between occupied and empty states, labeled i and k respectively, and thus a sharp discontinuity at the Fermi energy of the occupation probability, from the value of 1 to 0. **(g)** This decoupling allows for the definition of two annihilation operators: $a_k(b_i)$ particle (hole) annihilation operators, implying the existence of hole (antiparticle) states ($b_i^\dagger|HF\rangle$) with quantum numbers time reversed to that of particle states, (for details see e.g. Brink, D. and Broglia (2005) App. A). In other words, the $|HF\rangle$ ground (vacuum) state is filled to the rim (ϵ_F) with N nucleons. The system with $(N - 1)$ nucleons can, within the language of (Feynman’s) field theory, be described in terms of the degrees of freedom of that of the missing nucleon (hole–, antiparticle state). Such a description is considerably more economic than that corresponding to an antisymmetric wavefunction with $(N - 1)$ spatial and spin coordinates (\mathbf{r}_i, σ_i) . Within the above scenario, a stripping reaction $N(d, p)(N + 1)$ can be viewed as the creation of a particle state ($a_k^\dagger|HF\rangle = |k\rangle$) and that of a pickup reaction $N(p, d)(N - 1)$ as that of a hole state ($b_i^\dagger|HF\rangle \equiv |\tilde{i}\rangle$) (see also App. 5.10).

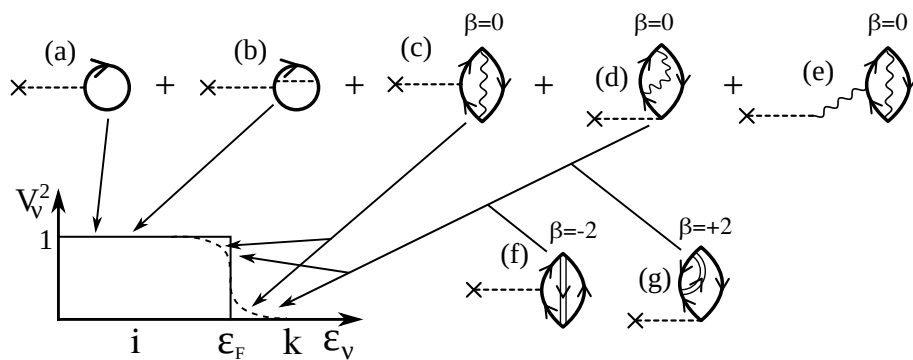


Figure 2.2.2: Schematic representation of the Fermi distribution. The sharp, continuous line drawn step function schematically represents the Hartree–Fock occupation numbers. The associated nuclear density measured with the help of an external field (cross attached to a dashed line) through processes of type (a) (Hartree: H) and (b) (Fock: F) is expected to display a diffusivity of the order of the strong force range. Zero Point Fluctuations (ZPF) associated with collective particle–hole vibrations, i.e. processes with transfer quantum number $\beta = 0$ (Bohr (1964)) and shown in (c), (d) and (e), and with pairing vibrations, i.e. pair removal (graph (f)) and pair addition modes (graph (g)), smooth out the occupation numbers around the Fermi energy (dashed curve) and lead to a nuclear density of larger (dynamical) diffusivity than that associated with HF. One- and two-particle strengths which in this (mean field) approximation are found in a single A -mass system, are as a result of ZPF ($\beta = 0, \pm 1, \pm 2$) distributed over a number of nuclei ($A, A \pm 1, A \pm 2$) (see also App. 5.10, Fig. 5.10.1).

that,

$$\begin{aligned} S(E1) &= \sum_n |\langle n|F|\tilde{0}\rangle|^2(E_n - E_0) \\ &= \sum_{k,i} |\langle k, i|F|gs(MF)\rangle|^2(\epsilon_k - \epsilon_i), \end{aligned} \quad (2.2.6)$$

provided $|\tilde{0}\rangle$ contains the ground state correlations mentioned in connection with Eq. (2.2.2), and that $|gs(MF)\rangle$ those associated with $\Delta x \Delta p \geq \hbar$ (see Fig. 2.2.1). In other words, provided

$$|HF\rangle = |gs(MF)\rangle = \prod_{i \in occup} a_i^\dagger |0\rangle \quad (2.2.7)$$

where $|0\rangle$ is the particle vacuum state ($a_j|0\rangle = 0$), and $\Gamma_\alpha|\tilde{0}\rangle = 0$, Γ_α^\dagger being the creation operator of a dipole Random Phase Approximation (RPA) correlated particle-hole like mode ($\Gamma_\alpha^\dagger = \sum_{ki} X_{ki}^\alpha a_k^\dagger a_i + Y_{ki}^\alpha (a_k^\dagger a_i)^\dagger$)³⁷. Relation (2.2.6) is a consequence of the fact that $S(E1)$ is proportional to the average value of the double commutator $[[H, F], F]$ in the ground state of the system ($|\tilde{0}\rangle$ or $|HF\rangle$). Because F is a function of only the nucleon coordinates, and assuming $v(|\mathbf{r} - \mathbf{r}'|)$ to be velocity independent, the only contribution to the double commutator arises from the (universal) kinetic energy term of the Hamiltonian. Thus, the value (2.2.1) is model independent. In other words, this value does not depend on the correlations acting among the nucleons, but on the number of them participating in the motion and on their mass (inertia) as testified by the fact that $\sum_\alpha \hbar\omega_\alpha \left(\frac{\hbar\omega_\alpha}{2C_\alpha} \right) = \sum_\alpha \left(\frac{\hbar^2}{2D_\alpha} \right)$. It is then not surprising that the TRK sum rule was used in the early stages of quantum mechanics, to determine the number of electrons in atoms.

Let us now go back to two-nucleon transfer (pairing) processes. The absolute cross sections associated with the population of final states can be set essentially on equal footing with respect to each other concerning Q -value and recoil effects, with the help of empirically determined global functions³⁸. In this way, the theoretical absolute cross section associated with e.g. the $A(t, p)A + 2$ population (we assume N to be even) of the n th final state of spin J and parity $(-1)^J$ can be written as

$$\sigma^{(n)}(J = L, Q_0) = \left| \sum_{j_1 \geq j_2} B(j_1 j_2; J_n) S(j_1 j_2; L, Q_0) \right|^2, \quad (2.2.8)$$

where

$$S^2(j_1 j_2; L, Q_0) = \sigma(j_1, j_2; L, Q_0), \quad (2.2.9)$$

³⁷Bertsch and Broglia (2005), Ch. 4, and Brink, D. and Broglia (2005) Ch. 8, Sect. 8.3, Bohr, A. and Mottelson (1975) Sect. 6-5 h. As can be seen from Fig 2.C.1, in the RPA approximation no scattering vertices (Fig. 2.3.1) are present. Consequently, the coupling between one- and two-phonon states is, within this (harmonic) approximation, not possible.

³⁸see Broglia, R. A. et al. (1972)

the quantity $\sigma(j_1, j_2; L, Q_0)$ being the absolute two-nucleon transfer cross section associated with the two particle configuration $(j_1, j_2)_L$. The quantity

$$B(j_1 j_2; J_n) = \left\langle \Phi_{J_n}(\xi_{A+2}) \left| \Phi_{J_i=0}(\xi_A) \frac{[a_{j_1}^\dagger a_{j_2}^\dagger]_J}{[1 + \delta(j_1, j_2)]^{1/2}} \right. \right\rangle, \quad (2.2.10)$$

is the two-nucleon spectroscopic amplitude, $\Phi_{J_i=0}(\xi_A)$ being the wavefunction describing the ground state of the initial nucleus, $\Phi_{J_n}(\xi_{A+2})$ that of the final state, ξ labeling the relative radial and spin intrinsic coordinates. Assuming A to be a closed shell system, and $J = 0$, one can write

$$|0_n^+\rangle = \sum_{j_1 \geq j_2} c^{(n)}(j, j; J = 0) |j, j; J = 0\rangle, \quad (2.2.11)$$

where $n = 1, 2, 3, \dots$ labels the final nucleus states of spin and parity $J^\pi = 0^+$ in increasing energy order. Making use of the completeness relation of the coefficients $c^{(n)}(j, j; J = 0)$ one obtains,

$$\sum_n \sigma^{(n)}(J = L = 0, Q_0) = \sum_j \sigma(j, j; L = 0, Q_0). \quad (2.2.12)$$

The above equation parallels (2.2.6), aside from the fact that the Q -value effect is, in connection with (2.2.6), analytically dealt with, while $\sigma(\{Q\})$ is a functional of Q . The complete separation of the relative and intrinsic motion coordinates taking place in e.g. (2.2.6) is in keeping with the fact that in elastic and inelastic processes the mass partition is equal in both entrance and exit channels. Thus, the intrinsic (structure) and the relative motion (reaction) coordinates can be treated separately. This is not the case for transfer processes, both intrinsic and reaction coordinates being interwoven through the recoil process (particle-recoil mode coupling, see jagged curves Figs 2.1.2 and 2.1.3 as well as Figs. 2.9.2 and 2.9.3; see also Sect. 2.6).

A parallel with the discussion carried out in connection with (2.2.5) regarding the TRK sum rule, can be drawn defining two-particle units as,

$$\sigma_{2pu}^{max}(A, L, Q_0) = \max [\sigma(j_1, j_2; L, Q_0)], \quad (2.2.13)$$

where $\max[\]$ indicates that the largest two-particle absolute cross section in the single-particle subspace considered (*hot orbital*), is to be considered. In this way one can write the relation (2.2.12) in dimensionless units. Another quite useful, this time exact, two-particle transfer sum rule has been introduced in the literature³⁹, which relates two-nucleon stripping and pick-up reactions cross sections, with single-particle transfer processes⁴⁰.

³⁹Bayman, B. F. and Clement (1972). In this connection, and within the context of a schematic model, see Eq. (2.7.79) and subsequent discussion.

⁴⁰Lanford (1977)

The above arguments carried out for nuclei around closed shells can, equally well, be applied to the case of open shell nuclei, making use of the corresponding two-nucleon spectroscopic amplitudes⁴¹. In particular, in the case of independent pair motion, i.e. the BCS mean field solution of the pair problem, the summed spectroscopic pair transfer amplitudes, each term weighted with $(j + 1/2)^{1/2}$, is given by

$$\begin{aligned}\alpha'_0 &= \langle BCS(N+2) | P'^{\dagger} | BCS(N) \rangle \\ &= \sum_j \frac{2j+1}{2} U'_j(N) V'_j(N+2),\end{aligned}\quad (2.2.14)$$

where⁴²

$$P'^{\dagger} = \sum_{m>0} a'_{jm}^{\dagger} a'_{\widetilde{jm}}^{\dagger} = \sum_j \sqrt{\frac{2j+1}{2}} T'^{\dagger}(j^2(0)), \quad (2.2.15)$$

creates two nucleons in time reversal states,

$$T'^{\dagger}(j^2(0)) = \frac{[a'_j^{\dagger} a'_j^{\dagger}]^0}{\sqrt{2}}, \quad (2.2.16)$$

being the two-nucleon (Cooper pair) transfer operator. The associated expectation value in the $|BCS\rangle$ ground state is the two-nucleon transfer spectroscopic amplitude

$$B(j^2(0), N \rightarrow N+2) = \sqrt{\frac{2j+1}{2}} U'_j(N) V'_j(N+2). \quad (2.2.17)$$

The ZPF associated with pairing vibrations, similar to those associated with particle-hole-like excitations, smooth out the sharp HF Fermi surface (Fig. 2.2.2). The number of pairs in each level participating in this smoothing is $(2j+1)/2$ their occupancy being measured by the simultaneous, and apparently contradictory, property of being a particle (amplitude V'_j) and a hole (amplitude U'_j). In other words α'_0 measures the number of pairs of nucleons (Cooper pairs) participating in the smoothing out of the Fermi surface⁴³ and thus can be viewed as the spectroscopic amplitude associated with the population of pairing rotational bands in two-nucleon transfer processes. It is expected that α'_0 depends weakly on N and is about conserved along a pairing rotational band. Because $d\sigma(gs(N) \rightarrow gs(N+2))/d\Omega \approx |\alpha'_0|^2$, conservation is also expected for these absolute cross section. But in this case, it is a conservation of a physical character, and not a mathematical one (see

⁴¹See App. 2 of Broglia, R.A. et al. (1973), Yoshida (1962).

⁴²The primed quantities are the particle creation operators and BCS occupation amplitudes referred to the intrinsic system of reference in gauge space (see Sect. 3.4 and 4.7). See also Potel, G. et al. (2013b).

⁴³Schrieffer (1964); Potel et al. (2017) and refs. therein.

Sect. 7.4.1). If one finds that at the angle where $L = 0$ two-nucleon transfer differential cross sections have the first maximum, as a rule close to 0° , the two nucleon strength function is dominated by a single peak, that associated with the ground state, and this is so for a number of isotopes differing in mass number by two, it can be concluded that one is in presence of a pairing rotational band (see Figs. 3.1.3 and 3.1.4). This is one of the reasons why (2.2.14) can be viewed as the order parameter of the nuclear superfluid phase and, in keeping with (2.2.15), two-nucleon transfer reaction to be the specific tool to probe pairing in nuclei.

Because in a finite many-body system like the nucleus, quantal fluctuations in general and those of particle number in particular, are much larger than in bulk systems, a dynamic parallel to α_0 (Eq. (2.2.14)) can be defined at profit (see Fig. 3.5.7)⁴⁴.

2.3 Particle–vibration coupling

The Hamiltonian describing a system of independent particles and of collective surface vibrations can be written as⁴⁵

$$H = H_M + H_{coll} + H_c, \quad (2.3.1)$$

where

$$H_M = T + U \quad (2.3.2)$$

is the mean field Hamiltonian, sum of the single-particle kinetic energy and of the self-consistent potential $U = f(\rho)$, functional of the density. That is,

$$U = U_H + U_x, \quad (2.3.3)$$

where

$$U_H = \int d\mathbf{r}' \rho(r') v(|\mathbf{r} - \mathbf{r}'|), \quad (2.3.4)$$

is the Hartree potential, and

$$U_x = - \sum_{i(\epsilon_i \leq \epsilon_F)} \varphi_i^*(\mathbf{r}') v(|\mathbf{r} - \mathbf{r}'|) \varphi_i^*(\mathbf{r}), \quad (2.3.5)$$

is the exchange (Fock) potential. It is well established that the nucleus can react collectively to external solicitations. In particular the nuclear surface⁴⁶ can vibrate in certain normal modes which, in the harmonic approximation can be described as⁴⁷

$$H_{coll} = \frac{\hat{\Pi}_\alpha^2}{2D_\alpha} + \frac{C_\alpha}{2} \hat{a}^2, \quad (2.3.6)$$

⁴⁴See also Potel et al. (2017).

⁴⁵Bohr, A. and Mottelson (1975); Brink, D. and Broglia (2005)

⁴⁶We consider in the present section only this type of collective modes

⁴⁷Concerning the dimension of the parameters C_α and D_α see App. 2.A, Eq. (2.A.10) and subsequent discussion. See also Sect. 5.3.1 of App. 5.3, Eq. (5.3.19) and following comments.

where,

$$\hat{\alpha} = \sqrt{\frac{\hbar\omega_\alpha}{2C_\alpha}} (\Gamma_\alpha^\dagger + \Gamma_\alpha), \quad (2.3.7)$$

is the collective coordinate, $\hat{\Pi}_\alpha$ being the corresponding conjugate momentum, while $\Gamma_\alpha^\dagger(\Gamma_\alpha)$ is the creation (annihilation) operator of the corresponding quanta. Microscopically, these modes can be calculated in the RPA as correlated particle-hole excitations⁴⁸.

The particle-vibration coupling Hamiltonian can be written as,

$$H_c = \kappa \hat{\alpha} \hat{F}, \quad (2.3.8)$$

with

$$\hat{F} = \sum_{\nu_1 \nu_2} \langle \nu_1 | F | \nu_2 \rangle a_{\nu_1}^\dagger a_{\nu_2}, \quad (2.3.9)$$

and

$$F = -\frac{1}{\kappa} R_0 \frac{\partial U(r)}{\partial r} Y_{LM}^*(\hat{r}). \quad (2.3.10)$$

It is of notice that κ characterizes the relationship between potential and density, of the mode considered. The self-consistent value is ($\langle F \rangle = \alpha$)⁴⁹,

$$\kappa = \int R_0 \frac{\partial U}{\partial r} R_0 \frac{\partial \rho}{\partial r} r^2 dr. \quad (2.3.11)$$

Both the coupling constant and the potential U are negative, for attractive fields. H_c embodies the coupling of the motion of a single-nucleons with the collective vibrations of the surface, with a matrix element (see Fig.2.3.1)

$$V_{\nu, \alpha'} = \langle n_\alpha = 1, \nu' | H_c | \nu \rangle = \Lambda_\alpha \langle \nu' | F | \nu \rangle, \quad (2.3.12)$$

where

$$\Lambda_\alpha = \kappa \sqrt{\frac{\hbar\omega_\alpha}{2C_\alpha}} \sim \frac{\kappa \beta_\alpha}{\sqrt{2L_\alpha + 1}}, \quad (2.3.13)$$

is the particle-vibration coupling strength, while β_α is the (dynamic) deformation parameter. For didactical purposes we shall assume in this section that $\beta_L^2 \ll \beta_L$ and thus treat H_c perturbatively. It is of notice that confronted with processes requiring to be summed to infinite order of perturbation theory, this can be done without much difficulty (see e.g. App. 5.4).

Making use of the single-particle energies obtained by solving (2.3.2) and of the particle vibration matrix element (2.3.12) the microscopic, RPA description of the collective states can be obtained by solving the dispersion relation displayed in the inset of Fig. 2.3.1.

⁴⁸Bohm and Pines (1951); Pines and Bohm (1952); Bohm and Pines (1953); see also Bertsch and Broglia (2005), Ch. 4 and refs. therein.

⁴⁹Bohr, A. and Mottelson (1975) Sect. 6-5 h.

Making the ansatz that the physical (clothed) single-particle states results from the coupling to only surface vibrations, the Hamiltonian (2.3.1) can be regarded as being complete to describe the elementary modes of excitation and their couplings. Adding to (2.3.1) the terms describing the spin, spin-isospin, etc. particle-hole modes, as well as those associated with multipole pairing vibrations (see Sect. 3.5 as well as caption to Fig. 2.1.3), i.e. pair addition and pair subtraction modes (with $\lambda^\pi = 0^+, 2^+, 4^+ \dots$, and eventually $1^-, 3^- \dots$, concerning 1^- see App. 7.12), and the corresponding coupling terms, and diagonalizing perturbatively the resulting Hamiltonian, will lead to the physical single-particle states of spherical normal systems (nuclei around close shells). For spherical open-shell nuclei effects arising from the coupling to the condensate⁵⁰ will somewhat affect the actual value of the results, e.g. the energy of the two-quasiparticle phonon states⁵¹.

2.3.1 Fluctuation and damping

To second order in the particle-vibration coupling strength one finds⁵²,

$$\begin{aligned} \left(-\frac{\hbar^2}{2m} \nabla_r^2 + U_H(r) \right) \varphi_j(r) &+ \int d^3 r' U_x(\vec{r}, \vec{r}') \varphi_j(\vec{r}'), \\ &+ (\Delta E_j + iW_j) \varphi_j(\vec{r}) \\ &\approx \left(-\frac{\hbar^2}{2m_k} \nabla_r^2 + U''_H(r) + \Delta E''_j + iW''_j \right) \varphi_j(\vec{r}), \\ &= \varepsilon_j \varphi_j(\vec{r}), \quad \left(U''_H = \frac{m}{m_k} U \text{ and similarly for } \Delta E'' \text{ and } W'' \right), \end{aligned} \quad (2.3.14)$$

where $m_k = \left(1 + \frac{m}{\hbar^2 k} \partial U_x / \partial k \right)^{-1} \approx 0.7m$ is the k -mass⁵³, while

$$\Delta E_j(\omega) = \lim_{\Delta \rightarrow 0} \sum_{\alpha'} \frac{V_{\nu, \alpha'}^2(\omega - E_{\alpha'})}{(\omega - E_{\alpha'})^2 + (\frac{\Delta}{2})^2}, \quad (2.3.15)$$

and

$$W_j(\omega) = \lim_{\Delta \rightarrow 0} \sum_{\alpha'} \frac{V_{\nu, \alpha'}^2}{(\omega - E_{\alpha'})^2 + (\frac{\Delta}{2})^2}, \quad (2.3.16)$$

are the real and imaginary contributions to the self-energy calculated in second order of perturbation theory, where ω is the single-particle energy⁵⁴ (see Fig. 2.3.2; note that in this case $E_{\alpha'} = \epsilon_{\nu_2} + \hbar\omega_\alpha$).

⁵⁰see Bès, D. R. and Kurchan (1990)

⁵¹see Barranco et al. (2004)

⁵²see e.g. Brink, D. and Broglia (2005), Mahaux, C. et al. (1985) and references therein. See also Bernard and Giai (1981).

⁵³This is in keeping with the fact that the non-local component of the mean field can be parametrized at profit as $0.4E$, where $E = |(\hbar^2 k^2 / 2m) - \epsilon_F|$ (Perey and Buck (1962)) see also Sect.

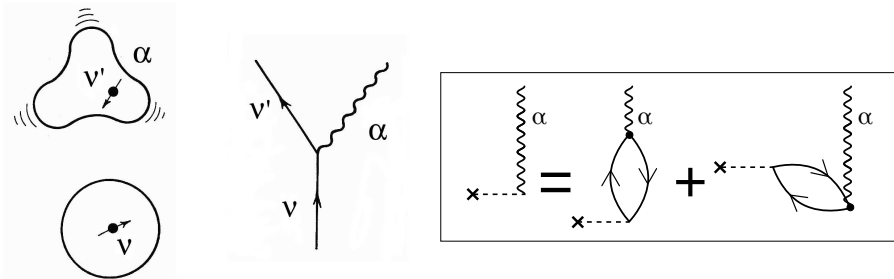


Figure 2.3.1: Schematic representation of the process by which a nucleon excites vibrations of the nuclear surface through the particle–vibration coupling vertex. In the inset, the graphical RPA dispersion relation which determines the properties of the collective mode α , e.g. the low–lying octupole vibration of ^{208}Pb , is displayed.

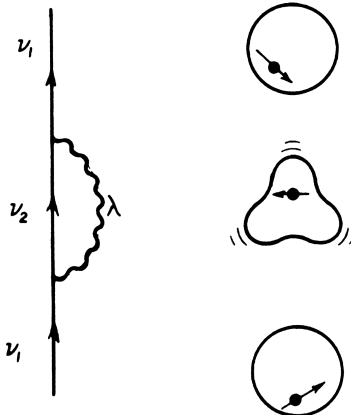


Figure 2.3.2: Self-energy (polarization, PO, see e.g. Fig. 7.2.2 and App. 5.10) graph renormalizing a single-particle. Time ordering leads to the corresponding correlation diagram (CO) (see e.g. Fig. 2.4.2 diagrams (e) and (f), as well as Figs. 5.4.1 and 5.5.2; within this context see also Brink, D. and Broglia (2005) Fig. 9.2 of this reference).

2.9.1.

⁵⁴Given a Hamiltonian H_c , the contribution to the energy in second order perturbation theory is

$$\Sigma_\nu(\omega) = \sum_{\alpha'} \frac{V_{\nu,\alpha'}^2}{\omega - E_{\alpha'}},$$

where $|\alpha'\rangle \equiv |n_a = 1, \nu'\rangle$ are the intermediate states which can couple to the initial single-particle state ν . Note that the expression above is not well defined, in that the energy denominator may vanish. As a rule, textbooks in quantum mechanics deal with such a situation by stating that accidental degeneracies are to be eliminated by diagonalization. Now, this is not a real solution of the problem, because it does not contemplate the case where there are many intermediate states with $E_{\alpha'} \approx \omega$. In other words, where the particle can decay into a more complicated (doorway-) states $|\alpha'\rangle$ (Feshbach (1958)), starting in the single-particle level ν of energy ω , without changing its energy (real process).

For many purposes ΔE can be treated in terms of an effective mass

$$m_\omega = m(1 + \lambda), \quad (2.3.17)$$

where

$$\lambda = -\frac{\partial \Delta E}{\partial \omega}, \quad (2.3.18)$$

is the *mass enhancement factor*, while

$$Z_\omega = m/m_\omega,$$

measures the single-particle content (discontinuity) at the Fermi energy.

Consequently, Eq.(2.3.14) can be rewritten as

$$\left(-\frac{\hbar^2}{2m^*} \nabla_r^2 + U'_H + iW'(\omega) \right) \varphi_j(\vec{r}) = \varepsilon_j \varphi_j(\vec{r}), \quad (2.3.19)$$

with

$$m^* = \frac{m_k m_\omega}{m}. \quad (2.3.20)$$

and $U'_H = (m/m^*)U$ and similarly for W' . Because $\lambda \approx 0.4$ (i.e. the dressed single-particle m_ω is heavier than the bare nucleon, as it has to carry a phonon along or, better, move in a cloud of phonons) and $m_k = 0.7m$, $m^*/m \approx 1$ and $Z_\omega \approx 0.7$. Furthermore, due to the fact that $\hbar\omega_\alpha \approx 2 - 2.5 \text{ MeV}$, the range of single-particle energy $E = \varepsilon - \varepsilon_F$ over which the particle-vibration coupling process displayed in Fig.2.3.2 is effective is $\approx \pm 2\hbar\omega_\alpha \approx 4 - 5 \text{ MeV}$ around the Fermi energy (see Figs.2.3.3 and 2.3.4)

It is of notice that ΔE_j (Eq.(2.3.15)) indicates the shift of the centroid of the "dressed" single-particle state due to the coupling to the doorway states, while $\Gamma = 2W$ measures the energy range over which the single-particle state spreads due to this coupling (see Fig.2.3.5). While a large number of states contribute to ΔE ("off-the-energy-shell process", i.e. intermediate, virtual processes in which energy is not conserved), only "on-the-energy-shell processes", that is processes which conserve energy, contribute to Γ . In fact

$$\lim_{\Delta \rightarrow 0} \frac{\Delta}{(\omega - E_{\alpha'})^2 + \left(\frac{\Delta}{2}\right)^2} = 2\pi\delta(\omega - E_{\alpha'}),$$

and

$$\Gamma(\omega) \approx 2\pi\bar{V}^2 n(\omega), \quad (2.3.21)$$

This is a typical dissipative (diffusion) process, and has to be solved by direct diagonalization (see Fig.2.3.5 and App. 5.4). Another way around, is to extend the function $\sum_v(\omega)$ into the complex plane ($E_{\alpha'} \rightarrow E_{\alpha'} + \frac{i\Delta}{2}$) thus *regularizing the divergence* through a coarse grain approximation, determining the finite contributions and then taking the limit for $\Delta \rightarrow 0$ (Eqs.(2.3.15) and (2.3.16)). The resulting complex potential (*optical potential* from the *complex dielectric function* of optics), parametrizes in simple terms the shift of the centroid of the single-particle state and its finite lifetime.

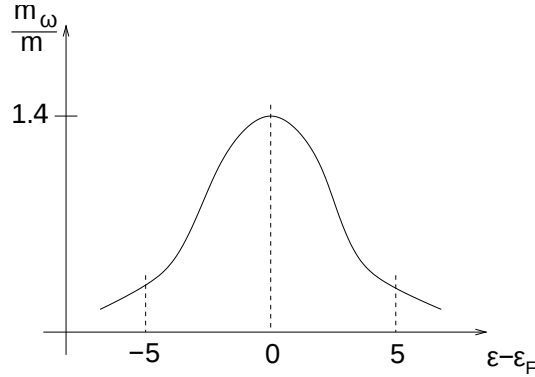


Figure 2.3.3: Schematic representation of the ω -mass as a function of the single-particle energy.

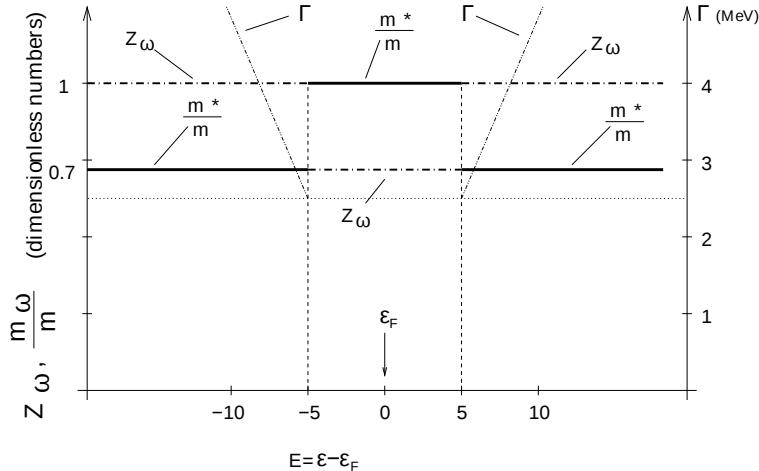


Figure 2.3.4: Schematic representation of the behaviour of m_ω/m , $Z_\omega = (m_\omega/m)^{-1}$ and Γ as a function of $E = \epsilon - \epsilon_F$.

where \bar{V}^2 is the average value of $V_{\nu,\alpha'}^2$, while

$$n(\omega) = \sum_{\alpha'} \delta(\omega - E_{\alpha'}), \quad (2.3.22)$$

is the density of energy-conserving states α' . Eq.(2.3.21) is known as *Fermi Golden rule*.

Assuming the distribution of single-particle levels is symmetric with respect to the Fermi energy,

$$\Delta E(\omega) = \lim_{\Delta \rightarrow 0} \sum_{\alpha'} \frac{V_{\nu_1 \alpha'}^2 (\omega - E_{\alpha'})}{(\omega - E_{\alpha'})^2 + \left(\frac{\Delta}{2}\right)^2} = 0 \quad (2.3.23)$$

as there are equally many states pushing the state down than up in energy (see

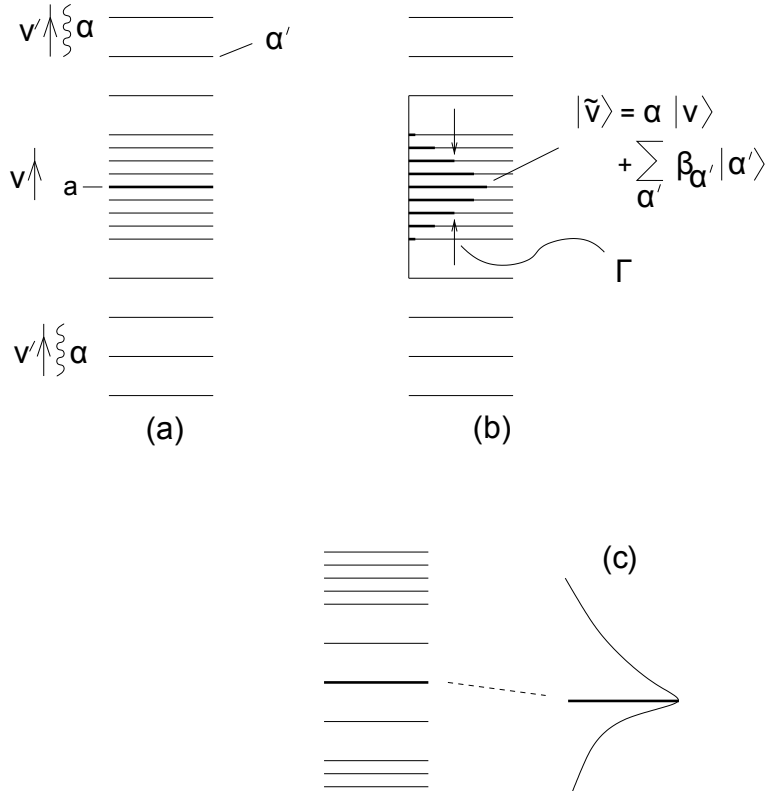


Figure 2.3.5: Schematic representation of the result of the diagonalization of H_c in a basis consisting of the single-particle states $|v\rangle$ and the $|\alpha'\rangle = |\nu', \alpha\rangle$ doorway states. In (c) we show a situation where there are more states $|\alpha'\rangle$ above $|a\rangle$ than below.

Fig.2.3.5).

In the above discussion, the imaginary potential was introduced as an approximation to the breaking of a stationary state into many, more complicated stationary states through the coupling to doorway states (Fig. 2.3.5(b)). This is the correct picture to describe the coupling of a nucleon moving in a single-particle state with more complicated configurations^{55,56}. However, such a description can become quite involved. On the other hand, to account for the change of the centroid energy and of its spreading width in terms of an *optical potential* $\Delta E + iW$ is very eco-

⁵⁵See however Caldeira and Leggett (1981), Caldeira and Leggett (1983) and refs. therein.

⁵⁶To be noted that if we spread the strength of a stationary quantal state in a number of doorway stationary states over an energy range Γ (of the order of few MeV in the case of the GDR), and set all components in phase at $t = 0$, they will essentially be out of phase at time $t = \tau = \hbar/\Gamma$. In other words, each component will behave independent of each other and the original correlated state, created at $t = 0$ with probability 1 essentially ceases to exist at $t = \tau$. This does not imply that each of the incoherent members of the original coherent state cannot γ -decay at a much later stage ($\Gamma_{\gamma_0}/\Gamma \lesssim 10^{-2}$), see Bortignon, P. F. et al. (1998). Discussions with B. Herskind on this issue are acknowledged.

nomic and convenient. In any case Γ measures the range of energy over which the "pure" single-particle state $|a\rangle$ spreads due to the coupling to the more complicated doorway states $|\alpha'\rangle$. In other words, a stationary state

$$\varphi_\nu(\vec{r}, t) = e^{i\omega t} \varphi_\nu(\vec{r}), \quad (2.3.24)$$

has a probability density

$$\int d^3 r |\varphi_\nu(\vec{r}_i t)|^2 = \int d^3 r |\varphi_\nu(\vec{r})|^2 = 1, \quad (2.3.25)$$

which does not depend on time. That is, if at $t = 0$, the probability that the particle is in a state ν is 1, it will have this probability also at $t = \infty$, implying an infinite lifetime. If however

$$\begin{aligned} \hbar\omega &= \varepsilon_\nu^{(0)} + \Delta E_\nu(\omega) + i\frac{\Gamma_\nu}{2}(\omega), \quad = \varepsilon_\nu + i\frac{\Gamma_\nu}{2}(\omega) \quad , (\varepsilon_\nu = \varepsilon_\nu^{(0)} + \Delta E_\nu) \\ \varphi_\nu(\vec{r}_i t) &= e^{i\frac{\varepsilon_\nu t}{\hbar}} e^{-\frac{\Gamma_\nu t}{2\hbar}}, \\ \int d^3 r |\varphi_\nu(\vec{r}_i t)|^2 &= e^{-\frac{\Gamma_\nu t}{\hbar}}, \end{aligned} \quad (2.3.26)$$

implying a lifetime for the single-particle state given by

$$\tau = \Gamma_\nu / \hbar. \quad (2.3.27)$$

One may ask, how is it possible that the coupling to complicate (but still simple) states like $|\alpha'\rangle = |n_\alpha = 1, \nu'\rangle$ made out of a nucleon in the state ν' and a one phonon state of quantum numbers α , can explain the damping of a single-particle state lying 8-10 MeV from the Fermi energy ε_F , where the density of levels is expected to be consistent? This is because the Hamiltonian given in Eq. (2.3.1) contains the basic physics needed to describe the dressed single-particle motion as far as surface modes are concerned (within this context see the discussion carried out following Eq. (2.3.13)). Couplings to more complicated states go through a hierarchy of couplings. In other words, the variety of couplings should first go through the coupling to states of type $|\alpha'\rangle$ which act as proper doorway states (see Fig. 2.3.6)⁵⁷. Summing up, in the nuclear case, the *doorway coupling provides the basic mechanism to break the single-particle strength, while higher-order couplings essentially fill in valleys* (see Fig. 2.3.7).

In the case of the $1s_{1/2}$ orbital of ^{40}Ca ($\varepsilon - \varepsilon_F = -8$ MeV), simple estimates⁵⁸ lead to $\bar{V}^2 \approx 0.3$ MeV for the coupling to an $L = 2$ phonon, and $n(\varepsilon_F) \approx 2$ MeV $^{-1}$. Consequently

$$\Gamma \approx 4$$
 MeV, (2.3.28)

in overall agreement with the experimental findings (see Fig. 2.3.8).

⁵⁷Feshbach (1958).

⁵⁸Mahaux, C. et al. (1985)

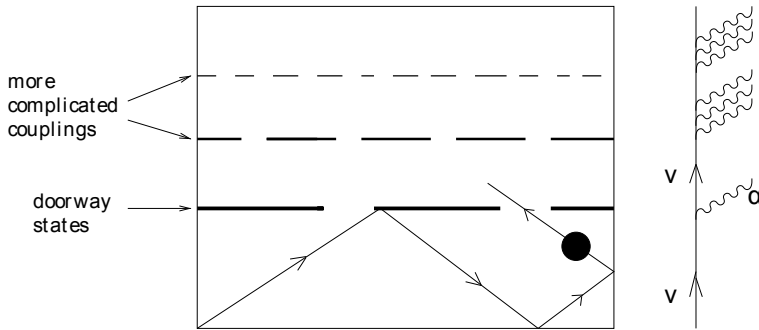


Figure 2.3.6: Schematic representation of the different levels of couplings leading to the damping of a single-particle state. It is essentially the first doorway coupling which controls the probability the ball (black dot) reflecting elastically on the walls of the box has to remain passed the first compartment.

The result given in Eq.(2.3.28) is a particular example of the general (empirical) result (see Fig. 2.3.4)⁵⁹.

$$\Gamma_{sp}(E) = \begin{cases} 0.5|E| & |E| > 5 \text{ MeV}, \\ 0 & E \leq 5 \text{ MeV}, \end{cases} \quad (2.3.29)$$

where

$$E = |\varepsilon - \varepsilon_F|. \quad (2.3.30)$$

2.3.2 Induced interaction

A nucleon close to the Fermi energy which, by bouncing inelastically off the nuclear surface excites a collective mode moving in the process to another, or remaining in the same state, has no other choices than to continue in such a state, or to reabsorb the vibration at a later instant of time (self-energy, Fig. 2.3.2). In the presence of another nucleon, the excited collective vibration by one nucleon may be absorbed by the second one (Fig. 2.3.9), the exchange of a vibration leading to an (induced) interaction.

Simple estimates of this induced interaction leads, in the case of ^{210}Pb , that is two neutrons above the $N = 126$ closed shell, to correlation energies for pairs of particles moving around it and coupled to angular momentum $J^\pi = 0^+$ of ≈ -1.5 MeV (see Fig. 2.3.10), when α is summed over the different multipolarities ($\lambda^\pi = 2^+, 3^-, 5^-$, label α in Fig. 2.3.9), and about half that value if one takes into account the fact that $Z_\omega \approx 0.7$ for each of the interacting particles. From this result one can conclude that the pairing interaction induced by the process depicted in Fig. 2.3.9, renormalizes in an important way the bare, $NN(^1S_0)$ -short range pairing interaction. This issue is taken up in detail later on, in particular in connection with

⁵⁹Bertsch et al. (1983)

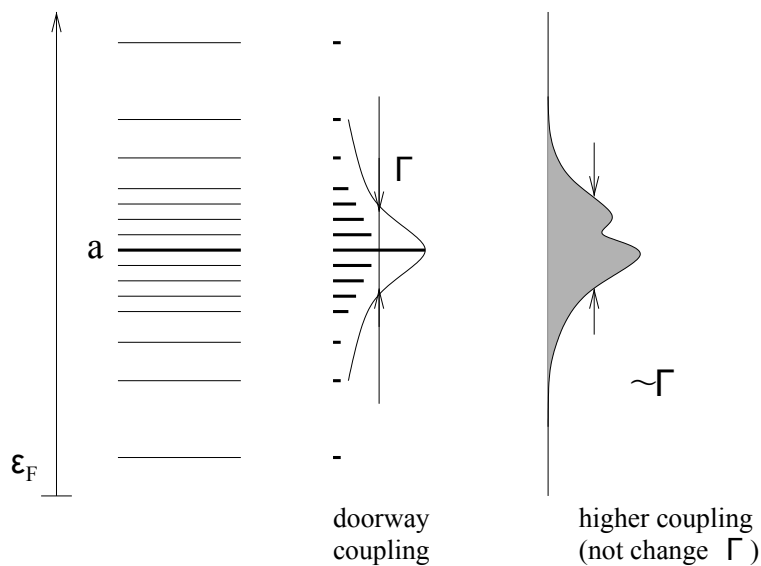


Figure 2.3.7: Schematic representation of the breaking of a single particle state $|a\rangle$ (heavy black horizontal line) through the coupling to doorway states ($|\alpha'\rangle = |n_\alpha = 1, \nu'\rangle$; thin horizontal lines) and eventually to increasingly more complicated (many-particle)–(many-hole) configurations.

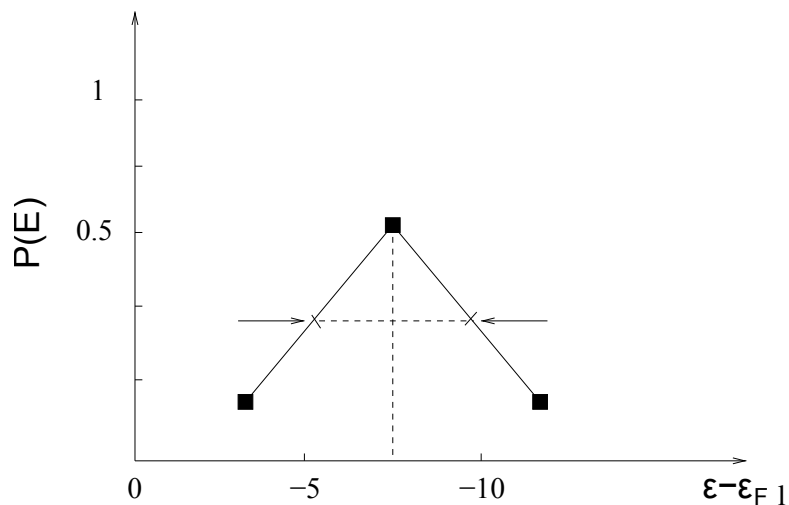


Figure 2.3.8: Schematic representation of the experimental strength function (solid squares) associated with the $2s$ state of ^{40}Ca . Also indicated is the full width at half maximum (FWHM) (after Mahaux, C. et al. (1985) Fig. 2.12).

exotic halo nuclei (see e.g. Fig. 2.9.1 and Sect. 3.6.1). Concerning nuclei lying along the stability valley, see next section.

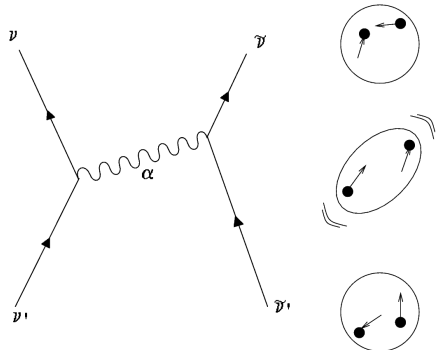


Figure 2.3.9: Schematic representation of the exchange of phonons between nucleons.

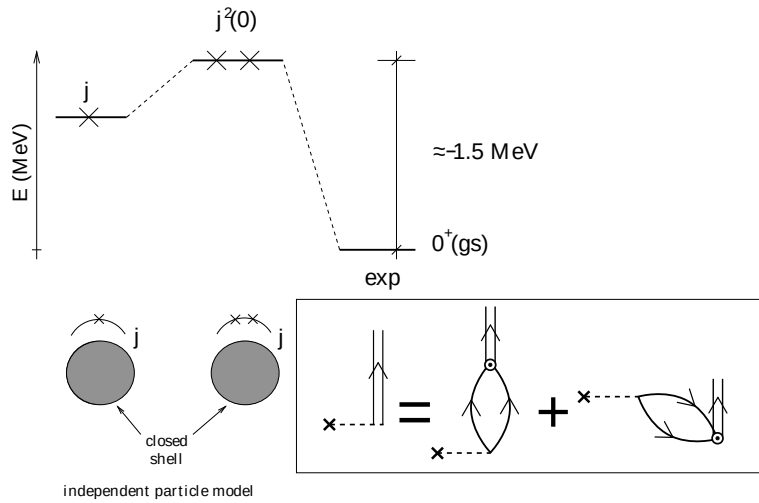


Figure 2.3.10: Schematic representation of the predictions of the independent particle model for one- and two-particles outside closed shell, in comparison with the experimental findings (e.g. for the case of ^{210}Pb , where $j = g_{9/2}$). In the inset, the graphical RPA dispersion relation of the monopole pair addition mode of ^{208}Pb , i.e. $|^{210}\text{Pb(gs)}\rangle$ is shown.

2.4 Well funneled nuclear structure landscape

Let us now return to the subject of the finite overlap existing between the elementary modes of nuclear excitation⁶⁰. That is, to the fact that one is working in a basis of states which contains already much of the physics one likes to describe, but which has the shortcoming of being overcomplete. An orthogonalization protocol, like a generalized Gram–Schmidt procedure, but leading to an effective field theory, where the different modes melt to some extent together, is called for.

A similar situation is found in the case of transfer processes in general, and of two–nucleon transfer in particular. One can work out the associated transfer amplitude by orthogonalizing, making use of second order perturbation theory, the single–particle wavefunctions of target and projectile. This can be done both within the semiclassical approximation (see App. 6.5, and Sect. 2.6) or the DWBA (Sect. 4.2 and 6.1; see also Sect. 4.6 in connection with weak coupled metallic superconductors and of the Josephson effect).

Because the coupling between elementary modes of excitation is proportional to their overlap, and in keeping with the fact that mean field theory is the natural starting point of nuclear structure and reaction calculations, overcompleteness of the basis is tantamount to the appearance of linear couplings between quasiparticles and collective modes⁶¹, which in the case of reactions corresponds to the recoil modes⁶².

Basis orthogonalization thus implies the diagonalization of the bare NN -interaction (four-point vertices) and of the associated particle-vibration coupling Hamiltonian H_c (three–point vertices). The rules to do so have been casted into a graphical effective field theory, namely the Nuclear Field Theory. In it, the free fields are to be calculated in the HF (HFB) approximation (particle (quasiparticle)) and in the RPA (QRPA) (vibrations). These elementary modes of excitation interact through the particle-vibration coupling vertices, while particles can also interact through four-point vertices (NN -bare interaction)⁶³.

The NFT rules for evaluating the effect of these couplings between fermions and bosons involve a number of restrictions concerning initial and intermediate states as compared with the usual rules of perturbation theory that are to be used in evaluating the effect of the original (bare) nucleon–nucleon interaction properly renormalized by the exchange of vibrations between nucleons. This is in keeping with the fact that the collective modes contain, from the start, the correlations arising from forwards and backwards going particle–hole ($\beta = 0$) as well as particle–particle ($\beta = +2$) and hole–hole ($\beta = -2$) bubbles, where β is the transfer quantum

⁶⁰And of which the particle–vibration coupling discussed above is a consequence.

⁶¹See Sect. 2.3 and App. 2.A in the case of surface modes and Sect. 2.7.4 in the case of the simultaneous treatment of surface and of pairing modes; see also Fig. 2.7.10.

⁶²See e.g. Figs. 2.1.2, 2.1.3 and 2.9.2–2.9.6. Also Figs. 6.5.1, 6.5.2, 5.1.1 and App. 2.C.

⁶³In connection with the reaction processes one finds again four–point (e.g. the proton-neutron interaction in the (p, d) reaction) and three–point vertices (e.g. particle-recoil coupling vertices).

number⁶⁴. Furthermore these (quasi) bosons are not elementary but composite fields, made out of pairs of fermions, and thus subject to the Pauli principle.

The general validity of NFT rules have been demonstrated by proving the equivalence existing, to each order of perturbation theory, between the many-body finite nuclear system propagator calculated in terms of Feynman diagrams involving only the fermionic degrees of freedom i.e. explicitly respecting Pauli in a complete and not overcomplete basis, also known as Feynman–Goldstone propagator, and the propagator constructed in terms of Feynman diagrams involving fermion and phonon degrees of freedom (NFT Feynman diagrams) in the case of a general two-body interaction and an arbitrary distribution of single-particle levels⁶⁵.

Concerning the actual embodiment of NFT one can recognize the practical difficulties of respecting the corresponding rules. This is in keeping with the fact that at present there is not a single bare, well behaved, low- k NN -force (eventually with $3N$ and higher order corrections) with which it is possible to generate a mean field (Eq. (2.2.3), also Fock potential see Fig. 2.2.1 (c)) to determine the single-particle states and, by introducing a periodic time-dependence with the constrain

$$\delta U(r) = \int d\mathbf{r} \delta\rho(r') v(|\mathbf{r} - \mathbf{r}'|), \quad (2.4.1)$$

calculate the collective modes associated with the variety of particle-hole ($\beta = 0$; density, spin, isospin, etc.) and pairing ($\beta = \pm 2$; monopole and multipole pair addition and pair subtraction) modes. If this was possible, one could then diagonalize, within the framework of NFT and to the desired order of perturbation, also infinite order, the resulting particle-vibration couplings, and thus obtain renormalized quantities which can be directly compared with the data. In other words, a real physical *ab initio* calculation could be done, resulting in a single, common ground state which, corrected with the corresponding ZPF lead eventually to the “exact” ground state concerning the degrees of freedom considered, as well as to properly dressed modes and interactions.

On the other hand, implementation of the NFT rules (renormalization)⁶⁶ have been carried out, making use of the bare Argonne v_{14} potential, and of Skyrme like SLy4⁶⁷ forces (or Saxon–Woods parametrizations and $m_k \approx 0.7m$) to determine the mean field and spin vibrational channels, and of multipole–multipole forces with self-consistent coupling constants for the variety of density vibrational channels.

The resulting predictions are, as a rule, able to provide, together with the specific reaction software, in particular COOPER and SINGLE, an overall account of “complete” sets of experimental data, obtained with the help of Coulomb, inelastic and one- and two-nucleon transfer data, able to map out the nuclear structure and reaction landscape⁶⁸. Similar, but more accurate results are obtained by freely

⁶⁴Bohr (1964).

⁶⁵Bès and Broglia (1975) and Bès et al. (1976a); see also Baranger (1969) and the lecture notes of McFarlane (1969).

⁶⁶Broglia et al. (2016).

⁶⁷Chabanat et al. (1997)

⁶⁸Idini et al. (2015); Idini, A. et al. (2014); Potel, G. et al. (2013a).

parametrising the bare potential so that the dressed particle reproduce experiment⁶⁹ (Table 2.4.1, last column). Summing up, the nuclear structure description given by the elementary modes of nuclear excitation approach within the framework of NFT, provides a unified description of the variety of observables. At the same time, each cross section or transition probability is connected to essentially all others.

To illustrate this point we bring together in this Section one- and two-particle transfer with the rest of the observables for the open-shell nucleus ^{120}Sn lying along the stability valley. From this example one can see that: 1) it is possible to predict, with few free parameters, most of them strongly constrained by empirical input, the experimental findings within a 10% level of accuracy; 2) the nuclear landscape, as it emerges from NFT based on elementary modes of excitation and of their interweaving through the particle-vibration coupling, is well funneled (Fig. 2.4.1, see also table 2.4.1), its minimum essentially coinciding with the global minimum resulting from the empirical renormalization⁷⁰ choice of basic quantities (m_k , strength bare pairing, properties of few low-lying collective ($p-h$) modes and pairing vibrations) An important proviso concerning the above parlance is that one considers a group of homogeneous nuclei as e.g. open shell spherical superfluid nuclei (like the Sn isotopes), or nuclei around closed shells (like $^{208,209,210}\text{Pb}$, ^{209}Bi , ^{210}Po , etc., or $^{10,11,12}\text{Be}$, $^{9,10,11}\text{Li}$, etc.)⁷¹. In connection with light exotic halo nuclei we refer to Sect. 2.9 of the present Chapter and to Sects. 5.2.2, 7.2 and 7.6.

Let us now comment on Fig. 2.4.1. In it, the root mean square deviations $\sigma(x)$ (see Table 2.4.1) between theoretical predictions and experimental values of the different structural properties which “completely” characterize ^{120}Sn are displayed. The calculations involve the island of open-shell superfluid nuclei $^{118,119,120,121,122}\text{Sn}$. The root mean square deviations are displayed in Fig. 2.4.1 (see also Table 2.4.1) as a function of the pairing coupling constant G (referred to $G_0 = 0.22$ MeV), the k -mass m_k ($(m_k)_0 = 0.7m$), the dynamical quadrupole deformation parameter β_2 ($(\beta_2)_0 = 0.13$) and in general of x (x_0), measured with respect to the minimum value $\sigma_{\min} = \sigma(x_{\min})$, displayed in the interval $0.5 \leq x/x_0 \leq 1.5$ and normalized according to $0 \leq N(\sigma(x) - \sigma_{\min}) \leq 1$. The curves represent (color online): the deviation of the pairing gap associated with the $h_{11/2}$ orbital ($\Delta_{h_{11/2}}(G/G_0)$ (solid black curve); $\Delta_{h_{11/2}}(m_k/(m_k)_0)$ (dotted blue curve); $\Delta_{h_{11/2}}(\beta_2/(\beta_2)_0)$ (dashed green curve)); the deviation of the quasiparticle spectrum ($E_{qp}(G/G_0)$ (dashed brown curve); $E_{qp}(\beta_2/(\beta_2)_0)$ (dash-dotted green curve)); the deviation of the $h_{11/2} \otimes 2^+$ multiplet splitting $E_{h_{11/2} \otimes 2^+}(\beta_2/(\beta_2)_0)$ (dash-dotted purple curve); the deviation of the centroid position of the $d_{5/2}$ strength function $S_{d_{5/2}}(\beta_2/(\beta_2)_0)$ (dash-dotted cyan curve); the deviation of the width of the $d_{5/2}$ strength function $S_{d_{5/2}}(\beta_2/(\beta_2)_0)$ (dash-dotted pink curve); the deviation of the quadrupole transition strength $B(E2)(\beta_2/(\beta_2)_0)$ (dashed orange curve). For an overview see⁷² Fig. 2.10.1. The remarkable feature of Fig. 2.4.1 is the fact that, in spite of the fluctua-

⁶⁹Barranco et al. (2017). This approach parallels renormalization in QED (see Sect. 7.6).

⁷⁰See Sect. 7.5.

⁷¹Within this context we refer to the conclusions of Idini et al. (2015).

⁷²For details see Idini et al. (2015).

tions of the results typical of finite many–body systems, they clearly define a funnel in which all minima fall within a narrow window of x/x_0 values (1 ± 0.2). This is a novel and unexpected result, which can be considered as an emergent property of a description of structure and reactions carried out in a basis of elementary modes of excitations, interacting through the PVC and PRC vertices according to the NFT rules.

The concept of a well funneled energy landscape is easy to understand in the case in which the number of particles $N \rightarrow \infty$ (thermodynamic limit). For example, a swing will have a very simple and well funneled potential energy landscape. A similar concept which still retains the classical viewpoint, but now referred to the free energy of large molecules, has been used in an attempt to describe protein folding⁷³. One has hypothesized that the results of an all atom, explicit solvent classical molecular dynamic simulations can be interpret in terms of a somewhat rugged, but still well funneled free energy landscape.

When we see such a behaviour in the nuclear case, even not so well defined, and somehow imperfect, we recognize that the nucleus is, after all, not macroscopic. Concepts strictly valid for $N \rightarrow \infty$ are strongly renormalized by quantal finite size effects, in particular zero point fluctuations (ZPF, Fig. 2.4.2)⁷⁴.

In other words, it is likely that the “imperfect” nature of the nuclear structure landscape funnel, an example of which is shown in Fig. 2.4.1, embodies more accurately the physics of quantal many–body systems than that of a smooth, more pedagogical construct essentially based on potential energy, even with the entropic contribution (free energy). This is in keeping with the fact that the interaction terms (potential energy) of the Hamiltonian contain the last vestiges of Newton’s conception of force or, causation, being thus too much anchored to classical mechanics⁷⁵.

Within this context we refer to Fig. 2.4.2, and to the fact that the ground state (nuclear vacuum) contains all the physics of the system in terms of virtual processes. This is demonstrated by the fact that acting on the system with the variety of probes available in the laboratory one obtains as on–shell final states, which eventually can be observed with the help of the appropriate detectors and setups,

⁷³Wolynes (2016); Wolynes et al. (2012); see also cover figure of the issue of PNAS in which this reference was published.

⁷⁴This nuclear result in turn, may be used at profit to shed light into the physics which is at the basis of protein folding. These systems are after all quantal systems, and the associated quantal fluctuations are likely to play an important role in fleeting transition states. The fact that average values and shapes of the transit–time distributions agree well with the simplest one–dimensional theory may only reflect the large uncertainties of the tunneling probabilities, small changes in the barrier’s parameters compensating for the lack of quantal phenomena, let alone the fact that being most high–dimensional models, as well as real processes, “sloppy”, their behavior depend on very few parameters (collective variables (CV), see Buchanan (2015), Transtrum et al. (2015), and references therein). It is unlikely that one or few of them are not related to quantal fluctuations. This is particularly true if one considers a NMR chemical shift biased molecular dynamic simulation, in keeping with the fact that NMR, based on the precession of nuclear spins is by its essence, a quantal phenomenon. Within this context one is reminded of α – and exotic–decay (see e.g. Ch. 7 of Brink, D. and Broglia (2005) and references therein).

⁷⁵Born (1948) pp. 95,103; Pais (1986) p 258.

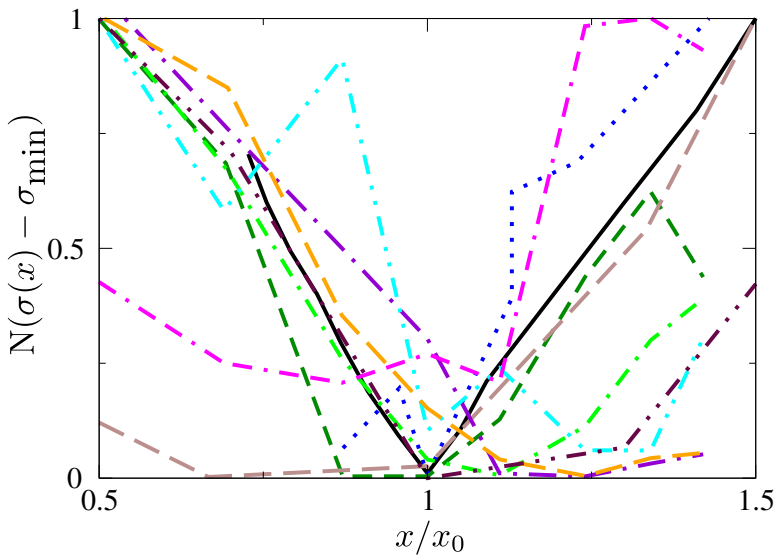


Figure 2.4.1: (Color online) Root mean square deviations $\sigma(x)$ (see Table 2.4.1) between theoretical predictions and experimental values of the different structural properties which “completely” characterize the open-shell nucleus ^{120}Sn (Idini et al. (2015)). After Broglia et al. (2016).

the variety of dressed (renormalized) elementary modes of excitation of the nucleus under study. In particular, diagrams **(b)**, **(c)** of Fig 2.4.2 describe inelastic and two-nucleon transfer processes while diagrams **(d)**–**(f)** portray one-nucleon transfer reactions.

In all orders in the particle vibration coupling vertex ((PVC), solid dot), starting from second order (graph (f)), NFT diagrams take care of the Pauli principle acting between the quasiparticles considered explicitly (continuous curves) and those participating in the modes (double wavy lines), as well as between modes. As a consequence, self energy processes based on pure or little collective two quasiparticle excitations are screened out or eliminated.

2.5 Non-orthogonality

Let us now consider a system based on a closed shell nucleus, namely two protons moving around ^{208}Pb . The ground state of $^{210}_{84}\text{Po}_{126}$ can be viewed as the proton pair addition mode of the doubly closed shell nucleus $^{208}_{82}\text{Pb}_{126}$, mode displaying $J^\pi = 0^+$ and $\beta = +2$ (transfer-) quantum numbers. Within this framework $^{209}_{83}\text{Bi}_{126}$ is expected to be a *bona fide* proton single-particle system ($\beta = +1$), in which the $g_{7/2}, d_{5/2}, h_{11/2}, d_{3/2}$ and $s_{1/2}$ valence orbitals are occupied, the odd proton occupying, in the ground state, a substate of the $h_{9/2}$ orbital.

This picture can be specifically probed through one-proton stripping and pick

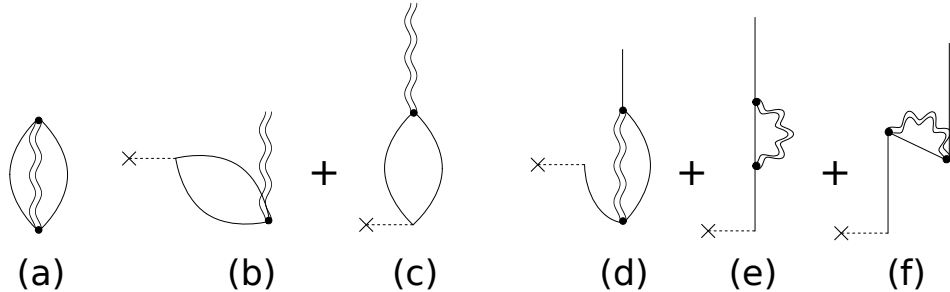


Figure 2.4.2: Schematic representation of the NFT(s+r) diagrams at the basis of the characterization of a superfluid nucleus like e.g. ^{120}Sn . (a) Nuclear structure (NFT(s)). Zero point fluctuations (ZPF) characterizing the nucleus ground state. Continuous lines describe quasiparticle (qp) states, double wavy curves correlated two quasiparticle ($2qp$) vibrational modes. Because $\alpha_\nu^\dagger = U_\nu a_\nu^\dagger - V_\nu a_\nu$ these modes encompass both particle-hole (ph) like vibrations, e.g. surface quadrupole vibrations, as well as correlated (pp) and (hh) monopole and multipole pairing vibrations. Intervening with an external field (cross followed by dashed line) one can excite (b) and (c) multipole (ph -like; inelastic scattering) and pairing ($2p$ -like) vibrations (two-particle transfer) as well as (d)-(f) single-quasiparticle states.

Observables	SLy4	$d_{5/2}$ shifted	Opt. levels
Δ	10 (0.7%)	10 (0.7 %)	50 (3.5 %)
E_{qp}	190 (19%)	160 (16%)	45 (4.5 %)
Mult. splitt.	50 (7%)	70 (10%)	59 (8.4 %)
$d_{5/2}$ strength (centr.)	200 (20%)	40 (4%)	40 (4%)
$d_{5/2}$ strength (width)	160 (20%)	75 (9.3%)	8 (1%)
$B(E2)$	1.4 (14%)	1.34 (13%)	1.43 (14%)
$\sigma_{2n}(p, t)$	40 (2%)	40 (2%)	40 (2%)

Table 2.4.1: Root mean square deviation σ between the experimental data and the theoretical values expressed in keV for the pairing gap, quasiparticle energies, multiplet splitting, centroid and width of the $5/2^+$ low-lying single-particle strength distribution (Fig. 5.2.3). In single-particle units B_{sp} for the γ -decay ($B(E2)$ transition probabilities) and in mb for $\sigma_{2n}(p, t)$ (Fig. 7.4.1). In brackets the ratio $\sigma_{rel} = \sigma/L$ between σ and the experimental range L of the corresponding quantities: 1.4 MeV (Δ), 1 MeV (E_{qp}), 700 keV (mult. splitting), 1 MeV ($d_{5/2}$ centroid), 809 keV (=1730–921) keV ($d_{5/2}$ width), 10 B_{sp} ($B(E2)$), 2250 μb ($\sigma_{2n}(p, t)$)) is given (for details see Idini et al. (2015), also Fig. 2.10.1). Columns 2,3, and 4 contain the results of NFT calculations making use of bare single-particle levels from Hartree–Fock with Sly4, same but for a 600keV shift towards the Fermi energy of the $\epsilon_{d_{5/2}}$ orbital, and optimal values of ϵ_j for all valence levels so that the dressed quasiparticle states provide the best fit to that data, respectively.

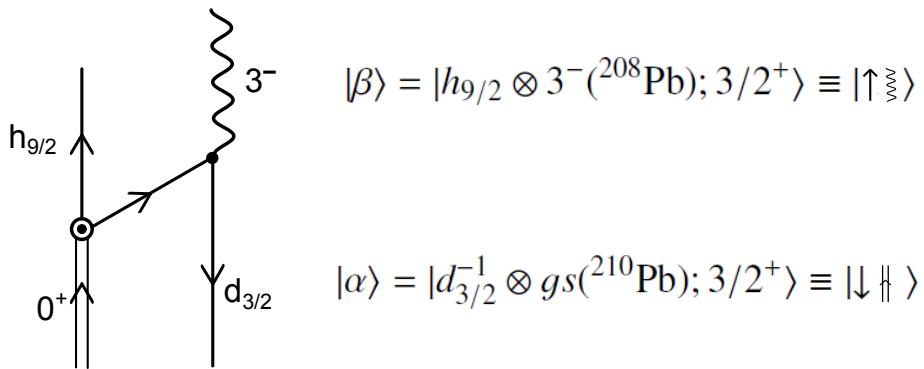


Figure 2.5.1: NFT diagram describing one of the most important processes coupling the $2p - 1h$ states $|\alpha\rangle$ and $|\beta\rangle$ (see Eqs. (2.5.1) and (2.5.2)), product of bare elementary modes of excitation consisting in the ${}^{208}\text{Pb}$, 0^+ pair addition mode and the $d_{3/2}$ proton hole state, and of the lowest octupole vibration of ${}^{208}\text{Pb}$ and of a proton moving in the $h_{9/2}$ orbital.

up reactions, e.g. with the help of ${}^{210}\text{Po}(t, \alpha){}^{209}\text{Bi}$ and ${}^{208}\text{Pb}({}^3\text{He}, d){}^{209}\text{Bi}$ transfer processes⁷⁶. The pick-up reaction cross section is, in the case of e.g. the states $1/2^+(s_{1/2})$ and $11/2^-(h_{11/2})$, essentially consistent with a single peak displaying full $(2j + 1)$ occupancy. On the other hand, two $3/2^+$ states with essentially equal strength and exhausting the associated $(2j + 1 (= 4))$ strength are observed. Furthermore, the four peaks mentioned above are essentially not excited in the stripping process (see Table 2.5.1). In an attempt to further clarify the structure of the two $3/2^+$, use is made of the inelastic process ${}^{209}\text{Bi}(d, d')$. Both states are excited in inelastic scattering, the associated angular distributions revealing the octupole character of such excitation (Tables 2.5.2 and 2.5.3).

In keeping with the fact that the same experiment reveals a multiplet (septuplet) of states with centroid around 2.6 MeV and with summed $L = 3$ inelastic cross section consistent with that of the lowest collective (2.615 MeV, $B(E3)/B_{sp} \approx 32$) octupole vibration of ${}^{208}\text{Pb}$, one can posit that the two $3/2^+$ states are a linear combination of the unperturbed (two particles)-(one hole) ($2p-1h$) states,

$$|\alpha\rangle = |d_{3/2}^{-1} \otimes gs({^{210}\text{Pb}}); 3/2^+\rangle, \quad (2.5.1)$$

and

$$|\beta\rangle = |h_{9/2}^- \otimes 3^-({^{208}\text{Pb}}); 3/2^+\rangle. \quad (2.5.2)$$

Because these states lie very close in energy they mix. According to NFT, the most important contribution to this mixing arises from the process given in Fig. 2.5.1.

⁷⁶It is of notice that in the present case, as well as in Sect. 2.7, and at variance with the rest of the monograph, use will be made, for the sake of being didactic, of spectroscopic factors (see end of Sect. 3.1 as well as App. 5.10).

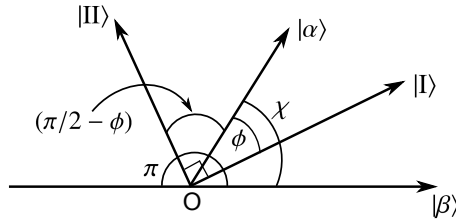


Figure 2.5.2: Schematic representation of the $3/2^+$ states entering the NFT calculation of the process displayed in Fig. 2.5.1. The basis state $|\alpha\rangle$ carries the full (t, α) transfer strength (tr) σ^{tr} , while the basis state $|\beta\rangle$ the full octupole (oct) strength σ^{oct} (see Tables 2.5.1–2.5.3). The overlap between these states is $\cos \chi$. The physical states obtained through the (Feynman) diagrammatic “orthogonalization process” are denoted $|I\rangle$ and $|II\rangle$ (see Eqs. (2.5.3) and (2.5.4)).

	$E_x(\text{MeV})$	$S(t, \alpha)(2j + 1)$	$S(^3\text{He}, d)$
$3/2^+$	2.49	$1.8 \pm 0.3 (4)$	< 0.01
$3/2^+$	2.95	$2.2 \pm 0.3 (4)$	< 0.01
$1/2^+$	2.43	$1.8 (2)$	< 0.02
$11/2^-$	3.69	$10 (12)$	< 0.05

Table 2.5.1: Single-particle strength associated with the transfer reactions $^{210}\text{Po}(t, \alpha)^{209}\text{Bi}$ and $^{208}\text{Pb}(^3\text{He}, d)^{209}\text{Bi}$ (see Bortignon, P. F. et al. (1977)).

The resulting physical (mixed) states can be written as,

$$|I\rangle = -0.53|\alpha\rangle + 0.76|\beta\rangle, \quad (2.5.3)$$

and

$$|II\rangle = 1.02|\alpha\rangle + 0.80|\beta\rangle, \quad (2.5.4)$$

as resulting from the calculation of the diagram displayed in Fig. 2.5.1 to all orders of perturbation, with the help of Brillouin–Wigner perturbation theory (diagonalization of the corresponding effective Hamiltonian⁷⁷, see Sect. 2.7.4).

Let us now calculate the overlap $O = \langle \alpha | \beta \rangle$ between the basis states $|\alpha\rangle$ and $|\beta\rangle$, that is $O = \cos \chi$ (see Fig. 2.5.2). Following this figure one can write,

$$\sqrt{\sigma_I^{tr}} = \cos \phi; \quad \sqrt{\sigma_{II}^{tr}} = \cos \left(\frac{\pi}{2} - \phi \right) = \sin \phi, \quad (2.5.5)$$

where

$$\sigma^{tr} = \sigma_I^{tr} + \sigma_{II}^{tr} = 1, \quad (2.5.6)$$

in keeping with the fact that the absolute cross sections of the states $|I\rangle$ and $|II\rangle$ are normalized in terms of the total cross section.

⁷⁷See p. 316 Bortignon, P. F. et al. (1977) and references therein.

	$E_x(\text{MeV})$	$\frac{\sigma(^{209}\text{Bi}(9/2^-;gs) \rightarrow ^{209}\text{Bi}(3/2^+;E))}{\sigma(^{208}\text{Pb}(gs) \rightarrow (3^-;2.615 \text{ MeV}))}$
3/2	2.49	0.042 ± 0.003
3/2	2.95	0.011 ± 0.002

Table 2.5.2: The total inelastic cross section σ^{oct} associated with the lowest octupole vibrational state of ^{208}Pb can be written in terms of that associated with a single magnetic substate σ' as $\sigma_{3^-}^{oct} = 7\sigma'$. That associated with the multiplet $(h_{9/2} \otimes 3^-)_{J^+}(J = 3/2 - 15/2)$ as $\sigma_{3^-}^{oct} = 70\sigma'$, in keeping with the fact that the $h_{9/2}$ state has 10 magnetic substates. Thus, the strength associated with the 3/2 channel is $4/70=0.057$ to be compared with the observed summed (percentage) strength $0.053 \pm 0.005 (= (0.042 \pm 0.003) + (0.011 \pm 0.002))$ associated with the 2.45 MeV and the 2.95 MeV 3/2 $^+$ states; see Bortignon, P. F. et al. (1977) Table 4.11.

	$E_n(\text{MeV})$		$\frac{\sigma(h_{9/2} \rightarrow 3/2^+)}{\sigma(0^+ \rightarrow 3^-)} (\%)$		$S(t, \alpha)$		$S(^3\text{He}, d)$	
	Theory	Exp	Theory	Exp	Theory	Exp	Theory	Exp
3/2	2.480	2.494	3.76	4.2 ± 0.3	1.83	1.8 ± 0.3	0.02	< 0.01
3/2	3.125	2.95	1.56	1.1 ± 0.2	2.25	2.2 ± 0.3	10^{-5}	< 0.01

Table 2.5.3: Summary of NFT predictions concerning the structure of the two lowest 3/2 $^+$ state of ^{209}Bi , in comparison with the experimental data (see Table 4.7 of Bortignon, P. F. et al. (1977)).

In the same way

$$\sqrt{\sigma_I^{oct}} = \cos(\chi - \phi) = \cos \chi \cos \phi + \sin \chi \sin \phi, \quad (2.5.7)$$

and

$$\sqrt{\sigma_{II}^{oct}} = \cos \left(\pi - \left(\frac{\pi}{2} - \phi + \chi \right) \right) = -\cos \left(\frac{\pi}{2} + (\phi - \chi) \right) = \sin \phi \cos \chi + \sin \chi \cos \phi. \quad (2.5.8)$$

Thus

$$\sqrt{\sigma_I^{oct}} = \cos \chi \sqrt{\sigma_I^{tr}} + \sin \chi \sqrt{\sigma_{II}^{tr}}, \quad (2.5.9)$$

and

$$\sqrt{\sigma_{II}^{oct}} = -\cos \chi \sqrt{\sigma_{II}^{tr}} + \sin \chi \sqrt{\sigma_I^{tr}}. \quad (2.5.10)$$

Multiplying the above relations by $\sqrt{\sigma_I^{tr}}$ and $\sqrt{\sigma_{II}^{tr}}$ respectively one obtains,

$$\sqrt{\sigma_I^{tr} \sigma_I^{oct}} = \cos \chi \sigma_I^{tr} + \sin \chi \sqrt{\sigma_I^{tr} \sigma_{II}^{tr}}, \quad (2.5.11)$$

and

$$\sqrt{\sigma_{II}^{tr}\sigma_{II}^{oct}} = -\cos\chi\sigma_{II}^{tr} + \sin\chi\sqrt{\sigma_I^{tr}\sigma_{II}^{tr}}, \quad (2.5.12)$$

which, upon subtraction leads to the expression of the overlap

$$\cos\chi = \frac{\sqrt{\sigma_I^{tr}\sigma_I^{oct}} - \sqrt{\sigma_{II}^{tr}\sigma_{II}^{oct}}}{\sigma_I^{tr} + \sigma_{II}^{tr}}. \quad (2.5.13)$$

Making use of the values of Tables 2.5.1–2.5.3 (see also Fig. 2.7.11 (e) last column labeled *experiment*)⁷⁸ one obtains

$$O = \cos\chi = \frac{\sqrt{1.8 \times 4.2} - \sqrt{2.2 \times 1.1}}{4} = 0.298 \quad (2.5.14)$$

Regarding the NFT results related to the above questions we refer to Sect. 2.7.4 as well as to App. 2.B (Sect. 2.B.2). In what follows we provide simple, necessarily qualitative estimates making use of the relations⁷⁹.

$$\begin{aligned} \langle I|I\rangle &= (-0.53)^2 + (0.76)^2 - 2 \times 0.53 \times 0.75 O = 1, \\ \langle III|II\rangle &= (1.02)^2 + (0.80)^2 + 2 \times 1.02 \times 0.80 O = 1, \end{aligned}$$

and $\langle I|II\rangle = -0.53 \times 1.02 + 0.76 \times 0.80 + (-0.53 \times 0.80 + 0.76 \times 1.02) O = 0$ leading to $O = -0.18, -0.42$ and -0.19 respectively and, thus, to the average value of -0.26 . Of course, one can hardly expect to obtain the sign to agree with that of the NFT expression, as it is associated with a free choice of the axis of references (Fig. 2.5.2). Note also the fact that the quantities σ appearing above are well defined, while $\sqrt{\sigma}$ is indetermined by an overall sign.

2.6 Coupling between intrinsic and relative motion

In what follows, we consider the reaction



within the framework of the semiclassical approximation⁸⁰. In the center-of-mass system, the total Hamiltonian may be written

$$H = T_{aA} + H_a + H_A + V_{aA} = T_{bB} + H_b + H_B + V_{bA}, \quad (2.6.2)$$

in keeping with energy conservation. Within this context other, mixed, representations are possible.

⁷⁸See Table 4.7 of Bortignon, P. F. et al. (1977).

⁷⁹see Tables 4.5 and 4.6 Bortignon, P. F. et al. (1977).

⁸⁰Broglia and Winther (2004) and references therein.

One then solves the time-dependent Schrödinger equation

$$i\hbar \frac{\partial \Psi}{\partial t} = H\Psi, \quad (2.6.3)$$

with the initial conditions that the nuclei a and A are in their ground states, and where the relative motion is described by a narrow wavepacket of rather well defined impact parameter and velocity.

We expand Ψ on (stationary) channel wavefunctions

$$\Psi = \sum_{\beta} c_{\beta} (\langle \mathbf{r}_{\beta} - R_{\beta} \rangle) \Psi_{\beta} e^{-iE_{\beta}t/\hbar}, \quad (2.6.4)$$

where

$$\Psi_{\beta}(t) = \Psi_m^b(\xi_b) \Psi_n^B(\xi_B) \exp(i\delta_{\beta}). \quad (2.6.5)$$

The index β labels both the partition of nuclei (b, B) as well as the quantal states of the two nucleons (m, n) .

The phase δ_{β} is defined as

$$\delta_{\beta} = \frac{1}{\hbar} \left\{ m_{\beta} \mathbf{v}_{\beta}(t) \cdot (\mathbf{r}_{\beta} - \mathbf{R}_{\beta}(t)) - \int_0^t \left(U_{\beta}(R_{\beta}(t')) - \frac{1}{2} m_{\beta} \mathbf{v}_{\beta}(t')^2 \right) dt' \right\}, \quad (2.6.6)$$

where an extra phase has been added to eliminate, as far as possible, the diagonal matrix elements in the coupled equations. The phase factor $\exp(i\delta_{\beta})$ acting on the channel wavefunction is essentially a Galilean transformation (see jagged “phonon” in the NFT reaction diagrams displayed in Figs. 5.1.1 (one-particle transfer) and Figs. 6.5.1 and 6.5.2 (two-particle transfer); see also Figs. 2.1.2, 2.1.3 and 2.9.2–2.9.6).

The function c_{β} can be expressed as

$$c_{\beta} = a_{\beta}(t) \chi_{\beta}(\mathbf{r}_{\beta} - \mathbf{R}_{\beta}(t), t) \quad (2.6.7)$$

product of an amplitude a_{β} of asymptotic values ($t = \pm\infty, 0$ or 1), and a normalized shape (wavepacket) function, $R_{\beta}(t)$ being the relative motion elastic trajectory.

Properly combining the above quantities and making use of the time-dependent Schrödinger equation one obtains

$$i\hbar \sum_{\beta} \dot{a}_{\beta}(t) \langle \Psi_{\xi} | \Psi_{\beta} \rangle_{\mathbf{R}_{\xi\gamma}} e^{iE_{\beta}t/\hbar} = \sum_{\gamma} \langle \Psi_{\xi} | V_{\gamma} - U_{\gamma}(r_{\gamma}) | \Psi_{\gamma} \rangle_{\mathbf{R}_{\xi\gamma}} a_{\gamma}(t) e^{iE_{\beta}t/\hbar}, \quad (2.6.8)$$

where

$$f(\mathbf{R}) = \langle \Psi_{\xi} | V_{\gamma} - U_{\gamma}(r_{\gamma}) | \Psi_{\gamma} \rangle_{\mathbf{R}} \quad (2.6.9)$$

are the formfactors, and

$$g(\mathbf{R}) = \langle \Psi_{\xi} | \Psi_{\beta} \rangle_{\mathbf{R}} \quad (2.6.10)$$

the *overlaps between the intrinsic channel wavefunctions*.

The coupled equations can be written in a more compact form by introducing the adjoint channel wavefunction

$$\omega_\xi = \sum_\gamma g_{\xi\gamma}^{-1} \Psi_\gamma, \quad (2.6.11)$$

where g^{-1} is the reciprocal of the *overlap matrix*

$$g_{\xi\gamma} = \langle \Psi_\xi | \Psi_\gamma \rangle. \quad (2.6.12)$$

Thus

$$(\omega_\xi, \Psi_\beta) = \delta(\xi, \beta), \quad (2.6.13)$$

and

$$i\hbar \dot{a}_\beta(t) = \sum_\gamma \langle \omega_\beta | V_\gamma - U_\gamma | \Psi_\gamma \rangle_{\mathbf{R}_{\beta\gamma}} e^{(E_\beta - E_\gamma)t/\hbar} a_\gamma(t). \quad (2.6.14)$$

Consequently, the proper tunneling Hamiltonian is obtained by a *basis orthogonalization process*. These coupled equations, being first order in time, can be solved knowing the initial conditions at time $t = -\infty$,

$$a_\gamma(-\infty) = \delta(\gamma, \alpha), \quad (2.6.15)$$

where α labels the entrance channel, that is, the nuclei a and A in their ground state. The cross section for the reaction $\alpha \rightarrow \beta$ is

$$\left(\frac{d\sigma}{d\Omega} \right)_{\alpha \rightarrow \beta} \sim |a_\beta(t = +\infty)|^2. \quad (2.6.16)$$

2.7 Nuclear Field Theory for pedestrians

Nuclear Field Theory (NFT) was tailored after Feynman's graphical version of quantum electrodynamics (QED)⁸¹. It is then natural that in discussing NFT analogies with QED will be recurrent. Arguably, as a consequence of special relativity which put an end to the concept of ether, the field-free and matter-free vacuum was rightly considered as *bona fide* empty space. The advent of quantum mechanics changed this situation, the vacuum becoming populated. In quantum mechanics an oscillator, for example, cannot be at rest. The oscillatory nature of the radiation field requires zero point fluctuations (ZPF) of the electromagnetic fields in the vacuum state of lower energy. The occupation of the negative kinetic energy electron

⁸¹“The diagrams were intended to represent physical processes and the mathematical expressions to describe them... I would see electrons going along, being scattered at one point... emitting a photon and the photon goes over there... I thought that if they really turn out to be useful it would be fun to see them in the pages of Physical Review” R. P. Feynman.

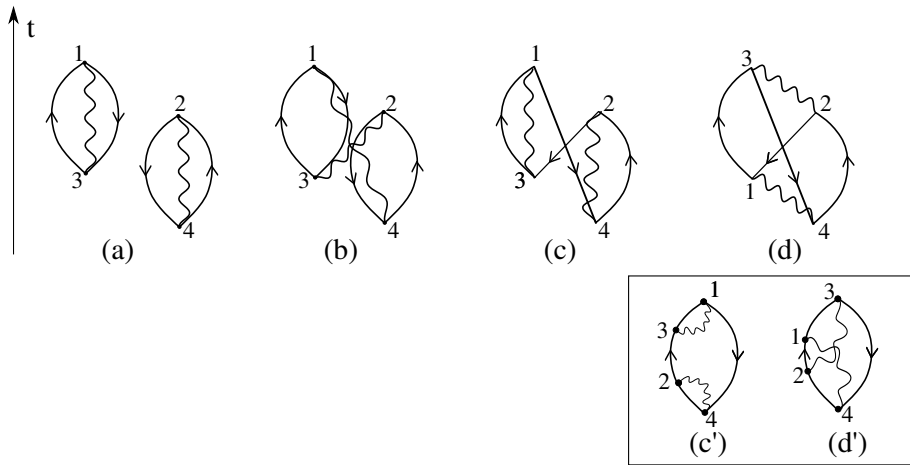


Figure 2.7.1: Oyster diagrams describing the correlation of the nuclear ground state associated with the ZPF of collective particle–hole–like excitations. In (a) we show two of such diagrams. In (b) and (c) we display a symmetrized (boson exchange), and antisymmetrized (fermion exchange) correction to (a), while (d) contains a simultaneous boson and fermion exchange. In all the diagrams shown, only ground state correlation vertices are present. They are connected with the $Y_{k_i}^\alpha$ –components ($\epsilon_k > \epsilon_F$, $\epsilon_i \leq \epsilon_F$) of the RPA wavefunction describing the collective mode (wavy line). While this is so for any time ordering, i.e., the sequence with which the particle-vibration coupling vertex (black dot) appear in the case of the processes shown in (a) and (b), this is not the case in connection with processes shown in (c) and (d) as can be seen from the corresponding diagrams (c') and (d') shown in the inset. Because of Pauli principle between particles (holes) present and those involved in the collective modes, the harmonic approximation has to be corrected. This is diagrammatically reflected by the presence of scattering vertices.

states and the subsequent calculation of the cross section for pair creation by photons, contributed another step in the understanding of the QED vacuum, let alone the Lamb shift⁸².

When the fields are expressed in terms of creation and annihilation operators, the interaction between fermion and boson fields is proportional to the product of two fermion creation or destruction operator a^\dagger or a , and of one boson operator Γ^\dagger or Γ : e.g. $a_\nu^\dagger a_\nu \Gamma_\alpha^\dagger$, (see Fig. 2.7.1). That is, bilinear in the fermion fields and linear in the boson fields.

⁸²In high energy collisions and accelerator laboratories some of the original beam energy can be consumed by ripping electron-positron pairs out of the vacuum (Bruce et al. (2007)).

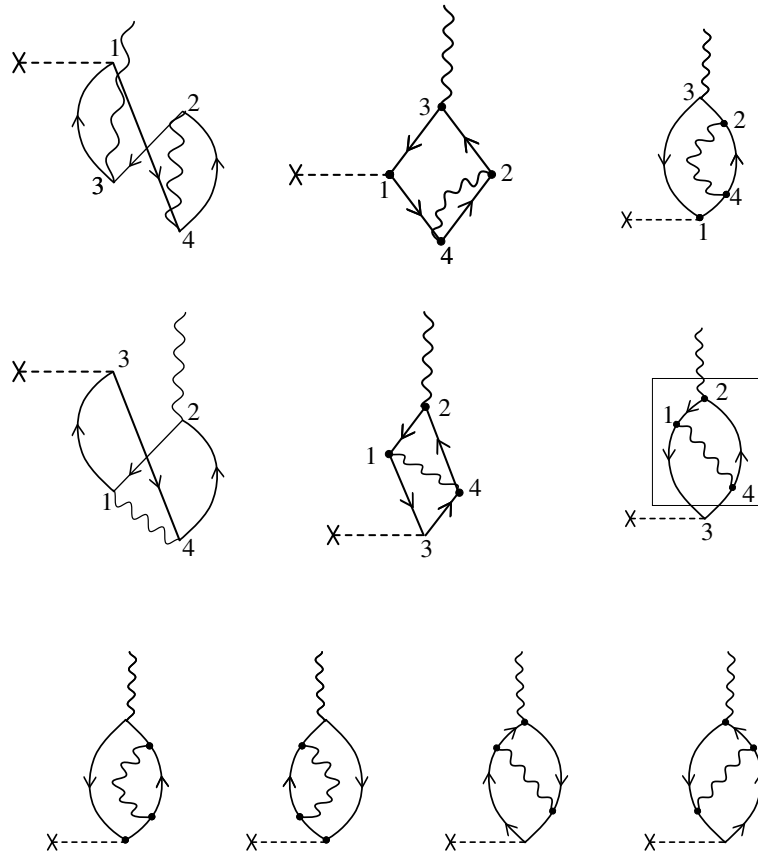


Figure 2.7.2: Some of the possible outcomes resulting from acting with an external single-particle field, i.e. that associated with inelastic processes (represented by a horizontal dashed line starting with a \times) on the ZPF of a nucleus ground state associated with particle-hole correlated vibrations. Within this context one returns to the question of renormalization mentioned in the text (see end of Sect. 2.1 and Sect. 2.4, see also Idini et al. (2015), Broglia et al. (2016), Barranco et al. (2017); see also Sect. 7.5) The diagrams of the first row result by intervening the virtual process shown in Fig. 2.7.1 (c) and eventual time orderings. Similar for those of the second row but in connection with diagram (b) of Fig. 2.7.1. The boxed processes correspond to particle self-energy (first row) and vertex correction (second row). Reversing the sense in which the fermions (arrowed lines) circle the loop from anticlockwise to clockwise, one obtains two new graphs. The complete set of processes obtained in this way are shown in the third and last row, and constitute a sum rule conserving set of diagrams.

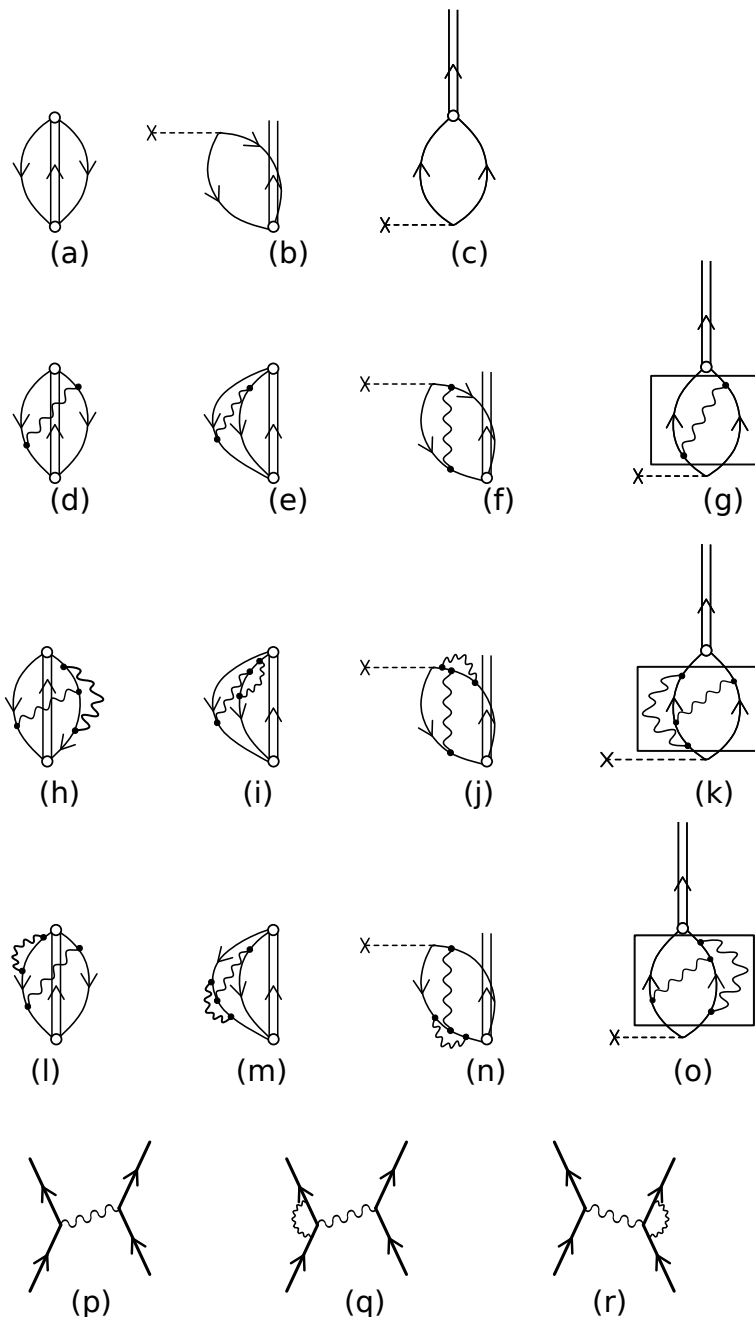


Figure 2.7.3: ZPF associated with the pair addition mode taking into account the interweaving of nucleons with density modes. The processes boxed in (g), (k) and (o), are associated with the induced pairing interaction (medium polarization effects; (p), (q), (r)) resulting from the exchange of density modes between nucleons moving in time reversal states, including also vertex corrections. The two-nucleon stripping and pickup external field is labeled by a dashed horizontal line which starts with a \times . The possibility of using pairing vibrational modes as intermediate bosons contributing to the induced pairing interaction, not only in 1S_0 channels but also in other channels (multipole modes) is discussed in App. 7.12. In particular, in connection with the possible presence of “vortex–like” pair addition modes, in exotic, halo nuclei, with $J^\pi = 1^-$ and $\beta = +2$ quantum numbers.

A detailed graphical NFT treatment of the vacuum has an important consequence concerning the probing of nuclear structure with reactions. By intervening it with an external field one will excite the modes whose properties can be compared with experiment without further ado.

In other words, if one is in doubt of which are the properly dressed elementary, physical modes of excitation, one should find out how to specifically excite the mode in question, by acting with an external field on the ZPF of the vacuum (Hawking-like radiation⁸³; see also Sect. 7.6.2 in particular Fig. 7.6.2). That is, carry out a *gedanken*, NFT-like *experiment* as in Fig. 2.7.2 for $p - h$ -vibrations and in Fig. 2.7.3 regarding pairing vibrations. Because the corresponding processes deal with physical states, they translate with ease into a laboratory setup. In keeping with the fact that the vacuum contains all the information (right physical degrees of freedom) of the quantal system under study. Forcing virtual processes associated with vacuum ZPF to become real, one is guaranteed to get, in each instance, the real, dressed, physical particle.

The fact that one can treat fully quantum mechanically and on equal footing both structure and reaction processes is apparent from these figures and considerations⁸⁴. Thus unification of structure and reactions, and dressing of energies, vertices (interactions) and formfactors (single-particle radial wavefunctions and associated transition densities), results in a single vacuum correlated state (e.g. Figs. 2.7.1 and 2.8.2). Vacuum states which through its fluctuations, reflect both single-particle, normal and abnormal (pairing) density vibrations and their interweaving. It also indicates the set of specific probes which make these virtual states to collapse into on-the-energy shell states, providing the corresponding physical information to the outgoing particles, also photons, which eventually interact with the corresponding detectors (e.g. Figs. 2.7.2, 2.7.3 and 2.9.2). Structure and reaction processes free of non-orthogonality, overcompleteness and Pauli violation contributions.

Summing up, the last line of Fig. 2.7.2 displays, together with the corresponding time orderings, the lowest order self-energy and vertex correction renormalising vibrational states. It thus gives rise to the physical collective vibrations whose properties can be directly compared with the experimental findings (within this context see last paragraph of the next section). In other words, the processes shown in the last line of Fig. 2.7.2 imply that the elementary modes participating in the virtual states have to display, exception made for energy (off-shell modes) the same properties of the physical, dressed (renormalized), on-shell modes whose properties can be directly compared with experiment⁸⁵ (renormalized NFT). This because one can, through an experiment force such virtual states to become real (on-shell) on short call.

Let us now provide an introduction to NFT for pedestrians and see how the

⁸³?

⁸⁴Full fledge embodiments being found in e.g. Figs. 2.9.1 and 2.9.2 and Figs. 7.3.1 and 7.6.2.

⁸⁵Examples of these processes in the case of giant resonances are found in Bortignon and Broglia (1981); Bertsch et al. (1983). For low-lying states see Barranco et al. (2004).

above considerations become concretely implemented⁸⁶

2.7.1 The concept of elementary modes of excitation⁸⁷

The Hamiltonian of a many–body system of noninteracting particles, bosons or fermions, can be written as

$$H = \sum_i H_i, \quad (2.7.1)$$

where the summation is over all the particles of the system and where each H_i depends only on the variables of the i -th particle. The single–particle Schrödinger equation is

$$H_i \psi_k(\mathbf{r}_i) = \epsilon_k \psi_k(\mathbf{r}_i), \quad (2.7.2)$$

where ϵ_k is the single–particle energy eigenvalue and

$$\psi_k(\mathbf{r}_i) \equiv \langle \mathbf{r}_i | a_k^\dagger | 0 \rangle \quad (2.7.3)$$

is the corresponding wave function. The operator a_k^\dagger creates a particle in the state k when acting in the vacuum state $|0\rangle$. The energy levels of the system are given by the equation

$$E_n = \sum_k n_k \epsilon_k, \quad (2.7.4)$$

the corresponding eigenstates being

$$|n\rangle = \prod_k \frac{(a_k^\dagger)^{n_k}}{\sqrt{n_k!}} |0\rangle, \quad (2.7.5)$$

where $n_k = 0$ or 1 in the case of fermions and $n_k = 0, 1, 2, \dots$ in the case of bosons.

Now we consider a system of interacting particles. The Hamiltonian will in this case be

$$H = \sum_i H_i + \frac{1}{2} \sum_{i,j} H_{ij}, \quad (2.7.6)$$

where i, j label the co–ordinates of the i -th and j -th particle.

In some cases it is possible to recast the two–body Hamiltonian in the form

$$H = \sum_\tau H'_\tau, \quad (2.7.7)$$

⁸⁶For details we refer to Bortignon, P. F. et al. (1977) and refs. therein.

⁸⁷Bès and Broglia (1977)

with the associated Schrödinger equation

$$H'_\tau \psi_\tau(\zeta) = \epsilon_\tau \psi_\tau(\zeta), \quad (2.7.8)$$

ζ representing a general variable⁸⁸ (e.g. the single-particle co-ordinate, the gap parameter, the shape of the nucleus, etc.). The wave function $\psi_\tau(\zeta)$ is the ζ -co-ordinate representation of the eigenstate $\alpha_\tau^\dagger |\tilde{0}\rangle$. The operator α_τ^\dagger creates an excitation with the quantum number τ when acting in the state $|\tilde{0}\rangle$, the correlated vacuum of all the excitations τ .

The energy of the levels of the system, or at any rate of the most important ones to determine the physical response of it to external probes can be written in the form

$$E_m = \sum_\tau n_\tau \epsilon_\tau. \quad (2.7.9)$$

The corresponding eigenstate can be written in the same way as before, *i.e.*

$$|n\rangle = \prod_\tau \frac{(\alpha_\tau^\dagger)^{n_\tau}}{\sqrt{n_\tau!}} |\tilde{0}\rangle. \quad (2.7.10)$$

Additivity features similar to (2.7.9) hold for other physical quantities, *i.e.*

$$\langle n|O|m\rangle = \sum_\tau A_\tau \sqrt{n_\tau} \delta(n_\tau, m_\tau + 1), \quad (2.7.11)$$

where

$$O = \sum_\tau A_\tau \alpha_\tau^\dagger \quad (2.7.12)$$

is the operator which specifically excites the eigenstates described by $\psi_\tau(\xi)$. Because the excitation energies E_m and observables $|\langle m'|O|m\rangle|^2$ (e.g. absolute two-particle transfer cross-section, electromagnetic-transition probabilities, etc.) are linear combinations of ϵ_τ and A_τ , respectively, the eigenstates with energy ϵ_τ and associated observable A_τ are called the *elementary excitations of the system*.

The elementary modes of excitation of a many-body system represent a generalization of the idea of normal modes of vibration. They provide the building blocks of the excitation spectra, giving insight into the deep nature of the system one is studying, aside from allowing for an economic description of complicated spectra in terms of a gas of, as a rule, weakly interacting bosons and fermions. In the nuclear case they correspond to clothed particles and empirically renormalised vibrations (rotations).

⁸⁸Collective, also in the sense of independent particle motion (see Mottelson (1962)) variable or order parameter.

There lie two ideas behind the concept of elementary modes of excitation⁸⁹. First, that one does not need to be able to calculate the total binding energy of a nucleus to accurately describe the low energy excitation spectrum, in much the same way in which one can calculate the normal modes of a metal rod not knowing how to calculate its total cohesive energy. The second idea is that low-lying states ($\hbar\omega \ll \epsilon_F \ll BE$, i.e. binding energy) are of a particularly simple character, and are amenable to a simple treatment, their interweaving being carried out at profit, in many cases, in perturbation theory⁹⁰. Within this context it is necessary to have a microscopic description of the ground state of the system which ensures that it acts as the vacuum state $|\tilde{0}\rangle$ of the elementary modes of excitation. In other words $a_\nu |\tilde{0}\rangle = 0$, $\Gamma_\alpha |\tilde{0}\rangle = 0$, where $a_\nu^+ |\tilde{0}\rangle = |\nu\rangle$ and $\Gamma_\alpha^+ |\tilde{0}\rangle = |\alpha\rangle$ represent a single-particle and a one-phonon state. This implies, in keeping with the indeterminacy relations⁹¹ $\Delta x \Delta p \geq \hbar/2$, $\Delta I \Delta \Omega \geq 1$, $\Delta N \Delta \phi \geq 1$, etc. that $|\tilde{0}\rangle = |0\rangle_F |0\rangle_B$ displays the quantal zero point fluctuations (ZPF) of the many-body system under study.

Within the framework of nuclear field theory (NFT) used below, in which single-particle (fermionic, F) and vibrational (bosonic, B) elementary modes of excitation are to be calculated within the framework of HFB and QRPA respectively, $|\tilde{0}\rangle$ must display the associated ZPF (cf. App. 2.D). In particular for (harmonic) vibrational modes the indeterminacy relation achieves its lowest possible value $\Delta x \Delta p = \hbar/2$, the associated zero point energy amounting to $\hbar\omega/2$ for each degree of freedom. For example $5\hbar\omega/2$ for quadrupole vibrations, $\hbar\omega$ being the energy of the collective vibrational mode under consideration.

An illustrative example of the above arguments is provided by the low-lying quadrupole vibrational state of ^{120}Sn . Diagonalizing SLy4 in QRPA leads to a value of $B(E2)$ ($890 e^2 \text{ fm}^2$) which is about a factor of 2 smaller than experimentally observed ($2030 e^2 \text{ fm}^2$). Taking into account renormalisation effects in NFT, namely in a conserving approximation (self-energy and vertex corrections, generalised Ward identities, see last line of Fig. 2.7.2 and Fig. 5.5.3), one obtains a value ($2150 e^2 \text{ fm}^2$), which essentially coincides with the experimental findings. One does not know how to accurately calculate the absolute ground state energy E_0 (total binding energy) of e.g. ^{120}Sn , but one can accurately work out the properties of the low-energy mode of this nucleus, also the collective energies $\hbar\omega_L = E_L - E_0$, and thus the associated ZPF and zero point energy E_0 , by renormalizing QRPA

⁸⁹This concept was introduced by Landau (Landau (1941)) to describe the spectrum of HeII. It was subsequently utilized by Bohr and Mottelson (Bohr, A. and Mottelson (1975)) to obtain a unified description of the nuclear spectrum.

⁹⁰More precisely, and in keeping with the fact that boson degrees of freedom have to decay through linear particle-vibration coupling vertices of strength Λ into their fermionic components to interact with another vibrational mode, the interweaving between the variety of many-body components clothing a single-particle state or a collective vibration will be described at profit in terms of an arrowed matrix which, assuming perturbation theory to be valid, can be transformed, neglecting contributions of the order of Λ^3 or higher, into a co-diagonal matrix, namely a matrix whose non-zero elements are $(i, i-1)$ and $(i, i+1)$, aside from the diagonal ones (i, i) .

⁹¹The quantities I , N and Ω , ϕ are the angular momentum and particle number, conjugate variables to the Euler and gauge angles respectively.

solutions through self-energy and vertex corrections contributions⁹². Now, if the collective phonons are not the main object of the study, but are to be used to cloth the single-particle states and give rise to the induced pairing interaction, one can make use of phonons which account for the experimental findings (renormalization^{93,94}).

2.7.2 NFT rules and applications

A field theory can be formulated in which the nuclear elementary modes of excitation play the role of the free fields and in which their mutual interweaving takes place through the particle–vibration coupling vertices⁹⁵. This theory provides a graphical perturbative approach to obtain the exact solution of the many-body nuclear-structure problem in the product basis $\psi_\tau(\zeta)\psi_\eta(\Delta)\dots\psi_\gamma(\Gamma)$

Note that the nuclear bosonic fields are built out by utilizing those degrees of freedom (particles and holes) which already exhaust all the nuclear degrees of freedom. It is thus an essential feature of the product basis to be over-complete and to violate the Pauli principle. On the other hand, this basis is directly related to observables of the system. The different experiments project out only one or two of its components.

In what follows we state and apply the nuclear–field–theory rules, to calculate the interactions between the nuclear free fields and the reaction processes between the resulting physical states making use of a schematic model.

⁹²Barranco et al. (2004), Bortignon and Broglia (1981).

⁹³Idini et al. (2015); Broglia et al. (2016); Barranco et al. (2017).

⁹⁴As already mentioned, with the help of experimental probes which couple weakly to the nucleus, i.e. in such a way that the system can be expressed in terms of the properties of the excitation in the absence of probes (see however Sect. 7.6.3), it has been possible to identify the following elementary excitations in systems around closed shells:

- a) single–particle and –holes,
- b) shape vibrations,
- c) spin and isospin vibrations and charge exchange modes,
- d) pairing vibrations.

Away from closed shells one has to add to the above modes:

- e) rotations in 3D–space (e.g. quadrupole rotations)
- f) rotations in gauge space (pairing rotations).

Different probes have been utilized in the process of the identification of the different modes. In particular two-neutron transfer reactions induced by tritons and protons have played a central role in unraveling the basic features of the pairing modes.

⁹⁵Bès et al. (1974); Broglia et al. (1976); Bohr, A. and Mottelson (1975); Mottelson (1976a).

Schematic model

The model considered consists of two single-particle levels, each with pair degeneracy⁹⁶ Ω and with a schematic monopole particle-hole interaction coupling the particles in the two levels.

The total Hamiltonian is equal to

$$H = H_{sp} + H_{TB} \quad (2.7.13)$$

where

$$H_{sp} = \frac{\epsilon}{2} N_0, \quad N_0 = \sum_{\sigma=\pm 1, m} \sigma a_{m,\sigma}^\dagger a_{m,\sigma}, \quad (2.7.14)$$

and

$$H_{TB} = -\frac{V}{2} (A^\dagger A + AA^\dagger), \quad A^\dagger = \sum_m a_{m,1}^\dagger a_{m,-1}. \quad (2.7.15)$$

The index σ ($=\pm 1$) labels the two levels, while m labels the degenerate states within each level. The strength of the monopole coupling is denoted by V and the energy difference between the two levels is ϵ . The matrix element of (2.7.15) is given by

$$\langle m, 1; m', -1 | H_{TB} | m'', 1; m''', -1 \rangle = -V \delta(m, m') \delta(m'', m'''). \quad (2.7.16)$$

Field-theoretical solutions

The bare nuclear fields are the elementary modes of excitation comprising surface vibrations and single particles. The boson fields are defined through the random-phase approximation, in terms of particle-hole excitations. The basis utilized to describe the nuclear systems is a product of the different free fields. The closed-shell system of the schematic model under consideration corresponds to the lowest ($\sigma = -1$) level filled with Ω particles, while the upper ($\sigma = 1$) level remains empty. The basis particle and hole states are obtained by adding or removing a single particle to/from this closed-shell configuration. The corresponding wave functions and energies, which should include the Hartree-Fock corrections (see Fig. 2.2.1 (b), (c)) generated by the residual interaction⁹⁷, are

$$\begin{cases} |m, 1\rangle = a_{m,1}^\dagger |0\rangle, & E(m, 1) = \frac{1}{2}(\epsilon + V), \\ |m, -1\rangle = a_{m,-1}^\dagger |0\rangle, & E(m, -1) = \frac{1}{2}(\epsilon + V). \end{cases} \quad (2.7.17)$$

⁹⁶It is of notice the difference of a factor of 2 in the degeneracy of each level as compared to Sect. 2 of Bortignon, P. F. et al. (1977) in which case it is 2Ω . This is in keeping with the fact that, as a rule, $\Omega = (2j+1)/2$. See also Eq. (2.7.89) and related discussion.

⁹⁷The Hartree-Fock energy associated with the Hamiltonian (2.7.13) can be obtained from the linearization relation $[H, a_{\sigma,m}^\dagger] = E(m, \sigma) a_{\sigma,m}^\dagger$ acting on the Hartree-Fock vacuum, which in this case coincides with the single-particle vacuum defined by $a_{m,-1}^\dagger |0\rangle = a_{m,1} |0\rangle = 0$



Figure 2.7.4: Graphical representation of the amplitude of the collective phonon (wavy line) on a given particle–hole excitation $((m, 1), (m, -1))$. This amplitude can be written in terms of the interaction vertex denoted by Λ_i , and the energy denominator $\omega_i - \epsilon'$. The particles (holes) are depicted by upward– (downward–) going arrowed lines.

Thus the unperturbed energy for producing a particle–hole excitation with respect to the ground state is

$$\epsilon' = E(m, 1) + E(m, -1) = \epsilon + V. \quad (2.7.18)$$

The contribution V in (2.7.18) is the Hartree–Fock contribution to the particle–hole excitation.

If we define the creation operator of the normal modes as

$$\beta_\nu^\dagger = \sum_m \lambda_m^\nu a_{m,1}^\dagger a_{m,-1}, \quad (2.7.19)$$

the linearization equation

$$[H, \beta_\nu^\dagger] = \omega_\nu \beta_\nu^\dagger, \quad (2.7.20)$$

yields

$$\begin{cases} \omega_1 = \epsilon' - V\Omega, \\ \omega_\nu = \epsilon' \quad (\nu = 2, 3, \dots, \Omega). \end{cases} \quad (2.7.21)$$

Utilizing (2.7.20) and the normalization condition

$$[\beta_\nu, \beta_{\nu'}^\dagger] = \delta(\nu, \nu'), \quad (2.7.22)$$

we obtain for the amplitudes associated with the lowest mode

$$\lambda_m^1 = \frac{1}{\sqrt{\Omega}}. \quad (2.7.23)$$

One can also write this amplitude as the ratio between a coupling matrix element and an energy denominator, i.e.

$$\lambda_m^1 = \frac{\Lambda_1}{\omega_1 - \epsilon'}. \quad (2.7.24)$$

From (2.7.21), (2.7.23) and (2.7.24) we obtain

$$\Lambda_1 = -V \sqrt{\Omega}, \quad (2.7.25)$$

which is the strength with which a particle hole excitation ($m, 1; m, -1$) couples to the collective phonon (see Fig. 2.7.4). This can also be seen by calculating the matrix element of the interaction Hamiltonian (2.7.15) between the normal modes and the single particle-hole state

$$\Lambda_\nu = \langle n_\nu = 1 | H_{TB} | m, 1; m', -1 \rangle = -V \sqrt{\Omega} \delta(m, m') \delta(\nu, 1). \quad (2.7.26)$$

Note that the particle–vibration coupling strengths associated with the other normal modes lying at an energy ϵ' (see (2.7.21)) are equal to zero. The exact solution of (2.7.13) is reproduced by utilizing as the basic degrees of freedom both the vibrations (see (2.7.21)) and the particles (see (2.7.17)) coupled through the interactions (2.7.16) (four-point vertex) and (2.7.26) (particle–vibration coupling)⁹⁸. A significant part of the original interaction has already been included in generating the collective mode (2.7.21). This implies that the rules for evaluating the effect of the couplings (2.7.16) and (2.7.26) between fermions and bosons involve a number of restrictions as compared with the usual rules of perturbation theory that are to be utilized in evaluating the effect of the original interaction (2.7.15) acting in a fermion space. They read as follows:

- I) In initial and final states, proper diagrams involve collective modes and particle modes, but not any particle configuration that can be replaced by a combination of collective modes. This restriction permits an initial state comprising the configuration ($n_\nu = 1; m$), but excludes ($m', 1; m', -1; m, 1$).
- II) The couplings (2.7.16) and (2.7.26) are allowed to act in all orders to generate the different diagrams of perturbation theory; the restriction I) does not apply to internal lines of these diagrams.
- III) The internal lines of diagrams are, however, restricted by the exclusion of diagrams in which a particle–hole pair is created and subsequently annihilated without having participated in subsequent interactions.
- IV) The energies of the uncoupled particle and phonon fields are to be calculated by utilizing the Hartree–Fock approximation (see eq. (2.7.17)) and the RPA (see eq. (2.7.21)), respectively. The contributions of all allowed diagrams are evaluated by the usual rules of perturbation theory.

⁹⁸Bès et al. (1974); Broglia et al. (1976)

We note that the external fields acting on the system are allowed to create any state which may generate the different diagrams of perturbation theory. The corresponding matrix elements should be weighted with the amplitude of the component through which the final state is excited.

The above rules are also valid for those situations which cannot be treated in perturbation theory and where a full diagonalization is called for. Thus, *e.g.*, when the system displays a spurious state (see Sect. 2.7.3).

In what follows we discuss the energy of the $2p - 1h$ -like excitations, simplest modes which can display spuriously. We distinguish between two types of states, namely

$$|n_i = 1; m, 1\rangle, \quad \begin{cases} \omega_1 = \epsilon' - V\Omega, & \Lambda_1 = -\sqrt{\Omega}V \\ & (i = 1; m = 1, 2, \dots, \Omega), \\ \omega_i = \epsilon', & \Lambda_i = 0 \\ & (i = 2, \dots, \Omega; m = 1, 2, \dots, \Omega), \end{cases} \quad (2.7.27)$$

and⁹⁹

$$|m', 1; m', -1; m, 1\rangle, \quad \epsilon' \quad (m, m' = 1, 2, \dots, \Omega), \quad (2.7.28)$$

where as in (2.7.27) only the energy of the particle-hole excitation is given (see (2.7.18)). One can also displace the zero point of the odd system to the value $\epsilon/2$, in which case the unperturbed energy of the basis states $|n_i; m, 1\rangle$ is ω_i . The physical states are to be written as

$$|qm\rangle = \sum_i \xi_{iqm} |n_i = 1; m, 1\rangle, \quad (2.7.29)$$

as (2.7.28) cannot be basis states according to rule I), but only intermediate states. The quantities ξ_{iqm} are the amplitudes of the physical state in the different components of the product basis of elementary excitations. Rule (I) eliminates most of the double counting of two-particle, one-hole states. The model state contains Ω “proper” states of the form $|n_i; m, 1\rangle$, in which case the odd particle is in the state $(m, 1)$. That is $|n_1; m, 1\rangle$ ($\omega_1 = \epsilon' - V\Omega$) and $|n_i; m, 1\rangle$ ($\omega_i = \epsilon'$, $i = 2, \dots, \Omega$). However, there are only $\Omega - 1$ two-particle, one-hole states in which the odd particle is in the state $(m, 1)$ (Fig. 2.7.6). Therefore, a spurious state remains in the spectrum based on elementary modes of excitation. In other words, allowing the quantum number m to run over all possible Ω -states, the model space contains Ω^2 states (one for each value of m), while the correct number is $\Omega(\Omega - 1)$.

Thus the basis $|n_1 = 1; m, 1\rangle$ contains Ω spurious states. Its origin can be traced back to the violation of the Pauli principle (see also Sect. 2.7.3). To obtain the energy of $|qm\rangle$ we have to allow the states $|n_1 = 1; m, 1\rangle$ to interact through the vertices (2.7.16) and (2.7.26) and generate all the different perturbation theory diagrams (see rule II) except those containing bubbles (see rule III)).

⁹⁹Since the states (2.7.28) are restricted to be intermediate states of the perturbation expansion, the configuration $(m, 1; m, -1; m', 1)$ is allowed.

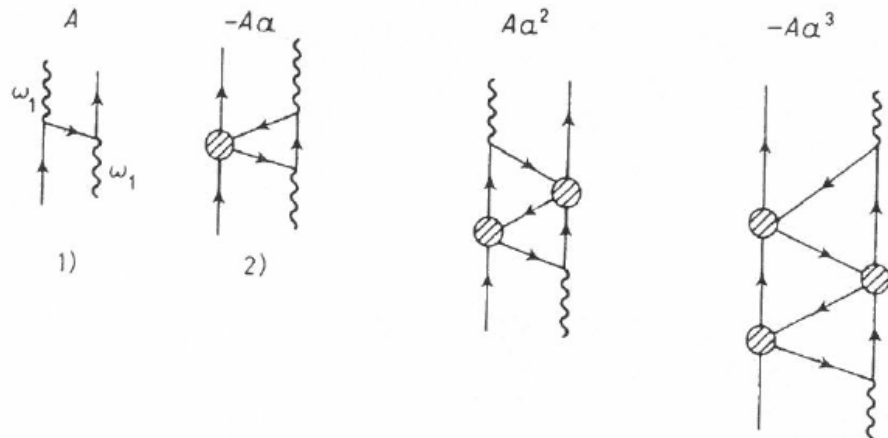


Figure 2.7.5: Contributions to the interaction of a fermion and a collective boson ω_i to order $1/\Omega^4$. The secular equation $E - E^{(0)} = A \sum_n a^n (-1)^n$ is given in terms of the quantities $A = 4\Omega V^2/(3\epsilon' - 2E)$ and $a = 2V/(3\epsilon' - 2E)$. The hatched circle represents the (particle-hole) four-point vertex (2.7.16) (see Fig. 2.7.8, third and fourth diagrams).

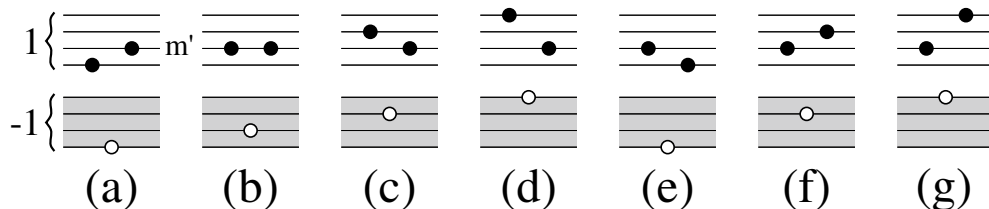


Figure 2.7.6: Schematic two-level model. Count of the states $|m, 1; m-1, m', 1\rangle$ in the case of $j = 3/2$ and $\Omega = 2j+1 = 4$. State (b) is not allowed because of Pauli principle. The states ((a),(e)), ((c),(f)) and ((d),(g)) are pairwise identical, in keeping with the indistinguishability of the particles. Thus, the states (a), (c) and (d) (equivalent (e), (f), (g)) exhaust the degrees of freedom of type (2.7.28). In other words, there are only $\Omega - 1 = 3$ two-particle one-hole states in which the odd particle is in the state $(m', 1)$.

The different graphical contributions calculated in the framework of the Brillouin–Wigner perturbation theory are displayed in Fig. 2.7.6. There is only one (diagonal) matrix element given by a single summation, which can be carried to all orders in the interaction vertices¹⁰⁰, and can be written as

$$\begin{aligned} X_{ii'} &= A \sum_n (-1)^n a^n \delta(i, i') = \\ &= \frac{A}{1+a} \delta(i, i') \delta(n, 1) = -K(E) (\sqrt{\Omega} V)^2 \delta(i, i') \delta(i, 1), \end{aligned} \quad (2.7.30)$$

where a and A are defined in the caption to the figure and

$$K(E) = \left(\frac{3}{2}\epsilon' - E + V \right)^{-1}. \quad (2.7.31)$$

The associated secular equation

$$|(\omega_i - E)\delta(i, i') + X_{ii'}| = 0 \quad (2.7.32)$$

is equivalent to the dispersion relation

$$\frac{1}{K(E)} = \sum_i \frac{(\sqrt{\Omega} V)^2}{\omega_i - E} \delta(i, 1). \quad (2.7.33)$$

Thus the energies of the system are determined by the equation

$$E = \omega_1 + \frac{\Omega V^2}{\frac{3}{2}\epsilon' - E + V}. \quad (2.7.34)$$

It admits the two solutions

$$E_{qm} = \begin{cases} \frac{3}{2}\epsilon', \\ \frac{1}{2}\epsilon' + \omega_1 + V = \frac{3}{2}\epsilon' - \Omega V + V, \end{cases} \quad (2.7.35)$$

and agree with the exact value¹⁰¹.

Because $A = 0$ for $i \neq 1$, there is no summation in (2.7.29) and

$$|qm\rangle = N_{qm}^2 |n_1 = 1; m, 1\rangle, \quad (2.7.36)$$

where

$$1 = N_{qm}^2 \left(1 - \frac{\partial X_{11}}{\partial E} \right) = N_{qm}^2 \left(1 - \frac{\Omega V^2}{\left(\frac{3}{2}\epsilon' - E + V \right)^2} \right). \quad (2.7.37)$$

¹⁰⁰Concerning the proper expansion parameter see Sect. 2.7.4, Eq. (2.7.89).

¹⁰¹The exact solutions can be obtained by noting that the operators A^\dagger, A and $\frac{1}{2}N_0$ are generators of the SU_2 group (see Bortignon, P. F. et al. (1977)).

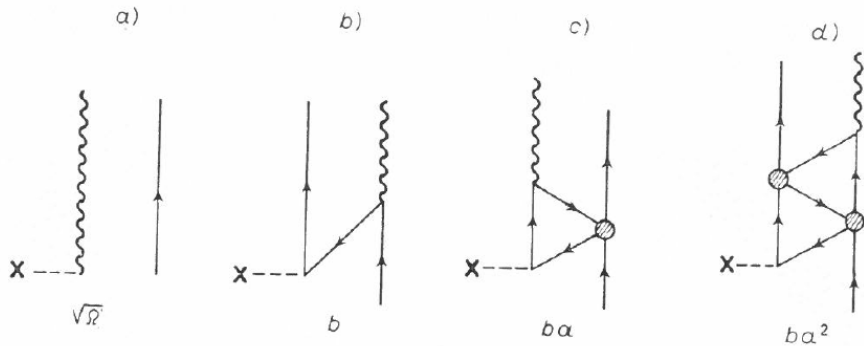


Figure 2.7.7: Graphical representation of the different terms contributing to the matrix element of the inelastic operator $\sqrt{\Omega} A^\dagger$ up to order $1/\Omega^3$. Note that the different contributions b), c), etc. have a one-to-one correspondence with the different contributions to E (see Fig. 2.7.5); $a = -2V/(3\epsilon' - 2E)$, $b = 2\Lambda_1/(3\epsilon' - 2E)$.

For $E_{qm} = \frac{1}{2}\epsilon' + \omega_1 + V$ we obtain

$$N_{qm}^2 = \frac{\Omega}{\Omega - 1}, \quad (2.7.38)$$

while for $E_{qm} = \frac{3}{2}\epsilon'$ the state is non-normalizable as the quantity in parentheses in (2.7.37) is either negative ($\Omega > 1$) or zero ($\Omega = 1$). The state defined by

$$|q, m\rangle = \sqrt{\frac{\Omega}{\Omega - 1}} |n_1 = 1; m, 1\rangle, \quad (2.7.39)$$

and

$$E_{qm} = \frac{1}{2}\epsilon' + \omega_1 + V = \frac{3}{2}\epsilon' - V(\Omega - 1), \quad (2.7.40)$$

exhausts the inelastic sum rule in agreement with the exact results. Note that (2.7.39) is specifically excited in inelastic processes, as can be seen by direct inspection. The external inelastic field can act in two ways, exciting either a particle-hole pair or a phonon, with amplitudes

$$\langle m, 1; m', -1 | A_1^\dagger | 0 \rangle = \delta(m, m'), \quad (2.7.41)$$

and

$$\langle n_i = 1 | A_1^\dagger | 0 \rangle = \sqrt{\Omega} \delta(i, 1), \quad (2.7.42)$$

respectively. The different graphical contributions to the inelastic-scattering process are displayed in Fig. 2.7.7, and can again be summed to all orders in the interaction vertices giving

$$\langle n_1 = 1; m, 1 | A_1^\dagger | m, 1 \rangle = \sqrt{\Omega} + \frac{\Lambda_1}{\frac{3}{2}\epsilon' - E_{qm} + V}. \quad (2.7.43)$$

For $E_{qm} = \frac{3}{2}\epsilon'$ this quantity is equal to zero. Thus, the corresponding states do not carry any inelastic strength, a feature which is closely related to the fact that they cannot be normalized and that they do not display any correlation energy¹⁰². On the other hand, the matrix element associated with (2.7.39) is

$$\langle qm|A^\dagger|m, 1\rangle = \sqrt{\frac{\Omega}{\Omega-1}} \frac{\Omega-1}{\sqrt{\Omega}} = \sqrt{\Omega-1}, \quad (2.7.44)$$

value which agrees with the exact answer. The results (2.7.40) and (2.7.44) can be traced down to Pauli-principle corrections. In fact, the state $|n_i = 1; m, 1\rangle$ has a nonvanishing matrix element, implying a single particle-vibration coupling vertex, with the state $|m, 1; m, -1; m, 1\rangle$. This component, which is spurious, is removed by the different graphs displayed in Figs. 2.7.5 and 2.7.7. The presence of the odd particle $(m, 1)$ blocks the particle-hole excitation $(m, 1; m, -1)$ which was present in the uncoupled system. Thus the system increases its energy by a quantity V . The reduction of the inelastic amplitude from $\sqrt{\Omega}$ to $\sqrt{\Omega-1}$ also indicates that there is one less particle-hole excitation responding to the external probe.

2.7.3 Spurious states

While the model space product of elementary modes of excitation discussed in the last section contains Ω^2 states, only $\Omega(\Omega-1)$ are physically possible, the number of spurious states being Ω , i.e. for each value of m . On the other hand, the agreement between the exact and the nuclear-field-theoretical results shows that the effects of those spurious states are eliminated from all the matrix elements associated with physical observables.

In what follows we show that, in fact, the spurious states are isolated in an explicit way in the nuclear field theory¹⁰³. Their energy coincides with the initial unperturbed energy, while all physical operators have zero off-diagonal matrix elements between any physical state and a spurious state, in particular the unit operator, which measures the overlap of the two types of states. For this purpose we use again a schematic model consisting in a number, Ω , of single-particle levels in which particles interact by means of a “monopole” force,

$$H = H_{sp} + H_{int}, \quad (2.7.45)$$

where

$$H_{sp} = \frac{1}{2} \sum_{m=1}^{\Omega} \epsilon_m (a_{m,1}^\dagger a_{m,1} - a_{m,-1}^\dagger a_{m,-1}), \quad (2.7.46)$$

and

$$H_{int} = -VA^\dagger A, \quad (2.7.47)$$

¹⁰²Note that, even if $N(E_{qm} = \epsilon_m) \rightarrow \infty$, the matrix elements associated with the different transitions tend to zero more rapidly and the final result converges and is equal to zero as expected.

¹⁰³Broglia et al. (1976)

with

$$A^\dagger = \sum_{m=1}^{\Omega} a_{m,1}^\dagger a_{m,1}. \quad (2.7.48)$$

The energy of the i -th phonon is determined by the RPA dispersion relation (see rule IV))

$$\sum_{m=1}^{\Omega} \frac{1}{\epsilon_m - \omega_i} = \frac{1}{V}. \quad (2.7.49)$$

The eigenfunction corresponding to the different modes is

$$|n_i = 1\rangle = \sum_m \frac{\Lambda_i}{\epsilon_m - \omega_i} a_{m,1}^\dagger a_{m,-1}|0\rangle. \quad (2.7.50)$$

The particle-vibration coupling constant is given by

$$\Lambda_i = -\langle n_i = 1 | H_{int} | m, 1; m', -1 \rangle = \left[\sum_m \frac{1}{(\epsilon_m - \omega_i)^2} \right]^{-\frac{1}{2}} \delta(n, n'), \quad (2.7.51)$$

where $|n_i = 1\rangle$ denotes a state containing one phonon, while $|m, 1; m', -1\rangle$ is the eigenstate associated with particle-hole excitation. The other interaction to be included (rule II)) is the four-point vertex which has the value

$$\langle m, 1; m', -1 | H_{int} | m'', 1; m', -1 \rangle = -V \delta(m, m') \delta(m'', m''). \quad (2.7.52)$$

The single-particle energies to be used in calculating the different graphs are $\frac{1}{2}\epsilon_m$, as the Hartree-Fock contribution (see rule IV)) of H_{int} is zero.

Similarly to H_{int} the “inelastic operator” has two different matrix elements, namely

$$\langle n_i = 1 | a_{m',1}^\dagger a_{m',-1} | 0 \rangle = \frac{\Lambda_i}{\epsilon_{m'} - \omega_i} \quad (2.7.53)$$

and

$$\langle m', 1; m'', -1 | a_{m,1}^\dagger a_{m,-1} | 0 \rangle = \delta(m, m') \delta(m', m''). \quad (2.7.54)$$

In what follows we discuss again the system comprising an odd particle, in the orbit $(m, 1)$, in addition to a single phonon excitation of the vacuum. According to rule I) initial and final states may involve both collective modes and particle modes, but not any particle configuration that can be replaced by a combination of collective modes. The exclusion of the states $|m, 1; m', 1; m', -1\rangle$ eliminates most of the double counting of two-particle, one-hole states. The Ω “proper” states of the form $|n_i = 1; m, 1\rangle$ are allowed. However, there are only $\Omega - 1$ (two-particle, one-hole) states in which the odd particle is in the state $(m, 1)$ (see Fig. 2.7.6).

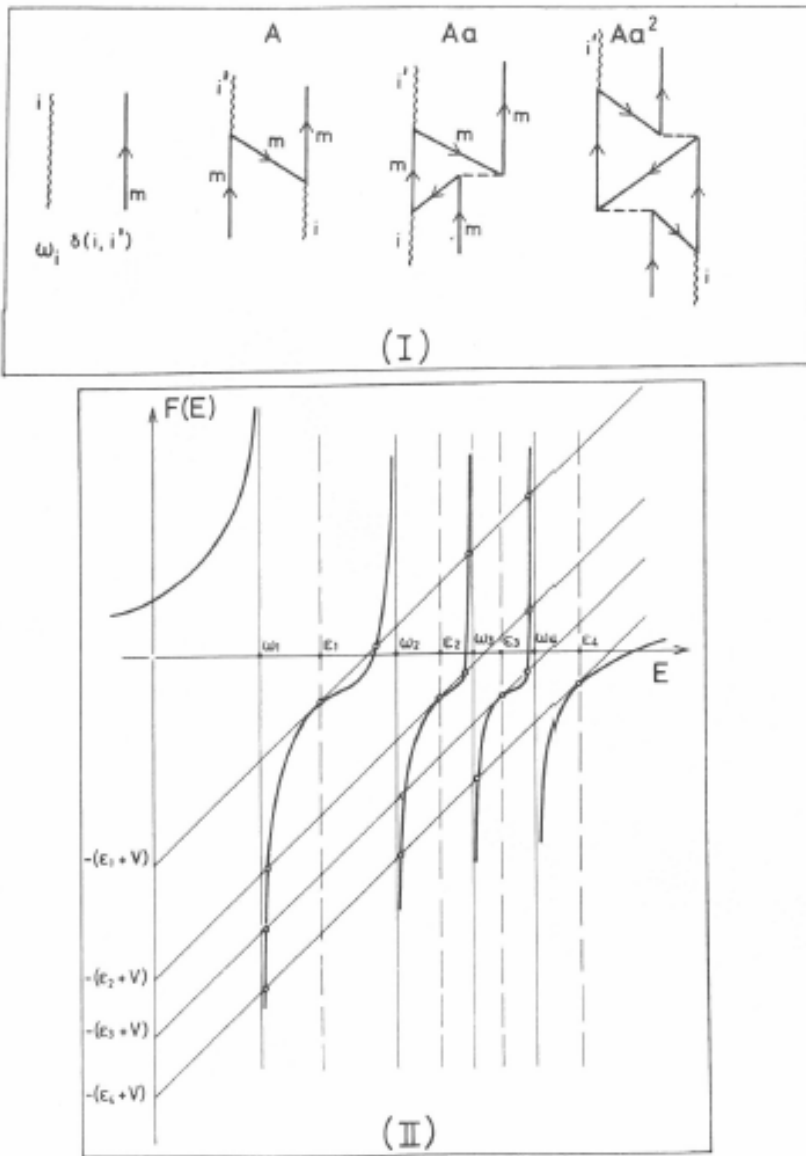


Figure 2.7.8: Lower order contributions to the energy matrix element between the basis states $|n_i = 1; m, 1\rangle$. The dashed line stands for the model bare interaction (see eq. 2.7.52). The quantity $X_{ii'}(E) = A \sum_n a^n = -\Lambda_i \Lambda'_i / (E - \epsilon_m - V)$, where $A = -\Lambda_i \Lambda'_i / (E - \epsilon_m)$ and $a = V / (E - \epsilon_m)$, is the matrix element iterated to all orders in $1/\Omega$. The secular equation of the problem is $|\omega_i \delta(i, i') + X_{ii'}| = 0$, and is equivalent to the dispersion relation (2.7.57). II) Graphical solution of the dispersion relation (2.7.57), for the case $\Omega = 4$. The function $F(E) = \sum_i \Lambda_i^2 / (\omega_i - E)$ is displayed as a continuous thick line, while the parallel lines $E - \epsilon_m - V$ have been drawn as thin continuous lines intersecting the ordinates axis at $-(\epsilon_m + V)$. The intersections between the two functions give the eigenvalues of the secular equation. For each value of ϵ_m there are $\Omega + 1$ roots, the root at $E = \epsilon_m$ being double.

Therefore, a spurious state remains in the spectrum of the elementary modes of excitation.

The lower-order corrections to this energy which do not contain bubbles are drawn in Fig. 2.7.8 (I). Iterating these processes to infinite order we obtain the secular equation

$$|(\omega_i - E)\delta(i, i') + X_{ii'}(E)| = 0, \quad (2.7.55)$$

where

$$X_{ii'} = -\frac{\Lambda_i \Lambda_{i'}}{E - \epsilon_m - V}. \quad (2.7.56)$$

The different contributions calculated in the framework of the Brillouin–Wigner perturbation theory are energy dependent, and take into account renormalization effects of the states not explicitly included in the calculations. The dispersion relation fixing the energies E_m of the physical states is (see App. 2.B)

$$E - \epsilon_m - V = \sum_{i=1}^{\Omega} \frac{\Lambda_i^2}{\omega_i - E} = F(E). \quad (2.7.57)$$

There is one equation for each single-particle level because the monopole force cannot change the m-state of the odd particle. The relation (2.7.57) can be solved graphically as shown in Fig. 2.7.8 (II). The energy $E = \epsilon_m$ is always a root of (2.7.57), in fact a double root since

$$\left[\frac{dF(E)}{dE} \right]_{E=\epsilon_m} = \sum_i \frac{\Lambda_i^2}{(\omega_i - \epsilon_m)^2} = 1, \quad (2.7.58)$$

and the line $E - \epsilon_m - V$ is at 45° . The remaining intersections of this line and the function $F(E)$ give rise to $\Omega - 1$ additional roots denoted by (qm) , whose energy E_{qm} agrees with the physical eigenvalues obtained from the exact solution of the model. The eigenvectors associated with the physical states (qm) are

$$|qm\rangle_F = \sum_i \xi_{iqm} |i; m, 1\rangle, \quad (2.7.59)$$

where

$$\xi_{iqm} = -N_{qm} \frac{\Lambda_i}{\omega_i - E_{qm}} = \langle i; m, 1 | qm \rangle_F. \quad (2.7.60)$$

The normalization condition which determines N_{qm} is

$$\begin{aligned} {}_F \langle qm | qm \rangle_F &= 1 = \sum_{i,i'} \left(\delta(i, i') - \frac{\partial X_{ii'}}{\partial E} \right) \xi_{iqm}^* \xi_{i'qm} = \\ &= N_{qm}^2 \left[\sum_i \frac{\Lambda_i^2}{(\omega_i - E_{qm})^2} - \frac{1}{(E_{qm} - \epsilon_m - V)^2} \sum_{i,i'} \frac{\Lambda_i^2 \Lambda_{i'}^2}{(\omega_i - E_{qm})(\omega_{i'} - E_{qm})} \right] = \\ &= N_{qm}^2 \left[\sum_i \frac{\Lambda_i^2}{(\omega_i - E_{qm})^2} - 1 \right], \end{aligned} \quad (2.7.61)$$

where the dispersion relation (2.7.57) has been utilized, and where $X_{ii'}$ is the matrix element appearing in (2.7.55) and defined in (2.7.56). For $E_{qm} = \epsilon_m$ the factor multiplying N_{qm}^2 is zero (see eq. (2.7.58)). Thus, there are only $\Omega - 1$ states which can be normalized when solving the Hamiltonian (2.7.45) in the framework of the nuclear field theory. The full spuriousity of the elementary-mode product basis is concentrated in a single state¹⁰⁴.

The subscript F has been utilized in (2.7.59) to indicate that we are dealing with the nuclear-field solution of the Hamiltonian (2.7.45) (for simplicity it will not be used in the following). Note that these eigenvectors are expressed in terms of only allowed initial or final states (see rule I))

$$|i; m, 1\rangle \equiv a_{m,1}^\dagger |i\rangle, \quad (2.7.62)$$

which are assumed to form an orthonormal basis, in particular in deriving the relation (2.7.61). This is equivalent to the basic assumption of nuclear field theory of the independence of the different modes of excitation, i.e., in the present case,

$$[\Gamma_i, a_{m,1}^\dagger] = 0. \quad (2.7.63)$$

Rules I–IV) discussed in the last section give the proper mathematical framework to this ansatz, which has played a basic role in developing a unified theory of nuclear structure. The above discussion can be illuminated by utilizing a conventional treatment of the residual interaction. Expanding the states $|n_i = 1; m, 1\rangle$ in terms of particle and hole states, we can write, with the help of (2.7.50),

$$a_{m,1}^\dagger |n_i = 1\rangle = a_{m,1}^\dagger \sum_{m' \neq m} \frac{\Lambda_i}{\epsilon' - \omega_i} a_{m',1}^\dagger |0\rangle \quad (2.7.64)$$

The overlap between the states $|n_i = 1; m, 1\rangle$ is thus given by,

$$\begin{aligned} Z(i, i') &= \langle i' | a_{m,1} a_{m,1}^\dagger | i \rangle \\ &= \sum_{m' \neq m} \frac{\Lambda_i \Lambda_{i'}}{(\epsilon_{m'} - \omega_i)(\epsilon_{m'} - \omega_{i'})} = \delta(i, i') - \frac{\Lambda_i \Lambda_{i'}}{(\epsilon_m - \omega_i)(\epsilon_m - \omega_{i'})}, \end{aligned} \quad (2.7.65)$$

where the orthogonality relation,

$$\sum_{m'} \frac{\Lambda_i \Lambda_{i'}}{(\epsilon_{m'} - \omega_i)(\epsilon_{m'} - \omega_{i'})} = \delta(i, i'), \quad (2.7.66)$$

of the RPA solutions in the even system has been utilized. Because of the non-orthogonality of the basis, the eigenvalues of the system are determined by the relation

$$|Z(E)(H - E)| = 0. \quad (2.7.67)$$

¹⁰⁴Note that the mathematical relation $N^2 f(E) = 1, N^2$, being the norm of the state with energy E , implies that such state is spurious if $f(E) = 0$ or $f(E) < 0$ (see eq. (2.7.37) and subsequent discussion).

This is fulfilled for

$$|H - E| = 0, \quad (2.7.68)$$

which yields the $\Omega - 1$ physical roots, as well as for

$$|Z(E)| = 0. \quad (2.7.69)$$

This solution corresponds to the spurious root $E_{qm} = \epsilon_m$ (i.e. $\omega_1 = 0$). In fact¹⁰⁵,

$$\begin{aligned} \lim_{\delta \rightarrow 0} \sum_i \xi_{iqm}(E_{qm} = \epsilon_m + \delta) Z_{ii'} &= \lim_{\delta \rightarrow 0} N_{qm}(E_{qm} = \epsilon_m + \delta) \\ &\times \sum_i \frac{\Lambda_i}{\omega_i - (\epsilon_m + \delta)} \sum_{m' \neq m'} \frac{\Lambda_i \Lambda_{i'}}{(\epsilon_{m'} - \omega_i)(\epsilon_{m'} - \omega_{i'})} = 0, \end{aligned} \quad (2.7.70)$$

since¹⁰⁶

$$\sum_{m' \neq m} \frac{\Lambda_i \Lambda_{i'}}{(\epsilon_{m'} - \omega_i)(\epsilon_{m'} - \omega_{i'})} = \delta(m, m'). \quad (2.7.71)$$

Note that this solution in terms of the overlap Z gives the exact answer in the present case, because of the simplicity of the model. In a general case which includes ground-state correlations this may not be true any longer.

Before dealing with the consequences of the above discussion in connection with reaction matrix elements (one-particle transfer amplitudes), let us return to (2.7.61). The physical amplitudes ξ_{iqm} are connected to $\tilde{\xi}_{iqm}$ by the relation

$$\xi_{iqm} = \frac{\tilde{\xi}_{iqm}}{\sqrt{N_{qm}}}. \quad (2.7.72)$$

Thus,

$$N_{qm} = \sum_{i,i'} \left(\delta(i, i') - \frac{\partial X_{ii'}}{\partial E} \right) \tilde{\xi}_{qm}^* \tilde{\xi}_{qm} = \sum_{i,i'} \tilde{M}_{ii'}^{mm} \tilde{\xi}_{qm}^* \tilde{\xi}_{qm}. \quad (2.7.73)$$

In usual perturbation theory

$$\frac{\partial X_{ii'}}{\partial E} \tilde{\xi}_{qm}^* \tilde{\xi}_{qm} < 0, \quad (2.7.74)$$

¹⁰⁵Within the context of renormalization, one first calculates the expressions for a finite value of δ and then takes the limit.

¹⁰⁶It is of notice that the validity of the relations (2.7.66) and (2.7.71) is related to the fact that the RPA conserves the EWSR.

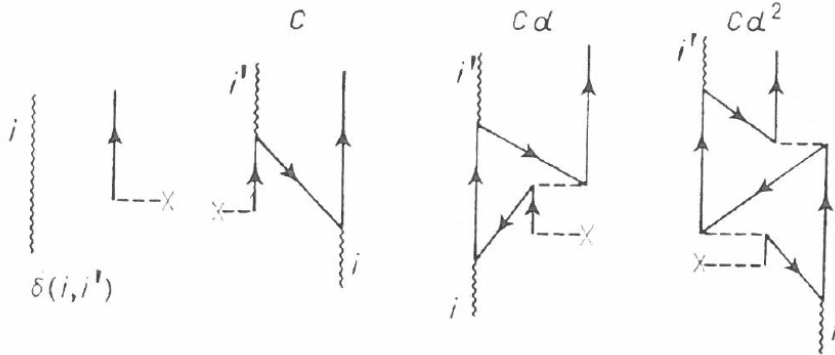


Figure 2.7.9: Lower order contributions to the one-particle transfer reaction induced by $a_{m,1}^\dagger$. The result of iterating the different contributions to all orders in $1/\Omega$ is equal to $T_{qm}(ii') = C \sum_n d^n = -\Lambda_i \Lambda_{i'} / ((\omega_i - \epsilon_m)(E_{qm} - \epsilon_m - V))$, $C = -\Lambda_i \Lambda_{i'} / ((\omega_i - \epsilon_m)(E_{qm} - \epsilon_m))$, $d = |V/(E_{qm} - \epsilon_m)|$.

and N_{qm} is always > 1 . In the present case, however, because the matrix elements of the effective Hamiltonian have to be calculated excluding the contributions containing bubbles, the quantity

$$\sum_{ii'} \frac{\partial X_{ii'}}{\partial E} \xi_{qm}^* \xi_{qm}, \quad (2.7.75)$$

can be either positive, or negative¹⁰⁷. From the above discussion it can be concluded that N_{qm} can vanish for certain states, eliminating the redundant degrees of freedom. Examples are discussed in Sect. 2.7.4 (see also 2.B.2).

We now calculate the one-particle stripping process leading to the odd system. This calculation illustrates the explicit concentration of the whole spuriousity into a single state which has zero correlation energy¹⁰⁸ and zero amplitude for the different physical processes exciting the $\Omega - 1$ physical states.

One has first to calculate the amplitude for the transition to a basis component ($n_i = 1; m, 1$) including only those graphs in which all intermediate states are excluded from appearing as initial or final states. This exclusion reflects the fact that the diagonalization procedure has included all interaction effects that link these allowed states. The final amplitude for the transition to the state (qm) is obtained by summing the amplitudes ($n_i = 1; m, 1$) each weighted by ξ_{iqm} given in Eq. (2.7.60).

The lower-order contributions to the one-particle transfer amplitude between the state $|n_i = 1\rangle$ and the state $|qm\rangle$ are displayed in Fig. 2.7.9. They can be summed

¹⁰⁷Within this context see Bès et al. (1976b) in particular App. B, footnote p. 25.

¹⁰⁸This is because the spurious state has zero phase space to correlate.

up to all orders of $1/\Omega$, the result being equal to

$$\begin{aligned}
 & \langle qm | a_{m,1}^\dagger | n_i = 1 \rangle \\
 &= \sum_{i'} \xi_{i'qm} \left\{ \delta(i, i') - \frac{\Lambda_i \Lambda_{i'}}{(\omega_i - \epsilon_m)(E_{qm} - \epsilon_m)} \left[\frac{1}{1 - V/(E_{qm} - \epsilon_m)} \right] \right\} \\
 &= \sum_{i'} \xi_{i'qm} \{ \delta(i, i') - T_{qm}(i, i') \} = \\
 &= -N_{qm} \left[\frac{\Lambda_i}{\omega_i - E_{qm}} - \frac{\Lambda_i}{(\omega_i - \epsilon_m)(E_{qm} - \epsilon_m - V)} \sum_{i'} \frac{\Lambda_{i'}^2}{\omega_{i'} - E_{qm}} \right] \\
 &= \frac{N_{qm}(E_{qm} - \epsilon_m)\Lambda_i}{(E_{qm} - \omega_i)(\omega_i - \epsilon_m)}. \tag{2.7.76}
 \end{aligned}$$

This quantity is zero for the spurious roots¹⁰⁹ (*i.e.* $E_{qm} = \epsilon_m$) and agrees with the exact result for the $\Omega - 1$ remaining physical roots.

Utilizing the relations

$$\frac{1}{V} = \sum_m \frac{1}{\epsilon_m - \omega_i}, \tag{2.7.77}$$

and

$$\frac{1}{V} = \sum_{m' \neq m} \frac{1}{\epsilon_{m'} - E_{qm}}, \tag{2.7.78}$$

we obtain

$$\sum_{m' \neq m} \frac{1}{(\epsilon_{m'} - E_{qm})(\epsilon_{m'} - \omega_i)} = \frac{1}{(E_{qm} - \omega_i)(\epsilon_m - \omega_i)}. \tag{2.7.79}$$

With the help of this relation we can derive the *one-particle transfer sum rule*. Note that (2.7.77) is the dispersion relation for the free phonon field. The second relation is, however, alien to the field theory results. Nevertheless, one can show that the solutions E_{qm} of (2.7.78) and of the nuclear-field-theory dispersion relation (2.7.57) are identical, except for the root $E_{qm} = \epsilon_m$. One can, therefore, utilize (2.7.78) as a mathematical relation without further justifications in the present context. One obtains

$$\begin{aligned}
 \sum_{qm} \left| \langle qm | a_{m,1}^\dagger | n_i = 1 \rangle \right|^2 &= \sum_{qm} \Lambda_{qm}^2 \Lambda_i^2 \sum_{m' \neq m} \frac{1}{(\epsilon_{m'} - E_{qm})(\epsilon_{m'} - \omega_i)} \\
 &\times \sum_{m' \neq m} \frac{1}{(\epsilon_{m'} - E_{qm})(\epsilon_{m'} - \omega_i)}, \tag{2.7.80}
 \end{aligned}$$

¹⁰⁹In fact, $\lim_{\delta \rightarrow 0} [(E_{qm} - \epsilon_m)N_{qm}]_{E_{qm} + \delta} = \lim_{\delta \rightarrow 0} \left\{ \sqrt{2} \delta^{3/2} / [\sum_i \frac{\Lambda_i}{\omega_i - \epsilon_m}]^{1/2} \right\} = 0$.

where

$$\Lambda_{qm} = -N_{qm}(E_{qm} - \epsilon_m) = \left[\sum_{m' \neq m} \frac{1}{(\epsilon_{m'} - E_{qm})} \right]^{-\frac{1}{2}}. \quad (2.7.81)$$

Thus

$$\sum_{qm} \left| \langle qm | a_{m,1}^\dagger | n_i = 1 \rangle \right|^2 = \Lambda_i^2 \sum_{m' \neq m} \frac{1}{(\epsilon_{m'} - \omega_i)^2} = 1 - \frac{\Lambda_i^2}{(\epsilon_m - \omega_i)^2}, \quad (2.7.82)$$

where use has been made of the orthogonality relation

$$\sum_{m' \neq m} \frac{1}{(\epsilon_{m'} - E_{qm})(\epsilon_{m''} - E_{qm})} = \delta(m', m'') \quad (m', m'' \neq m). \quad (2.7.83)$$

The result (2.7.82) coincides with the exact result. Physically it means that the single-particle orbital $(m, 1)$ is blocked by the amount $\Lambda_i^2/(\epsilon_m - \omega_i)^2$, which is the probability that the phonon $(n_i = 1)$ is in the particle-hole configuration $(m, 1; m, -1)$, *i.e.* with its particle in the orbital $(m, 1)$.

2.7.4 Applications

In what follows we discuss some aspects of the low-lying spectrum of the nucleus ^{209}Bi in terms of fermions, surface ($\beta_n^\dagger(0\lambda)$) and pairing ($\beta_n^\dagger(2\lambda)$) vibrational modes.

The unperturbed states of the closed-shell-plus-one-particle system can be written in terms of the free fields as

$$|n2\lambda, j; IM\rangle = [\beta_n^\dagger(2\lambda)a_j]_{IM}|0\rangle, \quad (2.7.84)$$

and

$$|n0\lambda, j; IM\rangle = [\beta_n^\dagger(0\lambda)a_j^\dagger]_{IM}|0\rangle. \quad (2.7.85)$$

This constitutes the basis set of states $\{\alpha_i\}$. All other states give rise to the complementary Hilbert space $\{a_i\}$.

The elementary modes of excitation interact through the particle-vibration and four-point vertices displayed in Fig. 2.7.10 giving rise to the matrix elements

$$M_1(nj, n'j') \equiv \langle [\beta_n^\dagger(0\lambda)a_{j'}^\dagger]_{IM} | h_{eff}(E) | [\beta_n^\dagger(0\lambda)a_j^\dagger]_{IM} \rangle, \quad (2.7.86)$$

$$M_2(nj, n'j') \equiv \langle [\beta_{n'}^\dagger(2\lambda)a_{j'}]_{IM} | h_{eff}(E) | [\beta_n^\dagger(2\lambda)a_j]_{IM} \rangle, \quad (2.7.87)$$

and

$$M_3(nj, n'j') \equiv \langle [\beta_{n'}^\dagger(2\lambda)a_{j'}]_{IM} | h_{eff}(E) | [\beta_n^\dagger(0\lambda)a_j^\dagger]_{IM} \rangle. \quad (2.7.88)$$

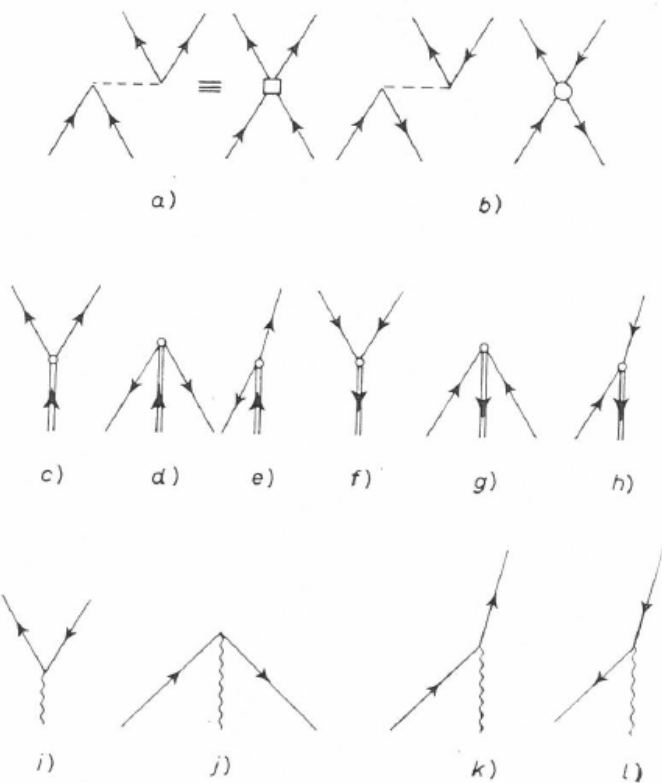


Figure 2.7.10: Interactions coupling the fermion fields with the pairing and surface vibrations. The different fermion and boson free fields are particles, holes, pairing vibrations ($\beta = \pm 2$) and surface vibrations ($\beta = 0$), β being the transfer quantum number. The two possible four-point vertices are given in a) and b). They correspond to the pairing and particle-hole model bare interactions. In graphs c)–h) all possible couplings between the fermion fields (arrowed lines) and the pairing vibrational fields (double lines arrowed) are displayed. Graphs i)–l) are all the possible coupling vertices between the surface vibrations (wavy line) and the fermion fields. Note that there is no direct coupling between the two boson fields, as the field theory we are dealing with is linear in the different field coordinates.

They are to be calculated by utilizing the graphical techniques of perturbation theory and the rules discussed in Sect. 2.7.2. *There are two parameters on which to expand upon in carrying out a perturbative calculation. The first one is the strength of the interaction vertices measured in terms of the average distance between single-particle levels. The second is $1/\Omega$, where $\Omega = \sum_j(j + \frac{1}{2})$ is the effective degeneracy of the valence shells (in connection to this “standard” definition of Ω we refer to footnote⁹⁶). These two parameters are in general connected through involved expressions. In the schematic model discussed in Sect. 2.7.2, however, their relation is explicit and can be expressed as*

$$\epsilon = O(1), \quad \Lambda = O\left(\frac{1}{\sqrt{\Omega}}\right) \quad \text{and} \quad V = O\left(\frac{1}{\Omega}\right). \quad (2.7.89)$$

Another feature which determines the family of diagrams to select to a given order of perturbation is the number of internal lines which can be freely summed up. Each of these summations introduces a multiplicative factor Ω . Based on a wealth of detailed calculations for realistic distributions of levels one can conclude that relations (2.7.89) are valid also in such cases¹¹⁰. In what follows, we give an example of NFT in a realistic situation, namely ^{209}Bi . This nucleus has been investigated by means of high-resolution anelastic process¹¹¹. Through these experiments a septuplet of states around 2.6 MeV of excitation was identified, with spins ranging from $\frac{3}{2}^+$ to $\frac{15}{2}^+$.

In zeroth order these states can be interpreted in terms of a proton moving in the $h_{9/2}$ orbital coupled to the lowest octupole vibration of ^{208}Pb . The $\frac{3}{2}^+$ of this multiplet displays also a large parentage based on the proton pair addition and proton hole moving in the $d_{3/2}$ orbital, as revealed by the (t, α) reaction¹¹² on ^{210}Po . The above results indicate that the (two-particle, one-hole) type of states in ^{209}Bi are amenable to a simple description in term of the basis states

$$|(\beta = 2), \lambda^\pi, j_1^{-1}; IM\rangle \equiv |j_1^{-1} \otimes \lambda^\pi(^{210}\text{Po}); IM\rangle \quad (\lambda^\pi = 0^+, 2^+, 4^+) \quad (2.7.90)$$

and

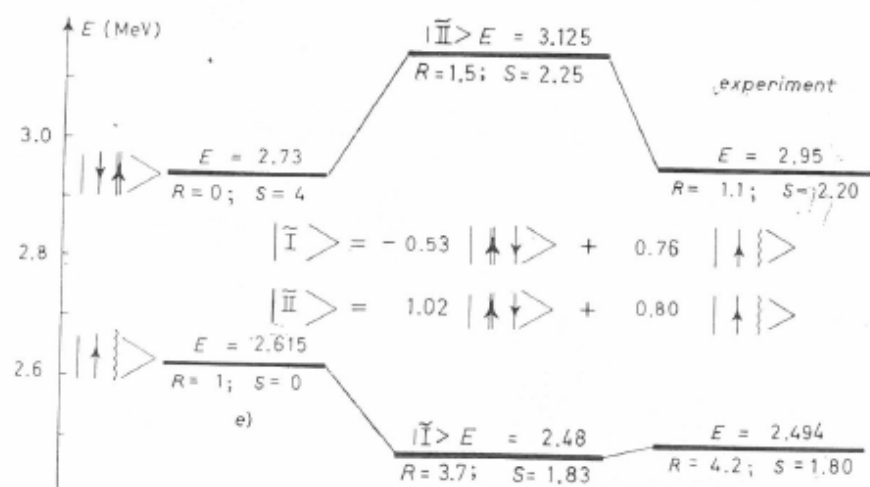
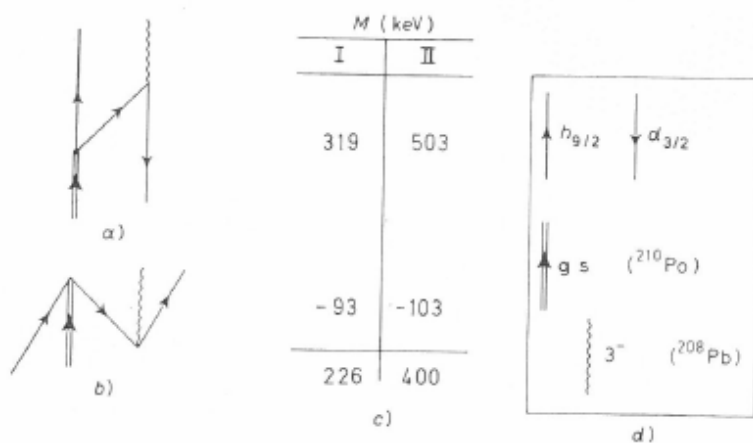
$$|(\beta = 0), \lambda^\pi, j_2; IM\rangle \equiv |j_2 \otimes \lambda^\pi(^{208}\text{Pb}); IM\rangle \quad (\lambda^\pi = 3^-) \quad (2.7.91)$$

Only the lowest states of each spin and parity λ^π are included in the basis states,

¹¹⁰An alternative way to argue concerning the expansion parameter, and in this case in connection with pairing vibrations, is to use the dimensionless quantity $x = 2G\Omega/D$ appropriate of a model made of two j -shells separated by an energy $D = 2\epsilon$ in which pairs of nucleons moving in time-reversal states interact through a pairing coupling constant G . Phase transition takes place at $x \geq 1$, while situations away from phase transitions but still displaying consistent fluctuations typical of nuclei displaying low-lying collective vibrations, correspond to $x \approx 0.5$. Assuming $D(O(\epsilon)) = O(1)$, one obtains $G(O(V)) = O(1/\Omega)$ and naturally $\Lambda = O(1/\sqrt{\Omega})$, in keeping with the fact that the induced interaction can be written as $\Lambda^2/(\epsilon - \omega)$.

¹¹¹Ungrin et al. (1971), Broglia, R. A. et al. (1970).

¹¹²Barnes, P. et al. (1972).



$$\begin{aligned} & \left\{ -0.53 \begin{bmatrix} \text{---} \\ \text{---} \\ \text{---} \end{bmatrix} + 1.02 \begin{bmatrix} \text{---} \\ \text{---} \\ \text{---} \end{bmatrix} \right\}^2 = 2 \times 10^{-2} \\ & \quad -0.103 \qquad \qquad \qquad 0.135 \\ & \quad -0.103 \qquad \qquad \qquad 0.135 \end{aligned}$$

f)

$$\begin{aligned} & 4 \times \left\{ -0.53 \begin{bmatrix} \text{---} \\ \text{---} \\ \text{---} \end{bmatrix} + 1.02 \begin{bmatrix} \text{---} \\ \text{---} \\ \text{---} \end{bmatrix} \right\}^2 = 1.12 \\ & \quad 1.12 \\ & \quad 4.16 \\ & 4 \times \left\{ -0.53 \begin{bmatrix} \text{---} \\ \text{---} \\ \text{---} \end{bmatrix} + 1.02 \begin{bmatrix} \text{---} \\ \text{---} \\ \text{---} \end{bmatrix} + -0.010 \begin{bmatrix} \text{---} \\ \text{---} \\ \text{---} \end{bmatrix} + -0.011 \begin{bmatrix} \text{---} \\ \text{---} \\ \text{---} \end{bmatrix} \right\}^2 = 1.82 \\ & \quad 1.82 \\ & \quad 2.27 \\ & \quad -0.211 \qquad \qquad \qquad 0.014 \\ & \quad -0.333 \qquad \qquad \qquad 0.015 \end{aligned}$$

g)
h)

$$\frac{1}{10} \left\{ 0.76 \begin{bmatrix} \text{---} \\ \text{---} \\ \text{---} \end{bmatrix} + 0.80 \begin{bmatrix} \text{---} \\ \text{---} \\ \text{---} \end{bmatrix} \right\}^2 = \frac{1.92 \times 10^{-2}}{2.13 \times 10^{-2}} \quad e^2 b^3$$

(3.3 %)
i)
= 0.577

$$\begin{aligned}
 & \frac{1}{10} \left\{ -0.53 \left[\begin{array}{c} \text{Diagram 1} \\ \text{Diagram 2} \end{array} \right] + 1.02 \left[\begin{array}{c} \text{Diagram 3} \\ \text{Diagram 4} \end{array} \right] \right\} \\
 & + 0.76 \left[\begin{array}{c} \text{Diagram 5} \\ \text{Diagram 6} \\ \text{Diagram 7} \\ \text{Diagram 8} \\ \text{Diagram 9} \\ \text{Diagram 10} \end{array} \right] + 0.80 \left[\begin{array}{c} \text{Diagram 11} \\ \text{Diagram 12} \\ \text{Diagram 13} \\ \text{Diagram 14} \\ \text{Diagram 15} \\ \text{Diagram 16} \end{array} \right] = \\
 & = \frac{0.0216}{(e^2 b^3)} \quad (3.7\%) \\
 & \quad 0.0087 \quad (1.5\%) \quad j)
 \end{aligned}$$

Figure 2.7.11: In **a), b)** and **c)** we give the two graphical contributions and the corresponding numerical values to the matrix element $M(E) = \langle d_{3/2}^{-1} \otimes gs(^{210}\text{Po}) | h_{eff}(E) | h_{9/2} \otimes 3^{-}(^{208}\text{Pb}); 3/2 \rangle$ in lowest order in $1/\Omega$. The resulting wave functions $|\tilde{I}\rangle$ and $|\tilde{II}\rangle$ are displayed in **e)** normalized according to (2.7.72). In **e)** we also give the unperturbed, and the renormalized theoretical energies of the levels. The (t, α) spectroscopic factor corresponding to the reaction $^{210}\text{Po}(t, \alpha)^{209}\text{Bi}$ is denoted by S , while

$$R = \frac{d\sigma(h_{9/2} \rightarrow J)}{d\sigma(gs(^{208}\text{Pb}) \rightarrow 3^{-}(^{208}\text{Pb}))}.$$

is the ratio of inelastic cross sections. In **d)** we display the free fields, while in **e)** we provide a summary of the results of the calculations in comparison with the data. The zeroth and order $1/\Omega$ contributions to the electromagnetic excitations are collected in **i)** and **j)**. The value $0.58e^2b^3$ is the $B(E3; 0 \rightarrow 3)$ value associated with the 2.615 MeV state in ^{208}Pb . In **g)** and **h)** we give the zeroth and order $1/\Omega$ contributions to the spectroscopic factor associated with the $^{210}\text{Po}(t, \alpha)^{209}\text{Bi}$ reaction. Finally in **f)** we display the lowest contribution to the spectroscopic factor associated with the $^{208}\text{Pb}(^3\text{He}, d)$ reaction, which gives a measure of the ground state correlations of ^{208}Pb associated with the existence of an octupole and a pairing vibration (see also Tables 2.5.1–2.5.3).

while all the RPA solutions are included in the intermediate states. The quadrupole surface vibrational modes were allowed only as intermediate states. The single hole and particle states j_1^{-1} and j_2 , respectively, correspond to experimentally known levels around the $Z = 82$ shell closure. In what follows, the two $\frac{3}{2}^+$ states built out of the $|d_{3/2}^{-1} \otimes gs(^{210}\text{Po})\rangle$ and $|h_{9/2} \otimes 3^-(^{208}\text{Pb})\rangle$ configurations are studied in this space. This two-state system provides a rich laboratory to learn about the interplay of surface and pairing modes.

The two basis states

$$|\alpha\rangle \equiv |d_{3/2}^{-1} \otimes gs(^{210}\text{Po}); 3/2^+\rangle \quad (2.7.92)$$

and¹¹³

$$|\beta\rangle \equiv |h_{9/2} \otimes 3^-(^{208}\text{Pb}); 3/2^+\rangle \quad (2.7.93)$$

are 118 keV apart. They mix strongly through the couplings depicted by the graphs a) and b) of Fig. 2.7.11.

Because of the energy dependence of h_{eff} there is a different matrix element for each final state. The diagonalization of the matrices was carried out self-consistently, *i.e.* the energy denominators of the different graphs are to be calculated by utilizing the exact energies¹¹⁴. The corresponding graphical contributions to the spectroscopic factor and inelastic cross-sections are also collected in fig. 2.7.11. To be noted is the very different ratio of the (d, d') and (t, α) cross sections. While $R_1 = B(E3; (\frac{3}{2})_1)/B(E3; (\frac{3}{2})_2)$ is approximately equal to 2.5, the ratio $R_2 = \sigma((t, \alpha); (\frac{3}{2})_2)/\sigma((t, \alpha); (\frac{3}{2})_1)$ is close to one. Because the component $|\beta\rangle$ carries the inelastic-scattering strength, while the (t, α) reaction proceeds mainly through the component of type $|\alpha\rangle$, the difference between R_1 and R_2 can be traced back to the corrections associated with the over-completeness of the unperturbed basis states which give rise to rather different normalizations of the two physical states (see Sects. 2.5 and 2.7.3, see also App. 2.B, Sect. 2.B.2).

2.8 Competition between the variety of ZPF, in particular those associated with density ($\beta = 0$) and pairing ($\beta = \pm 2$)

Particle-hole like vibrations, as e.g. collective surface quadrupole vibrations, induce dynamical distortions of the mean field which virtually break the magnetic degeneracy of levels into two-fold (Kramer's) degenerate (Nilsson-like) levels and to a reduction of the size of the discontinuity at the Fermi surface typical of non-interacting Fermi systems. Pairing vibrations also smooth out the sharp discontinuity of occupancy taking place around the Fermi energy displayed by closed shell

¹¹³Although not likely, the reader is advised not to confuse the label of the state $|\beta\rangle$ with the transfer quantum number β used above.

¹¹⁴for more details, see ref. Bortignon, P. F. et al. (1977); see also Bortignon et al. (1976).

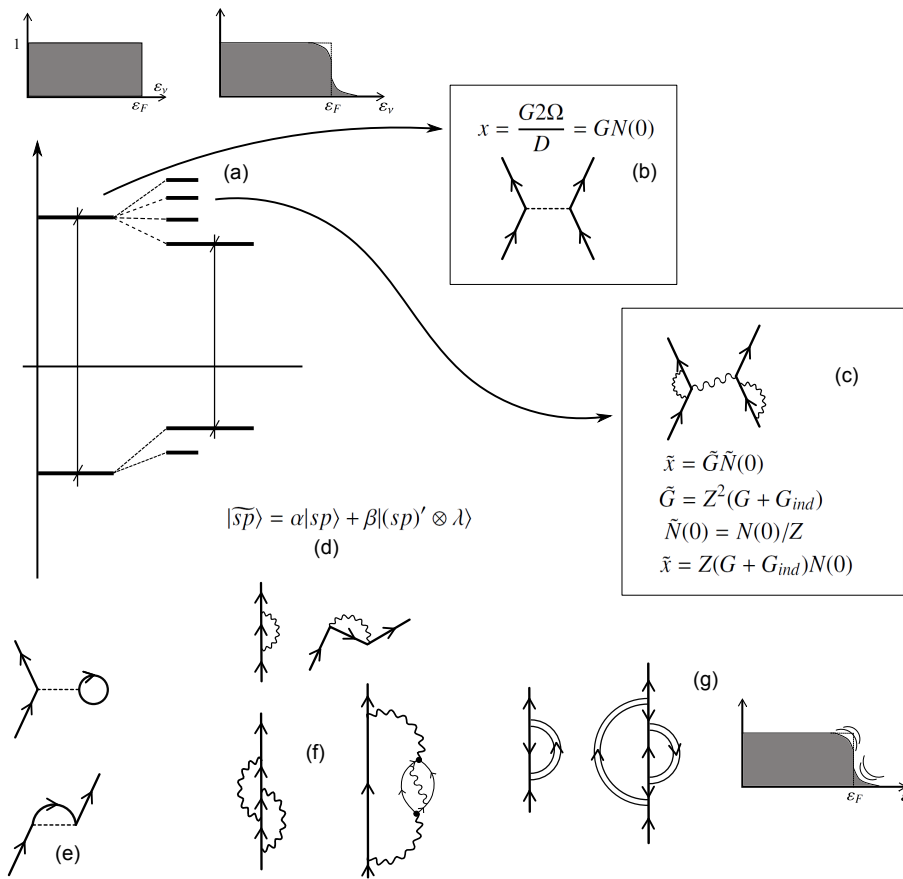


Figure 2.8.1: Schematic representation of some of the consequences the interweaving of the elementary modes of excitation with varied transfer quantum number ($\beta = 0, \pm 1, \pm 2$; (f), (g)) have in the (mainly single-particle) nuclear spectrum (a) (e). In particular pair correlations (b, c), as measured by the (two-level) dimensionless parameter $x = G2\Omega/D = GN(0)$, product of the bare coupling constant G and the density of states (DOS) at the Fermi energy (ratio of the single-particle degeneracy $2\Omega = (2j+1)$, and the single-particle energy separation; see Högaasen-Feldman (1961); Broglia, R.A. et al. (1968)). Coupling with surface modes (f) reduce the effective value of D leading to an increase of $N(0)$ as measured by $1/Z$ but, at the same time decreases, through the breaking of the single-particle strength, the single-particle content (d) of each level (as measured by Z ; see e.g. Barranco et al. (2005) and refs. therein). The eventual increase of x , as reflected by \tilde{x} , results from a delicate balance of the two effects eventually overwhelmed by the induced pairing interaction resulting from the exchange of collective ($\beta = 0$) vibrations between pairs of nucleons moving in time reversal states close to the Fermi energy, and by the dynamical smoothing of the Fermi energy through the coupling of single-particle states to $\beta \pm 2$ pairing vibrations (g).

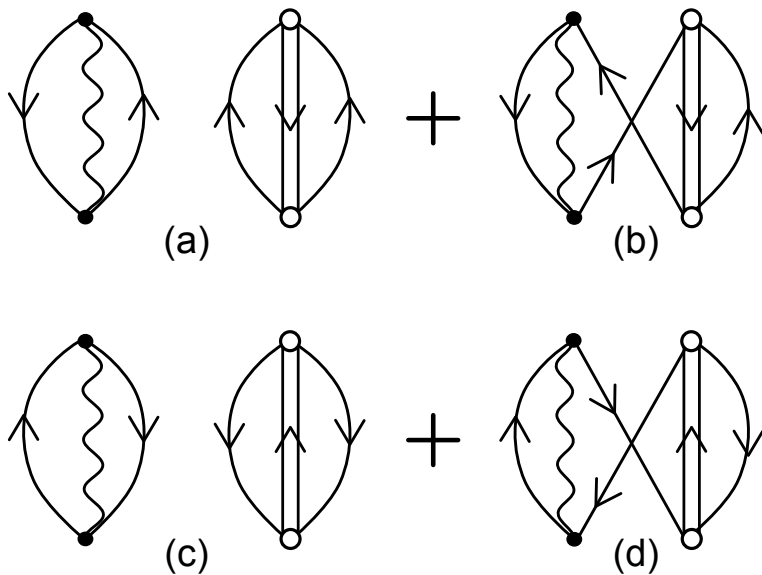


Figure 2.8.2: (a) (c) ZPF associated with $p-h$ and pairing vibrations (pair subtraction and pair addition modes) make use of the same nucleon degrees of freedom to simultaneously, and independently, correlate $p-h$, $p-p$ and $h-h$ excitations, thus violating Pauli principle (harmonic approximation). The NFT processes (b) and (d), which contribute to the correlation energy of the nucleus with opposite sign to that contributed by (a) and (c) (each unavoidable crossing of fermion lines contributes a minus sign), remove Pauli violating contributions to the corresponding order of perturbation in $1/\Omega$ (see Eq. (2.7.89) and related text).

systems through dynamical ($U_j V_j$) weighting factors (see Fig. 4.3.2), which are operative in an energy region¹¹⁵ $\epsilon_F \pm E_{corr}(\beta = \pm 2)$ (see Fig. 2.8.1 (g)). At the same time the dressing of nucleons by particle-hole and pairing vibrations, leads to an effective ω -mass making nucleons heavier, thus approaching the centroid of the valence orbitals lying above and in the Fermi sea towards the Fermi surface. In Fig. 2.8.1 a schematic representation of the subtle effects the interweaving of single-particle motion and collective vibrations has on pairing correlations, is displayed (see also Fig. 5.10.1).

Zero point fluctuations induced by particle-hole like and by pairing modes compete with each other for phase space, through Pauli principle (see Fig. 2.8.2), thus eventually leading to a single ground state containing all of the dressed renormalized ZPF (see Sect. 2.7). The Pauli principle NFT diagrams showed in Figs. 2.8.2 (b) and 2.8.2 (d) are at the basis of the stabilization of the ground state in general and of the competition between (as a rule quadrupole) deformations in 3D-space which breaks single-particle degeneracy (Nilsson potential), and in gauge space which thrives on large degeneracies¹¹⁶. It is also the reason why single open shell nuclei are usually spherical. When tidal-like polarization effects in doubly open shell nuclei become overwhelming, the nucleus makes use of a Jahn-Teller mechanism. This to profit at best and simultaneously, of the quadrupole-quadrupole (alignment) and of the pairing (independent pair motion in Kramers degenerate levels) interactions. In other words, of potential energy (quadrupole deformation, localization) and of pairs of nucleons solidly anchored to each other (localization), over distances $\xi (\gg R_0)$ resulting in strongly overlapping entities and thus little sensitive to the orientation of the quadrupole deformed field (small moment of inertia), effect weakened in turn because of low spatial degeneracy. The fact that the moment of inertia \mathcal{J} of e.g. quadrupole deformed nuclei is found to be appreciably smaller (by about a factor of 2) than the rigid moment of inertia testifies to the role pairing correlations play in nuclei. The fact that \mathcal{J} is considerably larger than the irrotational moment of inertia¹¹⁷ (by a factor of 5), testifies to the subtle effects that spatial quantization, medium polarization effects (within this context see Fig. 4.9.5), let alone the $^1S_0 - NN$ potential, eventually corrected by three-body effects, have in Cooper pair binding.

¹¹⁵ E_{corr} is the correlation energy associated with the pair addition ($\beta = +2$) and pair removal mode ($\beta = -2$).

¹¹⁶ This is an example of the competition between pairing and aligned scheme (Bayman (1961); Bès and Sorensen (1969); Mottelson (1962); Bohr, A. and Mottelson (1975)).

¹¹⁷ Bohr, A. and Mottelson (1975) p. 75.

2.9 Optical potential and transfer

In this Section the unification of NFT of structure and reactions is further developed using as example the light exotic two-neutron halo nucleus ^{11}Li . In particular, we dwell upon the variety of renormalization processes and associated form factors needed to calculate one- and two- neutron transfer reactions. The use of the same elements in the eventual calculation of the polarization contribution to the optical potential is also discussed.

2.9.1 Bare particles and Hartree–Fock field

Nucleon elastic scattering experiments at energies of tens of MeV can be accurately described in terms of an optical potential in which the real component is parametrized according to the (Woods–Saxon) potential¹¹⁸,

$$U(r) = Uf(r), \quad (2.9.1)$$

$f(r)$ being a Fermi (sigmoidal) function, of radius $R_0 = r_0 A^{1/3}$ ($r_0 = 1.2$ fm), diffusivity $a = 0.65$ fm, and strength

$$U = U_0 + 0.4E \quad (2.9.2)$$

where

$$U_0 = V_0 + 30 \frac{N - Z}{A} \text{ MeV}, \quad V_0 = -51 \text{ MeV}, \quad (2.9.3)$$

while E is the energy of the scattered particle $\epsilon_k = \hbar^2 k^2 / 2m$, measured from the Fermi energy, m being the nucleon mass. In the case of $^9\text{Li}_6$, $U_0 \approx -41$ MeV. One can replace the k -dependence in (2.9.2) by the so-called k -mass¹¹⁹

$$m_k = m \left(1 + \frac{m}{\hbar^2 k} \frac{dU}{dk} \right)^{-1}, \quad (2.9.4)$$

where the energy independent Woods–Saxon potential has a depth given by $\left(\frac{m}{m_k}\right) U_0 = U'_0$ ¹²⁰. For the nucleons of the core, i.e. of ^9Li , $m_k = m(1 + 0.4)^{-1} \approx 0.7m$. For the halo neutrons¹²¹, $m_k/m = (1 + O \times 0.4)^{-1}$, where $O (= (R_0/R)^3)$ is the overlap between the core and the halo nucleons. Making use of the values $R_0 = 2.66$ fm and $R = 4.58$ fm (see Eq. 4.11.4) one obtains $O \approx 0.2$ (see (3.6.8)) and thus, $m_k \approx 0.93m$.

¹¹⁸cf. e.g. Bohr and Mottelson (1969) and refs. therein.

¹¹⁹What in nuclear matter is called the k -mass and is a well defined quantity, in finite systems like the atomic nucleus, in which linear momentum is not a conserved quantity, is introduced to provide a measure of the spatial non-locality of the mean field, and is defined for each state as the expectation value of the quantity inside the parenthesis in Eq. (2.9.4), calculated making use of the corresponding single-particle wavefunction (see e.g. ref. Bernard and Giai (1981), in which case m_k is referred to as the non-locality effective mass)

¹²⁰See e.g. Fig. 2.14 Mahaux, C. et al. (1985).

¹²¹Assuming a velocity independent v , the k -dependence of the mean field stems from the exchange (Fock) potential $U_x(\mathbf{r}, \mathbf{r}') = -\sum_i \varphi_i^*(\mathbf{r}') v(|\mathbf{r} - \mathbf{r}'|) \varphi_i(\mathbf{r})$ (linear in O), while the central potential

2.9.2 Physical particles and optical potential

Within the framework of the above scenario, each nucleon moves independently in the average field created by all the other nucleons¹²² feeling their pushings and pullings only when trying to leave the nucleus, the summed effect being to be forced to scatter elastically off the nuclear surface. Schematically, the full complexity of the many-body nuclear Hamiltonian

$$H = T + v, \quad (2.9.5)$$

has been reduced to

$$H_{HF} = T + U(r) + U_x(\mathbf{r}, \mathbf{r}'). \quad (2.9.6)$$

In other words, and making use of the expression,

$$H = T + v(|\mathbf{r} - \mathbf{r}'|) = H_{HF} + (v(|\mathbf{r} - \mathbf{r}'|) - (U(r) + U_x(|\mathbf{r} - \mathbf{r}'|))) \quad (2.9.7)$$

the full many-body nuclear Hamiltonian has been approximated by the Hartree-Fock Hamiltonian by neglecting the term in parenthesis. That is, by assuming that the sum of the direct and exchange potential gives a sensible approximation to the full two-body interaction v . This approximation (adding an appropriate spin-orbit potential), although providing a number of important insights into the nuclear structure and reactions as the sequence of single-particle levels¹²³ (and associated magic numbers), and sensible nucleon-nucleus, elastic phase shifts, disagrees with experiment on a number of points. In particular, leading to a too low level density at the Fermi energy, to an infinite mean free path, also for nucleons moving in states (e.g. deep hole states) far removed from the Fermi energy, let alone the lack of collective electromagnetic transitions and the large value of the elastic cross section.

To move further, one has to go beyond independent particle as well as potential scattering motion. That is, one has to allow the particles (both bound and projectile nucleons) to interact among themselves through four point vertices (see e.g. (2.7.16) and diagrams a) and b) of Fig. 2.7.10), aside from coupling to the nuclear and to the Fermi surface (diagrams c)-i) of Fig. 2.7.10). Also with spin, spin-isospin, etc. modes (particle vibration coupling, which in the case of surface modes has been introduced in (2.7.26); see also (2.3.13)). In other words, to allow the elementary modes of excitation to interact according to the NFT rules. In the case in which one nucleon moves with asymptotic waves for $r = -\infty$ (e.g. projectile), the interaction in parentheses in (2.9.7) can lead to the coupling to open

is written as $U(r) = \sum_i \int d\mathbf{r}' |\varphi_i(\mathbf{r}')|^2 v(|\mathbf{r} - \mathbf{r}'|)$, (independent of O). It is of notice that the coupling between e.g. the quadrupole vibration of the core (⁸He) and a halo neutron is also linear in O , i.e. $\langle H_c \rangle_{2^+(\text{core}), n(\text{halo})} = \beta_2 \left\langle \frac{R_0}{\sqrt{5}} \frac{\partial U}{\partial r} \right\rangle O \langle j||Y^2||1/2 \rangle$, where $\langle j||Y^2||1/2 \rangle \approx 0.7$ ($j = 5/2, 3/2$), and $\left\langle R_0 \frac{\partial U}{\partial r} \right\rangle \approx 1.44 U_0 \approx -60$ MeV, see Brink, D. and Broglia (2005) Eqs. (D20) p. 303 and (D26) p. 304 (see Sect. 2.9.2 and Fig. 2.9.1).

¹²²Pauli principle (Fock potential) takes care of not to count the contribution of a nucleon on itself.

¹²³Mayer and Jensen (1955).

reaction channels. In particular, one- and two-particle transfer reactions, in which the mass partition changes between entrance and exit channels. Let us exemplify the consequences of the interaction between elementary modes of excitation in the case of $^{11}\text{Li}+p$.

2.9.3 $^{11}_3\text{Li}_8$ structure in a nutshell

The sequence of single-particle levels for the $^{10}_3\text{Li}_7$ associated with the mean field potential (2.9.3) implies that the distance between the last occupied neutron state $0p_{1/2}(\epsilon_{1/2^-} = -1.2 \text{ MeV})$ and the first empty one, $1s_{1/2}(\epsilon_{1/2^+} = 1.5 \text{ MeV})$ is 2.7 MeV (see Fig. 2.9.1). In other words, in ^{10}Li the $0s_{1/2}, 0p_{3/2}$ neutron orbitals are fully occupied, while $0p_{1/2}$ carries one neutron, making ^{11}Li a single closed shell system. There is experimental evidence which testifies to the fact that the first unoccupied states of ^{10}Li are a virtual $1/2^+$ ($\epsilon_{1/2^+} = 0.2 \text{ MeV}$) and a resonant $1/2^-$ ($\epsilon_{1/2^-} = 0.5 \text{ MeV}$) state¹²⁴. According to NFT, this is a consequence of the self-energy renormalization of the bare $1/2^+$ state and of the $1/2^-$ state through a mainly PO (polarization) and CO (correlation) process respectively¹²⁵ (Fig. 2.9.1). Thus parity inversion and the melting of the $N = 8$ closed shell in favor of the new magic number $N = 6$. While ^{10}Li is not bound, ^{11}Li displays a two-neutron separation energy $S_{2n} \approx 400 \text{ keV}$. This value is the result of a subtle bootstrap mechanism. Being at threshold and basically not feeling a centrifugal barrier, the $1/2^+$ and $1/2^-$ states, are essentially not available for the short range bare NN -pairing interaction, requiring a Cooper pair binding mechanism mediated by the exchange of long wavelength collective modes. This is the natural scenario of a very low-lying collective dipole mode for two main reasons. First, the presence of an eventual dipole particle-hole transition $1/2^+ \rightarrow 1/2^-$, with energy about 1 MeV. The second one is related to the fact that the neutron halo in ^{11}Li can hardly sustain multiple surface vibrations, e.g. quadrupole vibrations, aside from displaying a very large radius as compared to that of the closed shell core $^9_3\text{Li}_6$, and thus a small overlap with it. This single-particle controlled phenomenon¹²⁶ has a three-fold consequence: i) to screen the bare $NN^{-1}S_0$ short range pairing

¹²⁴Zinser et al. (1995). Note however Cavallaro et al. (2017) and Sanetullaev et al. (2016); see also Barranco et al. (2018) and Moro et al. (2019).

¹²⁵Barranco, F. et al. (2001), CO (involving ground state correlation vertices), PO (particle moving around closed shells and polarizing the core).

¹²⁶Within this context one is essentially forced to make a subtle extension of the statement according to which the single-particle motion is the most collective of all nuclear motions (Mottelson (1962)), emerging from the same properties of the nuclear interaction (both bare and induced) as collective motion does, and in turn at the basis of the detailed properties of each collective mode, acting as scaffolds and filters of the variety of embodiments. In fact, one has to add the characterisation of “physical” to “single-particle motion” (i.e. clothed) to englobe in the above statement also the present situation (parity inversion). In other words, while the bare $s_{1/2}$ and $p_{1/2}$ orbitals could never lead to a low-lying dipole strength, the corresponding clothed, physical states do so in a straightforward manner, the dressing effects being in this case of the same order of magnitude of the mean field effects. Consequently: “physical, clothed single-particle motion, is one of the most collective of nuclear motions”, seems to be the right statement.

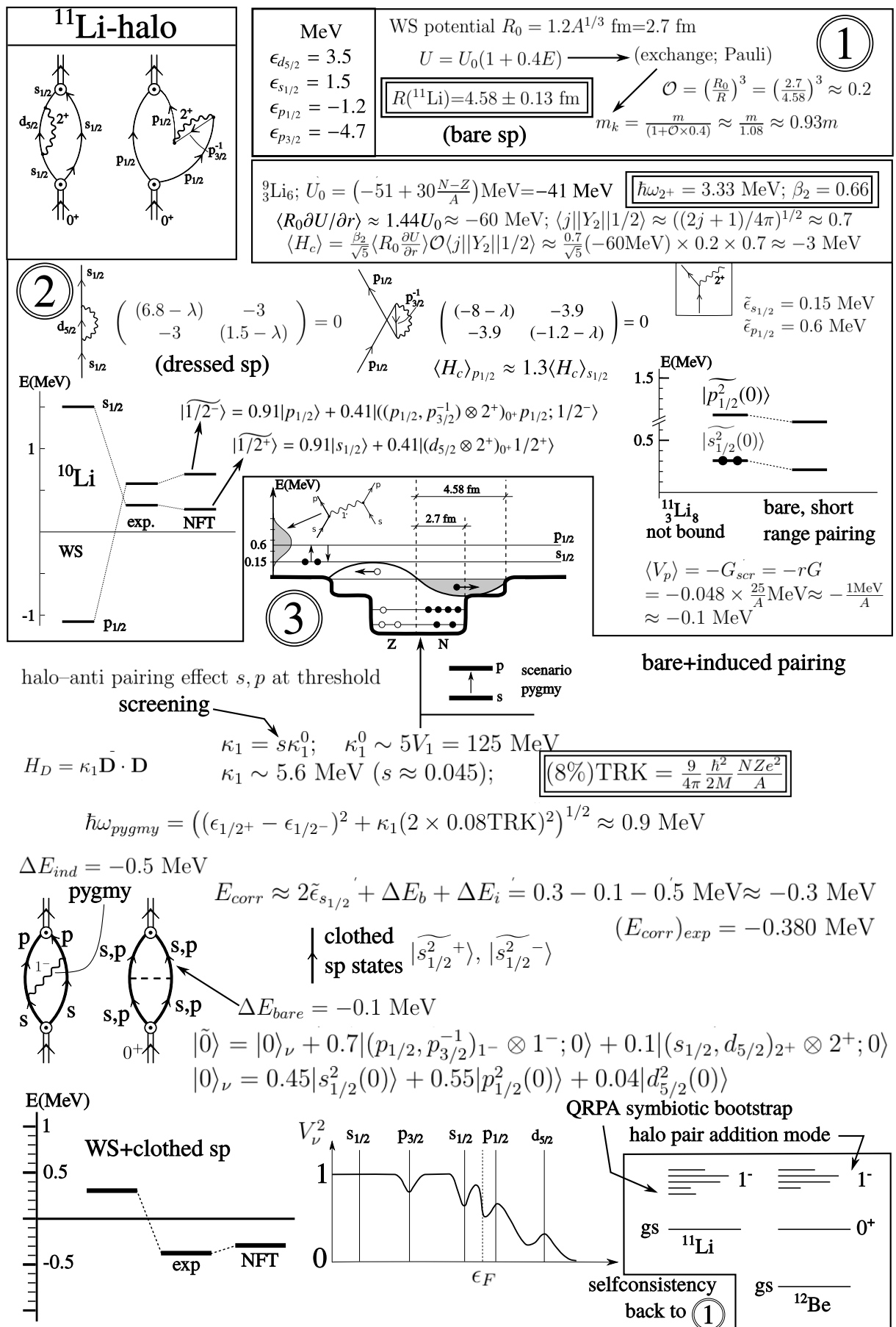


Figure 2.9.1

interaction making it subcritical, ii) to screen the (repulsive) symmetry interaction, and (consequently), iii) to allow the presence at low energies of a consistent fraction of the TRK–sum rule associated with the GDR at ≈ 36 MeV. In fact, a 1^- resonance carrying $\approx 8\%$ of the TRK sum rule and with centroid at an energy $\lesssim 1$ MeV have been observed¹²⁷. Thus, the connotation of pygmy dipole resonance (PDR)¹²⁸. Exchanged between the heavily dressed neutrons moving in parity inverted states provides, together with the contribution of the strongly screened, bare NN –pairing interaction, the glue needed to bind the neutron halo Cooper pair to the ${}^9\text{Li}$ core. With some experimental input¹²⁹, NFT allows to, accurately and economically, propagate dressing effects which not only renormalizes mean field, but overwhelms it providing an overall account of the experimental findings. The many–body effects at the basis of these phenomena are carried out in three steps, as schematically displayed in Fig. 2.9.1 and described below (for details see Sect. 3.6)¹³⁰.

1 Starting with well defined elements: Woods–Saxon (WS) potential, and the parameters characterizing the low–lying quadrupole vibration of the core ${}^9\text{Li}$ (**input**, double boxed quantities), calculate the single–particle levels and collective vibration (separable interaction) and determine the corresponding particle–vibration coupling vertices (strength and form factors). From the ratio of the WS radius (R_0) and of the observed one ($R({}^{11}\text{Li})$ **input**) determine the overlap O . Because $O \ll 1$, the contribution of the exchange (Fock) potential to the empirical WS potential is small concerning the halo neutrons¹³¹. Consequently the neutron halo k –mass m_k has a value close to the bare mass m .

2 Making use of the above elements one can cloth the bare single–particle states, in particular the $s_{1/2}$ and $p_{1/2}$ states. Parity inversion ensues, with $1/2^+$ and $1/2^-$ at threshold. As a consequence the $N = 8$ shell closure melts away, $N = 6$ becoming a new magic number, testifying to the fact that large amplitude fluctuations can be, in nuclei, as important or even more important than static mean field effects. As a result ${}^9\text{Li}_7$ is not bound. Adding one more neutron and switching on the bare pairing interaction (e.g. a contact force $V(r_{12}) = -4\pi V_0 \delta(\mathbf{r}_1 - \mathbf{r}_2)$ with constant matrix element¹³² $G = 1.2 \text{ fm}^{-3} V_0/A \approx (25/A) \text{ MeV}$), the screening $r = \frac{(M_j)\text{halo}}{(M_j)\text{core}} \approx \frac{2}{2j+1} \left(\frac{R_0}{R} \right)^3 \approx 0.048$ (see Eq. (3.6.3)) resulting from the poor overlap between halo and core neutrons leads to a value of the strength of the pairing interaction $(G)_{scr} = r \times G$ which is subcritical, and thus to an unbound system (see Sect. 3.6 and App. 3.8). In fact, $G_{scr} = 0.048 \times 25/A \text{ MeV} \approx 0.1 \text{ MeV}$ and $\Delta E = 2\tilde{\epsilon}_{s_{1/2}} - G_{scr} \approx 0.3 \text{ MeV} - 0.1 \text{ MeV} \approx 0.2 \text{ MeV}$. Summing up,

¹²⁷Kanungo et al. (2015); Sackett et al. (1993); Zinser, M. et al. (1997)

¹²⁸See Broglia et al. (2019) and references therein.

¹²⁹See e.g. the corresponding discussion in Barranco et al. (2017).

¹³⁰It is of notice that in discussing Fig. 2.9.1 use is made of the values calculated in NFT. This is also true in connection with the estimates carried out in Sect. 3.6.1.

¹³¹See Sect. 2.9.1.

¹³²Brink, D. and Broglia (2005), pp 40–42. It is of notice that the difference with the number found in this reference $G \approx 28/A \text{ MeV}$ is within the margin of uncertainties.

$G_{scr} < G_c$, G_c being the minimum value of the pairing coupling constant leading to a bound state¹³³.

3 Considering the sloshing back and forth of the halo neutrons (with a small contribution from the core neutrons) against the core protons, leads to a dipole mode feeling a strongly screened repulsive symmetry potential. In keeping with the fact that $\kappa_1^0 \sim 1/R^2(^{11}\text{Li})$, the screening factor can be estimated as $((R(^{11}\text{Li})/\xi)^2(R = 4.58 \text{ fm}, \xi = 20 \text{ fm}, s \approx 0.052)$, the value obtained in Sect. 3.6 being $s = 0.043$. In other words, while it takes a quantity proportional to $5V_1 = 125 \text{ MeV}$ to separate protons from neutrons in the core, this price is reduced to $s \times 5V_1 = 5.4 \text{ MeV}$ ($(V_1)_{scr} = sV_1 \approx 1 \text{ MeV}$) for halo neutrons. This is at the basis of the fact that $\approx 8\%$ of the Thomas–Reiche–Kuhn sum rule (**input**) gets down to $\lesssim 1 \text{ MeV}$. Another way to say the same thing is that $(V_1)_{scr} = sV_1$ is at the basis of the fact that the $s_{1/2} - p_{1/2}$ energy difference ($\Delta\epsilon \approx 0.45 \text{ MeV}$) is only increased by a modest value ($\hbar\omega_{pygmy} \approx 1 \text{ MeV} \approx 10^{21} \text{ Hz}$), while the $E1$ single-particle strength remains essentially unchanged. Typical values in the case of nuclei lying along the stability valley being $\approx 10^{-4}B_W(E1)$ for low-energy single-particle transitions, while in the present case one finds a value close to $1B_W(E1)$.

Now, the two halo neutrons dressed by the vibrations of the core (heavy arrowed lines in lowest left corner of Fig. 2.9.1) and interacting through the bare NN -pairing force are not bound. Consequently, the pygmy resonance will fade away almost as soon as it is generated (essentially lasting the neutron transversal time $\approx 10^{-21} \text{ s}$). This, unless it is exchanged between the two neutrons forcing them to jump from the configuration $s_{1/2}^2(0)$ at threshold ($2 \times \tilde{\epsilon}_{s_{1/2}} \approx 0.3 \text{ MeV}$) into $p_{1/2}^2(0)$, also close to threshold ($2 \times \tilde{\epsilon}_{p_{1/2}} \approx 1.2 \text{ MeV}$). In other words, one finds the dipole pygmy resonance acting as an intermediate boson which couples to the halo neutrons with a strength $\Lambda \approx 0.5 \text{ MeV}$ (QRPA calculation). As a result, it contributes to the binding of the neutron halo Cooper pair with $\approx 0.5 \text{ MeV}$ binding. Thus, the corresponding correlation energy $E_{corr} \approx -0.3 \text{ MeV}$ is mainly due

¹³³ At the basis of superconductivity one finds the result obtained by Cooper (1956). He worked out the problem of two electrons interacting through an attractive interaction above a quiescent Fermi sea. Thus, all but two of the electrons are assumed to be noninteracting. The background of electrons enter the total problem only through the Pauli principle by blocking states below the Fermi surface from participating in the remaining two-particle problem. If one measures the kinetic energy ϵ_k relative to its value at the Fermi surface only states with $\epsilon_k > 0$ are available to the interacting pair of electrons. Cooper found that a bound state of the pair always exists for arbitrarily weak coupling so long as the potential is attractive near the Fermi surface, a mechanism which implies the instability of the normal phase, and found at the basis of superconductivity. Cooper pair binding is a rather remarkable result for the usual two-body problem. If one has only two particles coupled by an attractive interaction of finite range, they would not form bound states unless the attractive interaction exceeds a certain critical value, Cooper reduces the above 3-dimensional to a 1-dimensional quantal system (Gor'kov (2012)) Now, in ¹¹Li the last two neutrons are very weakly bound. Consequently they move away from the neutron closed shell core ⁹Li, lowering in the process their relative momentum and forming a misty cloud or halo. One can thus view this system as the nuclear embodiment of a Cooper pair. The question then arises, why there is a critical value for the pairing interaction. The answer is spatial quantization, which is a three-dimensional feature, and is associated with the fact that the nucleus is a finite system.

to the dipole pygmy exchange process. The resulting symbiotic halo pair addition mode of ^{11}Li can, in principle, be used as a building block of the nuclear spectrum, amenable to be moved around. A possible candidate for such a role is the first excited 0^+ state of ^{12}Be , together with the associated dipole state built on it and eventually other fragments of the associated $E1$ –low energy–strength.

To calculate the pygmy dipole resonance (PDR) of ^{11}Li one needs to know the ground state of this nucleus (halo–pair addition mode) so as to be able to determine microscopically the occupation factors of the $1s_{1/2}, 1p_{3/2}, \epsilon s_{1/2}, \epsilon p_{1/2}, \epsilon d_{5/2}, \dots$, etc. states. This is the basic input needed to work out the corresponding QRPA equations, whose diagonalization provide the energy, transition density and probability of the mode. But to do so one is required to know the PDR. Arrived to this point, the protocol schematically presented in Fig. 2.9.1 implies to go back to 1 and repeat the whole procedure until convergence is achieved.

2.9.4 $^{11}\text{Li}(p, p)^{11}\text{Li}$ optical potential and transfer reaction channels

NFT is based on elementary modes of excitation, modes which carry a large fraction of the nuclear correlation. Because its rules have no limitations concerning whether the excitations studied lie or not in the continuum, or whether the single-particle motion displays asymptotic conditions, it allows for a unified description of structure (s) and reactions (r) (NFT(s+r)). An example of the above statement is provided by Fig. 2.9.2. Graph (a) is a NFT-diagram describing one of the processes contributing to the elastic reaction $^{11}\text{Li}(p, p)^{11}\text{Li}$ as the system propagates in time. This graph describes a polarization contribution to the global (mean field) optical potential describing proton elastic scattering off ^9Li .

In what follows we describe the processes taking place in Fig. 2.9.2 (a) in the interval of time $t_1 - t_{11}$, starting from the $t = -\infty$ situation in which a proton impinges on ^{11}Li . At time t_1 , the halo pair addition mode $|0_\nu\rangle$ couples to a pure, bare configuration $s_{1/2}^2(0)$. At time t_2 , and due to the zero point fluctuations associated with the quadrupole vibration of the ^{11}Li core, the virtual state $((p_{1/2}, p_{3/2}^{-1})_{2^+} \otimes 2^+)_{0^+}$ is created. At time t_4 , one of the continuum $s_{1/2}$ neutrons excites the quadrupole vibration of the core reabsorbing it at time t_6 . As a result of this self energy process, its energy is lowered to threshold, becoming a virtual state. The other $s_{1/2}$ continuum neutron state excites at t_3 the PDR and moves into the $p_{1/2}$ orbital after which, and due to Pauli principle, becomes exchanged with the homologous $p_{1/2}$ of the $(p_{1/2}, p_{3/2}^{-1})_{2^+}$ configuration, exchange process which is completed by time t_5 . As a result the $p_{1/2}$ state undergoes a conspicuous repulsion, becoming a resonant state. At time t_7 the $s_{1/2}$ neutron absorbs the PDR and moves into a $p_{1/2}$ state. At time t_8 it interacts, through the bare 1S_0 –(pairing) interaction, with the other $p_{1/2}$ neutron, completing the process by which the halo pair addition mode binds to the core ^{11}Li . Before the two $p_{1/2}$ neutrons couple to the $|0_\nu\rangle$ state one of them is picked up at time t_9 under the action of the proton–neutron interaction v_{np} , by the projectile (proton), to form a virtual deuteron. The recoil effect associated with the new mass partition being taken care of by the particle–recoil

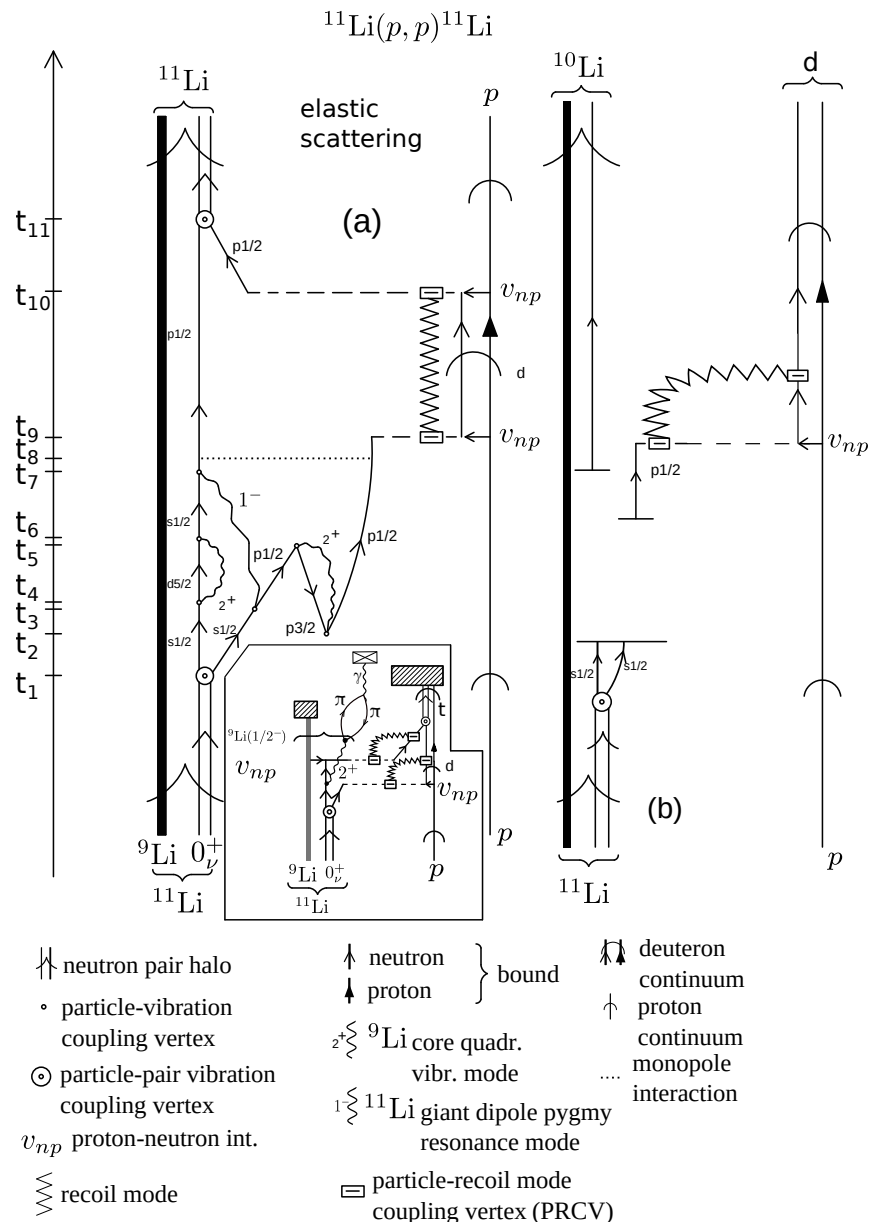


Figure 2.9.2: (a) NFT-diagram describing one of the processes contributing to the elastic reaction $^{11}\text{Li}(p, p)^{11}\text{Li}$ as the system propagates in time (polarization contribution to the global (mean field) optical potential). In the inset, a schematic NFT diagram describing the process $^{11}\text{Li}(p, t)^9\text{Li}(1/2^-)$ is displayed. A dashed open rectangle indicates the particle-recoil coupling vertex. A crossed box represents a γ -detector, while hatched rectangles particle detectors. (b) Schematic NFT diagram describing the reaction $^{11}\text{Li}(p, d)^{10}\text{Li}$, i.e. same as in (a) up to time t_8 (reason for which no details are repeated between t_2 and t_8). From there on the deuteron continues to propagate to the detector bringing to it, aside from nuclear structure information, the information resulting from its interaction with the recoil mode. Likely, the neutron in ^{10}Li will break up almost as soon as it is formed. Summing up, in the center of mass reference frame both p and ^{11}Li display asymptotic states in entrance as well as in exit channels in case (a), and only in the entrance channel in case (b), while in the exit channel it is the ^{10}Li ($^9\text{Li} + n$) and the deuteron that do so.

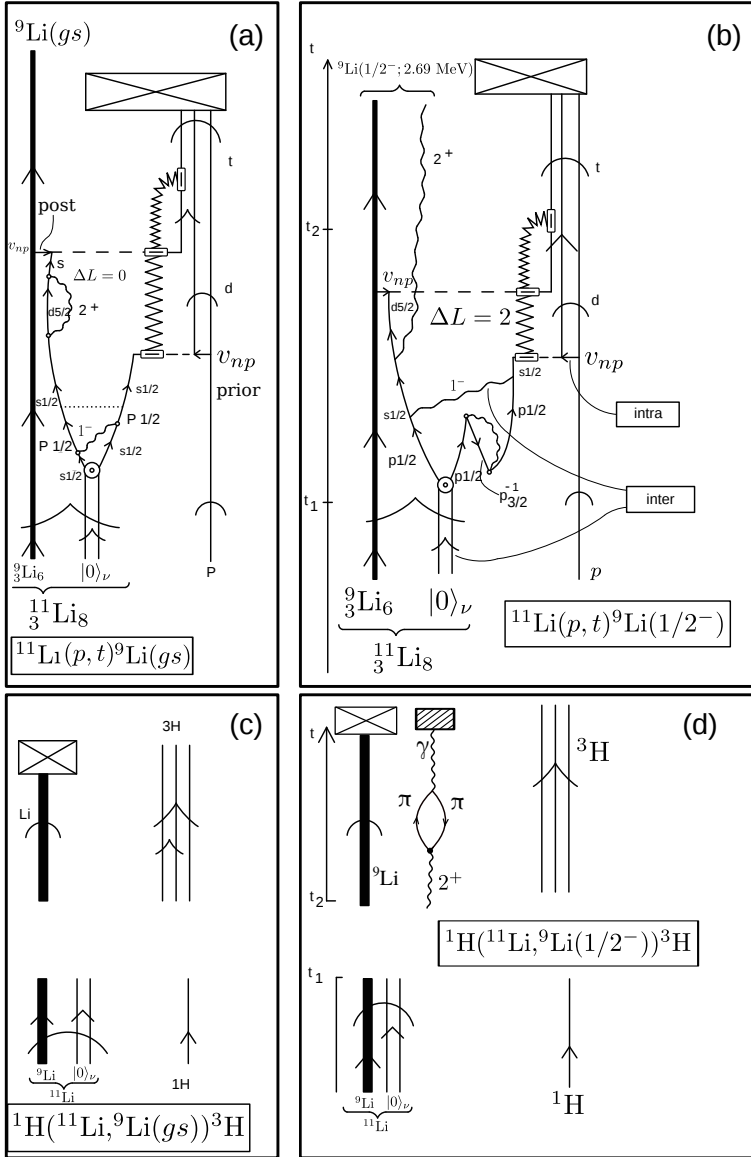


Figure 2.9.3: NFT representation of the reactions (a) $^{11}\text{Li}(p, t)^9\text{Li}(\text{gs})$, (b) $^{11}\text{Li}(p, t)^9\text{Li}(1/2^-)$, (c) $^1\text{H}(^{11}\text{Li}, ^9\text{Li}(\text{gs}))^3\text{H}$ and (d) $^1\text{H}(^{11}\text{Li}, ^9\text{Li}(1/2^-))^3\text{H}$. Time is assumed to run upwards. A single arrowed line represents a fermion (proton) (p) or neutron (n). A double arrowed line two correlated nucleons. In the present case two correlated (halo) neutrons (halo-neutron pair addition mode $|0>_\nu$). A heavy arrowed line represents the core system $|^9\text{Li}(\text{gs})>$. A standard pointed arrow refers to structure, while "round" arrows refer to reaction. A wavy line represents (particle-hole) collective vibrations, like the low-lying quadrupole mode of ^9Li , or the dipole pygmy resonant state which, together with the bare pairing interaction (horizontal dotted line) binds the neutron halo Cooper pair to the core. A short horizontal arrow labels the proton–neutron interaction v_{np} responsible for the single–particle transfer processes, represented by an horizontal dashed line. A dashed open square indicates the particle-recoil coupling vertex. The jagged line represents the recoil normal mode resulting from the mismatch between the relative centre of mass coordinates associated with the mass partitions $^{11}\text{Li}+p$, $^{10}\text{Li}+d$ (virtual) and $^9\text{Li}+t$. The γ -detector is represented by a hatched box (see Fig. 7.6.2), the particle detector by a crossed rectangle. For further details see caption Fig. 2.9.2.

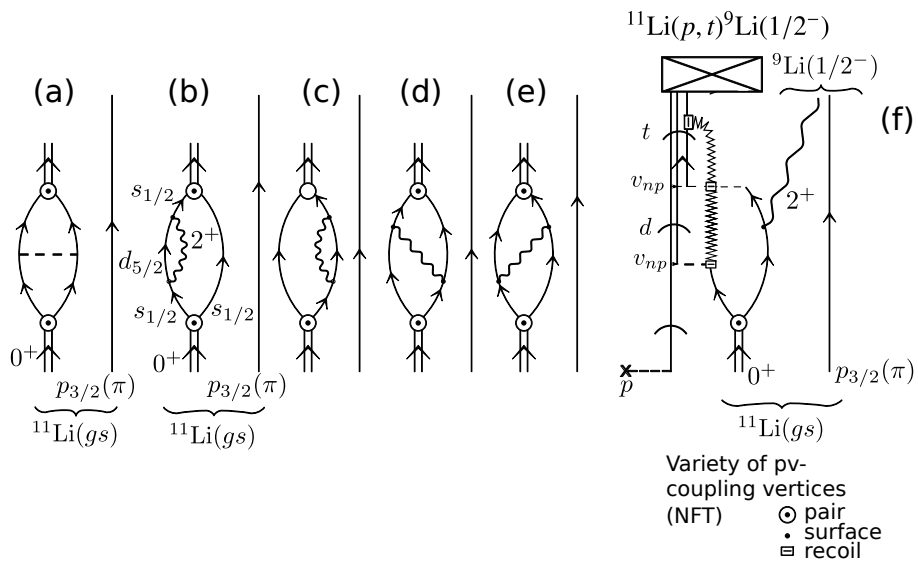


Figure 2.9.4: (a–e) Lowest order, NFT diagrams associated with the processes contributing to the binding of the neutron halo Cooper pair (double arrowed line) of ^{11}Li to the core ^9Li through the bare pairing interaction (dashed line) as well as the exchange of the core quadrupole phonon and of the soft dipole mode of ^{11}Li (wavy line). Single arrowed lines describe the nucleon independent-particle motion of neutrons ($s_{1/2}, d_{5/2}$, etc.) as well as of the $p_{3/2}(\pi)$ proton considered as a spectator; (a) Bare pairing interaction, four-point vertex (horizontal dotted line); (b, c) self energy, effective mass polarization (PO) process dressing the $s_{1/2}(v)$ single-particle state (a similar diagram, but corresponding to correlation (CO) processes (see Fig. 5.2.4) dressing the $p_{1/2}$ state is not shown, see Figs. 2.9.2 and 2.9.3); (d, e) vertex correction (induced interaction) renormalizing the vertex with which the pair addition mode couples to the fermion (dotted open circle); (f) NFT diagram describing the reaction $^{11}\text{Li}(p, t)^{9}\text{Li}(1/2^-)$ populating the first excited state of ^9Li , the dashed horizontal line starting with a cross standing for the (p, t) probe. The successive transfer of the two halo neutrons ($^{11}\text{Li}(\text{gs}) + p \rightarrow ^{10}\text{Li} + d \rightarrow ^9\text{Li}(1/2^+) + t$) is shown, in keeping with the fact that this process, that is successive transfer, provides the largest contribution to the absolute differential cross section. The jagged line represents the recoil mode carrying to the outgoing particle the effect of the momentum mismatch associated with the transfer process (recoil).

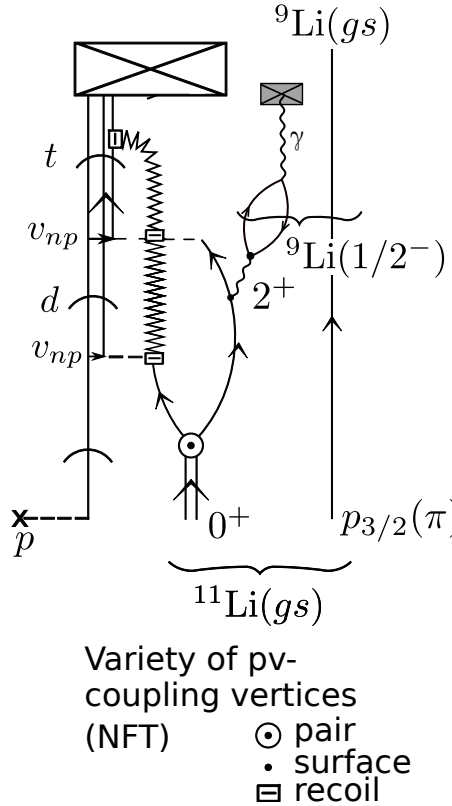


Figure 2.9.5: Gedanken γ -ray coincidence experiment $^1\text{H}(^{11}\text{Li}, ^9\text{Li})^3\text{H}$ and $^9\text{Li}(\text{gs}) + \gamma(E2; 2.69 \text{ MeV})$. In this case, the virtual quadrupole phonon associated with self-energy and vertex correction processes becomes real through the action of the (p, t) external field. Thus, it is not only that recoil modes are “measured” by detectors in connection with outgoing particles which have asymptotic wavefunctions, but also the quadrupole vibration, whose eventual γ -decay (see Fig. 7.6.2 (II)) can be measured by the γ -detector. The apparent bubble process made out of a proton particle-hole component of the quadrupole mode does not contradict NFT rule III (Sect. 2.7). In fact, the initial vertex (solid dot) corresponds to a nuclear PVC, while the second couples the proton excitation to the electromagnetic field, leading to spontaneous γ -decay.

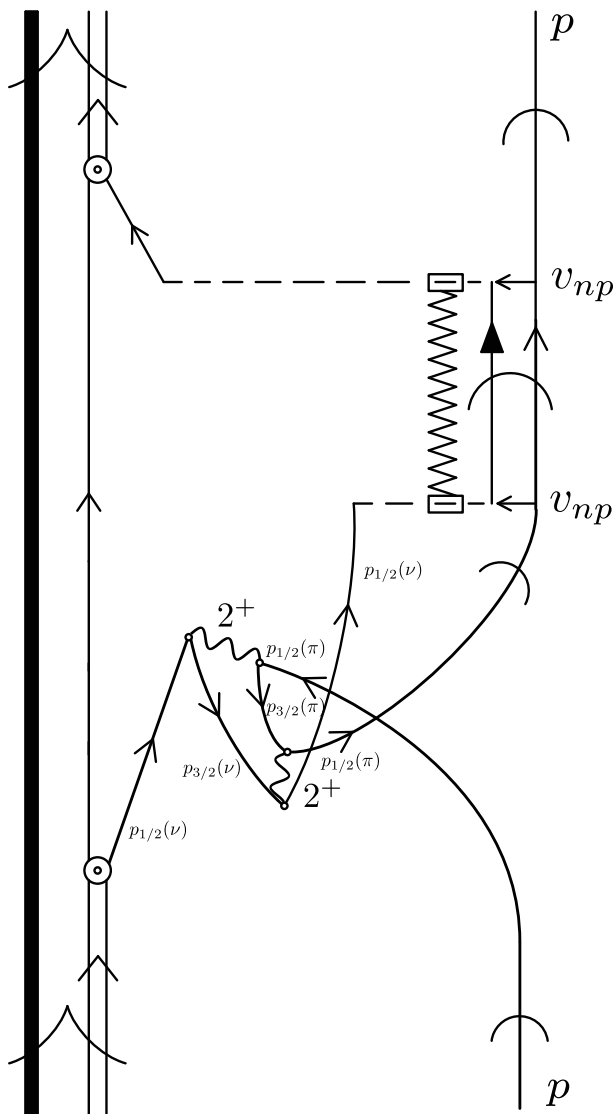


Figure 2.9.6: In keeping with standard direct reaction praxis, neither in Fig. 2.9.2 nor in 2.9.3 antisymmetrization is carried out between the impinging proton and the protons of ^{11}Li . Within the present discussion ($^{11}\text{Li}(p, p)^{11}\text{Li}$), an example of such processes corresponds to the exchange of a proton participating in the quadrupole vibration of the core, with the projectile, as shown in the figure. Such a process will not only be two orders higher in perturbation in the particle–vibration coupling vertex than the original one shown in graph (a) of Fig. 2.9.2. It will be strongly reduced by the square of the overlap between a proton moving in the continuum, and a $p_{1/2}$ proton of the ^9Li core.

coupling vertex. At time t_{10} , again under the effect of v_{np} , the neutron of the virtual deuteron is transferred back to the virtual ${}^{10}\text{Li}$ nucleus to form again ${}^{11}\text{Li}$ and thus the original mass partition, as testified by the fact that the recoil phonon (jaggy line initiated at time t_9) is reabsorbed by a second particle–recoil coupling vertex. The resulting ($p_{1/2}^2(0)$) configuration couples to the $|0_\nu\rangle$ state leading to the $|{}^{11}\text{Li(gs)}\rangle$ state. The system has thus returned to the entrance channel configuration, namely that of ${}^{11}\text{Li} + p$, which propagates to $t \rightarrow +\infty$, the proton eventually bringing the nuclear structure information to the detector.

The real and imaginary part of the diagram shown in Fig 2.9.2 (a), contribute to the corresponding terms of the polarization components of the optical potential, providing the A -dependence of, and to be added to, the experimentally determined (global) ${}^A X + p$ elastic scattering optical potential¹³⁴. The mass number A represents the region of the mass table¹³⁵ associated with nuclei close to the neutron drip line region $A \approx 11$. It is of notice that Fig. 2.9.2 exemplifies the elements needed to extend and formalize NFT rules of structure so as to be able to deal also with reactions.

As schematically shown in Fig. 2.9.1, to each nuclear structure process displayed in diagram (a) of Fig. 2.9.2, it corresponds a specific equation, amplitude, etc., and thus a number with appropriate units. This is also so regarding the reaction aspects of the diagram, and thus reaction amplitudes and eventual absolute differential cross sections. A fact which is exemplified in detail in Sect. 7.1 and App. 7.8 in connection with graphs (a) and (b) of Fig. 2.9.3.

In Fig. 2.9.2 (b) one assumes the same processes to take place as in (a) up to time t_8 (reason for which no details are repeated between t_2 and t_8). From there on the deuteron continues to propagate to the detector, and the effect of the particle–recoil coupling vertex is to be worked out and the corresponding outgoing distorted waves modified accordingly. Likely, the neutron in ${}^{10}\text{Li}$ will break up before it can be recorded by the particle detector. Summing up, in the center of mass reference frame both p and ${}^{11}\text{Li}$ display asymptotic states in entrance as well as in exit channels in case (a), and only in the entrance channel in case (b), while in the exit channel only ${}^{10}\text{Li}({}^9\text{Li}+n)$ and the deuteron do so.

Another examples of the NFT diagrams of structure and reactions are given in Fig. 2.9.3. In (a) one contribution associated with the reaction ${}^{11}\text{Li}(p, t){}^9\text{Li(gs)}$ is shown, while in (b) one associated with the population of the first excited $1/2^-$ (2.69 MeV) state of ${}^9\text{Li}$. Within this context we refer to Figs. 2.9.4 and 2.9.5

¹³⁴In relation with the program of NFT(r+s) one can mention that Landau felt that a Feynman diagram have an independent basic importance, because the possibility of relating them directly to physical observables. Feynman diagrams allow to describe processes where one set of particles with given energies, momenta, angular momenta, go in and another set (or the same) comes out. At the basis of this approach one finds vertex processes and dispersion relations. Now, vertex processes can simply mean the variety of processes connecting the incoming particles with the outgoing ones. In other words, within the present framework the processes taking place between times $t_2 - t_{11}$ (Fig. 2.9.2) and $t_1 - t_2$ (Fig. 2.9.3) (Landau (1959); ter Haar (1969)). See also Sect. 7.5.

¹³⁵Similar to the island of superfluid nuclei involved in the characterization of ${}^{120}\text{Sn}$ discussed in the next Section (see Idini et al. (2015) and references therein).

for a compact graphical representation of this last process. The importance of such process is that it provided, likely for the first time, direct evidence of phonon mediated pairing interaction in nuclei as theoretically predicted¹³⁶.

Returning to the process displayed in Fig.2.9.2 concerning the question of Pauli principle in reaction processes (also essential in the case of structure NFT), in this case not between e.g. the two halo neutrons, but between the incoming proton and the collective modes of the core (${}^9\text{Li}$) we refer to¹³⁷ Fig. 2.9.6.

2.10 Characterization of an open-shell nucleus: ${}^{120}\text{Sn}$

In this section we aim at giving an overall view of the versatility of $(\text{NFT})_{\text{ren}}(\mathbf{s}+\mathbf{r})$ to describe both structure as well as the results of experimental probes which provide an essentially complete characterization of an atomic nucleus. Details of the structure and reaction calculations, techniques and software employed to achieve such characterization will be provided in the following chapters.

In keeping with the fact that ${}^{120}\text{Sn}$ is a typical example of superfluid nuclei, it has been studied extensively with a variety of probes. Elastic, anelastic (Coulomb excitation and subsequent γ -decay as well as inelastic scattering). Also one- and two-particle transfer reactions. The corresponding absolute differential cross sections and transition probabilities involve as targets and residual systems the island of superfluid nuclei ${}^{118,119,120,121,122}\text{Sn}$.

A theoretical description of the variety of observables have been carried out solving the Nambu Gorkov equation to propagate the different $(\text{NFT})_{\text{ren}}(\mathbf{s})$ processes dressing the single-particle states and renormalizing the bare pairing interaction, as well as spectroscopic and transition amplitudes¹³⁸. With the help of the softwares SINGLE and COOPER, tailored to propagate the $(\text{NFT})_{\text{ren}}(\mathbf{s})$ spectroscopic amplitude content to the detector, one- and two- nucleon transfer reactions have been worked out $((\text{NFT})_{\text{ren}}(\mathbf{r}))$. Also the γ -decay transition probabilities. In Fig. 2.10.1 theory is compared to experiment in terms of renormalized energies, absolute differential cross sections and electromagnetic transition probabilities.

In what follows we describe the contents of this figure. In the **upper left** part, (color online), the cartoon representation displayed in Fig. 2.1.1 is here used to schematically illustrate¹³⁹ anelastic processes, Coulomb excitation and the quadrupole γ -decay of ${}^{119}\text{Sn}$ (**middle left** (a) experiment, (b) theory, (c) standard

¹³⁶Barranco, F. et al. (2001) Tanihata, I. et al. (2008); Potel et al. (2010); Tanihata et al. (2013); Beceiro–Novo et al. (2015).

¹³⁷It is of notice that making use of global optical potentials to describe the elastic channel, or mean field optical potentials to which one adds polarization contributions like those displayed in Fig. 2.9.2 (a), the effect of Pauli principle between a nucleon projectile and the nucleons of the target can, approximately be taken care of through the energy-dependent Perey–Buck potential (Perey and Buck (1962)), intimately connected with the k -mass.

¹³⁸See Idini et al. (2015) and refs. therein, see also Broglia et al. (2016).

¹³⁹While in Fig. 2.1.1 one refers to the excitation of an octupole mode, in the present case we deal with a quadrupole vibration.

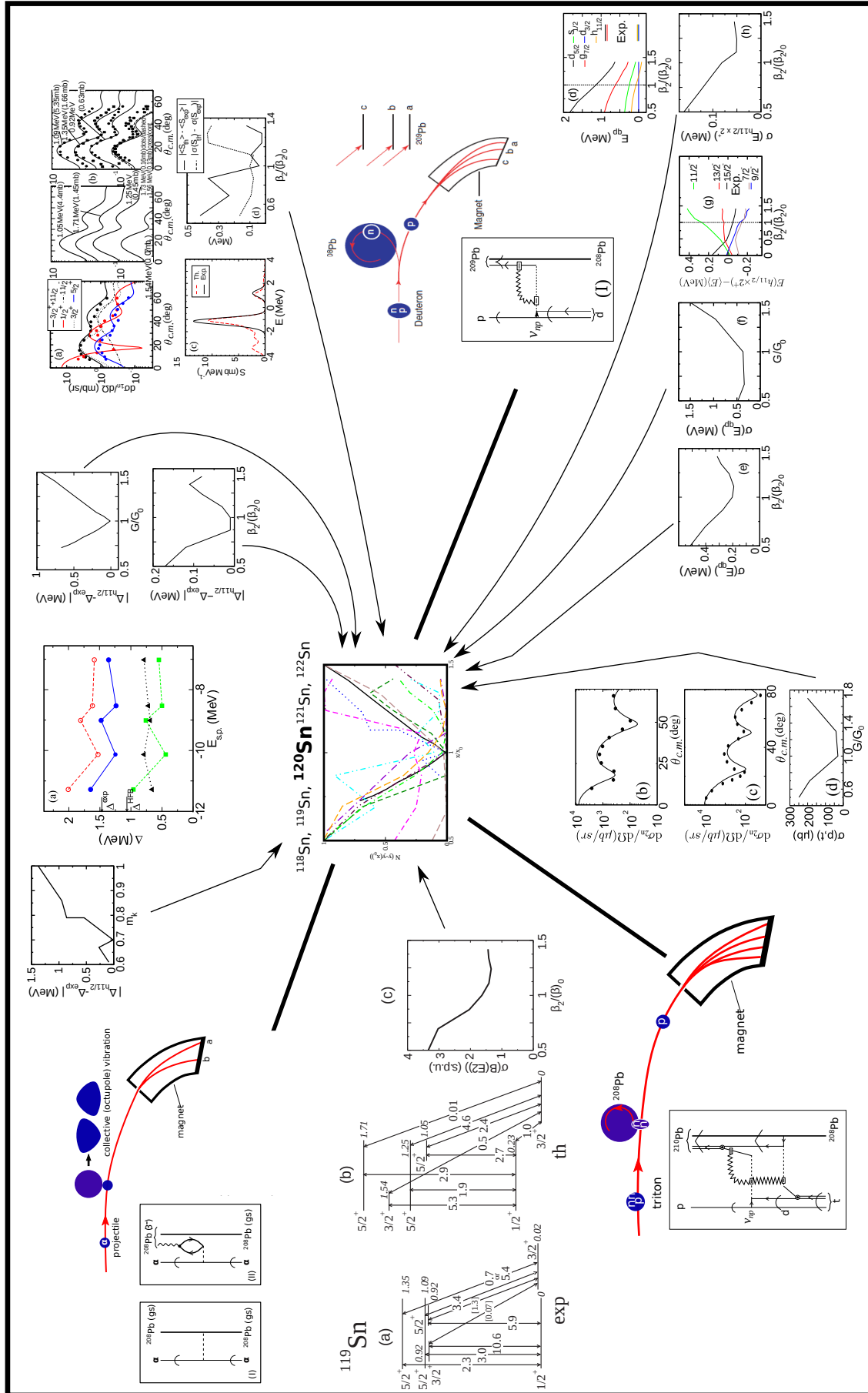


Figure 2.10.1: Characterization of ^{120}Sn .

deviation between theory and experiment calculated as a function of β_2 normalized with respect to the experimental value ($\beta_2)_0$). The resulting values are displayed in terms of the dashed orange curve of the center boxed landscape (see Fig. 2.4.1 and Table 2.4.1). Also displayed in the upper left part of the figure are NFT diagrams describing elastic and inelastic processes.

In the **bottom left** part of the figure, a schematic representation of an experimental setup to measure two–nucleon transfer processes is given. Also a (NFT)_{ren(s+r)} diagram describing successive transfer is displayed. In the **bottom middle** part of the figure, the theoretical absolute differential cross sections (continuous curves) associated with the reactions $^{120}\text{Sn}(p, t)^{118}\text{Sn}(\text{gs})$ and $^{122}\text{Sn}(p, t)^{120}\text{Sn}(\text{gs})$ are displayed ((b) and (c)), in comparison with the experimental data (solid dots). The theoretical cross sections were recalculated as a function of the pairing strength G , normalized with respect to the (equivalent) value G_0 of v_{14} (Argonne 1S_0 bare NN –interaction), and the corresponding standard deviation with respect to the experimental value determined (only the values corresponding to $^{120}\text{Sn}(p, t)^{118}\text{Sn}$ are displayed in (d)). It is of notice that the corresponding relative standard deviation σ/L for $G = G_0$ (L being the experimental cross section), is quite small ($70\mu\text{b}/2250\mu\text{b} \approx 0.03$)¹⁴⁰.

In the **upper middle** part of the figure and under the label (a), the state dependent pairing gap for the five valence orbitals of ^{120}Sn (blue line) is displayed, in comparison with the experimental findings ($\Delta^{\text{exp}} \approx 1.45$ MeV, arrow left). The gap associated with the lowest quasiparticle state $h_{11/2}$ calculated as a function of m_k (different Skyrme interaction) as well as of G/G_0 and $\beta_2/(\beta_2)_0$ have been used to work out the corresponding standard deviations with respect to the experimental findings and are displayed to the right and the left of (a) (see also dotted blue curve, dashed brown curve and dashed green curve in the central boxed plot, i.e. Fig. 2.4.1). In the **upper right** part of the figure absolute differential cross sections and strength functions associated with the one–particle transfer processes $^{120}\text{Sn}(d, p)^{121}\text{Sn}$, are displayed. In (a), the absolute differential cross sections associated with the low–lying states $h_{11/2}, d_{3/2}, s_{1/2}$ and $d_{5/2}$ are shown (theory: continuous curve; data: solid dots). In (b) (left) the calculated $^{121}\text{Sn}(5/2^+)$ absolute differential cross sections (continuous curves) are shown and compared with the experimental data (right, solid dots; also given here are DWBA fits used in the analysis of the experimental data). In (c) the calculated strength function associated with the $5/2^+$ state (red dashed curve) is compared to the data (black continuous curve), while in (d) the difference between the centroid width of the experimental and calculated $d_{5/2}$ strength function is shown as a function of the ratio $\beta_2/(\beta_2)_0$ in terms of the solid and dashed curves. In the **middle right** part of the figure,

¹⁴⁰This result is related with the fact that $\sigma \sim |\alpha_0|^2$, α_0 being the BCS order parameter (number of Cooper pairs participating in the condensate which measure the deformation in gauge space). Because the state $|BCS\rangle$ describing independent pair motion (Cooper pair condensate) is a coherent state displaying off–diagonal–long–range–order (ODLO), it is not surprising that $|\alpha|^2 = \left| \sum_{v>0} U_v V_v \right|^2 = \langle BCS | P^\dagger | BCS \rangle^2 = \langle BCS | P | BCS \rangle^2$ plays the role of a, physical, non–energy weighted sum rule (Potel et al. (2017)). See Sect. 7.4.1.

a cartoon representation of a setup to measure one-nucleon transfer reactions is displayed. Also shown is a $(NFT)_{ren}(s+r)$ diagram describing the process. In the **lower right** part of the figure, the lowest quasiparticle energy values are displayed as a function of $\beta_2/(\beta_2)_0$ in comparison with the data. The root mean-square deviation between the experimental and theoretical levels as a function of a function of $\beta_2/(\beta_2)_0$ and of G/G_0 are shown in (e) and (f) respectively. In (g) the experimental energies of the members of the $h_{11/2} \times 2^+$ multiplet shown in (d), are compared with the theoretical values calculated as a function of the ratio $\beta_2/(\beta_2)_0$. Finally in (h) the root mean-square deviation between the experimental and theoretical energies of the members of the $h_{11/2} \times 2^+$ multiplet shown in (g) are given as a function of $\beta_2/(\beta_2)_0$.

Summing up, the nuclear structure landscape is well funneled and theory provides an overall account of the data, when the physical values of β_2 , G and m_k are used.

2.11 Summary

In Fig. 2.10.1 the results of a “complete” $(NFT)_{ren}(r+s)$ description of the open shell superfluid nucleus ^{120}Sn in terms of the $^{120}\text{Sn}(p, t)^{118}\text{Sn(gs)}$, $^{122}\text{Sn}(p, t)^{120}\text{Sn(gs)}$, $^{120}\text{Sn}(p, d)^{119}\text{Sn}$, $^{121}\text{Sn}(p, d)^{120}\text{Sn}$, $^{119}\text{Sn}(\alpha, \alpha')^{119}\text{Sn}$ (γ -decay) cross sections, energies and transition probabilities are displayed in comparison with the experimental findings. Arbitrarily forcing the particle-vibration coupling (PVC) strength, the strength of the bare pairing force and the value of the k -mass to depart from their “physical” values, one can test the robustness of the $NFT(r+s)$ picture of ^{120}Sn given, and of the well funneled character of the associated nuclear structure and reaction landscape.

In a very real sense this, namely the results collected in Fig. 2.10.1 is a nucleus¹⁴¹. That is, the summed experimental and theoretical structural information accessed through asymptotic states, outcome of simultaneously probing the system with a complete array of experiments (elastic, anelastic and associated γ -decay, as well as one- and two-nucleon transfer reactions), and of calculating the corresponding observables with an equally ample array of theoretical tools, as provided by $(NFT)_{ren}(r+s)$.

Appendix 2.A Inelastic Scattering

In this Appendix we briefly discuss how to extract values of the effective deformation parameter β_L from inelastic scattering absolute differential cross sections in the most simple and straightforward way, ignoring all the complications associated with the spin carried by the particles, the spin-orbit dependence of the

¹⁴¹For details, see Idini et al. (2015), and Broglia et al. (2016), see also Fig. 2.4.1.

optical model potential, etc. The deformation parameter β_L enter e.g. the particle-vibration coupling Hamiltonian (Eqs. (2.3.8–2.3.13)).

2.A.1 (α, α') -scattering

We start assuming that the interaction V'_β is equal to $V'_\beta = V'_\beta(\xi_\beta, r_\beta)$, which is usually called the stripping approximation. We can then write the differential cross section in the Distorted Wave Born Approximation (DWBA) as (see e.g. App 6.B) as,

$$\frac{d\sigma}{d\Omega} = \frac{k_\beta}{k_\alpha} \frac{\mu_\alpha \mu_\beta}{(2\pi\hbar^2)} |\langle \psi_\beta(\xi_\beta) \chi^{(-)}(k_\beta, \vec{r}_\beta), V'_\beta(\xi_\beta, r_\beta) \psi_\alpha(\xi_\alpha) \chi^{(+)}(k_\alpha, \vec{r}_\alpha) \rangle|^2. \quad (2.A.1)$$

For the case of inelastic scattering $\xi_\alpha = \xi_\beta = \xi$, thus

$$\psi_\beta(\xi_\beta) = \psi_{M_{I\beta}}^{I_\beta}(\xi), \quad (2.A.2a)$$

$$\psi_\alpha(\xi_\alpha) = \psi_{M_{I\alpha}}^{I_\alpha}(\xi), \quad (2.A.2b)$$

$$\vec{r}_\alpha = \vec{r}_\beta, \mu_\alpha = \mu_\beta, \quad (2.A.2c)$$

i.e we are always in the mass partition of the entrance channel.

Equation (2.A.1) can now be rewritten as

$$\frac{d\sigma}{d\Omega} = \frac{k_\beta}{k_\alpha} \frac{m_\alpha^2}{(2\pi\hbar^2)^2} \frac{1}{2I_\alpha + 1} \sum_{M_\alpha M_\beta} |\langle \chi^{(-)}(k_\beta, \vec{r}_\beta), V_{eff}(\vec{r}) \chi^{(+)}(k_\alpha, \vec{r}_\alpha) \rangle|^2, \quad (2.A.3)$$

where

$$\begin{aligned} V_{eff} &= \int d\xi \psi_{M_{I\beta}}^{I_\beta^*}(\xi) V'_\beta(\xi, \vec{r}) \psi_{M_{I\alpha}}^{I_\alpha}(\xi), \\ &= \int d\xi \psi_{M_{I\beta}}^{I_\beta^*}(\xi) V_\beta(\xi, \vec{r}) \psi_{M_{I\alpha}}^{I_\alpha}(\xi), \end{aligned} \quad (2.A.4)$$

as ψ^{I_β} and ψ^{I_α} are orthogonal (remember $V'_\beta = V_\beta - \bar{U}(r)$). We now expand the interaction in spherical harmonics, i.e.

$$\begin{aligned} V_\beta(\xi, \vec{r}) &= \sum_{LM} V_M^L(\xi, r) Y_M^L(\hat{r}) \\ &= \sum_{LM} V_M^L(\xi, \vec{r}). \end{aligned} \quad (2.A.5)$$

Defining

$$\int d\xi \psi_{M_{I\beta}}^{I_\beta^*}(\xi) [V_M^L(\xi, r) \psi^{I_\alpha}(\xi)]_{M_{I\beta}}^{I_\beta} = F_L(r), \quad (2.A.6)$$

we can write eq.(2.A.4) as

$$V_{eff}(\vec{r}) = \sum_{LM} (LMI_\alpha M_\alpha | I_\beta M_\beta) F_L(r) Y_M^L(\hat{r}). \quad (2.A.7)$$

Inserting (2.A.7) into (2.A.3) we obtain

$$\begin{aligned}
 \frac{d\sigma}{d\Omega} &= \frac{k_\beta}{k_\alpha} \frac{m_\alpha^2}{(2\pi\hbar^2)^2} \frac{1}{2I_\alpha + 1} \sum_{M_\alpha M_\beta} \left| \sum_{LM} (LMI_\alpha M_\alpha | I_\beta M_\beta) \right. \\
 &\quad \times \left. \int d\vec{r} \chi^{(-)*}(k_\beta, \vec{r}_\beta) F_L(r) Y_M^{L*}(\hat{r}) \chi^{(+)}(k_\beta, \vec{r}_\beta) \right|^2 \\
 &= \frac{k_\beta}{k_\alpha} \frac{m_\alpha^2}{(2\pi\hbar^2)^2} \frac{2I_\beta + 1}{2I_\alpha + 1} \\
 &\quad \times \sum_{LM} \frac{1}{2L + 1} \left| \int d\vec{r} \chi^{(-)*}(k_\beta, \vec{r}_\beta) F_L(r) Y_M^{L*}(\hat{r}) \chi^{(+)}(k_\beta, \vec{r}_\beta) \right|^2,
 \end{aligned} \tag{2.A.8}$$

where we have used the orthogonality relation between Clebsch-Gordan coefficients

$$\begin{aligned}
 &\sum_{M_\alpha M_\beta} (LMI_\alpha M_\alpha | I_\beta M_\beta) (L'MI_\alpha M_\alpha | I_\beta M_\beta) \\
 &= \sqrt{\frac{(2I_\beta + 1)^2}{(2L + 1)(2L' + 1)}} \sum_{M_\alpha M_\beta} (I_\beta - M_\beta I_\alpha M_\alpha | L - M) \\
 &\quad \times (I_\beta - M_\beta I_\alpha M_\alpha | L' - M) = \frac{2I_\beta + 1}{2L + 1} \delta_{LL'},
 \end{aligned} \tag{2.A.9}$$

(fixed M).

Let us now discuss the case of inelastic scattering of even spherical nuclei.

The macroscopic Hamiltonian describing the dynamics of the multipole surface vibrations in such nuclei can be written, in the harmonic approximation as

$$H = \sum_{L,M} \left\{ \frac{D_L}{2} |\dot{\alpha}_M^L|^2 + \frac{C_L}{2} |\alpha_M^L|^2 \right\} = \sum_{L,M} \left\{ \frac{|\Pi_M^L|^2}{2D_L} + \frac{C_L}{2} |\alpha_M^L|^2 \right\}, \tag{2.A.10}$$

where the collective coordinate α_M^L is defined through the equation of the radius

$$R(\hat{r}) = R_0 \left[1 + \sum_{L,M} \alpha_M^L Y_M^{L*}(\hat{r}) \right], \tag{2.A.11}$$

and where $R_0 = r_0 A^{1/3}$ fm, and

$$\Pi_M^L = D_L |\dot{\alpha}_M^L|. \tag{2.A.12}$$

It is of notice that α_M^L is a dimensionless variable. Consequently, the dimensions of the inertia and of the restoring force parameters are

$$[D_L] = \text{MeV s}^2 \quad \text{and} \quad [C_L] = \text{MeV}, \tag{2.A.13}$$

while that of the conjugate momentum is

$$[\Pi_M^L] = \text{MeV s.} \quad (2.A.14)$$

The collective mode is generated from the interaction of the multipole field carried by each particle and the field of the rest of the particles. In turn this coupling modifies the single-particle motion. In particular the incoming projectile would feel this coupling. The potential V'_β is equal to

$$\begin{aligned} V'_\beta(\xi, \vec{r}) &= U(r - R(\hat{r})) \\ &= U(r - R_0 - R_0 \sum_{L,M} a_M^L Y_M^{L*}(\hat{r})) \\ &= U(r - R_0) - R_0 \sum_{L,M} a_M^L Y_M^{L*}(\hat{r}) \frac{dU(r - R_0)}{dr} \end{aligned} \quad (2.A.15)$$

$$\begin{aligned} &= V_\beta(\xi, r) - \bar{U}_\beta(r), \\ \bar{U}_\beta(r) &= -U(r - R_0) \\ V_\beta(\xi, \vec{r}) &= R_0 \frac{d\bar{U}_\beta(r)}{dr} \sum_{L,M} a_M^L Y_M^{L*}(\hat{r}). \end{aligned} \quad (2.A.16)$$

Comparing with eq. (2.A.5) we obtain

$$V_M^L(\alpha, r) = R_0 \frac{d\bar{U}_\beta(r)}{dr} a_{+M}^L. \quad (2.A.17)$$

Note that H defined in Eq. (2.A.10) is the Hamiltonian of an L -dimensional harmonic oscillator, and that a_M^L is a classical variable. One can quantize this Hamiltonian in the standard way,

$$a_M^L = \sqrt{\frac{\hbar\omega_L}{2C_L}}(a_M^L - a_{-M}^{+L}), \quad (2.A.18)$$

where $\hbar\omega_L$ is the energy of the vibration, and a_M^{+L} is the creation operator of a phonon. For an even nucleus

$$\begin{aligned} |\Psi_{M_\alpha}^{I_\alpha}\rangle &= |0\rangle \quad (I_\alpha = M_\alpha = 0), \\ |0\rangle &: \quad \text{ground (vacuum) state.} \end{aligned} \quad (2.A.19)$$

The one-phonon state can be written as,

$$\begin{aligned} |\Psi_{M_\alpha}^{I_\alpha}\rangle &= |I; LM\rangle = a_M^{+L}|0\rangle, \\ (I_\beta &= L; M_{I_\beta} = M). \end{aligned} \quad (2.A.20)$$

We can now calculate the matrix element of the operator (2.A.17), which connects states which differ in one phonon. Starting from the ground state we obtain

$$\begin{aligned} \langle I; LM | V_M^L(\alpha, r) | 0 \rangle &= (-1)^{L-M} R_0 \frac{d\bar{U}_\beta(r)}{dr} \sqrt{\frac{\hbar\omega_L}{2C_L}} \langle 0 | (a_M^L - a_{-M}^{+L}) | 0 \rangle \\ &= R_0 \frac{d\bar{U}_\beta(r)}{dr} \sqrt{\frac{\hbar\omega_L}{2C_L}} = -\frac{R_0}{\sqrt{2L+1}} \frac{d\bar{U}_\beta(r)}{dr} \beta_L, \end{aligned} \quad (2.A.21)$$

where

$$\beta_L = \sqrt{\frac{(2L+1)\hbar\omega_L}{2C_L}}. \quad (2.A.22)$$

Substituting (2.A.21) into eq. (2.A.8) and making use of eqs. (2.A.19) and (2.A.20) we get

$$\begin{aligned} \frac{d\sigma}{d\Omega} &= \frac{k_\beta}{k_\alpha} \frac{\mu_\alpha^2}{(2\pi\hbar^2)^2} (\beta_L R_0)^2 \\ &\times \sum_M \frac{1}{2L+1} \left| \int d\vec{r} \chi^{(-)*}(k_\beta, \vec{r}) \frac{dU(r)}{dr} Y_M^{L*}(\hat{r}) \chi^{(+)}(k_\alpha, \vec{r}_\beta) \right|^2. \end{aligned} \quad (2.A.23)$$

Let us now assume that the nucleus has a permanent quadrupole ($L = 2$) axially-symmetric deformation. For a $K = 0$ band, the nuclear wave function has the form¹⁴²

$$\Psi_{IMK=0} = \sqrt{\frac{2I+1}{8\pi^2}} \mathcal{D}_{M0}^I(\omega) \chi_{K=0} \quad (\text{intrinsic}), \quad (2.A.24)$$

where we have used $(\omega) = (\theta, \phi, \psi)$ to label the Eulerian angles which serve as orientation parameters.

In the intrinsic frame (which we take to coincide with the space-fixed axis when $\theta = \phi = \psi = 0$) the nuclear surface has the shape

$$R(\hat{r}) = R_0 \left[1 + \sum_L b_L Y_0^L(\hat{r}) \right], \quad (2.A.25)$$

where the b_L introduced here is a_0^L in the intrinsic frame. When the nucleus has orientation ω , this shape is rotated into

$$\hat{R}_\omega R(\hat{r}) = R_0 \left[1 + \sum_L b_L \mathcal{D}_{M0}^L(\omega) Y_0^L(\hat{r}) \right]. \quad (2.A.26)$$

One can then write,

$$W(r - R(\hat{r})) = W(r - R_0) - R_0 \frac{dW(r - R_0)}{dr} \sum_L b_L \mathcal{D}_{M0}^L(\omega) Y_0^L(\hat{r}), \quad (2.A.27)$$

¹⁴²see e.g. Bohr, A. and Mottelson (1975) and refs. therein.

which is the equivalent to Eq. (2.A.15) for the case of deformed nuclei. Then

$$V_M^L(b, r; \omega) = -\frac{d\bar{U}_\beta(r - R_0)}{dr} b_L \mathcal{D}_{M0}^L(\omega). \quad (2.A.28)$$

The effective interaction is now equal to

$$\begin{aligned} \langle \Psi_{IMK=0}, V_M^L(b, r; \omega) \Psi_{000} \rangle &= \\ &- R_0 \frac{d\bar{U}(r - R_0)}{dr} b_L \sqrt{\frac{(2L+1)^2}{8\pi^2}} \int d\omega \mathcal{D}_{M0}^{L*}(\omega) \mathcal{D}_{M0}^L(\omega) = \\ &- R_0 \frac{d\bar{U}(r - R_0)}{dr} b_L = -\frac{R_0}{\sqrt{(2L+1)}} \frac{d\bar{U}(r - R_0)}{dr} \beta_L = F_L(r), \\ (\beta_L &= \sqrt{(2L+1)} b_L), \end{aligned} \quad (2.A.29)$$

in complete analogy to (2.A.21). Thus the same formfactor is used for both types of collective excitation. Within the above simple scheme of structure and reaction, the normalization factor $(\beta_L R_0)^2$ is the only free parameter that can be obtained from the comparison of the experimental and theoretical (DWBA) differential cross section. The quantity β_L is known as the multipole deformation (dynamic or static) parameter, and gives a direct measure of the coupling of the projectile to the vibrational field. The value of β_L can also be obtained from the $B(EL)$ reduced transition probability, in which case one has a measure of the electric moment, instead of the mass moment.

Appendix 2.B Technical details NFT

In this Appendix we briefly discuss two technical aspects related to the overcompleteness of the basis used in NFT.

2.B.1 Graphical solution

The dispersion relation (2.7.57), which is central in the discussion concerning spurious states in the overcomplete basis of elementary modes of excitation used to develop NFT, is solved numerically in Sect. 2.7 (Fig. 2.7.8 (II)). The technical details of the corresponding implementation emerges natural by making a parallel with the dispersion relation associated with the Cooper pair problem, taking into account the energy separation existing in nuclei between single-particle levels due to the fact that it is a finite system (spatial quantization). In this case, the wavefunction of the two-particle system can be written as

$$|0^+\rangle = \frac{1}{\sqrt{2}} \sum_j \alpha_j [a_j^\dagger a_j^\dagger]_0^0 |0\rangle, \quad (2.B.1)$$

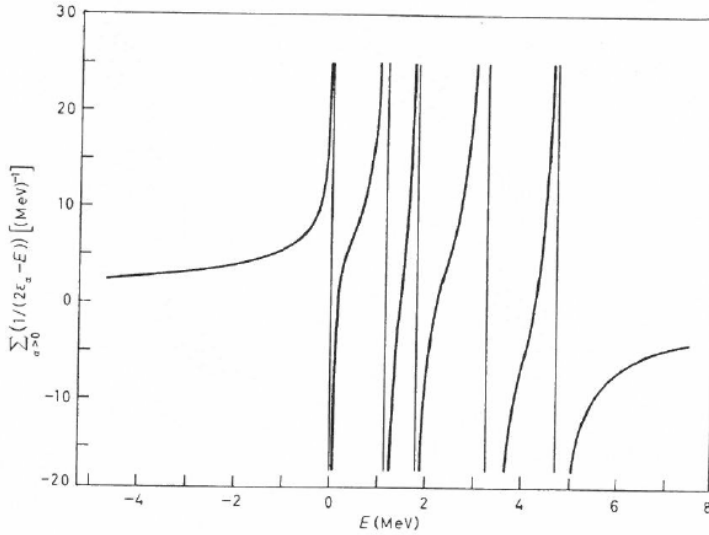


Figure 2.B.1: Dispersion relation for ^{206}Pb . The single-hole states available to the neutron holes (in MeV) are $p_{1/2}(0)$, $f_{5/2}(0.57)$, $p_{3/2}(0.89)$, $i_{13/2}(1.63)$, $f_{7/2}(2.34)$. The label α denotes the quantum numbers (j, m) (after Bayman (1960)).

where $|0\rangle$ is the vacuum state and a_j^\dagger creates a particle in the orbital j with time-reversal properties $\tau a_{jm}^\dagger \tau^{-1} = (-1)^{j-m} a_{j-m}^\dagger$. The amplitudes α_j are determined by the secular equation

$$(2\epsilon_j - E)\alpha_j = \sum_{j'} (j + 1/2)^{1/2} (j' + 1/2)^{1/2} G(j', j', j, j) \alpha_{j'}. \quad (2.B.2)$$

If one replaces the radial integrals $G(j', j', j, j) = -(V_0/4\pi) \int u_j^2(r) u_{j'}^2(r) r^2 dr$ (assuming the pairing force to be a contact interaction, see Sect. 3.6) by an average value G , the eigenvalues E are determined by the secular equation,

$$\frac{1}{G} = \sum_j \frac{(j + 1/2)}{2\epsilon_j - E} = \sum_j \sum_{m>0} \frac{1}{2\epsilon_j - E} = F(E). \quad (2.B.3)$$

The nature of the solution is illustrated in Fig. 2.B.1. When E goes from a value smaller to a value larger than $2\epsilon_j$, $F(E)$ decreases from $+\infty$ to $-\infty$ going through zero. The eigenvalues E are given by the intersection of $F(E)$ with the line G^{-1} . While all other eigenvalues than the lowest one, are trapped between the unperturbed energies $2\epsilon_j$, the ground state correlation can freely increase as G increases.

Making use of the correspondence

$$\sqrt{j + 1/2} \leftrightarrow \Lambda_1 \quad (2.B.4)$$

and

$$G \leftrightarrow (E - \epsilon_m - V)^{-1}, \quad (2.B.5)$$

one can transform (2.B.3) into (2.7.57). Consequently, the graphical solution shown in Fig. 2.B.1 can be used for this dispersion relation (Fig. 2.7.8).

Let us now return to the Cooper pair problem, and the dispersion relation (2.B.3). If the nucleus was a large box with the states j belonging to the continuum, Eq. (2.B.3) would indicate that there would exist a bound state for an arbitrary weak coupling provided that the potential was attractive near the Fermi surface. This result was first pointed out by Cooper in connection with the problem of electrons moving in a metal at low temperatures¹⁴³.

2.B.2 Overlap

The states $|\alpha\rangle$ and $|\beta\rangle$ mix strongly through the couplings depicted by the graphs (a) and (b) of Fig. 2.7.11. Because of the energy dependence of the effective Hamiltonian (see (2.7.55), (2.7.56)) there is one matrix element for each state. The eigenvectors resulting from the diagonalization procedure were normalized according to (2.7.73). The corresponding amplitudes ξ_{iqm} (2.7.60) are displayed in Fig. 2.7.11 (e).

The normalization matrices $\tilde{M}_{ii'}^{mm}$ associated with the two $3/2^+$ states discussed in Sect. 2.5 and 2.7, are given in Table 2.B.1. Details concerning the off-diagonal matrix elements are collected in Table 2.B.2.

It is of notice that in a conventional two-state model calculation implying a single matrix one would obtain

$$|I\rangle = A|\alpha\rangle + B|\beta\rangle$$

and

$$|II\rangle = -B|\alpha\rangle + A|\beta\rangle, \quad (2.B.6)$$

with $A^2 + B^2 = 1$. This model would predict the value $R = (\alpha/\beta)^2$ for the (t, α) ratio $R(t, \alpha) = \sigma_I^{tr}/\sigma_{II}^{tr}$ and $1/R$ for the (α, α') ratio $R(\alpha, \alpha') = \sigma_I^{oct}/\sigma_{II}^{oct}$ (see Sect. 2.7.4). The ratio $R_{th}(t, \alpha) = 1.83/2.25 = 0.81$ (against $R_{exp}(t, \alpha) = 1.8/2.2 = 0.82$) and $R_{th}(\alpha, \alpha') = 3.7/1.5 = 2.5$ (against $R_{exp}(\alpha, \alpha') = 4.2/1.1 = 3.8$) is a direct consequence of the overcompleteness of the basis which is taken care of by the nuclear field theory. While this is a systematic mathematical procedure to deal with the spurious state (in this case due to the overcompleteness of the basis $\{|\alpha\rangle, |\beta\rangle\}$) one can also relate, within the framework of shell model calculations (see Eq. (2.B.1)), the asymmetry between $R(t, \alpha)$ and $R(\alpha, \alpha')$ to the finite overlaps between states $|\alpha\rangle$ and $|\beta\rangle$, as discussed in Sect. 2.5.

2.B.3 NFT(r+s): linear theory

NFT is linear in the variety of particle-vibration coupling vertices (see e.g. Fig. 2.7.10). This is also valid concerning its extension to describe reaction processes,

¹⁴³Cooper (1956); Bayman (1960).

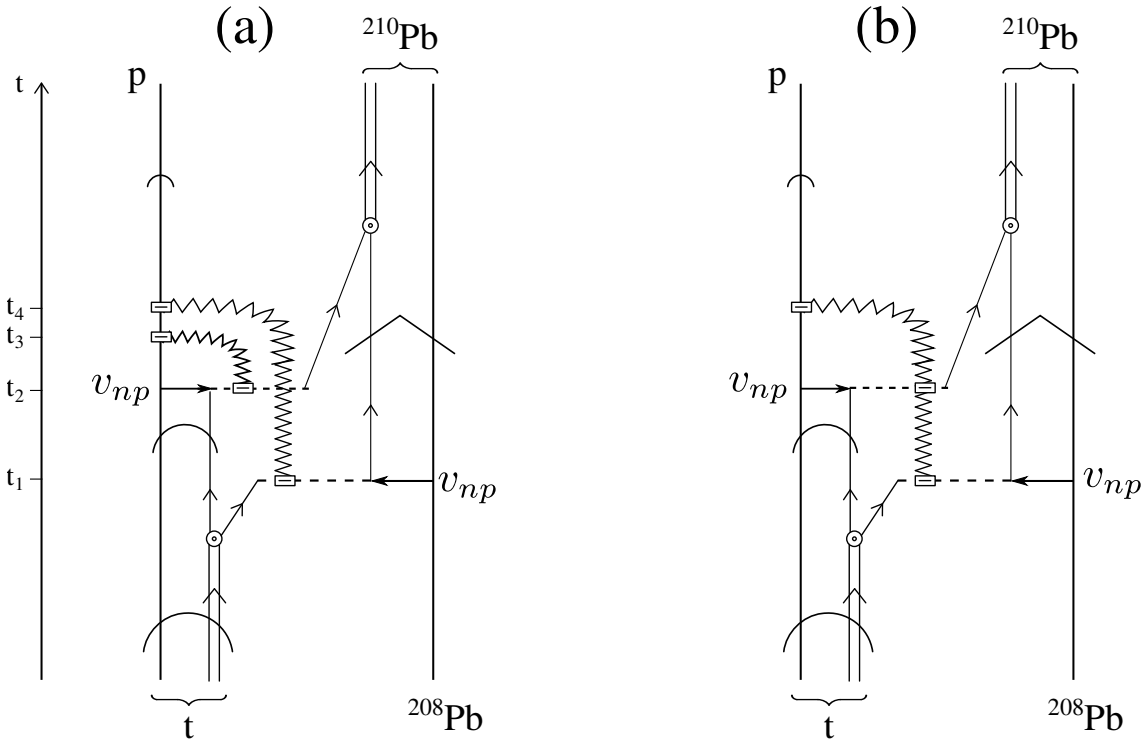


Figure 2.B.2: NFT($r+s$) diagram describing the reaction $^{208}\text{Pb}(t, p)^{210}\text{Pb}(\text{gs})$. That is the population of the lowest energy, monopole pair addition mode of ^{208}Pb . Concerning the different symbols used, we refer to Figs. 2.1.3 and 2.9.2. In particular concerning the recoil mode (jagged line) and the associated particle–recoil mode coupling vertex (dashed open rectangle). Also, of all the possible contributions associated with the different sequence of the processes taking place in this graph at times t_1, t_2, t_3 and t_4 , with the final outcome that the outgoing particle carries information to the detector of a transfer of two neutron masses. With this proviso in mind, and only for simplicity is that one may replace diagram (a) by diagram (b).

	$ \alpha\rangle$	$ \beta\rangle$		$ \alpha\rangle$	$ \beta\rangle$		$ \alpha\rangle$	$ \beta\rangle$
$ \alpha\rangle$	-0.010	-0.168	$ \alpha\rangle$	-0.012	-0.434	$ \alpha\rangle$	-0.011	-0.271
$ \beta\rangle$		0.009	$ \beta\rangle$		0.070	$ \beta\rangle$		0.03

Table 2.B.1: Normalization matrices (see Eq. (2.7.73)) associated with the two $3/2^+$ states of ^{209}Bi , $|I\rangle$ and $|II\rangle$ (Fig. 2.7.11 (e)) (Bortignon, P. F. et al. (1977), table 4.6).

		Fig. 1.7.10		
m	m'	(b)	(c)	(b)+(c)
I	II	0.013	-0.181	-0.168
II	II	0.016	-0.450	-0.434
I	II	0.014	-0.285	-0.271

Table 2.B.2: Contributions to the off diagonal elements of the overlap matrix $M_{ii'}^{mm'}$ associated with the $3/2$ states in the basis $|\alpha\rangle, |\beta\rangle$ (Table 2.B.1). See also figure 4.1 of Bortignon, P. F. et al. (1977).

as can be seen from graph (a) of Fig. 2.B.2. For simplicity, this diagram and similar ones are drawn as displayed in Fig. 2.B.2 (b) (see also Fig. 2.1.3). However, in all cases the effects of recoil are properly taken into account following (a), as shown in e.g. Fig. 4.1.2 as well as in Sect. 6.1 within the framework of DWBA, and in App. 6.5 (Eq. (6.5.7)) in the semiclassical approximation.

Appendix 2.C NFT and reactions

Nuclear Field Theory was systematically developed to describe nuclear structure processes. This fact did not prevent the translation into this graphical language of expressions which embodied the transition amplitude of a variety of reaction processes, in particular second order (in v_{np}) transition amplitudes associated with two nucleon transfer reactions¹⁴⁴.

The new feature to be considered regarding transfer processes and not encountered neither in structure, nor in elastic or anelastic processes, is the graphical representation of recoil effects. That is, a physical phenomenon associated with the change in the coordinate of relative motion reflecting the difference in mass partition between entrance (intermediate, if present) and exit channels. In fact, nuclear structure processes, do not affect the center of mass, with a proviso. In fact, the shell model potential violates the translational of the total nuclear Hamiltonian and, thus, single-particle excitations can be produced by a field proportional to the total center-of-mass coordinate. The translational invariance can be restored by including the effects of the collective field generated by a small displacement α of the nucleus. Such a displacement, in the x -direction, gives rise to a coupling which

¹⁴⁴Broglia (1975).

can be written as,

$$H_c = \kappa\alpha F, \quad (2.C.1)$$

where

$$F = -\frac{1}{\kappa} \frac{\partial}{\partial x}, \quad (2.C.2)$$

and

$$\kappa = \int \frac{\partial}{\partial x} \frac{\partial \rho_0}{\partial x} d\tau = -A \left\langle \frac{\partial^2 U}{\partial x^2} \right\rangle, \quad (2.C.3)$$

corresponding to a normalization of α such that $\langle F \rangle = \alpha$. It is of notice that both κ and U are negative for attractive fields (p. 356 of¹⁴⁵)

The spectrum of normal modes generated by the field coupling (2.C.1), namely by a Galilean transformation of amplitude α , contains an excitation mode with zero energy for which zero point fluctuations diverge in just the right way to restore translational invariance to leading order in α . In fact, while the zero point fluctuations (ZPF)

$$\lim_{\omega_\alpha \rightarrow 0} \left(\frac{\hbar\omega_\alpha}{2C_\alpha} \right)^{1/2} = \lim_{\omega_\alpha \rightarrow 0} \left(\frac{\hbar^2}{2D_\alpha \hbar\omega_\alpha} \right)^{1/2}, \quad (2.C.4)$$

diverge the inertia remains finite and equal to $D_\alpha = AM$, as expected, C_α being the restoring force constant. The additional dipole roots include, in particular, the isoscalar dipole modes associated with $\hat{D} = \sum_{i=1}^A r_i^3 Y_{1\mu}(\hat{r}_i)$, which can be viewed as a non-isotropic compression mode¹⁴⁶.

The operators leading to transformations associated with the change in the coordinates of relative motion (recoil effects) are Galilean operators ($\sim \exp(\mathbf{k}_{\alpha\beta} \cdot (\mathbf{r}_\beta - \mathbf{r}_\alpha))$). Their action (on e.g. the entrance channel), as that of (2.C.1) (on the shell model ground state), can be graphically represented in terms of NFT diagrams (or eventual extensions of them). In Figs 2.1.2 and 2.1.3 as well as 2.9.2–2.9.6 they are drawn in terms of jagged lines. How do we calculate such couplings? Let us elaborate on this point.

When one states that the small displacement α of the nucleus leads to a coupling (2.C.1) one means a coupling between the single-particle and the collective displacement of the system as a whole. When one talks about the spectrum of normal modes associated with such a coupling, one refers to the harmonic approximation (RPA). Thus, to the solutions of the dispersion relation¹⁴⁷,

$$-\frac{2\kappa}{\hbar} \sum_i \frac{|F|_i^2 \omega_i}{\omega_i^2 - \omega_d^2} = 1, \quad (2.C.5)$$

¹⁴⁵Bohr, A. and Mottelson (1975).

¹⁴⁶See e.g. Colò et al. (2000).

¹⁴⁷Bohr, A. and Mottelson (1975); Eq. (6-244), Brink, D. and Broglia (2005), Sect. 8.3.1.

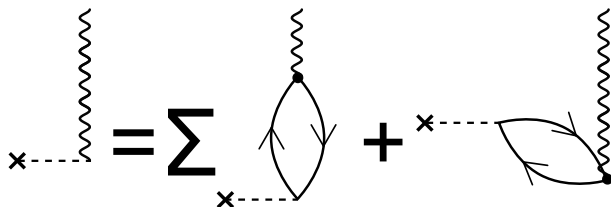


Figure 2.C.1: Self-consistent condition for normal modes

where the sum is over dipole particle–hole excitations. This dispersion relation can be represented graphically through the diagrams shown in Fig. 2.C.1. In particular, α acting on the vacuum creates the collective mode. This can also be seen by expressing α in second quantization, namely

$$\alpha = \sqrt{\frac{\hbar\omega_\alpha}{2C_\alpha}}(\Gamma_\alpha^\dagger + \Gamma_\alpha), \quad (2.C.6)$$

where $\sqrt{\hbar\omega_\alpha/2C_\alpha} = \sqrt{\frac{\hbar^2}{2D_\alpha} \frac{1}{\hbar\omega_\alpha}}$ is the zero-point amplitude of the collective (displacement) mode. Now, none of the above arguments lose their meaning in the case in which there is a root with $\omega_\alpha = 0$, also in keeping with the fact the inertia remains finite. In Figs. 2.9.2–2.9.6 we do something similar to what is done in Fig. 2.C.1. The dot, which in this figure represents the particle-vibration coupling, is replaced by a small dashed open square, which we label “particle-recoil coupling vertex” (see labels Fig. 2.9.2). It constitutes a graphical mnemonic to count the degrees of freedom that are at play. In this case the coordinates of relative motion. Also the fact that in connection with the appearance of such vertices one has to calculate matrix elements of precise form factors which involve the recoil phases. As far as the actual calculation of a particle-mode vertex in which $\omega_\alpha \rightarrow 0$, an empirical way out is that of a coarse-grained-like symmetry restoration. In this case κ is adjusted in such a way, that the lowest solution of Eq. (2.C.5), although being smaller than the rest of them, remains finite¹⁴⁸.

2.C.1 Potential scattering

The elastic differential cross section expressed in terms of partial waves is

$$\sigma(\theta) = |f(\theta)|^2 = \frac{1}{k^2} \left| \sum_{l=0}^{\infty} (2l+1) e^{i\delta_l} \sin \delta_l P_l(\cos \theta) \right|^2, \quad (2.C.7)$$

¹⁴⁸Within this context we refer to Bohr, A. and Mottelson (1975), p. 446. With no coupling H_c (Eq. (2.C.1)), the ZPF $\alpha_0^{(0)}$ of the nuclear CM are small ($\sim A^{-1/3}$). Thus, it is possible to tune κ so as to make the ZPF associated with the lowest root large as compared to $\alpha_0^{(0)}$, but still compatible with the ansatz at the basis of RPA (small amplitude harmonic vibrations).

where

$$f(\theta) = \frac{1}{2ik} \sum_{l=0}^{\infty} (2l+1) (e^{2i\delta_l} - 1) P_l(\cos \theta), \quad (2.C.8)$$

is the scattering amplitude. The total cross section

$$\sigma = 2\pi \int_0^\infty \sigma(\theta) \sin \theta d\theta = \frac{4\pi}{k^2} \sum_{l=0}^{\infty} (2l+1) \sin^2 \delta_l \quad (2.C.9)$$

expressed in term of f , namely,

$$\sigma = \frac{4\pi}{k} \Im f(0), \quad (2.C.10)$$

being a particular case of the optical theorem. The quantity δ_l is known as the phase shift of the l th partial wave, namely the difference in phase between the asymptotic form of the actual radial wavefunction describing the scattering process and the radial wavefunction $j_l(kr)$ in the absence of potential. The phase shifts which completely determine the scattering lead to a change in the scaling between incoming and outgoing waves which results, as expressed in (2.C.10), in the interference between them, so that particle intensity is smaller behind the scattering region ($\theta \approx 0$) than in front of it. It is of notice that δ_l cannot be measured directly. In fact, with the exception of the $l = 0$ phase shift, obtained from low-energy scattering experiments, the values of δ_l are inferred as empirical quantities from the parametrization of the potential. It is of notice that a degree of ambiguity concerning the uniqueness of the findings may remain.

2.C.2 Transfer

We now consider a general reaction



in which the nucleus a impinges on the nucleus A in the entrance channel $\alpha(a, A)$ and where the two nuclei in the exit channel β , namely b and B may differ from those in α , by the transfer of one or more nucleons.

In the center-of-mass system, the total Hamiltonian may be written as

$$\begin{aligned} H &= T_{aA} + H_a + H_A + V_{aA}, \\ &= T_{bB} + H_b + H_B + V_{bB}, \end{aligned} \quad (2.C.12)$$

where T_{aA} is the kinetic energy of the relative motion in channel α

$$T_{aA} = -\frac{\hbar^2}{2m_{aA}} \nabla_{aA}^2, \quad (m_{aA} = \frac{m_a m_A}{m_a + m_A}), \quad (2.C.13)$$

and similarly for T_{bB} . Assuming the nuclei in (2.C.11) to be heavy ions, we shall solve the time-dependent Schrödinger equation

$$i\hbar \frac{\partial \Psi}{\partial t} = H\Psi \quad (2.C.14)$$

with the initial condition that a and A are in their ground states, and that the relative motion is described as a narrow wave-packet of rather well-defined impact parameter and velocity. Because of the quantal nature of the process under consideration, we study the quantal description in the limit of small wavelength of relative motion (semiclassical approximation). One expands Ψ on the channel wavefunctions

$$\Psi_\beta(t) = \Psi_m^b(\xi_b)\Psi_n^B(\xi_B)e^{i\delta_\beta} \quad (2.C.15)$$

where Ψ^b and Ψ^B describe the structure of the two nuclei and satisfy the equations

$$H_b\Psi_m^b(\xi_b) = E_m^b\Psi_m^b(\xi_b) \quad (2.C.16)$$

and

$$H_B\Psi_n^B(\xi_B) = E_n^B\Psi_n^B(\xi_B), \quad (2.C.17)$$

while ξ_b and ξ_B denote the intrinsic coordinates. the phase δ_β is defined by

$$\delta_\beta = \frac{1}{\hbar} \left\{ m_\beta \mathbf{v}_\beta(t)(\mathbf{r}_\beta - \mathbf{R}_\beta(t)) - \int_0^t \left(U_\beta(R_\beta(t')) - \frac{1}{2}m_\beta v_\beta^2(t') \right) dt' \right\}. \quad (2.C.18)$$

The index β labels both the partition of nucleons into b and B , as well as the quantal states of the two nuclei. The quantity U_β is the ion-ion potential in this channel. It is equal to the expectation value of $V_\beta = V_{bB}$ in the channel β . The distance between the centers of mass of the two systems is denoted by

$$\mathbf{r}_\beta = \mathbf{r}_{bB} = \mathbf{r}_b - \mathbf{r}_B. \quad (2.C.19)$$

The quantity \mathbf{R}_β and its derivative $\mathbf{v}_\beta = \dot{\mathbf{R}}_\beta$ describe the motion of the centers of mass of the wavepackets, and satisfy the corresponding classical equation of motion,

$$m_\beta \dot{\mathbf{v}}_\beta = -\nabla U_\beta(\mathbf{R}_\beta). \quad (2.C.20)$$

The phase factor $e^{i\delta_\beta}$ in the channel wavefunction, is essentially a Galilean transformation where an additional phase (related with the Q -value) has been added to eliminate, as far as possible, the diagonal matrix elements of the coupled equations. Using the notation $E_\beta = E_m^b + E_n^B$ and inserting the ansatz

$$\Psi = \sum_\beta c_\beta((r_\beta - R_\beta), t)\Psi_\beta(t)e^{-iE_\beta t/\hbar} \quad (2.C.21)$$

in eq. (2.C.14) one obtains, assuming narrow wavepackets, product of an amplitude $a_\beta(t)$ and a shape $\chi_\beta(\mathbf{r} - \mathbf{R}_\beta(t), t)$, ($c_\beta = a_\beta \chi_\beta$),

$$\begin{aligned} i\hbar \sum_\beta \dot{a}_\beta(t) \langle \Psi_\xi | \Psi_\beta \rangle_{\mathbf{R}_\xi} e^{-iE_\beta t/\hbar} \\ = \sum_\gamma \langle \Psi_\xi | V_\gamma - U_\gamma(r_\gamma) | \Psi_\gamma \rangle_{\mathbf{R}_\xi} a_\gamma(t) e^{-iE_\gamma t/\hbar}. \end{aligned} \quad (2.C.22)$$

where the sub-index on the matrix elements indicate that the integration over the degree of freedom of the two nuclei, the average center-of-mass coordinate $\mathbf{r}_{\beta\gamma} = (\mathbf{r}_\beta + \mathbf{r}_\gamma)/2$ should be identified with the average classical coordinate, i.e.

$$\mathbf{r}_{\beta\gamma} \rightarrow \mathbf{R}_{\beta\gamma} = \frac{1}{2}(\mathbf{R}_\beta + \mathbf{R}_\gamma), \quad (2.C.23)$$

and the functions $\langle \Psi_\xi | V_\gamma - U_\gamma(r_\gamma) | \Psi_\gamma \rangle_{\mathbf{R}_\xi}$ are the form factors. The coupled equations (2.C.22) can be written in a more compact way by an orthogonalization procedure, which makes use of the *adjoint channel wavefunctions*

$$\omega_\xi = \sum_\gamma g_{\xi\gamma}^{-1} \Psi_\gamma, \quad (2.C.24)$$

where g^{-1} is the inverse of the overlap matrix

$$g_{\xi\gamma} = \langle \Psi_\xi | \Psi_\gamma \rangle, \quad (2.C.25)$$

that is

$$\sum_\xi g_{\gamma\xi} g_{\xi\beta}^{-1} = \sum_\xi g_{\gamma\xi}^{-1} g_{\xi\beta} = \delta(\gamma, \beta). \quad (2.C.26)$$

With this definition,

$$(\omega_\xi, \Psi_\beta) = \delta(\xi, \beta), \quad (2.C.27)$$

which takes care of non-orthogonality. Making use of the above relations one can rewrite (2.C.22) in the form

$$i\hbar \dot{a}_\beta(t) = \sum_\gamma \langle \omega_\beta | V_\gamma - U_\gamma | \Psi_\gamma \rangle_{\mathbf{R}_\beta} e^{i(E_\beta - E_\gamma)t/\hbar} a_\gamma(t). \quad (2.C.28)$$

That is, the proper transfer (tunneling) equations are obtained from (2.C.22) by a basis orthogonalization process¹⁴⁹. By solving these coupled equations with the condition that at $t = -\infty$ the system is in the ground state of a and A (entrance channel α), that is $a_\gamma(-\infty) = \delta_{\gamma,\alpha}$, one can calculate the differential cross section

$$\frac{d\sigma_{\alpha \rightarrow \beta}}{d\Omega} = P_{\alpha \rightarrow \beta} \sqrt{\left(\frac{d\sigma_\alpha}{d\Omega} \right)_{el} \left(\frac{d\sigma_\beta}{d\Omega} \right)_{el}}, \quad (2.C.29)$$

¹⁴⁹Within this connection we refer to Sect. 4.6 where the tunneling Hamiltonian used in connection with the Josephson effect is discussed.

where $P_{\alpha \rightarrow \beta}$ is the absolute value squared of the transition amplitude $|a_\beta(t = +\infty)|^2$. It gives the probability that the system at $t = +\infty$ is in the final channel. The quantities $(d\sigma/d\Omega)_{el}$ are the (semiclassical) elastic cross sections.

We now solve the coupled equations in first order perturbation theory. For this purpose we insert $\delta(\gamma, \alpha)$ at the place of $a_\gamma(t)$ obtaining

$$\begin{aligned} a_\beta(t) &= \frac{1}{i\hbar} \int_{-\infty}^t \langle \omega_\beta | V_\alpha - U_\alpha | \Psi_\alpha \rangle_{\mathbf{R}_{\beta\alpha}(t)} \exp^{i(E_\beta - E_\alpha)t'/\hbar} dt' \\ &= \frac{1}{i\hbar} \int_{-\infty}^t dt' \langle \Psi_\beta | V_\alpha - U_\alpha | \Psi_\alpha \rangle_{\mathbf{R}_{\beta\alpha}(t)} \exp^{i(E_\beta - E_\alpha)t'/\hbar} \end{aligned} \quad (2.C.30)$$

where the expansion,

$$\omega_\beta = \Psi_\beta - \langle \Psi_\alpha | \Psi_\beta \rangle_{\mathbf{R}_{\beta\alpha}(t)}, \quad (2.C.31)$$

has been used, and the ansatz made, that the global optical potentials (U : real part), and standard nucleon–nucleon interactions V fulfill the relation

$$\langle \Psi_\alpha | V_\alpha - U_\alpha | \Psi_\alpha \rangle = 0. \quad (2.C.32)$$

Let us consider for simplicity the one-particle transfer reaction¹⁵⁰

$$a (= b + 1) + A \rightarrow b + B (= A + 1). \quad (2.C.33)$$

Making use of (2.C.15), that is,

$$\Psi_\alpha = \Psi^a \Psi^A e^{i\delta_\alpha}, \quad (2.C.34)$$

and

$$\Psi_\beta = \Psi^b \Psi^B e^{i\delta_\beta}, \quad (2.C.35)$$

one can write

$$\begin{aligned} \langle \Psi_\beta | V_\alpha - U_\alpha | \Psi_\alpha \rangle_{\mathbf{R}_{\alpha\beta}} &= \langle \Psi^b \Psi^B | (V_\alpha - U_\alpha) e^{i\sigma_{\alpha\beta}} | \Psi^a \Psi^A \rangle_{\mathbf{R}_{\alpha\beta}} e^{i\gamma_{\alpha\beta}} \\ &= \langle \phi^{B(A)}(S^B(n), r_{1A}), U(r_{1b}) e^{i\sigma_{\alpha\beta}} \phi^{a(b)}(S^a(n), r_{1b}) \rangle_{\mathbf{R}_{\alpha\beta}} e^{i\gamma_{\alpha\beta}}. \end{aligned} \quad (2.C.36)$$

To obtain the above relation, we have separated the difference $\delta_{\alpha\beta} = \delta_\alpha - \delta_\beta$ between the phases δ_α and δ_β into a part $\gamma_{\alpha\beta}$ which only depends on time and is related to the effective Q -value of the reaction process, and a phase $\sigma_{\alpha\beta}$ which also depends on the center-of-mass coordinate of the transferred particles. That is

$$\begin{aligned} \gamma_{\alpha\beta}(t) &= \int_0^t \left\{ U_\alpha(R_\alpha(t)) - \frac{1}{2} m_\alpha v_\alpha^2(t') - U_\beta(R_\beta(t')) + \frac{1}{2} m_\beta v_\beta^2(t') \right\} \\ &\quad + \mathbf{k}_{\alpha\beta}(t)(\mathbf{R}_\alpha - \mathbf{R}_\beta), \end{aligned} \quad (2.C.37)$$

¹⁵⁰Concerning the question of non-orthogonality in one-particle transfer processes, the first contribution arises in second order of perturbation theory, within the framework of DWBA (Thompson and Nunes (2009)).

where $\mathbf{k}_{\alpha\beta}$ is the average wave vector

$$\mathbf{k}_{\alpha\beta} = \frac{1}{2\hbar} (m_\alpha \mathbf{v}_\alpha(t) + m_\beta \mathbf{v}_\beta(t)). \quad (2.C.38)$$

Similarly

$$\sigma_{\alpha\beta} = \mathbf{k}_{\alpha\beta}(t) \cdot (\mathbf{r}_\beta - \mathbf{r}_\alpha). \quad (2.C.39)$$

The phase σ is characteristic for transfer processes since the dynamical variables \mathbf{r}_α and \mathbf{r}_β are identical for inelastic scattering. It arises from the change in the center-of-mass coordinate taking place when mass is transferred from one system to other. It gives rise to the recoil effect. Within the framework of DWBA it leads to a change of scaling of the DW (see also section elastic transfer). Summing up, the one-particle transfer amplitude reads

$$\begin{aligned} (a_\beta(t = +\infty))^{(1)} &= \int_{-\infty}^{\infty} \langle \phi^{B(A)}(S^B(n), \mathbf{r}_{1A}), U_{1b}(r_{1b}) e^{\sigma_{\alpha\beta}} \phi^{a(b)}(S^a(n), \mathbf{r}_{1b}) \rangle_{\mathbf{R}_{\alpha\beta}} \\ &\times \exp \left\{ i \left[(E_\beta - E_\alpha)t'/\hbar + \gamma_{\alpha\beta} \right] \right\} \end{aligned} \quad (2.C.40)$$

The phases $\delta_{\alpha\beta}$ ($\sigma_{\alpha\beta} + \gamma_{\alpha\beta}$) play a similar role in the determination of transfer processes reaction amplitudes as δ_l does in connection with elastic scattering cross sections. In fact, $\delta_{\alpha\beta}$ determines the shift between incoming and outgoing waves and thus the interference process which is at the basis of the absolute value of the transfer differential cross section. In other words, the reaction part of the elastic and one-nucleon-transfer reaction cross section are embodied in δ_l and $\delta_{\alpha\beta}$ respectively. The nuclear structure part is contained in the reduced mass μ and potential U in the case of elastic scattering, and in the single-particle wavefunctions, potential U_{1b} and Q -value phase in the transfer case. Within the diagrammatic representation of particle-transfer reaction theory, the recoil phase is represented by a jagged line. Similar to δ_l , $\delta_{\alpha\beta}$ and $\sigma_{\alpha\beta}$ cannot be measured directly, but can in principle be inferred from the absolute differential cross section¹⁵¹. In other words, the jagged line does not display asymptotic behavior, representing in all cases a virtual process.

Let us conclude this section by making some comments concerning two nucleon transfer processes

$$\alpha \equiv a (= b + 2) + A \rightarrow b + B (= A + 2) \equiv \beta, \quad (2.C.41)$$

and associated sum rules. For such reactions, the overlap appearing in Eq. (2.C.31) contributes with an amplitude $\langle \Psi_\beta | \mathbb{1} | \Psi_\gamma \rangle \langle \Psi_\gamma | V_\alpha - U_\alpha | \Psi_\alpha \rangle$, where $\mathbb{1}$ is the unit operator, while $\gamma \equiv f (= b + 1) + F (= A + 1)$, denotes the mass partition of the intermediate channel. The above expression indicates that a consistent description of two-nucleon transfer reactions in a non-orthogonal basis involves three strongly

¹⁵¹For more detail see Broglia and Winther (2004), in particular Section V.4 p. 308 and subsequent.

interweaved reaction channels¹⁵², namely α, γ and β and consequently has to be worked out, at least, up to second order of perturbation theory, and thus the need to calculate also $a^{(2)}(t)$. That is, including simultaneous and successive transfer and non-orthogonality corrections.

Regarding the sum-rule subject we consider, for simplicity, the simultaneous transfer amplitude (2.C.30) (see also App. 6.5, Eq. (6.5.4)). That is,

$$\begin{aligned} a^{(1)}(t = +\infty) &= \frac{1}{i\hbar} \int_{-\infty}^{\infty} dt \exp\left[\frac{i}{\hbar}(E^{bB} - E^{aA})t + \gamma_{\beta\alpha}(t)\right] \\ &\times \langle \phi^{B(A)}(\mathbf{r}_{1A}, \mathbf{r}_{2A}) | U(r_{1b}) | e^{i\sigma_{\beta\alpha}} \phi^{a(b)}(\mathbf{r}_{1b}, \mathbf{r}_{2b}) \rangle_{\mathbf{R}_{\alpha\beta}(t)}, \end{aligned} \quad (2.C.42)$$

where

$$\sigma_{\beta\alpha} = \frac{1}{\hbar} \frac{m_n}{m_A} (m_{aA} \mathbf{v}_{aA}(t) + m_{bB} \mathbf{v}_{bB}(t)) \cdot (\mathbf{r}_\alpha - \mathbf{r}_\beta), \quad (2.C.43)$$

takes care of recoil effects, the phase factor $e^{\sigma_{\beta\alpha}}$ being a generalized Galilean transformation associated with the mismatch between entrance and exit channels, while the phase

$$\begin{aligned} \gamma_{\beta\alpha}(t) &= \int_0^t dt' \left\{ U_\beta(\mathbf{R}_\beta(t')) - \frac{1}{2} m_\beta v_\beta^2(t') - U_\alpha(\mathbf{R}_\alpha(t')) + \frac{1}{2} m_\alpha v_\alpha^2(t') \right\} \\ &+ \frac{1}{2\hbar} (m_\alpha \mathbf{v}_\alpha(t) + m_\beta \mathbf{v}_\beta(t)) \cdot (\mathbf{R}_\beta(t) - \mathbf{R}_\alpha(t)), \end{aligned} \quad (2.C.44)$$

is related to the effective Q -value of the reaction.

The rate of change of the formfactor $\langle \phi^{B(A)}, U(r_{1b}) e^{i\sigma_{\alpha\beta}} \phi^{a(b)} \rangle$ with time is slow, being completely overshadowed by the rapidly varying phase factor $\exp\left[\frac{i}{\hbar}(E^{bB} - E^{aA})t + \gamma_{\beta\alpha}(t)\right]$. Similar relations concerning recoil and Q -value effects can be obtained from the amplitudes associated to successive and to non-orthogonality terms i.e. $a^{(2)}$ and $a^{(NO)}$ (see Ch. 6, Sect. 6.5).

Summing up, to compare two-nucleon transfer cross sections on equal structural footing, one has to eliminate the kinematical oscillating phase which can completely distort the “intrinsic” (reduced matrix element) value of the two-nucleon cross section. And for that, one has to work on each of the three amplitudes to extract at best the phases which couple relative and intrinsic motion.

Let us make a parallel with the sum rule associated with electromagnetic decay (Coulomb excitation, γ -decay). The absolute transition probability for absorption (emission) of a photon from nuclear dipole states is measured in sec^{-1} by

$$T(E1; I_1 \rightarrow I_2) = (1.59 \times 10^{15}) \times (E)^3 \times B(E1; I_1 \rightarrow I_2), \quad (2.C.45)$$

¹⁵²This is also testified by the fact that their formal expression can be shifted around by changing representation, among post-post, prior-prior, and prior-post, see e.g. Eq. (2.6.2) as well as Fig. 6.5.2.

where E is the energy of the transition and $B(E1) = \langle I_2 || \mathcal{M}(E1) || I_1 \rangle / \sqrt{3}$ is¹⁵³ the reduced transition probability¹⁵⁴. The TRK-sum rule is written as

$$S(E1) = \langle 0 | [[H, \mathcal{M}(E1)], \mathcal{M}(E1)] | 0 \rangle / 2, \quad (2.C.46)$$

Now, in this particular case the Q -value dependence of the observed absolute transition probabilities can be eliminated analytically (E^3 dependence), as well as the overall factor (1.59×10^{15}), in keeping with the fact that the mass partition ($a+A \rightarrow a+A^*$) as well as the overall factor does not change between entrance and exit channels or, equivalently, the coordinate of relative motion $\mathbf{R}_{aa'}(t)$ is always that describing the relative center of mass position of target and projectile.

Expressed it differently, and returning to the expression of the first order (simultaneous) two-nucleon transfer amplitude $a^{(1)}(t = +\infty)$ one can only devise empirical protocols to try to extract the γ - and σ -phase dependence from it (see Eqs. (2.C.42)–(2.C.44)), and set differential absolute two-nucleon transfer cross sections $d\sigma/d\Omega \sim |a|^2$ on equal footing regarding kinematics, so as to be able to compare the intrinsic, reduced transition probabilities (structure). That is, extract the structure information contained in, e.g.,¹⁵⁵

$$\phi^{B(A)}(\mathbf{r}_{1A}, \mathbf{r}_{2A}) = \langle \mathbf{r}_{1A}, \mathbf{r}_{2A} | \Gamma_1^\dagger(\beta = +2) | \tilde{0} \rangle, \quad (2.C.47)$$

as well as in

$$\phi^{B(A)}(\mathbf{r}_{1A}, \mathbf{r}_{2A}) = \langle \mathbf{r}_{1A}, \mathbf{r}_{2A} | [a_k^\dagger a_k^\dagger]_0 | 0 \rangle. \quad (2.C.48)$$

Namely, in the RPA pair addition mode representation and in the pure two-particle configuration $|j_k^2(0)\rangle$ describing two nucleons moving in time reversal states around the close shell system $|0\rangle$. If one was able to disentangle the γ and σ dependence of $a^{(1)}$ (as well as that of $a^{(2)}$ and $a^{(NO)}$, see above) from its formfactor dependence, the comparison between the quantities $\sum_{n,k} |c_k^{(n)}|^2$, and¹⁵⁶ $\sum_{n,j} \left| \sum_k X_k^{(n)} \delta(j, k) - \sum_i Y_i^{(n)} \delta(j, i) \right|^2$ could eventually be phrased in terms of exact sum rules. This not being the case, one has to deal with approximate TNTR sum rules. With this proviso in mind, such sum rules are quite useful (see Sect. 7.4.1; also end of Sect. 2.2).

Appendix 2.D NFT vacuum polarization

The role zero point fluctuations play in the nuclear ground state, i.e. in the NFT vacuum can be clarified by relating it to the polarization of the QED vacuum. Let us briefly dwell on the "reality" of such a phenomenon by recalling the fact that

¹⁵³ $\mathcal{M}(E1) = e \sum_k \left(\left(\frac{N-Z}{A} - t_Z \right) r Y_{1\mu} \right)_k$.

¹⁵⁴ Bohr and Mottelson (1969) p. 382.

¹⁵⁵ Where $\Gamma_n^\dagger(\beta = +2) = \sum_k X_k^n [a_k^\dagger a_k^\dagger]_0 - \sum_i Y_i^n [a_i^\dagger a_i^\dagger]_0$, is the RPA pair creation addition mode acting on a closed shell system $|\tilde{0}\rangle$.

¹⁵⁶ See e.g. Broglia and Riedel (1967).

to the question of Rabi of whether the polarization of the QED vacuum could be measured¹⁵⁷ in particular the change in charge density felt by the electrons of an atom, e.g. the electron of a hydrogen atom, due to virtual creation and annihilation of electron–positron pairs - Lamb gave a quantitative answer, both experimentally and theoretically¹⁵⁸. The corresponding correction (Lamb shift) implies that the $2s_{1/2}$ level lies higher than the $2p_{1/2}$ level by about 1000 megacycles/s as experimentally observed.

In connection with the discussion of Feynman of vacuum polarisation, where a field produces a pair, the subsequent pair annihilation producing a new field, namely a close loop, he implemented in his space–time trajectories Wheeler’s idea of electrons going backwards in time (positrons). Such trajectories would be like an N in time, that is electrons which would back up for a while, and go forward again. Being connected with a minus sign, these processes are associated with Pauli principle in the self–energy of electrons (see Fig. 2.4.2 (f)). The divergences affecting such calculations could be renormalised by first computing the self-energy diagram in second order and finding the answer which is finite, but contains a cut-off to avoid a logarithmic divergence. Expressing the result in terms of the experimental mass, one can take the limit (cut-off $\rightarrow \infty$) which now exists (see also Sect. 7.6). Concerning radiative corrections to scattering, in particular that associated with the process in which the potential creates an electron-positron pair which then reannihilates, emitting a quantum which scatters the electron, the renormalisation procedure should be applied to the electric charge, introducing the observed one (Bethe and Pauli)¹⁵⁹.

In the nuclear case, for example Skyrme effective interactions give rise to particle-vibration coupling vertices which, because of the contact character of these interactions may lead to divergent zero point energies¹⁶⁰, unless a cut-off is introduced¹⁶¹. The Gogny force being finite range does not display such problems. Nonetheless, the associated results concerning zero point energies may not be very stable and/or accurate carrying out a complete summation over both collective and non collective contributions. In this case one can eliminate such a problem by going to higher orders in the oyster diagrams (see Figs. 2.4.2 (a), 2.7.1 and 2.8.2, as well as App. 6.3). The fermion exchange between two of these diagrams (Pauli

¹⁵⁷Pais (1986) pp. 450, 451; Pais (2000) pp. 255-267.

¹⁵⁸Lamb and Rutherford (1947); Kroll and Lamb (1949)

¹⁵⁹See Mehra (1996) p. 295; see also Bjorken and Drell (1998).

¹⁶⁰See Hellemans et al. (2013); Pastore et al. (2015) and refs. therein.

¹⁶¹Let alone the fact that the velocity dependent component of these forces weaken the PVC vertices leading to poorly collective low-lying vibrations, and to equally poor clothed valence states. The question emerges of which are the provisos to be taken in the use of effective forces to higher orders of the PVC. Within this context cf. Mahaux, C. et al. (1985), also Broglia et al. (2016); Barranco et al. (2017) concerning the implementation of renormalization in both configuration and 3D-spaces within the framework of NFT. In a nutshell, the bare mean field exists but its properties cannot be measured (not any more than the bare electron mass in renormalized quantum electrodynamics), and corresponds to a set of parameters of a Fermi-like function which ensure that the clothed states reproduce all of the experimental findings, for both structure and reactions.

principle) eliminates non-collective contributions, leading to convergent, accurate results.

An economic and reliable method to achieve a similar result, is that of using renormalization. That is, to calculate the lowest order diagrams but introducing, in the intermediate states, the dressed physical (empirical) states.

Bibliography Ch 2

- K. Alder and A. Winther. *Electromagnetic Excitations*. North Holland, Amsterdam, 1975.
- K. Alder, A. Bohr, T. Huus, B. Mottelson, and A. Winther. Study of Nuclear Structure by Electromagnetic Excitation with Accelerated Ions. *Rev. Mod. Phys.*, 28:432, 1956.
- P. W. Anderson. Special effects in superconductivity. In E. R. Caianello, editor, *The Many-Body Problem, Vol.2*, page 113. Academic Press, New York, 1964.
- N. Austern. *Direct nuclear reaction theories*. Interscience monographs and texts in physics and astronomy. Wiley-Interscience, 1970.
- M. Baranger. Recent progress in the understanding of finite nuclei from the two-nucleon interaction. In M. Jean and R. A. Ricci, editors, *Proceedings of the International school of physics “E. Fermi” Course XL Nuclear Structure and Nuclear Reactions*, page 511. Academic Press, New York, 1969.
- J. Bardeen, L. N. Cooper, and J. R. Schrieffer. Microscopic theory of superconductivity. *Physical Review*, 106:162, 1957a.
- J. Bardeen, L. N. Cooper, and J. R. Schrieffer. Theory of superconductivity. *Physical Review*, 108:1175, 1957b.
- Barnes, P., E. Romberg, C. Ellegard, R. Casten, O. Hansen, and J. Mulligan. Proton-hole states in ^{209}Bi From the $^{210}\text{Po} (t, \alpha)$ reaction. *Nucl. Phys. A*, 195: 146, 1972.
- F. Barranco, R. A. Broglia, G. Colò, G. Gori, E. Vigezzi, and P. F. Bortignon. Many-body effects in nuclear structure. *European Physical Journal A*, 21:57, 2004.
- F. Barranco, P. F. Bortignon, R. A. Broglia, G. Colò, P. Schuck, E. Vigezzi, and X. Viñas. Pairing matrix elements and pairing gaps with bare, effective, and induced interactions. *Phys. Rev. C*, 72:054314, 2005.
- F. Barranco, G. Potel, R. A. Broglia, and E. Vigezzi. Structure and reactions of ^{11}Be : many-body basis for single-neutron halo. *Phys. Rev. Lett.*, 119:082501, 2017.
- F. Barranco, G. Potel, E. Vigezzi, and R. A. Broglia. $d(^9\text{Li}, p)$, specific probe of ^{10}Li , paradigm of parity-inverted, soft-dipole isotones with one neutron outside the $N = 6$ closed shell. *arXiv:1812.01761 [nucl-th]*, 2018.
- Barranco, F., P. F. Bortignon, R. A. Broglia, G. Colò, and E. Vigezzi. The halo of the exotic nucleus ^{11}Li : a single Cooper pair. *Europ. Phys. J. A*, 11:385, 2001.

- B. Bayman. A derivation of the pairing-correlation method. *Nuclear Physics*, 15:33, 1960.
- B. F. Bayman. Seniority, Quasi-particle and Collective vibrations. *Lecture notes, Palmer Physical Laboratory, Princeton, unpublished*, 1961.
- Bayman, B. F. and C. F. Clement. Sum rules for two-nucleon transfer reactions. *Phys. Rev. Lett.*, 29:1020, 1972.
- S. Beceiro–Novo, T. Ahn, D. Bazin, and W. Mittig. Active targets for the study of nuclei far from stability. *Progress in Particle and Nuclear Physics*, 84:124, 2015.
- S. T. Belyaev. Effect of pairing correlations on nuclear properties. *Kgl. Danske Videnskab. Selskab, Mat.-fys. Medd.*, 31:No11, 1959.
- V. Bernard and N. V. Giai. Single-particle and collective nuclear states and the green's function method. In R. A. Broglia, R. A. Ricci, and C. H. Dasso, editors, *Proc. of the Int. School of Physics "Enrico Fermi", Course LXXVII*, p. 437. North Holland, Amsterdam, 1981.
- G. Bertsch and R. A. Broglia. *Oscillations in Finite Quantum Systems*. Cambridge University Press, Cambridge, 2005.
- G. F. Bertsch, P. F. Bortignon, and R. A. Broglia. Damping of nuclear excitations. *Rev. Mod. Phys.*, 55:287, 1983.
- D. R. Bès and R. A. Broglia. Equivalence between Feynman–Goldstone and particle–phonon diagrams for finite many body systems. In G. Alaga, V. Paar, and L. Sips, editors, *Problems of Vibrational Nuclei, in Procs. of the topical Conference on Problems of Vibrational Nuclei*, page 1, Amsterdam, 1975. North Holland.
- D. R. Bès and R. A. Broglia. Nuclear superfluidity and field theory of elementary excitations. In A. Bohr and R. A. Broglia, editors, *International School of Physics "Enrico Fermi" Course LXIX, Elementary Modes of Excitation in Nuclei*, page 55, Amsterdam, 1977. North Holland.
- D. R. Bès and R. A. Sorensen. The pairing–plus–quadrupole model. *Advances in Nuclear Physics*, 2:129, 1969.
- D. R. Bès, G. G. Dussel, R. A. Broglia, R. Liotta, and B. R. Mottelson. Nuclear field theory as a method of treating the problem of overcompleteness in descriptions involving elementary modes of both quasi-particles and collective type. *Phys. Lett. B*, 52:253, 1974.
- D. R. Bès, R. A. Broglia, G. G. Dussel, R. J. Liotta, and R. P. J. Perazzo. On the many-body foundation of the Nuclear Field Theory. *Nucl. Phys. A*, 260:77, 1976a.

- D. R. Bès, R. A. Broglia, G. G. Dussel, R. J. Liotta, and H. M. Sofía. The nuclear field treatment of some exactly soluble models. *Nucl. Phys. A*, 260:1, 1976b.
- D. R. Bès, R. A. Broglia, G. G. Dussel, R. J. Liotta, and H. M. Sofía. Application of the nuclear field theory to monopole interactions which include all the vertices of a general force. *Nucl. Phys. A*, 260:27, 1976c.
- Bès, D. R. and J. Kurchan. *The treatment of Collective Coordinates in Many-Body Systems*. World Scientific, Singapore, 1990.
- Bès, D. R. and Broglia, R. A. and Dussel, G. G. and Liotta. Simultaneous treatment of surface and pairing nuclear fields. *Phys. Lett. B*, 56:109, 1975.
- Bjerregaard, J. H., O. Hansen, Nathan, and S. Hinds. States of ^{208}Pb from double triton stripping. *Nucl. Phys.*, 89:337, 1966.
- J. B. Bjorken and S. D. Drell. *Relativistic quantum mechanics*. Mc Graw–Hill, New York, 1998.
- D. Bohm and D. Pines. A Collective Description of Electron Interactions. I. Magnetic Interactions. *Phys. Rev.*, 82:625, 1951.
- D. Bohm and D. Pines. A Collective Description of Electron Interactions: III. Coulomb Interactions in a Degenerate Electron Gas. *Phys. Rev.*, 92:609, 1953.
- A. Bohr. Elementary modes of excitation and their coupling. In *Comptes Rendus du Congrès International de Physique Nucléaire*, volume 1, page 487. Centre National de la Recherche Scientifique, 1964.
- A. Bohr. *Rotational Motion in Nuclei, in Les Prix Nobel en 1975*. Imprimerie Royale Norstedts Tryckeri, Stockholm, 1976. p. 59.
- A. Bohr and B. R. Mottelson. *Nuclear Structure, Vol.I*. Benjamin, New York, 1969.
- A. Bohr, B. R. Mottelson, and D. Pines. Possible analogy between the excitation spectra of nuclei and those of the superconducting metallic state. *Physical Review*, 110:936, 1958.
- Bohr, A. and B. R. Mottelson. *Nuclear Structure, Vol.II*. Benjamin, New York, 1975.
- M. Born. *Natural philosophy of cause and chance*. Oxford University Press, Oxford, 1948.
- P. F. Bortignon and R. A. Broglia. Role of the nuclear surface in an unified description of the damping of single-particle states and giant resonances. *Nucl. Phys. A*, 371:405, 1981.
- P. F. Bortignon, R. A. Broglia, D. R. Bès, R. Liotta, and V. Paar. On the role of the pairing modes in the ($h_{9/2} \otimes 3^-$) multiplet of ^{209}Bi . *Phys. Lett. B*, 64:24, 1976.

- Bortignon, P. F., R. A. Broglia, D. R. Bès, and R. Liotta. Nuclear field theory. *Physics Reports*, 30:305, 1977.
- Bortignon, P. F., R. A. Broglia, and D. R. Bès. On the convergence of nuclear field theory perturbation expansion for strongly anharmonic systems. *Phys. Lett. B*, 76:153, 1978.
- Bortignon, P. F., A. Bracco, and R. A. Broglia. *Giant Resonances*. Harwood Academic Publishers, Amsterdam, 1998.
- Brink, D. and R. A. Broglia. *Nuclear Superfluidity*. Cambridge University Press, Cambridge, 2005.
- Brink, D. M. *Semi-classical methods in nucleus-nucleus scattering*. Cambridge University Press, Cambridge, 1985.
- R. Broglia, F. Barranco, A. Idini, G. Potel, and E. Vigezzi. Pygmy resonances: what's in a name? *Phys. Scr.*, 94:114002, 2019.
- R. A. Broglia. Heavy ion reaction, Notes of lectures delivered during the academic years 1974–1976 at SUNY, Stony Brook at Brookhaven National Laboratory, and at Niels Bohr Institute, unpublished. <http://www.mi.infn.it/vigezzi/HIR/HeavyIonReactions.pdf>, 1975.
- R. A. Broglia and C. Riedel. Pairing vibration and particle-hole states excited in the reaction $^{206}\text{Pb}(\text{t}, \text{p})^{208}\text{Pb}$. *Nucl. Phys.*, 92:145, 1967.
- R. A. Broglia and A. Winther. *Heavy Ion Reactions*. Westview Press, Boulder, CO., 2004.
- R. A. Broglia, B. R. Mottelson, D. R. Bès, R. Liotta, and H. M. Sofía. Treatment of the spurious state in Nuclear Field Theory. *Physics Letters B*, 64:29, 1976.
- R. A. Broglia, P. F. Bortignon, F. Barranco, E. Vigezzi, A. Idini, and G. Potel. Unified description of structure and reactions: implementing the Nuclear Field Theory program. *Phys. Scr.*, 91:063012, 2016.
- Broglia, R. A., J. S. Lilley, R. Perazzo, and W. R. Phillips. Coulomb excitation of ^{209}Bi and the weak-coupling model. *Phys. Rev. C*, 1:1508, 1970.
- Broglia, R. A., C. Riedel, and T. Udagawa. Sum rules and two-particle units in the analysis of two-neutron transfer reactions. *Nuclear Physics A*, 184:23, 1972.
- Broglia, R.A., C. Riedel, and B. Sørensen. Two-nucleon transfer and pairing phase transition. *Nuclear Physics A*, 107:1, 1968.
- Broglia, R.A., O. Hansen, and C. Riedel. Two-neutron transfer reactions and the pairing model. *Advances in Nuclear Physics*, 6:287, 1973. URL www.mi.infn.it/?vigezzi/BHR/BrogliaHansenRiedel.pdf.

- R. Bruce, J. M. Jowett, S. Gilardoni, A. Drees, W. Fischer, S. Tepikian, and S. R. Klein. Observations of beam losses due to bound-free pair production in a heavy-ion collider. *Phys. Rev. Lett.*, 99:144801, 2007.
- M. Buchanan. Wheat from the chaff. *Nature Physics*, 11:296, 2015.
- A. O. Caldeira and A. J. Leggett. Influence of dissipation on quantum tunneling in macroscopic systems. *Phys. Rev. Lett.*, 46:211, 1981.
- A. O. Caldeira and A. J. Leggett. Quantum tunneling in a dissipative system. *Ann. of Phys.*, 149:374, 1983.
- M. Cavallaro, M. De Napoli, F. Cappuzzello, S. E. A. Orrigo, C. Agodi, M. Bondí, D. Carbone, A. Cunsolo, B. Davids, T. Davinson, A. Foti, N. Galinski, R. Kanningo, H. Lenske, C. Ruiz, and A. Sanetullaev. Investigation of the ^{10}Li shell inversion by neutron continuum transfer reaction. *Phys. Rev. Lett.*, 118:012701, 2017.
- E. Chabanat, P. Bonche, P. Haensel, J. Meyer, and R. Schaeffer. A Skyrme parametrization from subnuclear to neutron star densities. *Nuclear Physics A*, 627:710, 1997.
- G. Colò, N. V. Giai, P. F. Bortignon, and M. R. Quaglia. On dipole compression modes in nuclei. *Physics Letters B*, 485:362, 2000.
- L. N. Cooper. Bound Electron Pairs in a Degenerate Fermi Gas. *Phys. Rev.*, 104: 1189, 1956.
- Dickhoff, W. and D. Van Neck. *Many-Body Theory Exposed: Propagator description of quantum mechanics in many-body systems*. World Scientific, Singapore, 2005.
- H. Feshbach. Unified Theory of Nuclear Reactions. *Annals of Physics*, 5:357, 1958.
- R. Feynman. *Theory of fundamental processes*. Benjamin, Reading, Mass., 1975.
- Glendenning, N. K. *Direct nuclear reactions*. World Scientific, Singapore, 2004.
- L. P. Gor'kov. *Theory of Superconductivity: from phenomenology to microscopic theory*. CRC Press, 2012.
- W. Heisenberg. *The physical principles of quantum theory*. Dover, New York, 1949.
- V. Hellemans, A. Pastore, T. Duguet, K. Bennaceur, D. Davesne, J. Meyer, M. Bender, and P.-H. Heenen. Spurious finite-size instabilities in nuclear energy density functionals. *Phys. Rev. C*, 88:064323, 2013.

- J. Högaasen-Feldman. A study of some approximations of the pairing force. *Nuclear Physics*, 28:258, 1961.
- A. Idini, G. Potel, F. Barranco, E. Vigezzi, and R. A. Broglia. Interweaving of elementary modes of excitation in superfluid nuclei through particle-vibration coupling: Quantitative account of the variety of nuclear structure observables. *Phys. Rev. C*, 92:031304, 2015.
- Idini, A., G. Potel, Barranco, E. Vigezzi, and R. A. Broglia. Dual origin of pairing in nuclei. *Physics of Atomic Nuclei*, 79:807, 2014.
- D. F. Jackson. *Nuclear reactions*. Methuen, London, 1970.
- B. D. Josephson. Possible new effects in superconductive tunnelling. *Phys. Lett.*, 1:251, 1962.
- R. Kanungo, A. Sanetullaev, J. Tanaka, S. Ishimoto, G. Hagen, T. Myo, T. Suzuki, C. Andreoiu, P. Bender, A. A. Chen, B. Davids, J. Fallis, J. P. Fortin, N. Galinski, A. T. Gallant, P. E. Garrett, G. Hackman, B. Hadinia, G. Jansen, M. Keefe, R. Krücken, J. Lighthall, E. McNeice, D. Miller, T. Otsuka, J. Purcell, J. S. Randhawa, T. Roger, A. Rojas, H. Savajols, A. Shotter, I. Tanihata, I. J. Thompson, C. Unsworth, P. Voss, and Z. Wang. Evidence of soft dipole resonance in ^{11}Li with isoscalar character. *Phys. Rev. Lett.*, 114:192502, 2015.
- N. M. Kroll and W. E. Lamb. On the self-energy of a bound electron. *Phys. Rev.*, 75:388, 1949.
- W. E. Lamb and R. C. Rutherford. Fine structure of the hydrogen atom by a microwave method. *Phys. Rev.*, 72:241, 1947.
- L. Landau. The theory of superfluidity in ^2He . *Journ. Phys. USSR*, 5:71, 1941.
- L. Landau. On analytic properties of vertex parts in quantum field theory. *Nuclear Physics*, 13:181, 1959.
- W. A. Lanford. Systematics of two-neutron-transfer cross sections near closed shells: A sum-rule analysis of (p, t) strengths on the lead isotopes. *Phys. Rev. C*, 16:988, 1977.
- Mahaux, C., P. F. Bortignon, R. A. Broglia, and C. H. Dasso. Dynamics of the shell model. *Physics Reports*, 120:1–274, 1985.
- M. Mayer and J. Jensen. *Elementary Theory of Nuclear Structure*. Wiley, New York, NY, 1955.
- M. H. McFarlane. The reaction matrix in nuclear shell theory. In M. Jean and R. A. Ricci, editors, *Proceedings of the International school of physics “E. Fermi” Course XL Nuclear Structure and Nuclear Reactions*, page 457. Academic Press, New York, 1969.

- J. Mehra. *The beat of a different drum*. Clarendon Press, Oxford, 1996.
- A. Moro, J. Casal, and M. Gmez-Ramos. Investigating the ^{10}Li continuum through $^{9}\text{Li}(\text{d},\text{p})^{10}\text{Li}$ reactions. *Physics Letters B*, 793:13 – 18, 2019.
- B. R. Mottelson. Selected topics in the theory of collective phenomena in nuclei. In G. Racah, editor, *International School of Physics “Enrico Fermi” Course XV , Nuclear Spectroscopy*, page 44, New York, 1962. Academic Press.
- B. R. Mottelson. *Elementary Modes of Excitation in Nuclei, Le Prix Nobel en 1975*. Imprimerie Royale Norstedts Tryckeri, Stockholm, 1976a. p. 80.
- B. R. Mottelson. Atomkernens elementære eksitationer. *Naturens Verden*, 6:169, 1976b.
- S. G. Nilsson. Binding states of individual nucleons in strongly deformed nuclei. *Mat. Fys. Medd. Dan. Vid. Selsk.*, 29, 1955.
- A. Pais. *Inward bound*. Oxford University Press, Oxford, 1986.
- A. Pais. *The genius of science*. Oxford University Press, Oxford, 2000.
- A. Pastore, D. Tarpanov, D. Davesne, and J. Navarro. Spurious finite-size instabilities in nuclear energy density functionals: Spin channel. *Phys. Rev. C*, 92: 024305, 2015.
- F. Perey and B. Buck. A non-local potential model for the scattering of neutrons by nuclei . *Nuclear Physics*, 32:353, 1962.
- D. Pines and D. Bohm. A Collective Description of Electron Interactions: II. Collective vs Individual Particle Aspects of the Interactions. *Phys. Rev.*, 85:338, 1952.
- Pines, D. and Nozières. *The theory of quantum liquids*. Benjamin, New York, 1966.
- G. Potel, F. Barranco, E. Vigezzi, and R. A. Broglia. Evidence for phonon mediated pairing interaction in the halo of the nucleus ^{11}Li . *Phys. Rev. Lett.*, 105:172502, 2010.
- G. Potel, A. Idini, F. Barranco, E. Vigezzi, and R. A. Broglia. From bare to renormalized order parameter in gauge space: structure and reactions. *Phys. Rev C*, 96:034606, 2017.
- Potel, G., A. Idini, F. Barranco, E. Vigezzi, and R. A. Broglia. Cooper pair transfer in nuclei. *Rep. Prog. Phys.*, 76:106301, 2013a.
- Potel, G., A. Idini, F. Barranco, E. Vigezzi, and R. A. Broglia. Quantitative study of coherent pairing modes with two-neutron transfer: Sn isotopes. *Phys. Rev. C*, 87:054321, 2013b.

- H. Reinhardt. Foundation of nuclear field-theory. *Nucl. Phys. A*, 241:317, 1975.
- H. Reinhardt. Functional approach to Nuclear Field-theory - schematic model with pairing and particle-hole forces. *Nucl. Phys. A*, 298:60, 1978a.
- H. Reinhardt. Nuclear Field-Theory. *Nucl. Phys. A*, 251:77, 1978b.
- H. Reinhardt. Application of the nuclear-field theory to superfluid nuclei-quasiparticle-phonon multiplet. *Nucl. Phys. A*, 251:176, 1980.
- D. Sackett, K. Ieki, A. Galonsky, C. A. Bertulani, H. Esbensen, J. J. Kruse, W. G. Lynch, D. J. Morrissey, N. A. Orr, B. M. Sherrill, H. Schulz, A. Sustich, J. A. Winger, F. Deák, A. Horváth, A. Kiss, Z. Seres, J. J. Kolata, R. E. Warner, and D. L. Humphrey. Electromagnetic excitation of ^{11}Li . *Phys. Rev. C*, 48:118, 1993.
- A. Sanetullaev, R. Kanungo, J. Tanaka, M. Alcorta, C. Andreoiu, P. Bender, A. Chen, G. Christian, B. Davids, J. Fallis, J. Fortin, N. Galinski, A. Gallant, P. Garrett, G. Hackman, B. Hadinia, S. Ishimoto, M. Keefe, R. Krücken, J. Lighthall, E. McNeice, D. Miller, J. Purcell, J. Randhawa, T. Roger, A. Rojas, H. Savajols, A. Shotter, I. Tanihata, I. Thompson, C. Unsworth, P. Voss, and Z. Wang. Investigation of the role of ^{10}Li resonances in the halo structure of ^{11}Li through the $^{11}\text{Li}(p, d)^{10}\text{Li}$ transfer reaction. *Physics Letters B*, 755:481, 2016.
- G. Satchler. *Introduction to Nuclear Reactions*. Mc Millan, New York, 1980.
- G. Satchler. *Direct Nuclear Reactions*. Clarendon Press, Oxford, 1983.
- J. Schrieffer. *Superconductivity*. Benjamin, New York, 1964.
- J. Schwinger. *Quantum Mechanics*. Springer, Heidelberg, 2001.
- I. Tanihata, H. Savajols, and R. Kanungo. Recent experimental progress in nuclear halo structure studies. *Progress in Particle and Nuclear Physics*, 68:215, 2013.
- Tanihata, I., M. Alcorta, D. Bandyopadhyay, R. Bieri, L. Buchmann, B. Davids, N. Galinski, D. Howell, W. Mills, S. Mythili, R. Openshaw, E. Padilla-Rodal, G. Ruprecht, G. Sheffer, A. C. Shotter, M. Trinczek, P. Walden, H. Savajols, T. Roger, M. Caamano, W. Mittig, P. Roussel-Chomaz, R. Kanungo, A. Gallant, M. Notani, G. Savard, and I. J. Thompson. Measurement of the two-halo neutron transfer reaction $^1\text{H}(^{11}\text{Li}, ^9\text{Li})^3\text{H}$ at 3A MeV. *Phys. Rev. Lett.*, 100:192502, 2008.
- D. ter Haar. *Men of Physics: L. D. Landau II*. Bergamon Press, Oxford, 1969.
- I. J. Thompson and F. M. Nunes. *Nuclear Reactions for Astrophysics*. Cambridge University Press, Cambridge, 2009.
- M. K. Transtrum, B. B. Machta, K. S. Brown, B. C. Daniels, C. R. Myers, and J. P. Sethna. Perspective: Sloppiness and emergent theories in physics, biology, and beyond. *The Journal of Chemical Physics*, 143:010901, 2015.

- J. Ungrin, R. M. Diamond, P. O. Tjøm, and B. Elbek. Inelastic deuteron scattering in the lead region. *Mat. Fys. Medd. Dan. Vid. Selk.*, 38, 1971.
- P. G. Wolynes. Moments of excitement. *Science*, 352:150, 2016.
- P. G. Wolynes, W. A. Eaton, and F. A. R. Chemical physics of protein folding. *PNAS*, 109:17770, 2012.
- S. Yoshida. Note on the two-nucleon stripping reaction. *Nuclear Physics*, 33:685, 1962.
- M. Zinser, F. Humbert, T. Nilsson, W. Schwab, T. Blaich, M. J. G. Borge, L. V. Chulkov, H. Eickhoff, T. W. Elze, H. Emling, B. Franzke, H. Freiesleben, H. Geissel, K. Grimm, D. Guillemaud-Mueller, P. G. Hansen, R. Holzmann, H. Irnich, B. Jonson, J. G. Keller, O. Klepper, H. Klingler, J. V. Kratz, R. Kulessa, D. Lambrecht, Y. Leifels, and A. Magel. Study of the unstable nucleus ^{10}Li in stripping reactions of the radioactive projectiles ^{11}Be and ^{11}Li . *Phys. Rev. Lett.*, 75:1719, 1995.
- Zinser, M., F. Humbert, T. Nilsson, W. Schwab, H. Simon, T. Aumann, M. J. G. Borge, L. V. Chulkov, J. Cub, T. W. Elze, H. Emling, H. Geissel, D. Guillemaud-Mueller, P. G. Hansen, R. Holzmann, H. Irnich, B. Jonson, J. V. Kratz, R. Kulessa, Y. Leifels, H. Lenske, A. Magel, A. C. Mueller, G. Mnzenberg, F. Nickel, G. Nyman, A. Richter, K. Riisager, C. Scheidenberger, G. Schrieder, K. Stelzer, J. Stroth, A. Surowiec, O. Tengblad, E. Wajda, and E. Zude. Invariant-mass spectroscopy of ^{10}Li and ^{11}Li . *Nuclear Physics A*, 619:151, 1997.